

UNIVERSITY OF OKLAHOMA
GRADUATE COLLEGE

RADAR CROSS SECTION MODELING OF TORNADIC DEBRIS
AND APPLICATIONS

A DISSERTATION
SUBMITTED TO THE GRADUATE FACULTY
in partial fulfillment of the requirements for the
Degree of
DOCTOR OF PHILOSOPHY

By
YE ZHU
Norman, Oklahoma
2016

RADAR CROSS SECTION MODELING OF TORNADIC DEBRIS
AND APPLICATIONS

A DISSERTATION APPROVED FOR THE
SCHOOL OF ELECTRICAL AND COMPUTER ENGINEERING

BY

Dr. J. R. Cruz, Chair

Dr. Zhibo Yang

Dr. Robert D. Palmer

Dr. Mark B. Yeary

Dr. Caleb J. Fulton

©Copyright by YE ZHU 2016
All Rights Reserved.

Dedication

This dissertation is dedicated to my parents, Tonggeng Zhu and Shuxia Wang, for making an unforgettable impression on me and always offering their encouragement; to my supportive husband, Chuanbin Mao; and to my lovely, sweet daughter Angelina Mao, who is a talented psychologist, artist, and musician.

Acknowledgements

Over the past several years, many individuals have supported my doctoral studies. I would have never been able to finish my dissertation without the guidance of my new committee members, help from colleagues and friends, and the support from my family.

My progress toward the doctoral degree was interrupted when two of my advisors, Dr. Matthew Kane and Dr. Binil Starly, left the University of Oklahoma. I struggled for a long time to find a new advisor suitable for my interest of research. Fortunately, Dr. Cruz has been a supportive mentor, and has helped me through my toughest moments over and over again. The kindness in his heart has given me the strength and encouragement to finish my dissertation. Dr. Palmer, a co-advisor, and Dr. Fulton introduced me to radar as an area of research. This dissertation would not be possible without them. I would like to give a great “thank you” to everybody who supported me in finishing my doctoral program.

During the process of writing dissertation, Dr. Palmer and Dr. Fulton helped me write the outline for the dissertation. Dr. Cruz and Dr. Palmer also helped me answer questions to make the defense successful.

Finally, I would like to thank my lovely daughter and my husband. They are always there no matter what obstacles I face.

Table of Contents

Acknowledgements	iv
List of Tables	ix
List of Figures	x
Abstract	xlvi
1 Introduction	1
2 Background	12
2.1 Measurements.....	15
2.2 Full-wave simulations.....	18
2.2.1 Finite element method and HFSS modeling.	19
2.2.2 MoM-based method	20
2.3 Analytical approaches.....	21
2.3.1 PO.....	21
2.3.2 GO.....	23
2.3.3 GTD.....	24
2.4 Summary.....	24
3 PO-based calculations of the RCS of plate-like objects	26
3.1 Literature review.....	26
3.2 Motivation for detailed analysis.....	27
3.2.1 Circular vs. rectangular.....	28
3.2.2 Metal vs. dielectric (penetrable vs. non-penetrable).....	29
3.2.3 Thick plates vs. thin plates.....	30
3.2.4 Electrically small vs. electrically-large objects.....	30
3.3 Generic derivation for metal (non-penetrable) objects-rectangular and circular.....	31
3.3.1 Generic derivation for metal (non-penetrable)-perfect conducting rectangular plates.....	34
3.3.2 Generic derivation for metal (non-penetrable)-perfect conducting circular plates.....	36
3.3.3 Simulation vs. analytical results-conducting circular plates.....	38
3.3.3.1 Small (radius $< 0.5 \lambda$) conducting circular plates.....	39

3.3.3.2	Larger (radius $\geq 0.5 \lambda$) conducting circular plates	41
3.3.4	Simulation vs. analytical results – conducting rectangular plates	48
3.3.4.1	Small (a, b $< 1 \lambda$) conducting rectangular plates	49
3.3.4.2	Large (a, b $\geq 1 \lambda$) conducting rectangular plates	51
3.4	Generic derivation for penetrable objects- rectangular and circular plates	53
3.4.1	Thin sheet approximation –rectangular	53
3.4.2	Multi-layered approach for thicker plates-rectangular	57
3.4.3	Generic derivation of penetrable (non-metal) circular plates	62
3.4.3.1	Surface impedance circular plates (non-metal)	62
3.4.3.2	General non-metal circular plates (sheets)	64
3.4.3.3	Simulation vs. analytical results for non-metal circular plates	65
3.4.3.3.1	Small (radius $< 0.5 \lambda$) non-metal circular sheets	66
3.4.3.3.2	Larger (radius $> 0.5 \lambda$) non-metal circular sheets	70
3.4.3.3.3	Small (radius $< 0.5 \lambda$) non-metal circular thicker plates	74
3.4.3.3.4	Large (radius $> 0.5 \lambda$) circular non-metal thicker plates	76
3.4.3.4	Simulation vs. analytical results for non-metal rectangular sheets	77
3.4.3.4.1	Small (a, b $< 1 \lambda$) non-metal rectangular thin sheets	77
3.4.3.4.2	Large (a, b $> 1 \lambda$) non-metal rectangular thin sheets	79
3.4.3.5	Simulation vs. analytical results for rectangular thicker plates	83
3.4.3.5.1	One layer non-metal rectangular plates	83
3.4.3.5.1.1	Small (a, b $< 1 \lambda$) non-metal plates	83
3.4.3.5.1.2	Large (a, b $> 1 \lambda$) non-metal thicker plates	87
3.4.3.5.2	Multi-layer (two layers) rectangular thicker plates	90
3.5	The errors and limitations	97

3.5.1	Metal vs. non-metal – PO vs. simulations.....	98
3.5.1.1	Metal vs. non-metal for circular plates.....	98
3.5.1.2	Metal vs. non-metal for rectangular plates.....	105
3.5.2	Thick vs. thin – PO vs. simulations.....	112
3.5.2.1	Thin vs. thick for circular non-metal plates.....	112
3.5.2.2	Thin vs. thick for circular metal plates.....	121
3.5.2.3	Thin vs. thick for rectangular non-metal plates.....	127
3.5.2.4	Thin vs. thick for rectangular metal plates.....	134
3.6	Summary.....	138
4	PO-based calculations of the RCS of cylindrical objects	141
4.1	Review of standard results and current implementation of these standard results (PO).....	141
4.2	Motivation for detailed analysis.....	142
4.2.1	Metal vs. Non-metal (dielectric) cylinders.....	144
4.2.2	Long vs. short cylinders.....	144
4.3	Generic derivation for metal cylinders.....	146
4.3.1	Generic derivation for metal cylinders broadside.....	146
4.3.2	Simulation vs. analytical results for metal large, thin cylinders with and without endcaps.....	150
4.4	Generic derivation for dielectric cylinders.....	172
4.4.1	Generic derivation for dielectric cylinders broadside....	172
4.4.2	Generic derivation for dielectric cylinders endcaps.....	178
4.4.3	Simulation vs. analytical results for dielectric large, thin cylinders with and without endcaps.....	179
4.5	Short and fat dielectric cylinders.....	199
4.5.1	Analytical vs. simulated results with and without endcaps	200
4.5.2	Comparison to thin sheet results for short cylinders.....	218
4.5.3	Summary.....	226
5	Example applications	228
5.1	Leaf library generation examples.....	228
5.1.1	Describe and discuss the coordinate transformations to generate a library.....	228
5.1.2	Analytical simulation for a single leaf.....	231
5.2	Mean RCS of wood board study.....	261
5.2.1	Motivation.....	261
5.2.2	Calculation of the mean value of RCS for wood board..	263
5.2.3	The list of wood to a typical house and establishing a RCS library.....	268

6 Conclusions	274
References	285
Appendix A	
List of Acronyms.....	293
Appendix B	
List of Symbols.....	294

List of Tables

5.1	Approximation of RCS values for dry wood board at 10 square sizes at 5 different frequencies (2.8, 5.5, 9.7, 37.5, 100 GHz).....	271
5.2	Non-approximation of RCS values for dry wood board at 10 square sizes at 5 different frequencies (2.8, 5.5, 9.7, 37.5, 100 GHz).....	272
5.3	Non-approximation of RCS values for wet wood board at 10 square sizes at 5 different frequencies (2.8, 5.5, 9.7, 37.5, 100 GHz) (Moisture content 20%, $\epsilon_r = 4.6500 - 1.4600i$).....	273

List of Figures

1.1	Conceptual diagram of the time series radar simulator. Each point scatterer represents a discrete position from which the transmit pulse is reflected. Meteorological parameters from the Advanced Regional Prediction (ARPS) model are used to derive the reflectivity and velocity of each discrete scatterer. All reflected echoes are integrated to obtain the composite returned signal. As the number of points increases, the composite returned signal approximates well from volume scattering.....	6
3.1	Illustration of setup for the source and target.....	31
3.2	Procedure of RCS estimation.....	32
3.3	Block diagram for computing radiated fields from electric and magnetic sources.(Source: C.A. Balanis, <i>Antenna Theory: Analysis and Design</i> . 3 rd Edition, Copyright 2005, John Wiley & Sons, Inc.).....	33
3.4	Target far-field geometry approximation.....	33
3.5	Amplitude comparison for TE and TM mode in MATLAB and HFSS (offset 0.0001 (~0.001 λ) meters in thickness by 0.03 (~0.27 λ) meters in radius for a metal thin sheet ($\epsilon_r = 10^6$) located in half of $L = 0.6$ (~6 λ) meters). Amplitudes show a few dB differences for TE and TM.....	39
3.6	Phase comparison for TE and TM mode in MATLAB and HFSS (offset 0.0001 (~0.001 λ) meters in thickness by 0.03 (~0.27 λ) meters in radius for a metal thin sheet ($\epsilon_r = 10^6$) located in half of $L = 0.6$ (~6 λ) meters). The phase matches well for both TE and TM.....	40
3.7	Amplitude comparison for TE and TM mode in MATLAB and HFSS (offset 0.01 (~0.1 λ) meters in thickness by 0.03 (~0.27 λ) meters in radius for a perfect conducting plate located in half of $L = 0.6$ (~6 λ) meters). Amplitudes show a few dB differences for both TE and TM.....	40
3.8	Phase comparison for TE and TM mode in MATLAB and HFSS (offset 0.01 (~0.1 λ) meters in thickness by 0.03 (~0.27 λ) meters in radius for a perfect conducting plate located in half of $L=0.6$ (~6 λ) meters). The phase matches well for TE, and mismatches as the incident angle is close to 90 degrees for TM.....	41
3.9	Amplitude comparison for TE and TM mode in MATLAB and	

	HFSS (0.00011 (~0.001 λ) meters in length by 0.055 (~0.5 λ) meters in radius at $\epsilon_r = 10^6$ for a metal thin sheet at half of $L = 0.11$ (~1 λ) meters). Amplitudes overlap at 0 degrees for both TE and TM.....	41
3.10	Phase comparison for TE and TM mode in MATLAB and HFSS (0.00011 (~0.001 λ) meters in length by 0.055 (~0.5 λ) meters in radius at $\epsilon_r = 10^6$ for a metal thin sheet with endcap located at half of $L = 0.11$ (~1 λ) meters). The phase matches closely for both TE and TM.....	42
3.11	Amplitude comparison for TE and TM mode in MATLAB and HFSS (offset 0.0001 (~0.001 λ) meters in thickness by 0.11 (~1 λ) meters in radius for a metal ($\epsilon_r = 10^6$) thin sheet located in half of $L = 1.1$ (~10 λ) meters). Amplitudes match well as the incident angle is less than 30 degrees for both TE and TM.....	42
3.12	Phase comparison for TE and TM mode in MATLAB and HFSS (offset 0.0001 (~0.001 λ) meters in thickness by 0.11 (~1 λ) meters in radius for a metal ($\epsilon_r = 10^6$) thin sheet located in half of $L = 1.1$ (~10 λ) meters). The phase shows a little mismatch for both TE and TM.....	43
3.13	Amplitude comparison for TE and TM mode in MATLAB and HFSS (offset 0.001 (~0.01 λ) meters in thickness by 0.11 (~1 λ) meters in radius for a conducting thin plate located in half of $L = 1.1$ (~10 λ) meters). Amplitudes match well as the incident angle is less than 30 degrees for both TE and TM.....	43
3.14	Phase comparison for TE and TM mode in MATLAB and HFSS (offset 0.001 (~0.01 λ) meters in thickness by 0.11 (~1 λ) meters in radius for a conducting thin sheet located in half of $L = 1.1$ (~10 λ) meters). The phase shows a little mismatch for both TE and TM.....	44
3.15	Amplitude comparison for TE and TM mode in MATLAB and HFSS (offset 0.01 (~0.1 λ) meters in thickness by 0.11 (~1 λ) meters in radius for a conducting thick plate located in half of $L = 1.1$ (~10 λ) meters). Amplitudes match well as the incident angle is less than 20 degrees for both TE and TM.....	44
3.16	Phase comparison for TE and TM mode in MATLAB and HFSS (offset 0.01 (~0.1 λ) meters in thickness by 0.11 (~1 λ) meters in radius for a conducting thick plate located in half of $L = 1.1$ (~10 λ) meters). Slight phase mismatch for TE and TM is observed..	45
3.17	Amplitude comparison for TE and TM mode in MATLAB and HFSS (offset 0.0001 (~0.001 λ) meters in thickness by 0.165 (~1.5 λ) meters in radius for a metal thin sheet located in half of $L = 3.3$ (~30 λ) meters). Amplitudes match well as the incident	

	angle is less than 30 degrees for both TE and TM.....	45
3.18	Phase comparison for TE and TM mode in MATLAB and HFSS (offset 0.0001 (~0.001 λ) meters in thickness by 0.165 (~1.5 λ) meters in radius for a metal thin plate located in half of $L = 3.3$ (~30 λ) meters). The phase matches well for both TE and TM...	46
3.19	Amplitude comparison for TE and TM mode in MATLAB and HFSS (offset 0.0001 (~0.001 λ) meters in thickness by 0.33 (~3 λ) meters in radius for a perfect conducting thin sheet located in half of $L = 0.8$ (~8 λ) meters). Amplitudes match well as the incident angle is less than 30 degrees for both TE and TM.....	46
3.20	Phase comparison for TE and TM mode in MATLAB and HFSS (offset 0.0001 (~0.001 λ) meters in thickness by 0.33 (~3 λ) meters in radius for a perfect conducting thin sheet located in half of $L = 0.8$ (~8 λ) meters). The phase matches closely for both TE and TM.....	47
3.21	Amplitude comparison for TE and TM mode in MATLAB and HFSS (offset 0.001 (~0.01 λ) meters in thickness by 0.33 (~3 λ) meters in radius for a perfect conducting thin sheet located in half of $L = 0.8$ (~8 λ) meters). Amplitudes match well as the incident angle is less than 30 degrees for both TE and TM.....	48
3.22	Amplitude comparison for TE and TM mode in MATLAB and HFSS (offset 0.01 (~0.1 λ) meters in thickness by 0.33 (~3 λ) meters in radius for a perfect conducting plate located in half of $L = 0.8$ (~8 λ) meters). Amplitudes match well as the incident angle is less than 30 degrees for both TE and TM.....	48
3.23	Amplitude comparison for TE and TM mode in MATLAB and HFSS (offset 0.01 (~0.1 λ) meters in thickness for a metal rectangular plate at $a = 0.04$ (~0.4 λ) meters, $b = 0.06$ (~0.6 λ) meters located at origin). A few dB differences in amplitude are observed for both TE and TM.....	49
3.24	Phase comparison for TE and TM mode in MATLAB and HFSS (offset 0.01 (~0.1 λ) meters in thickness for a metal rectangular plate at $a = 0.04$ (~0.4 λ) meters, $b = 0.06$ (~0.6 λ) meters located at origin). The phase mismatch is observed for both TE and TM.....	50
3.25	Amplitude comparison for TE and TM mode in MATLAB and HFSS (offset 0.001 (~0.01 λ) meters in thickness for a metal rectangular thin plate at $a = 0.04$ (~0.4 λ) meters, $b = 0.06$ (~0.6 λ) meters located at origin). A few dB differences in amplitude are observed for both TE and TM.....	50
3.26	Phase comparison for TE and TM mode in MATLAB and HFSS (offset 0.001 (~0.01 λ) meters in thickness for a metal rectangular thin plate at $a = 0.04$ (~0.4 λ) meters, $b = 0.06$ (~0.6 λ) meters	

	located at origin). The phase mismatch is observed for both TE and TM.....	51
3.27	Amplitude comparison for TE and TM mode in MATLAB and HFSS (offset 0.01 (~0.1 λ) meters in thickness for a metal rectangular plate at a = 0.11 (~1 λ) meters, b = 0.11 (~1 λ) meters located at origin). They match well as the incident angle is less than 30 degrees for both TE and TM.....	51
3.28	Phase comparison for TE and TM mode in MATLAB and HFSS (offset 0.01 (~0.1 λ) meters in thickness for a metal rectangular plate at a = 0.11 (~1 λ) meters, b = 0.11 (~1 λ) meters located at origin). The phase does not match well for both TE and TM.....	52
3.29	Amplitude comparison for TE and TM mode in MATLAB and HFSS (offset 0.01 (~0.1 λ) meters in thickness for a metal rectangular plate at a = 1.1 (~10 λ) meters, b = 0.5 (~5 λ) meters located at origin). Amplitudes are in good agreement with HFSS as the incident angle is less than 40 degrees for both TE and TM.	52
3.30	Phase comparison for TE and TM mode in MATLAB and HFSS (offset 0.01 (~0.1 λ) meters in thickness for a metal rectangular plate at a = 1.1 (~10 λ) meters, b = 0.5 (~5 λ) meters located at origin). The phase matches closely for both TE and TM.....	53
3.31	Amplitude comparison for TE and TM mode in MATLAB and HFSS (offset 0.0001 (~0.001 λ) meters in thickness by 0.011 (~0.1 λ) meters in radius $\epsilon_r = 2.15$ for a thin sheet located in half of L = 1.1 (~10 λ) meters). Amplitudes show a few dB differences for TE with HFSS, and match closely with HFSS as the incident angle is less than 40 degrees for TM.....	66
3.32	Phase comparison for TE and TM mode in MATLAB and HFSS (offset 0.0001 (~0.001 λ) meters in thickness by 0.011 (~0.1 λ) meters in radius dielectric $\epsilon_r = 2.15$ for a thin sheet located in half of L = 1.1 (~10 λ) meters). The phase shows a little mismatch for TE and TM.....	66
3.33	Amplitude comparison for TE and TM mode in MATLAB and HFSS (offset 0.0001 (~0.001 λ) meters in thickness by 0.011 (~0.1 λ) meters in radius $\epsilon_r = 10-5j$ for a thin sheet located in half of L = 1.1 (~10 λ) meters). Amplitudes show a few dB differences for TE with HFSS, and match closely with HFSS as the incident angle is less than 60 degrees for TM.....	67
3.34	Phase comparison for TE and TM mode in MATLAB and HFSS (offset 0.0001 (~0.001 λ) meters in thickness by 0.011 (~0.1 λ) meters in radius dielectric $\epsilon_r = 10-5j$ for a thin sheet located in	

	half of $L = 1.1$ ($\sim 10 \lambda$) meters). The phase shows a little mismatch for TE and TM.....	67
3.35	Amplitude comparison for TE and TM mode in MATLAB and HFSS (offset 0.0001 ($\sim 0.001 \lambda$) meters in thickness by 0.033 ($\sim 0.3 \lambda$) meters in radius $\epsilon_r = 2.15$ (wood) for a thin sheet located in half of $L = 3.3$ ($\sim 30 \lambda$) meters). Amplitude matches closely with HFSS as the incident angle is less than 70 degrees for TE, and is less than 40 degrees for TM.....	68
3.36	Phase comparison for TE and TM mode in MATLAB and HFSS (offset 0.0001 ($\sim 0.001 \lambda$) meters in thickness by 0.033 ($\sim 0.3 \lambda$) meters in radius $\epsilon_r = 2.15$ for a thin sheet located in half of $L = 3.3$ ($\sim 30 \lambda$) meters). The phase shows a little mismatch, as the incident angle is less than 20 degrees for both TE and TM.....	68
3.37	Amplitude comparison for TE and TM mode in MATLAB and HFSS (offset 0.0001 ($\sim 0.001 \lambda$) meters in thickness by 0.033 ($\sim 0.3 \lambda$) meters in radius $\epsilon_r = 10-5j$ for a thin sheet located in half of $L = 3.3$ ($\sim 30 \lambda$) meters). Amplitudes show to be very close as the incident angle is less than 70 degrees for TE, and is less than 60 degrees for TM.....	69
3.38	Phase comparison for TE and TM mode in MATLAB and HFSS (offset 0.0001 ($\sim 0.001 \lambda$) meters in thickness by 0.033 ($\sim 0.3 \lambda$) meters in radius $\epsilon_r = 10-5j$ for a thin sheet located in half of $L = 3.3$ ($\sim 30 \lambda$) meters). The phase has a little mismatch, as the incident angle is less than 20 degrees for both TE and TM.....	69
3.39	Amplitude comparison for TE and TM mode in MATLAB and HFSS (offset 0.0001 ($\sim 0.001 \lambda$) meters in thickness by 0.055 ($\sim 0.5 \lambda$) meters in radius $\epsilon_r = 2.15$ for a thin sheet located in half of $L = 1.1$ ($\sim 10 \lambda$) meters). Amplitude for TE is in good agreement with HFSS and matches well for TM with HFSS as the incident angle is less than 40 degrees.....	70
3.40	Phase comparison for TE and TM mode in MATLAB and HFSS (offset 0.0001 ($\sim 0.001 \lambda$) meters in thickness by 0.055 ($\sim 0.5 \lambda$) meters in radius $\epsilon_r = 2.15$ for a thin sheet located in half of $L = 1.1$ ($\sim 10 \lambda$) meters). The phase shows a little mismatch for both TE and TM.....	71
3.41	Amplitude comparison for TE and TM mode in MATLAB and HFSS (offset 0.0001 ($\sim 0.001 \lambda$) meters in thickness by 0.055 ($\sim 0.5 \lambda$) meters in radius $\epsilon_r = 10-5j$ for a thin sheet located in half of $L = 1.1$ ($\sim 10 \lambda$) meters). Amplitude is in good agreement for TE with HFSS and matches well for TM with HFSS as the incident angle is less than 60 degrees.....	71

3.42	Phase comparison for TE and TM mode in MATLAB and HFSS (offset 0.0001 ($\sim 0.001 \lambda$) meters in thickness by 0.055 ($\sim 0.5 \lambda$) meters in radius $\epsilon_r = 10-5j$ for a thin sheet located in half of $L = 1.1$ ($\sim 10 \lambda$) meters). The phase shows a little mismatch for both TE and TM.....	72
3.43	Amplitude comparison for TE and TM mode in MATLAB and HFSS (offset 0.0001 ($\sim 0.001 \lambda$) meters in thickness by 0.11 ($\sim 1 \lambda$) meters in radius $\epsilon_r = 10-5j$ for a thin sheet located in half of $L = 1.1$ ($\sim 10 \lambda$) meters). Amplitudes for TE are in good agreement with HFSS and match well for TM with HFSS as the incident angle is less than 60 degrees.....	72
3.44	Phase comparison for TE and TM mode in MATLAB and HFSS (offset 0.0001 ($\sim 0.001 \lambda$) meters in thickness by 0.11 ($\sim 1 \lambda$) meters in radius $\epsilon_r = 10-5j$ for a thin sheet located in half of $L = 1.1$ ($\sim 10 \lambda$) meters). The phase shows a little mismatch for both TE and TM.....	73
3.45	Amplitude comparison for TE and TM mode in MATLAB and HFSS (0.0002 ($\sim 0.002 \lambda$) meters in length by 0.33 ($\sim 3 \lambda$) meters in radius at $\epsilon_r = 2.15$ for a dielectric thin sheet at $L = 1.1$ ($\sim 10 \lambda$) meters). Amplitudes are almost in good agreement except at 80-90 degrees for TE and TM.....	73
3.46	Phase comparison for TE and TM mode in MATLAB and HFSS 0.0002 ($\sim 0.002 \lambda$) meters in length by 0.33 ($\sim 3 \lambda$) meters in radius at $\epsilon_r = 2.15$ for a dielectric thin sheet at $L = 1.1$ ($\sim 10 \lambda$) meters). The phase is in good agreement with HFSS for both TE and TM.	74
3.47	Amplitude comparison for TE and TM mode in MATLAB and HFSS (offset 0.01 ($\sim 0.1 \lambda$) meters in thickness by 0.011 ($\sim 0.1 \lambda$) meters in radius $\epsilon_r = 2.15$ for a thicker plate located in half of $L = 1.1$ ($\sim 10 \lambda$) meters). Amplitudes for TE and TM are close as the incident angle is less than 40 degrees.....	74
3.48	Phase comparison for TE and TM mode in MATLAB and HFSS (offset 0.01 ($\sim 0.1 \lambda$) meters in thickness by 0.011 ($\sim 0.1 \lambda$) meters in radius $\epsilon_r = 2.15$ for a thicker plate located in half of $L = 1.1$ ($\sim 10 \lambda$) meters). The phase shows a little mismatch, as the incident angle is less than 50 degrees for both TE and TM.....	75
3.49	Amplitude comparison for TE and TM mode in MATLAB and HFSS (offset 0.01 ($\sim 0.1 \lambda$) meters in thickness by 0.033 ($\sim 0.3 \lambda$) meters in radius $\epsilon_r = 10-5j$ for a thin plate located in half of $L =$	

	3.3 (~30 λ) meters). Amplitudes for TE and TM match well as the incident angle is less than 40 degrees.....	75
3.50	Phase comparison for TE and TM mode in MATLAB and HFSS (offset 0.01 (~0.1 λ) meters in thickness by 0.033 (~0.3 λ) meters in radius $\epsilon_r = 10-5j$ for a thin plate located in half of $L = 3.3$ (~30 λ) meters). The phase shows a little mismatch, as the incident angle is less than 40 degrees for both TE and TM.....	76
3.51	Amplitude comparison for TE and TM mode in MATLAB and HFSS (offset 0.1 (~1 λ) meters in thickness by 0.11 (~1 λ) meters in radius $\epsilon_r = 2.15$ for a thick plate located in half of $L = 1.1$ (~10 λ) meters). Amplitudes match closely as the incident angle is less than 30 degrees for both TE and TM.....	76
3.52	Phase comparison for TE and TM mode in MATLAB and HFSS (offset 0.1 (~1 λ) meters in thickness by 0.11 (~1 λ) meters in radius $\epsilon_r = 2.15$ for a thick plate located in half of $L = 1.1$ (~10 λ) meters). The phase matches well as incident angle is close to 90 degrees for TE and 60-90 degrees for TM.....	77
3.53	Amplitude comparison for TE and TM mode in MATLAB and HFSS (offset 0.0001 (~0.001 λ) meters in thickness by 0.04 (~0.4 λ) meters by 0.06 (~0.6 λ) meters $\epsilon_r = 2.15$ for a rectangular thin sheet located at origin). Amplitude matches well for TM as the incident angle is less than 40 degrees. Amplitude has a few dB differences from 0-90 degrees for TE.....	78
3.54	Phase comparison for TE and TM mode in MATLAB and HFSS (offset 0.0001 (~0.001 λ) meters in thickness by 0.04 (~0.4 λ) meters by 0.06 (~0.6 λ) meters $\epsilon_r = 2.15$ for a rectangular thin sheet located at origin). The phase shows a big gap for both TE and TM.....	78
3.55	Amplitude comparison for TE and TM mode in MATLAB and HFSS (offset 0.0002 (~0.002 λ) meters in thickness by 0.22 (~2 λ) meters by 0.14 (~1.27 λ) meters $\epsilon_r = 34.56-12.34j$ (leaf) for a rectangular sheet located at origin). Amplitudes match well as the incident angle is less than 50 degrees for both TE and TM.....	79
3.56	Phase comparison for TE and TM mode in MATLAB and HFSS (offset 0.0002 (~0.002 λ) meters in thickness by 0.22 (~2 λ) meters by 0.14 (~1.27 λ) meters $\epsilon_r = 34.56-12.34j$ (leaf) for a rectangular sheet located at origin). The phase matches closely to both TE and TM.....	80
3.57	Amplitude comparison for TE and TM mode in MATLAB and	

	HFSS (offset 0.0001 ($\sim 0.001 \lambda$) meters in thickness by 0.22 ($\sim 2 \lambda$) meters by 0.14 ($\sim 1.27 \lambda$) meters $\epsilon_r = 2.15$ for a rectangular sheet located at origin). Amplitudes match closely as the incident angle is less than 50 degrees for both TE and TM.....	80
3.58	Phase comparison for TE and TM mode in MATLAB and HFSS (offset 0.0001 ($\sim 0.001 \lambda$) meters in thickness by 0.22 ($\sim 2 \lambda$) meters by 0.14 ($\sim 1.27 \lambda$) meters $\epsilon_r = 2.15$ for a rectangular sheet located at origin). The phase matches closely to both TE and TM.....	81
3.59	Amplitude comparison for TE and TM mode in MATLAB and HFSS (offset 0.0001 ($\sim 0.001 \lambda$) meters in thickness by 0.22 ($\sim 2 \lambda$) meters by 0.14 ($\sim 1.27 \lambda$) meters $\epsilon_r = 10-5j$ for a rectangular sheet located at origin). Amplitudes match closely as the incident angle is less than 70 degrees for both TE and TM.....	81
3.60	Phase comparison for TE and TM mode in MATLAB and HFSS (offset 0.0001 ($\sim 0.001 \lambda$) meters in thickness by 0.22 ($\sim 2 \lambda$) meters by 0.14 ($\sim 1.27 \lambda$) meters $\epsilon_r = 10-5j$ for a rectangular sheet located at origin). The phase matches closely to both TE and TM.....	82
3.61	Amplitude comparison for TE and TM mode in MATLAB and HFSS (offset 0.0002 ($\sim 0.002 \lambda$) meters in thickness by 0.44 ($\sim 4 \lambda$) meters by 0.28 ($\sim 2.54 \lambda$) meters $\epsilon_r = 34.56-12.34j$ (leaf) for a rectangular sheet located at origin). Amplitudes match closely as the incident angle is less than 50 degrees for TE, and less than 70 degrees for TM.....	82
3.62	Phase comparison for TE and TM mode in MATLAB and HFSS (offset 0.0002 ($\sim 0.002 \lambda$) meters in thickness by 0.44 ($\sim 4 \lambda$) meters by 0.28 ($\sim 2.54 \lambda$) meters $\epsilon_r = 34.56-12.34j$ (leaf) for a rectangular sheet located at origin). The phase matches closely to both TE and TM.....	83
3.63	Amplitude comparison for TE and TM mode in MATLAB and HFSS (offset 0.01 ($\sim 0.1 \lambda$) meters in thickness by 0.04 ($\sim 0.4 \lambda$) meters by 0.06 ($\sim 0.6 \lambda$) meters $\epsilon_r = 2.15$ for a rectangular thick plate located at origin). Amplitudes match closely as the incident angle is less than 40 degrees for both TE and TM.....	84
3.64	Phase comparison for TE and TM mode in MATLAB and HFSS (offset 0.01 ($\sim 0.1 \lambda$) meters in thickness by 0.04 ($\sim 0.4 \lambda$) meters by 0.06 ($\sim 0.6 \lambda$) meters $\epsilon_r = 2.15$ for a rectangular thick plate located at origin). The phase shows a big gap for both TE and TM.....	84

- 3.65 Amplitude comparison for TE and TM mode in MATLAB and HFSS (offset 0.02 (~0.2 λ) meters in thickness by 0.04 (~0.4 λ) meters by 0.06 (~0.6 λ) meters $\epsilon_r = 2.15$ for a rectangular thicker plate located at origin). Amplitudes match closely as the incident angle is less than 20 degrees for both TE and TM.....85
- 3.66 Phase comparison for TE and TM mode in MATLAB and HFSS (offset 0.02 (~0.2 λ) meters in thickness by 0.04 (~0.4 λ) meters by 0.06 (~0.6 λ) meters $\epsilon_r = 2.15$ for a rectangular thick plate located at origin). The phase shows a big gap for both TE and TM.85
- 3.67 Amplitude comparison for TE and TM mode in MATLAB and HFSS (offset 0.001 (~0.01 λ) meters in thickness by 0.04 (~0.4 λ) meters by 0.06 (~0.6 λ) meters $\epsilon_r = 2.15$ for a rectangular thin plate located at origin). Amplitudes match closely as the incident angle is less than 40 degrees for both TE and TM.....86
- 3.68 Phase comparison for TE and TM mode in MATLAB and HFSS (offset 0.001 (~0.01 λ) meters in thickness by 0.04 (~0.4 λ) meters by 0.06 (~0.6 λ) meters $\epsilon_r = 2.15$ for a rectangular thin plate located at origin). The phase shows a large gap for both TE and TM.....87
- 3.69 Amplitude comparison for TE and TM mode in MATLAB and HFSS (offset 0.1 (~1 λ) meters in thickness by 0.4 (~3.64 λ) meters by 0.6 (~5.45 λ) meters $\epsilon_r = 2.15$ for a rectangular thick plate located at origin). Amplitudes match closely as the incident angle is less than 40 degrees for both TE and TM.....87
- 3.70 Phase comparison for TE and TM mode in MATLAB and HFSS (offset 0.1 (~1 λ) meters in thickness by 0.4 (~3.64 λ) meters by 0.6 (~5.45 λ) meters $\epsilon_r = 2.15$ for a rectangular thick plate located at origin). The phase matches closely to TE and TM....88
- 3.71 Amplitude comparison for TE and TM mode in MATLAB and HFSS (offset 0.1 (~1 λ) meters in thickness by 0.4 (~3.64 λ) meters by 0.6 (~5.45 λ) meters $\epsilon_r = 10-5j$ for a rectangular thick plate located at origin). Amplitudes match closely as the incident angle is less than 30 degrees.....88
- 3.72 Phase comparison for TE and TM mode in MATLAB and HFSS (offset 0.1 (~1 λ) meters in thickness by 0.4 (~3.64 λ) meters by 0.6 (~5.45 λ) meters $\epsilon_r = 10-5j$ for a rectangular thick plate located at origin). The phase matches closely to TE and TM....89
- 3.73 Amplitude comparison for TE and TM mode in MATLAB and HFSS (offset 0.1 (~1 λ) meters in thickness by 0.4 (~3.64 λ) meters by 0.6 (~5.45 λ) meters $\epsilon_r = 2.15$ and $\epsilon_r = 10-5j$ for a

- rectangular thick plate located at origin). Resistance R at $\epsilon_r = 2.15$ is greater than resistance R at $\epsilon_r = 10-5j$, amplitudes for both analytical and HFSS are lower than $\epsilon_r = 10-5j$, which is consistent with previous research (Jenn 2005). Lower scattering amplitude for higher R accounts for more transmission and less reflection in the material.....89
- 3.74 Amplitude comparison for TE and TM mode in MATLAB and HFSS (water with $\epsilon_r = 80.4$, thickness 0.002 ($\sim 0.02 \lambda$) meters on the top of wood board $\epsilon_r = 2.15$, 0.01 ($\sim 0.1 \lambda$) meters in thickness for 0.4 ($\sim 3.64 \lambda$) meters by 0.6 ($\sim 5.45 \lambda$) meters rectangular 2-layer thick plate in comparison to 1 layer of the same size wood board $\epsilon_r = 2.15$, 0.01 ($\sim 0.1 \lambda$) meters in thickness, located at origin). The amplitude of two-layer water-coated wood board increases by 10 dB when compared to 1-layer wood board.....90
- 3.75 Amplitude comparison for TE and TM mode in MATLAB and HFSS (water with $\epsilon_r = 80.4$, thickness 0.005 ($\sim 0.05 \lambda$) meters on the top of wood board $\epsilon_r = 2.15$, 0.01 ($\sim 0.1 \lambda$) meters in thickness by 0.4 ($\sim 3.64 \lambda$) meters by 0.6 ($\sim 5.45 \lambda$) meters rectangular 2-layer thick plate in comparison to 1 layer of the same size wood board $\epsilon_r = 2.15$, 0.01 ($\sim 0.1 \lambda$) meters in thickness, located at origin). The amplitude of two-layer water-coated wood board increases by 10 dB when compared to 1-layer wood board.....91
- 3.76 Amplitude comparison for TE and TM mode in MATLAB and HFSS (water with $\epsilon_r = 80.4$, thickness 0.005 ($\sim 0.05 \lambda$) meters, 0.0001 ($\sim 0.001 \lambda$) meters, respectively, on the top of wood board $\epsilon_r = 2.15$, 0.01 ($\sim 0.1 \lambda$) meters in thickness by 0.4 ($\sim 3.64 \lambda$) meters by 0.6 ($\sim 5.45 \lambda$) meters of rectangular 2-layer thick plate in comparison to 1 layer of the same size wood board $\epsilon_r = 2.15$, 0.01 ($\sim 0.1 \lambda$) meters in thickness, located at origin). Wood board coated with a thicker layer of water increases 10 dB more than 1-layer wood board. Wood board coated with a thin sheet layer of water shows some variation from 0-90 degrees.....92
- 3.77 Amplitude comparison for TE and TM mode in MATLAB and HFSS (water with $\epsilon_r = 80.4$, thickness 0.005 ($\sim 0.05 \lambda$) meters, 0.0002 ($\sim 0.002 \lambda$) meters, respectively, on the top of wood board $\epsilon_r = 2.15$, 0.01 ($\sim 0.1 \lambda$) meters in thickness by 0.4 ($\sim 3.64 \lambda$) meters by 0.6 ($\sim 5.45 \lambda$) meters rectangular 2-layer thick plate in comparison to 1 layer of the same size wood board $\epsilon_r = 2.15$, 0.01 ($\sim 0.1 \lambda$) meters in thickness, located at origin). Wood board coated with a thicker layer of water increases by 10 dB when

	compared to 1-layer wood board. Wood board coated with a thin sheet layer of water shows some variation from 0-90 degrees...92
3.78	Amplitude comparison for TE and TM mode in MATLAB and HFSS (2-layers of water with $\epsilon_r = 80.4$, thickness 0.005 ($\sim 0.05 \lambda$) meters, 0.0003 ($\sim 0.003 \lambda$) meters, respectively, on the top of wood board $\epsilon_r = 2.15$, 0.01 ($\sim 0.1 \lambda$) meters in thickness by 0.4 ($\sim 3.64 \lambda$) meters by 0.6 ($\sim 5.45 \lambda$) meters of rectangular thick plate in comparison to 1 layer of the same size wood board, located at origin). Water coated in 2 layers increases by 10 dB, and 5 dB when compared to 1-layer wood board, respectively.....93
3.79	RCS FEKO plots for 2 layers with different water coating thicknesses at 0.01 ($\sim 0.1 \lambda$) meters, 0.005 ($\sim 0.05 \lambda$) meters, 0.002 ($\sim 0.02 \lambda$) meters, 0.0003 ($\sim 0.003 \lambda$) meters, 0.0002 ($\sim 0.002 \lambda$) meters, 0.0001 ($\sim 0.001 \lambda$) meters on top of wood board with a thickness of 0.01 ($\sim 0.1 \lambda$) meters. FEKO plots are very similar to analytical results for two layers.....96
3.80	Amplitude comparison for TE and TM mode in MATLAB and HFSS (offset 0.0001 ($\sim 0.001 \lambda$) meters in thickness by 0.11 ($\sim 1 \lambda$) meters in radius $\epsilon_r = 2.15$ for a thin sheet located in half of $L = 1.1$ ($\sim 10 \lambda$) meters). Amplitude for TE is in good agreement with HFSS, and matches well for TM as the incident angle is less than 60 degrees.....99
3.81	Phase comparison for TE and TM mode in MATLAB and HFSS (offset 0.0001 ($\sim 0.001 \lambda$) meters in thickness by 0.11 ($\sim 1 \lambda$) meters in radius $\epsilon_r = 2.15$ for a thin sheet located in half of $L = 1.1$ ($\sim 10 \lambda$) meters). The phase shows a little mismatch for both TE and TM.....100
3.82	Amplitude comparison for TE and TM mode in MATLAB and HFSS (offset 0.001 ($\sim 0.01 \lambda$) meters in thickness by 0.11 ($\sim 1 \lambda$) meters in radius $\epsilon_r = 2.15$ for a thin plate located in half of $L = 1.1$ ($\sim 10 \lambda$) meters). Amplitudes match well as the incident angle is less than 50 degrees for both TE and TM.....100
3.83	Phase comparison for TE and TM mode in MATLAB and HFSS (offset 0.001 ($\sim 0.01 \lambda$) meters in thickness by 0.11 ($\sim 1 \lambda$) meters in radius $\epsilon_r = 2.15$ for a thin plate located in half of $L = 1.1$ ($\sim 10 \lambda$) meters). The phase matches well to both TE and TM.....101
3.84	Amplitude comparison for TE and TM mode in MATLAB and HFSS (offset 0.01 ($\sim 0.1 \lambda$) meters in thickness by 0.11 ($\sim 1 \lambda$) meters in radius $\epsilon_r = 2.15$ for a thick plate located in half of $L =$

	1.1 ($\sim 10 \lambda$) meters). Amplitudes match well as the incident angle is less than 50 degrees for both TE and TM.....	101
3.85	Phase comparison for TE and TM mode in MATLAB and HFSS (offset 0.01 ($\sim 0.1 \lambda$) meters in thickness by 0.11 ($\sim 1 \lambda$) meters in radius $\epsilon_r = 2.15$ for a thick plate located in half of $L = 1.1$ ($\sim 10 \lambda$) meters). The phase matches well as the incident angle is between 60-90 degrees for both TE and TM.....	102
3.86	Amplitude comparison for TE and TM mode in MATLAB and HFSS (offset 0.0001 ($\sim 0.001 \lambda$), 0.001 ($\sim 0.01 \lambda$), and 0.01 ($\sim 0.1 \lambda$) meters in 3 different thicknesses by 0.11 ($\sim 1 \lambda$) meters in radius $\epsilon_r = 2.15$ for plates located in half of $L = 1.1$ ($\sim 10 \lambda$) meters). Each thickness produces roughly 20 dB of amplitude difference. Because there is more transmission and less reflection in thinner plates, a thinner thickness corresponds to lower amplitude.....	103
3.87	Amplitude comparison for TE and TM mode in MATLAB and HFSS (offset 0.01 ($\sim 0.1 \lambda$) meters in thickness by 0.11 ($\sim 1 \lambda$) meters in radius for metal and non-metal $\epsilon_r = 2.15$ for thick plates located in half of $L = 1.1$ ($\sim 10 \lambda$) meters). Amplitude in metal is about 10 dB greater than non-metal due to more reflection and less transmission in the metal plate.....	103
3.88	Amplitude comparison for TE and TM mode in MATLAB and HFSS (offset 0.001 ($\sim 0.01 \lambda$) meters in thickness by 0.11 ($\sim 1 \lambda$) meters in radius for metal and non-metal $\epsilon_r = 2.15$ for thick plates located in half of $L = 1.1$ ($\sim 10 \lambda$) meters). Amplitude in metal is about 30 dB greater than non-metal due to more reflection and less transmission in the metal plate.....	104
3.89	Amplitude comparison for TE and TM mode in MATLAB and HFSS (offset 0.01 ($\sim 0.1 \lambda$) meters in thickness by 0.11 ($\sim 1 \lambda$) meters in radius for $\epsilon_r = 2.15$ and $\epsilon_r = 10-5j$ for a thick plate located in half of $L = 1.1$ ($\sim 10 \lambda$) meters). There is about 10 dB difference in amplitude for different ϵ_r . The higher the resistance R for $\epsilon_r = 2.15$, the lower the amplitude.....	104
3.90	Amplitude comparison for TE and TM mode in MATLAB and HFSS (offset 0.001 ($\sim 0.01 \lambda$) meters in thickness by 0.11 ($\sim 1 \lambda$) meters in radius for $\epsilon_r = 2.15$ and $\epsilon_r = 10-5j$ for a thick plate located in half of $L = 1.1$ ($\sim 10 \lambda$) meters). An approximate 20 dB differences in amplitude for different ϵ_r are observed. The higher the resistance at $\epsilon_r = 2.15$, the lower the amplitude.....	105
3.91	Amplitude comparison for TE and TM mode in MATLAB and HFSS (offset 0.01 ($\sim 0.1 \lambda$) meters in thickness for a metal rectangular plate at $a = 0.4$ ($\sim 4 \lambda$) meters, $b = 0.6$ ($\sim 6 \lambda$) meters).	

	Amplitudes match well as the incident angle is less than 30 degrees for both TE and TM.....	106
3.92	Phase comparison for TE and TM mode in MATLAB and HFSS (offset 0.01 (~0.1 λ) meters in thickness for a metal rectangular plate at a = 0.4 (~4 λ) meters, b = 0.6 (~6 λ) meters). The phase matches closely for both TE and TM.....	106
3.93	Amplitude comparison for TE and TM mode in MATLAB and HFSS (offset 0.01 (~0.1 λ) meters in thickness by 0.4 (~3.64 λ) meters by 0.6 (~5.45 λ) meters $\epsilon_r = 2.15$ for a rectangular thick plate located at origin). Amplitudes match well as the incident angle is less than 50 degrees for TE, and closely matches to TM.	107
3.94	Phase comparison for TE and TM mode in MATLAB and HFSS (offset 0.01 (~0.1 λ) meters in thickness by 0.4 (~3.64 λ) meters by 0.6 (~5.45 λ) meters $\epsilon_r = 2.15$ for a rectangular thick plate located at origin). The phase matches closely to both TE and TM.	107
3.95	Amplitude comparison for TE and TM mode in MATLAB and HFSS (offset 0.01 (~0.1 λ) meters in thickness by 0.4 (~3.64 λ) meters by 0.6 (~5.45 λ) meters $\epsilon_r = 2.15$ for a metal rectangular thick plate at the same thickness located at origin). The amplitude for metal is 10 dB greater than non-metal as a consequence of more reflection and less transmission in metal.....	108
3.96	Amplitude comparison for TE and TM mode in MATLAB and HFSS (offset 0.01 (~0.1 λ) meters in thickness for a metal rectangular plate at a = 0.33 (~3 λ) meters, b = 0.33 (~3 λ) meters). Amplitudes are in good agreement with HFSS as the incident angle is less than 30 degrees for both TE and TM.....	109
3.97	Phase comparison for TE and TM mode in MATLAB and HFSS (offset 0.01 (~0.1 λ) meters in thickness for a metal rectangular plate at a = 0.33 (~3 λ) meters, b = 0.33 (~3 λ) meters). The phase matches closely to both TE and TM.....	109
3.98	Amplitude comparison for TE and TM mode in MATLAB and HFSS (offset 0.01 (~0.1 λ) meters in thickness 0.33 (~3 λ) by 0.33 (~3 λ) meters at $\epsilon_r = 10-5j$ for a rectangular thick plate located at origin). Amplitudes are in good agreement with HFSS as the incident angle is less than 30 degrees for both TE and TM.....	110
3.99	Phase comparison for TE and TM mode in MATLAB and HFSS (offset 0.01 (~0.1 λ) meters in thickness 0.33 (~3 λ) by 0.33 (~3 λ) meters at $\epsilon_r = 10-5j$ for a rectangular thick plate located at origin). The phase matches closely to TE and TM.....	110
3.100	Amplitude comparison for TE and TM mode in MATLAB and	

	HFSS (offset 0.01 ($\sim 0.1 \lambda$) meters in thickness 0.33 ($\sim 3 \lambda$) by 0.33 ($\sim 3 \lambda$) meters at $\epsilon_r = 10-5j$ for a metal rectangular thick plate located at origin). Amplitude in metal is higher than non-metal materials because of more reflection and less transmission in metal. Amplitude of a metal rectangular plate is close to a non-metal plate at a relative permittivity of 10-5j.....	111
3.101	Amplitude comparison for TE and TM mode in MATLAB and HFSS (offset 0.0001 ($\sim 0.001 \lambda$) meters in thickness by 0.165 ($\sim 1.5 \lambda$) meters in radius $\epsilon_r = 2.15$ for a thin sheet located in half of $L = 3.3$ ($\sim 30 \lambda$) meters). Amplitudes for TE and TM match closely as the incident angle is less than 50 degrees.....	113
3.102	Phase comparison for TE and TM mode in MATLAB and HFSS (offset 0.0001 ($\sim 0.001 \lambda$) meters in thickness by 0.165 ($\sim 1.5 \lambda$) meters in radius $\epsilon_r = 2.15$ for a thin sheet located in half of $L = 3.3$ ($\sim 30 \lambda$) meters). The phase shows a little mismatch for TE and TM with an incident angle of less than 20 degrees.....	113
3.103	Amplitude comparison for TE and TM mode in MATLAB and HFSS (offset 0.001 ($\sim 0.01 \lambda$) meters in thickness by 0.165 ($\sim 1.5 \lambda$) meters in radius $\epsilon_r = 2.15$ for a thin plate located in half of $L = 3.3$ ($\sim 30 \lambda$) meters). Amplitudes are in good agreement with HFSS as the incident angle is less than 50 degrees for both TE and TM.....	114
3.104	Phase comparison for TE and TM mode in MATLAB and HFSS (offset 0.001 ($\sim 0.01 \lambda$) meters in thickness by 0.165 ($\sim 1.5 \lambda$) meters in radius $\epsilon_r = 2.15$ for a thin plate located in half of $L = 3.3$ ($\sim 30 \lambda$) meters). The phase shows mismatch as the incident angle is less than 20 degrees.....	115
3.105	Amplitude comparison for TE and TM mode in MATLAB and HFSS (offset 0.01 ($\sim 0.1 \lambda$) meters in thickness by 0.165 ($\sim 1.5 \lambda$) meters in radius $\epsilon_r = 2.15$ for a thick plate located in half of $L = 3.3$ ($\sim 30 \lambda$) meters). Amplitudes are in good agreement with HFSS as the incident angle is less than 50 degrees for both TE and TM.....	115
3.106	Phase comparison for TE and TM mode in MATLAB and HFSS (offset 0.01 ($\sim 0.1 \lambda$) meters in thickness by 0.165 ($\sim 1.5 \lambda$) meters in radius $\epsilon_r = 2.15$ for a thick plate located in half of $L = 3.3$ ($\sim 30 \lambda$) meters). The phase shows mismatch as the incident angle is less than 20 degrees.....	116
3.107	Amplitude comparison for TE and TM mode in MATLAB and HFSS (offset 0.0001 ($\sim 0.001 \lambda$) meters, 0.001 ($\sim 0.01 \lambda$) meters, and 0.01 ($\sim 0.1 \lambda$) meters in thickness by 0.165 ($\sim 1.5 \lambda$) meters in	

	radius $\epsilon_r = 2.15$ for a thin plate located in half of $L = 3.3$ ($\sim 30 \lambda$) meters). The plots for both HFSS and the analytical results demonstrate that amplitude differs by about 20 dB as scales increase in thickness by multiples of ten.....	116
3.108	Amplitude comparison for TE and TM mode in MATLAB and HFSS (offset 0.0001 ($\sim 0.001 \lambda$) meters in thickness by 0.165 ($\sim 1.5 \lambda$) meters in radius $\epsilon_r = 10-5j$ for a thin sheet located in half of $L = 3.3$ ($\sim 30 \lambda$) meters). Amplitudes are in good agreement with HFSS as the incident angle is less than 50 degrees for both TE and TM.....	117
3.109	Phase comparison for TE and TM mode in MATLAB and HFSS (offset 0.0001 ($\sim 0.001 \lambda$) meters in thickness by 0.165 ($\sim 1.5 \lambda$) meters in radius $\epsilon_r = 10-5j$ for a thin sheet located in half of $L = 3.3$ ($\sim 30 \lambda$) meters). The phase shows a little mismatch for TE and TM, as the incident angle is less than 20 degrees.....	118
3.110	Amplitude comparison for TE and TM mode in MATLAB and HFSS (offset 0.001 ($\sim 0.01 \lambda$) meters in thickness by 0.165 ($\sim 1.5 \lambda$) meters in radius $\epsilon_r = 10-5j$ for a thin plate located in half of $L = 3.3$ ($\sim 30 \lambda$) meters). Amplitudes match well as the incident angle is less than 50 degrees for both TE and TM.....	118
3.111	Phase comparison for TE and TM mode in MATLAB and HFSS (offset 0.001 ($\sim 0.01 \lambda$) meters in thickness by 0.165 ($\sim 1.5 \lambda$) meters in radius $\epsilon_r = 10-5j$ for a thin plate located in half of $L = 3.3$ ($\sim 30 \lambda$) meters). The phase shows mismatch as the incident angle is less than 20 degrees.....	119
3.112	Amplitude comparison for TE and TM mode in MATLAB and HFSS (offset 0.01 ($\sim 0.1 \lambda$) meters in thickness by 0.165 ($\sim 1.5 \lambda$) meters in radius $\epsilon_r = 10-5j$ for a plate located in half of $L = 3.3$ ($\sim 30 \lambda$) meters). Amplitudes match well as the incident angle is less than 30 degrees for both TE and TM.....	120
3.113	Phase comparison for TE and TM mode in MATLAB and HFSS (offset 0.01 ($\sim 0.1 \lambda$) meters in thickness by 0.165 ($\sim 1.5 \lambda$) meters in radius $\epsilon_r = 10-5j$ for a thin plate located in half of $L = 3.3$ ($\sim 30 \lambda$) meters). The phase shows mismatch as the incident angle is less than 20 degrees.....	120
3.114	Amplitude comparison for TE and TM mode in MATLAB and HFSS (offset 0.0001 ($\sim 0.001 \lambda$) meters, 0.001 ($\sim 0.01 \lambda$) meters, and 0.01 ($\sim 0.1 \lambda$) meters in 3 different thicknesses by 0.165 ($\sim 1.5 \lambda$) meters in radius $\epsilon_r = 10-5j$ for plates located in half of $L = 3.3$ ($\sim 30 \lambda$) meters). It appears that amplitude differs by about 10 dB when comparing thicknesses of 0.001 ($\sim 0.01 \lambda$) meters and 0.01	

	(~0.1 λ) meters, and amplitude differs by about 20 dB when comparing thicknesses of 0.0001 (~0.001 λ) meters and 0.001 (~0.01 λ) meters.....	121
3.115	Amplitude comparison for TE and TM mode in MATLAB and HFSS (offset 0.0003 (~0.003 λ) meters in thickness by 0.03 (~0.3 λ) meters in radius for a conducting thin sheet located at origin). Amplitude differs by a few dB for both TE and TM.....	122
3.116	Amplitude comparison for TE and TM mode in MATLAB and HFSS (offset 0.003 (~0.03 λ) meters in thickness by 0.03 (~0.3 λ) meters in radius for a conducting thin plate located at origin). Amplitude differs by a few dB for both TE and TM.....	122
3.117	Amplitude comparison for TE and TM mode in MATLAB and HFSS (offset 0.03 (~0.3 λ) meters in thickness by 0.03 (~0.3 λ) meters in radius for a conducting thick plate located at origin). Amplitude matches well for TE as the incident angle is less than 40 degrees, and matches closely for TM as the incident angle is less than 20 degrees.....	123
3.118	Amplitude comparison for TE and TM mode in MATLAB and HFSS (offset 0.03 (~0.3 λ) meters and 0.003 (~0.03 λ) meters in 2 different thicknesses by 0.03 (~0.3 λ) meters in radius for a conducting thick plate located at origin). Amplitude is greater for thicker plates when compared to thinner plates as a consequence of more penetration in thinner plates.....	123
3.119	Amplitude comparison for TE and TM mode in MATLAB and HFSS (offset 0.03 (~0.3 λ) meters, 0.003 (~0.03 λ) meters, and 0.0003 (~0.003 λ) meters in 3 different thicknesses by 0.03 (~0.3 λ) meters in radius for a conducting thick plate located at origin). HFSS shows little difference for varying thickness.....	124
3.120	Amplitude comparison for TE and TM mode in MATLAB and HFSS (offset 0.0002 (~0.002 λ) meters in thickness by 0.3 (~3 λ) meters in radius for a conducting thin sheet located at origin). Amplitudes match well as the incident angle is less than 30 degrees for both TE and TM.....	125
3.121	Amplitude comparison for TE and TM mode in MATLAB and HFSS (offset 0.002 (~0.02 λ) meters in thickness by 0.3 (~3 λ) meters in radius for a conducting thin plate located at origin). Amplitudes match well as the incident angle is less than 30 degrees for both TE and TM.....	125
3.122	Amplitude comparison for TE and TM mode in MATLAB and HFSS (offset 0.02 (~0.2 λ) meters in thickness by 0.3 (~3 λ) meters in radius for a conducting plate located at origin). Amplitudes match well as the incident angle is less than 30 degrees for both TE and TM.....	126

- 3.123 Amplitude comparison for TE and TM mode in MATLAB and HFSS (offset 0.02 (~0.2 λ) meters, 0.002 (~0.02 λ) meters, and 0.0002 (~0.002 λ) meters in 3 different thicknesses by 0.3 (~3 λ) meters in radius for conducting plates located at origin). Amplitudes match well for all three thicknesses as the incident angle is less than 30 degrees for both TE and TM.....126
- 3.124 Amplitude comparison for TE and TM mode in MATLAB and HFSS (offset 0.001 (~0.01 λ) meters in thickness by 0.4 (~3.64 λ) meters by 0.6 (~5.45 λ) meters $\epsilon_r = 2.15$ for a rectangular thin plate located at origin). Amplitudes match well as the incident angle is less than 50 degrees for both TE and TM.....128
- 3.125 Phase comparison for TE and TM mode in MATLAB and HFSS (offset 0.001 (~0.01 λ) meters in thickness by 0.4 (~3.64 λ) meters by 0.6 (~5.45 λ) meters $\epsilon_r = 2.15$ for a rectangular thin plate located at origin). The phase matches closely to both TE and TM.128
- 3.126 Amplitude comparison for TE and TM mode in MATLAB and HFSS (offset 0.0001 (~0.001 λ) meters in thickness by 0.4 (~3.64 λ) meters by 0.6 (~5.45 λ) meters $\epsilon_r = 2.15$ for a rectangular thin sheet located at origin). Amplitudes match closely to both TE and TM as the incident angle is less than 50 degrees.....129
- 3.127 Phase comparison for TE and TM mode in MATLAB and HFSS (offset 0.0001 (~0.001 λ) meters in thickness by 0.4 (~3.64 λ) meters by 0.6 (~5.45 λ) meters $\epsilon_r = 2.15$ for a rectangular thin sheet located at origin). The phase matches closely to both TE and TM.....129
- 3.128 Amplitude comparison for TE and TM mode in MATLAB and HFSS (offset 0.0001 (~0.001 λ) meters, 0.001 (~0.01 λ) meters, and 0.01 (~0.1 λ) meters in 3 different thicknesses by 0.4 (~3.64 λ) meters by 0.6 (~5.45 λ) meters $\epsilon_r = 2.15$ for rectangular plates located at origin. Amplitudes vary by about 20 dB for each scale change in thickness (ten times bigger from thin to thick) for both MATLAB and HFSS.....130
- 3.129 Amplitude comparison for TE and TM mode in MATLAB and HFSS (offset 0.01 (~0.1 λ) meters in thickness by 0.22 (~2 λ) meters by 0.22 (~2 λ) meters $\epsilon_r = 10-5j$ for a rectangular thick plate located at origin). Amplitudes match closely as the incident angle is less than 30 degrees for both TE and TM.....130
- 3.130 Phase comparison for TE and TM mode in MATLAB and HFSS

- (offset 0.01 ($\sim 0.1 \lambda$) meters in thickness by 0.22 ($\sim 2 \lambda$) meters by 0.22 ($\sim 2 \lambda$) meters $\epsilon_r = 10-5j$ for a rectangular thick plate located at origin). The phase matches closely to both TE and TM.....131
- 3.131 Amplitude comparison for TE and TM mode in MATLAB and HFSS (offset 0.001 ($\sim 0.01 \lambda$) meters in thickness by 0.22 ($\sim 2 \lambda$) meters by 0.22 ($\sim 2 \lambda$) meters $\epsilon_r = 10-5j$ for a rectangular thin plate located at origin). Amplitudes match closely as the incident angle is less than 30 degrees for both TE and TM.....131
- 3.132 Phase comparison for TE and TM mode in MATLAB and HFSS (offset 0.001 ($\sim 0.01 \lambda$) meters in thickness by 0.22 ($\sim 2 \lambda$) meters by 0.22 ($\sim 2 \lambda$) meters $\epsilon_r = 10-5j$ for a rectangular thin plate located at origin). The phase matches closely to both TE and TM.132
- 3.133 Amplitude comparison for TE and TM mode in MATLAB and HFSS (offset 0.0001 ($\sim 0.001 \lambda$) meters in thickness by 0.22 ($\sim 2 \lambda$) meters by 0.22 ($\sim 2 \lambda$) meters $\epsilon_r = 10-5j$ for a rectangular sheet plate located at origin). Amplitudes match closely as the incident angle is less than 50 degrees for both TE and TM.....132
- 3.134 Phase comparison for TE and TM mode in MATLAB and HFSS (offset 0.0001 ($\sim 0.001 \lambda$) meters in thickness by 0.22 ($\sim 2 \lambda$) meters by 0.22 ($\sim 2 \lambda$) meters $\epsilon_r = 10-5j$ for a rectangular sheet located at origin). The phase matches closely to both TE and TM.133
- 3.135 Amplitude comparison for TE and TM mode in MATLAB and HFSS (offset 0.0001 ($\sim 0.001 \lambda$) meters, 0.001 ($\sim 0.01 \lambda$) meters, and 0.01 ($\sim 0.1 \lambda$) meters in 3 different thicknesses by 0.22 ($\sim 2 \lambda$) meters by 0.22 ($\sim 2 \lambda$) meters $\epsilon_r = 10-5j$ for a rectangular plate located at origin). Amplitudes have less than a 10 dB difference between two plates at 0.001 ($\sim 0.01 \lambda$) meters and 0.01 ($\sim 0.1 \lambda$) meters thicknesses. The amplitude for a “sheet” at 0.0001 ($\sim 0.001 \lambda$) meters in thickness is 20 dB or 30 dB lower than the other two plates.....133
- 3.136 Amplitude comparison for TE and TM mode in MATLAB and HFSS (offset 0.01 ($\sim 0.1 \lambda$) meters in thickness for a metal rectangular plate at $a = 0.5$ ($\sim 5 \lambda$) meters, $b = 0.5$ ($\sim 5 \lambda$) meters). They match well as the incident angle is less than 30~40 degrees for both TE and TM..... 134
- 3.137 Phase comparison for TE and TM mode in MATLAB and HFSS (offset 0.01 ($\sim 0.1 \lambda$) meters in thickness for a metal rectangular plate at $a = 0.5$ ($\sim 5 \lambda$) meters, $b = 0.5$ ($\sim 5 \lambda$) meters). The phase matches closely for both TE and TM.....135
- 3.138 Amplitude comparison for TE and TM mode in MATLAB and

	HFSS (offset 0.001 ($\sim 0.01 \lambda$) meters in thickness for a metal rectangular thin plate at $a = 0.5$ ($\sim 5 \lambda$) meters, $b = 0.5$ ($\sim 5 \lambda$) meters). Amplitudes match well as the incident angle is less than 40 degrees for both TE and TM.....	135
3.139	Phase comparison for TE and TM mode in MATLAB and HFSS (offset 0.001 ($\sim 0.01 \lambda$) meters in thickness for a metal rectangular thin plate at $a = 0.5$ ($\sim 5 \lambda$) meters, $b = 0.5$ ($\sim 5 \lambda$) meters). The phase matches closely for both TE and TM.....	136
3.140	Amplitude comparison for TE and TM mode in MATLAB and HFSS (offset 0.0001 ($\sim 0.001 \lambda$) meters in thickness for a metal rectangular thin sheet at $a = 0.5$ ($\sim 5 \lambda$) meters, $b = 0.5$ ($\sim 5 \lambda$) meters). Amplitudes match closely as the incident angle is less than 40 degrees for both TE and TM.....	136
3.141	Phase comparison for TE and TM mode in MATLAB and HFSS (offset 0.0001 ($\sim 0.001 \lambda$) meters in thickness for a metal rectangular thin sheet at $a = 0.5$ ($\sim 5 \lambda$) meters, $b = 0.5$ ($\sim 5 \lambda$) meters). The phase matches closely for both TE and TM.....	137
3.142	Amplitude comparison for TE and TM mode in MATLAB and HFSS (offset 0.0001 ($\sim 0.001 \lambda$) meters, 0.001 ($\sim 0.01 \lambda$) meters, and 0.01 ($\sim 0.1 \lambda$) meters in 3 different thicknesses by 0.5 ($\sim 5 \lambda$) meters by 0.5 ($\sim 5 \lambda$) meters for metal rectangular plates located at origin).....	137
4.1	Amplitude comparison for TE and TM mode in MATLAB and HFSS (0.4 ($\sim 3.64 \lambda$) meters in length by 0.02 ($\sim 0.2 \lambda$) meters in radius for a conducting cylinder without endcap). Amplitudes overlap at the peak of 90° for both TE and TM.....	151
4.2	Phase comparison for TE and TM mode in MATLAB and HFSS (0.4 ($\sim 3.64 \lambda$) meters in length by 0.02 ($\sim 0.2 \lambda$) meters in radius for a conducting cylinder without endcap). The phase shows mismatch for both TE and TM.....	151
4.3	Amplitude comparison for TE and TM mode in MATLAB and HFSS (0.4 ($\sim 3.64 \lambda$) meters in length by 0.02 ($\sim 0.2 \lambda$) meters in radius for a conducting cylinder with endcap). Amplitude increases 70 dB in TE at 0° . Amplitude increases 16 dB in TM at 0°	152
4.4	Phase comparison for TE and TM mode in MATLAB and HFSS (0.4 ($\sim 3.64 \lambda$) meters in length by 0.02 ($\sim 0.2 \lambda$) meters in radius for a conducting cylinder with endcap). The phase matches closely for both TE and TM.....	152
4.5	Amplitude comparison for TE and TM mode in MATLAB and HFSS (0.6 ($\sim 5.5 \lambda$) meters in length by 0.03 ($\sim 0.3 \lambda$) meters in radius for a conducting cylinder without endcap). Amplitudes	

	overlap at the peak of 90° but show big gaps at 0° for both TE and TM.....	153
4.6	Phase comparison for TE and TM mode in MATLAB and HFSS (0.6 (~5.5 λ) meters in length by 0.03 (~0.3 λ) meters in radius for a conducting cylinder without endcap). The phase shows mismatch between 0-60° for both TE and TM.....	153
4.7	Amplitude comparison for TE and TM mode in MATLAB and HFSS (0.6 (~5.5 λ) meters in length by 0.03 (~0.3 λ) meters in radius for a conducting cylinder with endcap). Amplitude increases 80 dB in TE at 0°. Amplitude increases 15 dB in TM at 0°.....	154
4.8	Phase comparison for TE and TM mode in MATLAB and HFSS (0.6 (~5.5 λ) meters in length by 0.03 (~0.3 λ) meters in radius for a conducting cylinder with endcap). The phase matches well in both TE and TM.....	154
4.9	Amplitude comparison for TE and TM mode in MATLAB and HFSS (0.8 (~7.27 λ) meters in length by 0.01 (~0.1 λ) meters in radius for a conducting cylinder without endcap). Amplitudes overlap at the peak of 90°, but show big gaps at 0° for both TE and TM.....	155
4.10	Phase comparison for TE and TM mode in MATLAB and HFSS (0.8 (~7.27 λ) meters in length by 0.01 (~0.1 λ) meters in radius for a conducting cylinder without endcap). The phase shows mismatch for TE and TM.....	155
4.11	Amplitude comparison for TE and TM mode in MATLAB and HFSS (0.8 (~7.27 λ) meters in length by 0.01 (~0.1 λ) meters in radius for a conducting cylinder with endcap). Amplitude increases 50 dB in TE at 0°. Amplitude increases 5 dB in TM at 0°.....	156
4.12	Phase comparison for TE and TM mode in MATLAB and HFSS (0.8 (~7.27 λ) meters in length by 0.01 (~0.1 λ) meters in radius for a conducting cylinder with endcap). The phase matches closely for both TE and TM.....	156
4.13	Amplitude comparison for TE and TM mode in MATLAB and HFSS (0.8 (~7.27 λ) meters in length by 0.03 (~0.3 λ) meters in radius for a conducting cylinder without endcap). Amplitudes overlap at the peak of 90°, but show big gaps at 0° for both TE and TM.....	157
4.14	Phase comparison for TE and TM mode in MATLAB and HFSS (0.8 (~7.27 λ) meters in length by 0.03 (~0.3 λ) meters in radius for a conducting cylinder without endcap). The phase shows mismatch between 0-60° for both TE and TM.....	157
4.15	Amplitude comparison for TE and TM mode in MATLAB and	

	HFSS (0.8 (~7.27 λ) meters in length by 0.03 (~0.3 λ) meters in radius for a conducting cylinder with endcap). Amplitudes match closely for both TE and TM.....	158
4.16	Phase comparison for TE and TM mode in MATLAB and HFSS (0.8 (~7.27 λ) meters in length by 0.03 (~0.3 λ) meters in radius for a conducting cylinder with endcap). The phase matches well for TE, and matches closely for TM.....	158
4.17	Amplitude comparison for TE and TM mode in MATLAB and HFSS (0.8 (~7.27 λ) meters in length by 0.04 (~0.36 λ) meters in radius for a conducting cylinder without endcap). Big gaps are observed at 0° and overlap at 90° for both TE and TM.....	159
4.18	Phase comparison for TE and TM mode in MATLAB and HFSS (0.8 (~7.27 λ) meters in length by 0.04 (~0.36 λ) meters in radius for a conducting cylinder without endcap). The phase shows mismatch between 0-60°.....	159
4.19	Amplitude comparison for TE and TM mode in MATLAB and HFSS (0.8 (~7.27 λ) meters in length by 0.04 (~0.36 λ) meters in radius for a conducting cylinder with endcap). Amplitudes match well for both TE and TM.....	160
4.20	Phase comparison for TE and TM mode in MATLAB and HFSS (0.8 (~7.27 λ) meters in length by 0.04 (~0.36 λ) meters in radius for a conducting cylinder with endcap). The phase matches well for both TE and TM.....	160
4.21	Amplitude comparison for TE and TM mode in MATLAB and HFSS (0.8 (~7.27 λ) meters in length by 0.06 (~0.55 λ) meters in radius for a conducting cylinder without endcap). Amplitudes show big gaps at 0° and overlap at 90° for both TE and TM....	161
4.22	Phase comparison for TE and TM mode in MATLAB and HFSS (0.8 (~7.27 λ) meters in length by 0.06 (~0.55 λ) meters in radius for a conducting cylinder without endcap). The phase shows mismatch between 0-60° for both TE and TM.....	161
4.23	Amplitude comparison for TE and TM mode in MATLAB and HFSS (0.8 (~7.27 λ) meters in length by 0.06 (~0.55 λ) meters in radius for a conducting cylinder with endcap). Amplitudes show good agreement with HFSS for both TE and TM.....	162
4.24	Phase comparison for TE and TM mode in MATLAB and HFSS (0.8 (~7.27 λ) meters in length by 0.06 (~0.55 λ) meters in radius for a conducting cylinder with endcap). The phase shows good agreement with HFSS for both TE and TM.....	162
4.25	Amplitude comparison for TE and TM mode in MATLAB and HFSS (1.1 (~10 λ) meters in length by 0.011 (~0.1 λ) meters in radius for a conducting cylinder without endcap). Amplitudes show big gaps at 0° and overlap at 90° for both TE and TM....	163

4.26	Phase comparison for TE and TM mode in MATLAB and HFSS (1.1 (~10 λ) meters in length by 0.011 (~0.1 λ) meters in radius for a conducting cylinder without endcap). The phase shows mismatch between 0-60° for both TE and TM.....	163
4.27	Amplitude comparison for TE and TM mode in MATLAB and HFSS (1.1 (~10 λ) meters in length by 0.011 (~0.1 λ) meters in radius for a conducting cylinder with endcap). Amplitudes have differences of less than 10 dB at 0° for both TE and TM.....	164
4.28	Phase comparison for TE and TM mode in MATLAB and HFSS (1.1 (~10 λ) meters in length by 0.011 (~0.1 λ) meters in radius for a conducting cylinder with endcap). The phase matches closely for both TE and TM.....	164
4.29	Amplitude comparison for TE and TM mode in MATLAB and HFSS (1.1 (~10 λ) meters in length by 0.055 (~0.5 λ) meters in radius for a conducting cylinder without endcap). Amplitudes show big gaps at 0° and overlap at 90° for both TE and TM....	165
4.30	Phase comparison for TE and TM mode in MATLAB and HFSS (1.1 (~10 λ) meters in length by 0.055 (~0.5 λ) meters in radius for a conducting cylinder without endcap). The phase shows mismatch between 0-60° for both TE and TM.....	165
4.31	Amplitude comparison for TE and TM mode in MATLAB and HFSS (1.1 (~10 λ) meters in length by 0.055 (~0.5 λ) meters in radius for a conducting cylinder with endcap). Amplitudes show very few differences at 0° for both TE and TM.....	166
4.32	Phase comparison for TE and TM mode in MATLAB and HFSS (1.1 (~10 λ) meters in length by 0.055 (~0.5 λ) meters in radius for a conducting cylinder with endcap). The phase is in good agreement with HFSS for both TE and TM.....	166
4.33	Amplitude comparison for TE and TM mode in MATLAB and HFSS (1.1 (~10 λ) meters in length by 0.11 (~1 λ) meters in radius for a conducting cylinder without endcap). Amplitudes show big gaps at 0° and overlap at 90° for both TE and TM.....	167
4.34	Phase comparison for TE and TM mode in MATLAB and HFSS (1.1 (~10 λ) meters in length by 0.11 (~1 λ) meters in radius for a conducting cylinder without endcap). The phase shows mismatch between 0-60° for both TE and TM.....	167
4.35	Amplitude comparison for TE and TM mode in MATLAB and HFSS (1.1 (~10 λ) meters in length by 0.11 (~1 λ) meters in radius for a conducting cylinder with endcap). Amplitudes almost overlap at 0° for both TE and TM.....	168
4.36	Phase comparison for TE and TM mode in MATLAB and HFSS	

	(1.1 (~10 λ) meters in length by 0.11 (~1 λ) meters in radius for a conducting cylinder with endcap). The phase is in good agreement with HFSS for both TE and TM.....	168
4.37	Amplitude comparison for TE and TM mode in MATLAB and HFSS (3.3 (~30 λ) meters in length by 0.033 (~0.3 λ) meters in radius for a conducting cylinder without endcap). Big gaps are shown at 0° for both TE and TM.....	169
4.38	Phase comparison for TE and TM mode in MATLAB and HFSS (3.3 (~30 λ) meters in length by 0.033 (~0.3 λ) meters in radius for a conducting cylinder without endcap). The phase shows mismatch between 0-60° for both TE and TM.....	169
4.39	Amplitude comparison for TE and TM mode in MATLAB and HFSS (3.3 (~30 λ) meters in length by 0.033 (~0.3 λ) meters in radius for a conducting cylinder with endcap). Only a very slight amplitude difference is shown at 0° for both TE and TM.....	170
4.40	Phase comparison for TE and TM mode in MATLAB and HFSS (3.3 (~30 λ) meters in length by 0.033 (~0.3 λ) meters in radius for a conducting cylinder with endcap). The phase is in good agreement with HFSS for both TE and TM.....	170
4.41	Amplitude comparison for TE and TM mode in MATLAB and HFSS (3.3 (~30 λ) meters in length by 0.165 (~1.5 λ) meters in radius for a conducting cylinder without endcap). Amplitudes overlap at the peak of 90°, but there are large gaps at 0° for both TE and TM.....	171
4.42	Phase comparison for TE and TM mode in MATLAB and HFSS (3.3 (~30 λ) meters in length by 0.165 (~1.5 λ) meters in radius for a conducting cylinder without endcap). The phase shows mismatch for both TE and TM.....	171
4.43	Amplitude comparison for TE and TM mode in MATLAB and HFSS (3.3 (~30 λ) meters in length by 0.165 (~1.5 λ) meters in radius for a conducting cylinder with endcap). Amplitudes overlap at 0° for both TE and TM.....	172
4.44	Phase comparison for TE and TM mode in MATLAB and HFSS (3.3 (~30 λ) meters in length by 0.165 (~1.5 λ) meters in radius for a conducting cylinder with endcap). The phase is in good agreement with HFSS for both TE and TM.....	172
4.45	Amplitude comparison for TE and TM mode in MATLAB and HFSS (1.1 (~10 λ) meters in length by 0.011 (~0.1 λ) meters in radius at $\epsilon_r = 2.15$ for a dielectric cylinder without endcap). Amplitudes have less than 20 dB differences at 0° for both TE and TM.....	180
4.46	Phase comparison for TE and TM mode in MATLAB and HFSS	

	(1.1 (~10 λ) meters in length by 0.011 (~0.1 λ) meters in radius at $\epsilon_r = 2.15$ for a dielectric cylinder without endcap). The phase shows mismatch for both TE and TM.....	180
4.47	Amplitude comparison for TE and TM mode in MATLAB and HFSS (1.1 (~10 λ) meters in length by 0.011 (~0.1 λ) meters in radius at $\epsilon_r = 2.15$ for a dielectric cylinder with endcap). Amplitude almost overlaps at 0° for TE. Amplitude matches closely for TM.....	181
4.48	Phase comparison for TE and TM mode in MATLAB and HFSS (1.1 (~10 λ) meters in length by 0.011 (~0.1 λ) meters in radius at $\epsilon_r = 2.15$ for a dielectric cylinder with endcap). The phase is in good agreement with HFSS for both TE and TM.....	181
4.49	Amplitude comparison for TE and TM mode in MATLAB and HFSS (1.1 (~10 λ) meters in length by 0.011 (~0.1 λ) meters in radius at $\epsilon_r = 10-5j$ for a dielectric cylinder without endcap). Big gaps are observed at 0° for both TE and TM.....	182
4.50	Phase comparison for TE and TM mode in MATLAB and HFSS (1.1 (~10 λ) meters in length by 0.011 (~0.1 λ) meters in radius at $\epsilon_r = 10-5j$ for a dielectric cylinder without endcap). The phase shows mismatch for both TE and TM.....	182
4.51	Amplitude comparison for TE and TM mode in MATLAB and HFSS (1.1 (~10 λ) meters in length by 0.011 (~0.1 λ) meters in radius at $\epsilon_r = 10-5j$ for a dielectric cylinder with endcap). Amplitude has less than 10 dB difference at 0° for TE. Amplitude has less than a 10 dB difference at 0° for TM.....	183
4.52	Phase comparison for TE and TM mode in MATLAB and HFSS (1.1 (~10 λ) meters in length by 0.011 (~0.1 λ) meters in radius at $\epsilon_r = 10-5j$ for a dielectric cylinder with endcap). The phase is in good agreement with HFSS for both TE and TM.....	183
4.53	Amplitude comparison for TE and TM mode in MATLAB and HFSS (1.1 (~10 λ) meters in length by 0.055 (~0.5 λ) meters in radius at $\epsilon_r = 2.15$ for a dielectric cylinder without endcap). Big gaps are observed at 0° for both TE and TM.....	184
4.54	Phase comparison for TE and TM mode in MATLAB and HFSS (1.1 (~10 λ) meters in length by 0.055 (~0.5 λ) meters in radius at $\epsilon_r = 2.15$ for a dielectric cylinder without endcap). The phase shows mismatch for both TE and TM.....	184
4.55	Amplitude comparison for TE and TM mode in MATLAB and	

	HFSS (1.1 (~10 λ) meters in length by 0.055 (~0.5 λ) meters in radius at $\epsilon_r = 2.15$ for a dielectric cylinder with endcap). Amplitudes show a few dB differences for both TE and TM at 0°	185
4.56	Phase comparison for TE and TM mode in MATLAB and HFSS (1.1 (~10 λ) meters in length by 0.055 (~0.5 λ) meters in radius at $\epsilon_r = 2.15$ for a dielectric cylinder with endcap). The phase is in good agreement with HFSS for both TE and TM.....	185
4.57	Amplitude comparison for TE and TM mode in MATLAB and HFSS (1.1 (~10 λ) meters in length by 0.055 (~0.5 λ) meters in radius at $\epsilon_r = 10-5j$ for a dielectric cylinder without endcap). Big gaps are observed at 0° for both TE and TM.....	186
4.58	Phase comparison for TE and TM mode in MATLAB and HFSS (1.1 (~10 λ) meters in length by 0.055 (~0.5 λ) meters in radius at $\epsilon_r = 10-5j$ for a dielectric cylinder without endcap). The phase shows mismatch between $0-60^\circ$ for both TE and TM.....	186
4.59	Amplitude comparison for TE and TM mode in MATLAB and HFSS (1.1 (~10 λ) meters in length by 0.055 (~0.5 λ) meters in radius at $\epsilon_r = 10-5j$ for a dielectric cylinder with endcap). A couple of dB differences are observed for both TE and TM....	187
4.60	Phase comparison for TE and TM mode in MATLAB and HFSS (1.1 (~10 λ) meters in length by 0.055 (~0.5 λ) meters in radius at $\epsilon_r = 10-5j$ for a dielectric cylinder with endcap). The phase is in good agreement with HFSS for both TE and TM.....	187
4.61	Amplitude comparison for TE and TM mode in MATLAB and HFSS (1.1 (~10 λ) meters in length by 0.11 (~1 λ) meters in radius at $\epsilon_r = 2.15$ for a dielectric cylinder without endcap). Big gaps are observed at 0° for both TE and TM.....	188
4.62	Phase comparison for TE and TM mode in MATLAB and HFSS (1.1 (~10 λ) meters in length by 0.11 (~1 λ) meters in radius at $\epsilon_r = 2.15$ for a dielectric cylinder without endcap). The phase shows mismatch for both TE and TM.....	188
4.63	Amplitude comparison for TE and TM mode in MATLAB and HFSS (1.1 (~10 λ) meters in length by 0.11 (~1 λ) meters in radius at $\epsilon_r = 2.15$ for a dielectric cylinder with endcap). Amplitudes have less than 5 dB differences at 0° for both TE and TM.....	189
4.64	Phase comparison for TE and TM mode in MATLAB and HFSS	

	(1.1 (~10 λ) meters in length by 0.11 (~1 λ) meters in radius at $\epsilon_r = 2.15$ for a dielectric cylinder with endcap). The phase is in good agreement with HFSS for both TE and TM.....	189
4.65	Amplitude comparison for TE and TM mode in MATLAB and HFSS (1.1 (~10 λ) meters in length by 0.11 (~1 λ) meters in radius at $\epsilon_r = 10-5j$ for a dielectric cylinder without endcap). Big gaps are observed at 0° for both TE and TM.....	190
4.66	Phase comparison for TE and TM mode in MATLAB and HFSS (1.1 (~10 λ) meters in length by 0.11 (~1 λ) meters in radius at $\epsilon_r = 10-5j$ for a dielectric cylinder without endcap). The phase shows mismatch for both TE and TM.....	190
4.67	Amplitude comparison for TE and TM mode in MATLAB and HFSS (1.1 (~10 λ) meters in length by 0.11 (~1 λ) meters in radius at $\epsilon_r = 10-5j$ for a dielectric cylinder with endcap). Amplitudes are in good agreement with HFSS for both TE and TM.....	191
4.68	Amplitude comparison for TE and TM mode in MATLAB and HFSS (1.1 (~10 λ) meters in length by 0.11 (~1 λ) meters in radius at $\epsilon_r = 10-5j$ for a dielectric cylinder with endcap). Phase is in good agreement with HFSS for both TE and TM.....	191
4.69	Amplitude comparison for TE and TM mode in MATLAB and HFSS (3.3 (~30 λ) meters in length by 0.033 (~0.3 λ) meters in radius at $\epsilon_r = 2.15$ for a dielectric cylinder without endcap). Big gaps are observed at 0° for both TE and TM.....	192
4.70	Phase comparison for TE and TM mode in MATLAB and HFSS (3.3 (~30 λ) meters in length by 0.033 (~0.3 λ) meters in radius at $\epsilon_r = 2.15$ for a dielectric cylinder without endcap). The phase shows mismatch for both TE and TM.....	192
4.71	Amplitude comparison for TE and TM mode in MATLAB and HFSS (3.3 (~30 λ) meters in length by 0.033 (~0.3 λ) meters in radius at $\epsilon_r = 2.15$ for a dielectric cylinder with endcap). Only a few amplitude differences are observed at 0° for both TE and TM.	193
4.72	Phase comparison for TE and TM mode in MATLAB and HFSS (3.3 (~30 λ) meters in length by 0.033 (~0.3 λ) meters in radius at $\epsilon_r = 2.15$ for a dielectric cylinder with endcap). The phase is in good agreement with HFSS for both TE and TM.....	193
4.73	Amplitude comparison for TE and TM mode in MATLAB and	

	HFSS (3.3 (~30 λ) meters in length by 0.033 (~0.3 λ) meters in radius at $\epsilon_r = 10-5j$ for a dielectric cylinder without endcap). Big gaps are observed at 0° for both TE and TM.....	194
4.74	Phase comparison for TE and TM mode in MATLAB and HFSS (3.3 (~30 λ) meters in length by 0.033 (~0.3 λ) meters in radius at $\epsilon_r = 10-5j$ for a dielectric cylinder without endcap). The phase shows mismatch for both TE and TM.....	194
4.75	Amplitude comparison for TE and TM mode in MATLAB and HFSS (3.3 (~30 λ) meters in length by 0.033 (~0.3 λ) meters in radius at $\epsilon_r = 10-5j$ for a dielectric cylinder with endcap). Amplitudes have a very few dB difference at 0° for both TE and TM.....	195
4.76	Phase comparison for TE and TM mode in MATLAB and HFSS (3.3 (~30 λ) meters in length by 0.033 (~0.3 λ) meters in radius at $\epsilon_r = 10-5j$ for a dielectric cylinder with endcap). The phase is in good agreement with HFSS for both TE and TM.....	195
4.77	Amplitude comparison for TE and TM mode in MATLAB and HFSS (3.3 (~30 λ) meters in length by 0.165 (~1.5 λ) meters in radius at $\epsilon_r = 2.15$ for a dielectric cylinder without endcap). Big gaps are observed at 0° for both TE and TM.....	196
4.78	Phase comparison for TE and TM mode in MATLAB and HFSS (3.3 (~30 λ) meters in length by 0.165 (~1.5 λ) meters in radius at $\epsilon_r = 2.15$ for a dielectric cylinder without endcap). The phase shows mismatch for both TE and TM.....	196
4.79	Amplitude comparison for TE and TM mode in MATLAB and HFSS (3.3 (~30 λ) meters in length by 0.165 (~1.5 λ) meters in radius at $\epsilon_r = 2.15$ for a dielectric cylinder with endcap). Amplitudes show differences of less than 10 dB at 0° for both TE and TM.....	197
4.80	Phase comparison for TE and TM mode in MATLAB and HFSS (3.3 (~30 λ) meters in length by 0.165 (~1.5 λ) meters in radius at $\epsilon_r = 2.15$ for a dielectric cylinder with endcap). The phase is in good agreement with HFSS for both TE and TM.....	197
4.81	Amplitude comparison for TE and TM mode in MATLAB and HFSS (3.3 (~30 λ) meters in length by 0.165 (~1.5 λ) meters in radius at $\epsilon_r = 10-5j$ for a dielectric cylinder without endcap). Big gaps are observed at 0° for both TE and TM.....	198
4.82	Phase comparison for TE and TM mode in MATLAB and HFSS	

	(3.3 (~30 λ) meters in length by 0.165 (~1.5 λ) meters in radius at $\epsilon_r = 10-5j$ for a dielectric cylinder without endcap). The phase shows mismatch for both TE and TM.....	198
4.83	Amplitude comparison for TE and TM mode in MATLAB and HFSS (3.3 (~30 λ) meters in length by 0.165 (~1.5 λ) meters in radius at $\epsilon_r = 10-5j$ for a dielectric cylinder with endcap). Amplitudes have differences of less than 5 dB at 0° for both TE and TM.....	199
4.84	Phase comparison for TE and TM mode in MATLAB and HFSS (3.3 (~30 λ) meters in length by 0.165 (~1.5 λ) meters in radius at $\epsilon_r = 10-5j$ for a dielectric cylinder with endcap). The phase is in good agreement with HFSS for both TE and TM.....	199
4.85	Amplitude comparison for TE and TM mode in MATLAB and HFSS (0.11 (~1 λ) meters in length by 0.055 (~0.5 λ) meters in radius at $\epsilon_r = 2.15$ for a dielectric cylinder without endcap). Big gaps are observed at 0° for both TE and TM.....	200
4.86	Phase comparison for TE and TM mode in MATLAB and HFSS (0.11 (~1 λ) meters in length by 0.055 (~0.5 λ) meters in radius at $\epsilon_r = 2.15$ for a dielectric cylinder without endcap). The phase shows mismatch for both TE and TM.....	200
4.87	Amplitude comparison for TE and TM mode in MATLAB and HFSS (0.11 (~1 λ) meters in length by 0.055 (~0.5 λ) meters in radius at $\epsilon_r = 2.15$ for a dielectric cylinder with endcap). Amplitudes have a few dB differences for both TE and TM....	201
4.88	Phase comparison for TE and TM mode in MATLAB and HFSS (0.11 (~1 λ) meters in length by 0.055 (~0.5 λ) meters in radius at $\epsilon_r = 2.15$ for a dielectric cylinder with endcap). The phase matches closely for both TE and TM.....	201
4.89	Amplitude comparison for TE and TM mode in MATLAB and HFSS (0.11 (~1 λ) meters in length by 0.055 (~0.5 λ) meters in radius at $\epsilon_r = 10-5j$ for a dielectric cylinder without endcap). Amplitudes show big gaps at 0° for both TE and TM.....	202
4.90	Phase comparison for TE and TM mode in MATLAB and HFSS (0.11 (~1 λ) meters in length by 0.055 (~0.5 λ) meters in radius at $\epsilon_r = 10-5j$ for a dielectric cylinder without endcap). The phase shows mismatch for both TE and TM.....	203
4.91	Amplitude comparison for TE and TM mode in MATLAB and HFSS (0.11 (~1 λ) meters in length by 0.055 (~0.5 λ) meters in radius at $\epsilon_r = 10-5j$ for a dielectric cylinder with endcap). Amplitudes show a few dB differences for both TE and TM....	203

4.92	Phase comparison for TE and TM mode in MATLAB and HFSS (0.11 (~1 λ) meters in length by 0.055 (~0.5 λ) meters in radius at $\epsilon_r = 10-5j$ for a dielectric cylinder with endcap). The phase matches closely for both TE and TM.....	204
4.93	Amplitude comparison for TE and TM mode in MATLAB and HFSS (0.11 (~1 λ) meters in length by 0.055 (~0.5 λ) meters in radius at $\epsilon_r = 10^6$ for a metal cylinder without endcap). Big gaps are observed at 0° for both TE and TM.....	204
4.94	Phase comparison for TE and TM mode in MATLAB and HFSS (0.11 (~1 λ) meters in length by 0.055 (~0.5 λ) meters in radius at $\epsilon_r = 10^6$ for a metal cylinder without endcap). The phase shows mismatch for both TE and TM.....	205
4.95	Amplitude comparison for TE and TM mode in MATLAB and HFSS (0.11 (~1 λ) meters in length by 0.055 (~0.5 λ) meters in radius at $\epsilon_r = 10^6$ for a metal cylinder with endcap). Amplitudes match well at 0° and 90°	205
4.96	Phase comparison for TE and TM mode in MATLAB and HFSS (0.11 (~1 λ) meters in length by 0.055 (~0.5 λ) meters in radius at $\epsilon_r = 10^6$ for a metal cylinder with endcap). The phase matches closely for both TE and TM.....	206
4.97	Amplitude comparison for TE and TM mode in MATLAB and HFSS (0.1 (~1 λ) meters in length by 0.11 (~1 λ) meters in radius at $\epsilon_r = 10-5j$ for a dielectric cylinder without endcap). Big gaps are observed at 0° for both TE and TM.....	206
4.98	Phase comparison for TE and TM mode in MATLAB and HFSS (0.1 (~1 λ) meters in length by 0.11 (~1 λ) meters in radius at $\epsilon_r = 10-5j$ for a dielectric cylinder without endcap). The phase shows a gap at 0° for TE, and matches closely for TM.....	207
4.99	Amplitude comparison for TE and TM mode in MATLAB and HFSS (0.1 (~1 λ) meters in length by 0.11 (~1 λ) meters in radius at $\epsilon_r = 10-5j$ for a dielectric cylinder with endcap). Amplitudes match closely for both TE and TM.....	207
4.100	Phase comparison for TE and TM mode in MATLAB and HFSS (0.1 (~1 λ) meters in length by 0.11 (~1 λ) meters in radius at $\epsilon_r = 10-5j$ for a dielectric cylinder with endcap). The phase matches closely for both TE and TM.....	208
4.101	Amplitude comparison for TE and TM mode in MATLAB and HFSS (0.1 (~1 λ) meters in length by 0.11 (~1 λ) meters in radius at $\epsilon_r = 2.15$ for a dielectric cylinder without endcap). Big gaps are observed at 0° for both TE and TM.....	209

4.102	Phase comparison for TE and TM mode in MATLAB and HFSS (0.1 (~1 λ) meters in length by 0.11 (~1 λ) meters in radius at $\epsilon_r = 2.15$ for a dielectric cylinder without endcap). Big gaps are observed at 0° and 90° for both TE and TM.....	209
4.103	Amplitude comparison for TE and TM mode in MATLAB and HFSS (0.1 (~1 λ) meters in length by 0.11 (~1 λ) meters in radius at $\epsilon_r = 2.15$ for a dielectric cylinder with endcap). Gaps appear at 90° for both TE and TM.....	210
4.104	Phase comparison for TE and TM mode in MATLAB and HFSS (0.1 (~1 λ) meters in length by 0.11 (~1 λ) meters in radius at $\epsilon_r = 2.15$ for a dielectric cylinder with endcap). Gaps appear at 90° for both TE and TM.....	210
4.105	Amplitude comparison for TE and TM mode in MATLAB and HFSS (0.1 (~1 λ) meters in length by 0.11 (~1 λ) meters in radius at $\epsilon_r = 10^6$ for a metal cylinder without endcap). Big gaps are observed at 0° for both TE and TM.....	210
4.106	Phase comparison for TE and TM mode in MATLAB and HFSS (0.1 (~1 λ) meters in length by 0.11 (~1 λ) meters in radius at $\epsilon_r = 10^6$ for a metal cylinder without endcap). Big gaps are observed at 0° for both TE and TM.....	211
4.107	Amplitude comparison for TE and TM mode in MATLAB and HFSS (0.1 (~1 λ) meters in length by 0.11 (~1 λ) meters in radius at $\epsilon_r = 10^6$ for a metal cylinder with endcap). Big gaps are observed at 0° for both TE and TM.....	211
4.108	Phase comparison for TE and TM mode in MATLAB and HFSS (0.1 (~1 λ) meters in length by 0.11 (~1 λ) meters in radius at $\epsilon_r = 10^6$ for a metal cylinder with endcap). Big gaps are observed at 0° for both TE and TM.....	212
4.109	Amplitude comparison for TE and TM mode in MATLAB and HFSS (0.1 (~1 λ) meters in length by 0.165 (~1.5 λ) meters in radius at $\epsilon_r = 2.15$ for a dielectric cylinder without endcap). Amplitudes show large gaps for both TE and TM.....	212
4.110	Phase comparison for TE and TM mode in MATLAB and HFSS (0.1 (~1 λ) meters in length by 0.165 (~1.5 λ) meters in radius at $\epsilon_r = 2.15$ for a dielectric cylinder without endcap). The phase shows a big gap for both TE and TM.....	213
4.111	Amplitude comparison for TE and TM mode in MATLAB and HFSS (0.1 (~1 λ) meters in length by 0.165 (~1.5 λ) meters in radius at $\epsilon_r = 2.15$ for a dielectric cylinder with endcap). Amplitudes have a few dB differences at 0° for both TE and TM.	

.....	213
4.112 Phase comparison for TE and TM mode in MATLAB and HFSS (0.1 (~1 λ) meters in length by 0.165 (~1.5 λ) meters in radius at $\epsilon_r = 2.15$ for a dielectric cylinder with endcap). The phase matches closely at 0° for both TE and TM.....	214
4.113 Amplitude comparison for TE and TM mode in MATLAB and HFSS (0.1 (~1 λ) meters in length by 0.165 (~1.5 λ) meters in radius at $\epsilon_r = 10-5j$ for a dielectric cylinder without endcap). Amplitudes show big gaps at 0° for both TE and TM.....	214
4.114 Phase comparison for TE and TM mode in MATLAB and HFSS (0.1 (~1 λ) meters in length by 0.165 (~1.5 λ) meters in radius at $\epsilon_r = 10-5j$ for a dielectric cylinder without endcap). The phase shows a big gap at 0° for both TE and TM.....	215
4.115 Amplitude comparison for TE and TM mode in MATLAB and HFSS (0.1 (~1 λ) meters in length by 0.165 (~1.5 λ) meters in radius at $\epsilon_r = 10-5j$ for a dielectric cylinder with endcap). Amplitudes are in good agreement with HFSS for both TE and TM.....	215
4.116 Phase comparison for TE and TM mode in MATLAB and HFSS (0.1 (~1 λ) meters in length by 0.165 (~1.5 λ) meters in radius at $\epsilon_r = 10-5j$ for a dielectric cylinder with endcap). The phase is in good agreement with HFSS for both TE and TM.....	216
4.117 Amplitude comparison for TE and TM mode in MATLAB and HFSS (0.1 (~1 λ) meters in length by 0.33 (~3 λ) meters in radius at $\epsilon_r = 2.15$ for a dielectric cylinder without endcap). Big gaps are observed at 0° for both TE and TM.....	216
4.118 Phase comparison for TE and TM mode in MATLAB and HFSS (0.1 (~1 λ) meters in length by 0.33 (~3 λ) meters in radius at $\epsilon_r =$ 2.15 for a dielectric cylinder without endcap). The phase shows mismatch for both TE and TM.....	217
4.119 Amplitude comparison for TE and TM mode in MATLAB and HFSS (0.1 (~1 λ) meters in length by 0.33 (~3 λ) meters in radius at $\epsilon_r = 2.15$ for a dielectric cylinder with endcap). Amplitudes have a few dB differences at 0° for both TE and TM.....	217
4.120 Phase comparison for TE and TM mode in MATLAB and HFSS (0.1 (~1 λ) meters in length by 0.33 (~3 λ) meters in radius at $\epsilon_r =$ 2.15 for a dielectric cylinder with endcap). The phase is in good agreement with HFSS for both TE and TM.....	218
4.121 Amplitude comparison for TE and TM mode in MATLAB and	

	HFSS (0.11 (~1 λ) meters in length by 0.055 (~0.5 λ) meters in radius at $\epsilon_r = 10-5j$ for a dielectric cylinder with endcap in comparison to a sheet 0.00011 (~0.001 λ) meters in thickness by 0.055 (~0.5 λ) meters in radius). Amplitudes show 25 dB differences for both TE and TM.....	219
4.122	Amplitude comparison for TE and TM mode in MATLAB and HFSS (0.11 (~1 λ) meters in length by 0.055 (~0.5 λ) meters in radius at $\epsilon_r = 2.15$ for a dielectric cylinder with endcap in comparison to a sheet 0.00011 (~0.001 λ) meters in thickness by 0.055 (~0.5 λ) meters in radius). Amplitudes show 40 dB differences for both TE and TM.....	220
4.123	Amplitude comparison for TE and TM mode in MATLAB and HFSS (0.11 (~1 λ) meters in length by 0.055 (~0.5 λ) meters in radius at $\epsilon_r = 10^6$ for a metal cylinder with endcap in comparison to a sheet 0.00011 (~0.001 λ) meters in thickness by 0.055 (~0.5 λ) meters in radius). Amplitudes for a metal thin sheet overlap with a metal cylinder at 0° , but have a gap with a metal cylinder at 90° for both TE and TM.....	220
4.124	Amplitude comparison for TE and TM mode in MATLAB and HFSS (0.1 (~1 λ) meters in length by 0.11 (~1 λ) meters in radius at $\epsilon_r = 10-5j$ for a dielectric cylinder with endcap in comparison to a sheet 0.0001 (~0.001 λ) meters in thickness by 0.11 (~1 λ) meters in radius). Amplitudes differ by about 30 dB for both TE and TM.....	221
4.125	Amplitude comparison for TE and TM mode in MATLAB and HFSS (0.1 (~1 λ) meters in length by 0.11 (~1 λ) meters in radius at $\epsilon_r = 2.15$ for a dielectric cylinder with endcap in comparison to a sheet 0.0001 (~0.001 λ) meters in thickness by 0.11 (~1 λ) meters in radius). Amplitudes differ by about 40 dB for both TE and TM.....	222
4.126	Amplitude comparison for TE and TM mode in MATLAB and HFSS (0.1 (~1 λ) meters in length by 0.11 (~1 λ) meters in radius at $\epsilon_r = 10^6$ for a metal cylinder with endcap in comparison to a sheet 0.0001 (~0.001 λ) meters in thickness by 0.11 (~1 λ) meters in radius). Amplitudes for a metal thin sheet overlap with a metal cylinder at 0° , but show a gap with a metal cylinder at 90° for both TE and TM.....	222
4.127	Amplitude comparison for TE and TM mode in MATLAB and HFSS (0.1 (~1 λ) meters in length by 0.165 (~1.5 λ) meters in radius at $\epsilon_r = 10-5j$ for a dielectric cylinder with endcap in comparison to a sheet 0.0001 (~0.001 λ) meters in thickness by	

	0.165 (~1.5 λ) meters in radius). Amplitudes differ by about 25-30 dB for both TE and TM.....	223
4.128	Amplitude comparison for TE and TM mode in MATLAB and HFSS (0.1 (~1 λ) meters in length by 0.165 (~1.5 λ) meters in radius at $\epsilon_r = 2.15$ for a dielectric cylinder with endcap in comparison to a sheet 0.0001 (~0.001 λ) meters in thickness by 0.165 (~1.5 λ) meters in radius). Amplitudes differ by about 40 dB for both TE and TM.....	224
4.129	Amplitude comparison for TE and TM mode in MATLAB and HFSS (0.1 (~1 λ) meters in length by 0.165 (~1.5 λ) meters in radius at $\epsilon_r = 10^6$ for a metal cylinder with endcap in comparison to a metal sheet 0.0001 (~0.001 λ) meters in thickness by 0.165 (~1.5 λ) meters in radius). Amplitudes for a metal thin sheet overlap with a metal cylinder at 0° , but have gap with a metal cylinder at 90° for both TE and TM.....	225
4.130	Amplitude comparison for TE and TM mode in MATLAB and HFSS (0.1 (~1 λ) meters in length by 0.33 (~3 λ) meters in radius at $\epsilon_r = 2.15$ for a dielectric cylinder with endcap in comparison to a sheet 0.0002 (~0.002 λ) meters in thickness by 0.33 (~3 λ) meters in radius). Amplitudes differ by 30 dB for both TE and TM.....	225
5.1	Spherical coordinate system used to specify the direction and the polarizationstate of a transverse electromagnetic wave. (Mishchenko 2000).....	229
5.2	Transformation of the laboratory reference system xyz into the particle reference frame $x' y' z'$. (Mishchenko 2000).....	229
5.3	Rotation of three axes for radar-laboratory transformation system.....	230
5.4	Rotation of three axes for radar-laboratory transformation system.....	230
5.5	Leaf rotations under the coordinate transformation system.....	232
5.6	An example of the RCS database for a maple leaf, which is comprised of the co-pol amplitude of E polarization S_{HH} (top), co-pol amplitude of H polarization S_{VV} (middle), and cross-pol amplitude of E polarization S_{HV} (bottom) of far-field RCS for a resistive sheet with a stem (cylinder) (width = 14 cm, height = 22 cm, thickness = 0.2 mm, stem length = 280 mm, stem diameter = 3.0 mm, moisture content: 80%) at 2.8 GHz. The red and blue arrows represent the horizontal and vertical polarizations, respectively.....	234
5.7	FEKO simulation for the RCS of the same size leaf at a different	

	polarization angle (total, theta, phi) at 2.8 GHz.....	235
5.8	An example of the RCS database for a maple leaf, which is comprised of the co-pol amplitude of E polarization S_{HH} (top), co-pol amplitude of H polarization S_{VV} (middle), and cross-pol amplitude of E polarization S_{HV} (bottom) of far-field RCS for a resistive sheet with a stem (cylinder) (width = 14 cm, height = 22 cm, thickness = 0.2 mm, stem length = 280 mm, stem diameter = 3.0 mm, moisture content: 80%) at 10 GHz. The red and blue arrows represent the horizontal and vertical polarizations, respectively.....	236
5.9	FEKO simulation for the RCS of the same size leaf at a different polarization angle (total, theta, phi) at 10 GHz.....	238
5.10	An example of the RCS database for a leaf, which is comprised of the co-pol amplitude of E polarization S_{HH} (top), co-pol amplitude of H polarization S_{VV} (middle), and cross-pol amplitude of E polarization S_{HV} (bottom) of far-field RCS for a resistive sheet with a stem (cylinder) (width = 6 cm, height = 8 cm, thickness = 0.2 mm, stem length = 120 mm, stem diameter = 1.5 mm, moisture content: 80%) at 2.8 GHz. The red and blue arrows represent the horizontal and vertical polarizations, respectively. (Cheong, Bodine, Zhu et al. 2015)	239
5.11	FEKO simulation for the RCS of the same size leaf at a different polarization angle (total, theta, phi) at 2.8 GHz.....	241
5.12	An example of the RCS database for a leaf, which is comprised of the co-pol amplitude of E polarization S_{HH} (top), co-pol amplitude of H polarization S_{VV} (middle), and cross-pol amplitude of E polarization S_{HV} (bottom) of far-field RCS for a resistive sheet with a stem (cylinder) (width = 6 cm, height = 8 cm, thickness = 0.2 mm, stem length = 120 mm, stem diameter = 1.5 mm, moisture content: 80%) at 10 GHz. The red and blue arrows represent the horizontal and vertical polarizations, respectively.....	242
5.13	FEKO simulation for the RCS of the same size leaf at a different polarization angle (total, theta, phi) at 10 GHz.....	244
5.14	An example of the RCS database for a leaf, which is comprised of the co-pol amplitude of E polarization S_{HH} (top), co-pol amplitude of H polarization S_{VV} (middle), and cross-pol amplitude of E polarization S_{HV} (bottom) of far-field RCS for a resistive sheet with a stem (cylinder) (width = 4 cm, height = 6 cm, thickness = 0.2 mm, stem length = 100 mm, stem diameter = 1.2 mm, moisture content: 80%) at 2.8 GHz. The red and blue arrows represent the horizontal and vertical polarizations, respectively.	245

5.15	FEKO simulation for the RCS of the same size leaf at a different polarization angle (total, theta, phi) at 2.8 GHz.....	247
5.16	An example of the RCS database for a leaf, which is comprised of the co-pol amplitude of E polarization S_{HH} (top), co-pol amplitude of H polarization S_{VV} (middle), and cross-pol amplitude of E polarization S_{HV} (bottom) of far-field RCS for a resistive sheet with a stem (cylinder) (width = 4 cm, height = 6 cm, thickness = 0.2 mm, stem length = 100 mm, stem diameter = 1.2 mm, moisture content: 80%) at 10 GHz. The red and blue arrows represent the horizontal and vertical polarizations, respectively.....	248
5.17	FEKO simulation for the RCS of the same size leaf at a different polarization angle (total, theta, phi) at 10 GHz.....	249
5.18	An example of the RCS database for a leaf, which is comprised of the co-pol amplitude of E polarization S_{HH} (top), co-pol amplitude of H polarization S_{VV} (middle), and cross-pol amplitude of E polarization S_{HV} (bottom) of far-field RCS for a resistive sheet with a stem (cylinder) (width = 2 cm, height = 4 cm, thickness = 0.2 mm, stem length = 80 mm, stem diameter = 1.0 mm, moisture content: 80%) at 2.8 GHz. The red and blue arrows represent the horizontal and vertical polarizations, respectively.....	250
5.19	FEKO simulation for the RCS of the same size leaf at a different polarization angle (total, theta, phi) at 2.8 GHz.....	252
5.20	An example of the RCS database for a leaf, which is comprised of the co-pol amplitude of E polarization S_{HH} (top), co-pol amplitude of H polarization S_{VV} (middle), and cross-pol amplitude of E polarization S_{HV} (bottom) of far-field RCS for a resistive sheet with a stem (cylinder) (width = 2 cm, height = 4 cm, thickness = 0.2 mm, stem length = 80 mm, stem diameter = 1.0 mm, moisture content: 80%) at 10 GHz. The red and blue arrows represent the horizontal and vertical polarizations, respectively.....	253
5.21	FEKO simulation for the RCS of the same size leaf at a different polarization angle (total, theta, phi) at 10 GHz.....	255
5.22	An example of the RCS database for a leaf, which is comprised of the co-pol amplitude of E polarization S_{HH} (top), co-pol amplitude of H polarization S_{VV} (middle), and cross-pol amplitude of E polarization S_{HV} (bottom) of far-field RCS for a resistive sheet with a stem (cylinder) (width = 1 cm, height = 3 cm, thickness = 0.2 mm, stem length = 60 mm, stem diameter = 0.8 mm, moisture content: 80%) at 2.8 GHz. The red and blue arrows represent the horizontal and vertical polarizations,	

	respectively.....	256
5.23	FEKO simulation for the RCS of the same size leaf at a different polarization angle (total, theta, phi) at 2.8 GHz.....	258
5.24	An example of the RCS database for a leaf, which is comprised of the co-pol amplitude of E polarization S_{HH} (top), co-pol amplitude of H polarization S_{VV} (middle), and cross-pol amplitude of E polarization S_{HV} (bottom) of far-field RCS for a resistive sheet with a stem (cylinder) (width = 1 cm, height = 3 cm, thickness = 0.2 mm, stem length = 60 mm, stem diameter = 0.8 mm, moisture content: 80%) at 10 GHz. The red and blue arrows represent the horizontal and vertical polarizations, respectively.....	259
5.25	FEKO simulation for the RCS of the same size leaf at a different polarization angle (total, theta, phi) at 10 GHz.....	261
5.26	Sphere for radar direction pointing to the wood slab with 651 points.....	266
5.27	RCS TE polarization on dry wood board (0.04157x 0.04157 meters) (left) and RCS TE polarization on wet wood board (0.04157x 0.04157 meters) (right) with two incident angles theta and phi scattered.....	267
5.28	RCS TM polarization on dry wood board (0.04157x 0.04157 meters) (left) and RCS TM polarization on wet wood board (0.04157x 0.04157 meters) (right) with two incident angles theta and phi scattered.....	267
5.29	Four lumber grades of lumber that homeowners need to see. (http://www.oldhouseweb.com/how-to-advice/buying-uides/what-to-look-for-when-buying-framing-lumber.shtml).....	270

Abstract

Tornadic debris plays an important role in the study of tornadoes due to the dramatic threat it poses to human life, and the devastation it causes to commercial and residential property. Radar cross section (RCS) modeling on plate-like and cylindrical objects is developed in this tornadic debris study. The sheets, plates, and cylinders used in this study are designed to represent leaves, wood board, flat building forms, metal rods, tree trunks, and branches, respectively.

Different techniques are evaluated in terms of the geometry of the object, accuracy, and math complexity and computation efficiency. Geometrical Optics (GO), Geometrical Theory of Diffraction (GTD), Finite Element Method (FEM), Finite Difference Time Domain method (FDTD), Moment of Method (MoM) and Physical Optics (PO) are introduced. Finally, the decision to use PO for deriving the formulation for plate-like objects throughout the dissertation was made.

Non-metal objects such as cylinder broadside, endcap, general circular sheets and plates, surface impedance circular plates, rectangular sheets and plates, as well as metal circular plates are derived by hand. Metal objects such as cylinder broadside and rectangular plates, as well as resistive rectangular thin sheet approximations, are verified and cited from published research books and papers.

Full wave simulation Ansys HFSS validates the analytical results in most cases. FEKO commercial software is used to compare the analytical results for two layer plates with different media and leaf sample applications.

After testing, metal vs. non-metal plates and thin vs. thick plates are distinguished by 5 dB, 10 dB, and 20 dB from the simulation results, respectively; this fact confirms the accuracy and limitations of theory. By adding endcaps, one is able to compensate the deficiency from normal to the cap surface of the finite cylinder by at least several wavelengths in length and at least half of a wavelength in radius. The theoretical analysis of the extension of PO indicates that more accurate results appear as the incident angle gets closer to normal. The errors and limitations of PO are described and demonstrated by comparison plots of analytical results vs. HFSS throughout.

The leaf library and wood board (dry and wet) studies are performed as sample applications for “real” debris types under the radar coordinate transformation system for all polarizations at oblique TEM incident wave.

Research questions are answered in the conclusions.

Chapter 1

Introduction

It is well-known that a tornado is one of the most threatening weather phenomena in the world. The introduction of the Weather Surveillance Radar 1988 Doppler (WSR-88D) network over two decades ago, significantly improved tornado lead time, and reduced storm-related fatalities and injuries (Simmons and Sutte 2005). The total estimated cost in damages from tornadoes in 2011 was \$28 billion (NOAA National Climatic Data Center, 2011). Even though the polarimetric measurements of tornadoes offer new discoveries in terms of the capacities of severe weather formation, these measurements are still limited because the scattering characteristics of tornadic debris are poorly understood.

Traditionally, the detection capabilities of the radar cross section (RCS) are considered in the design and operation of military aircraft, ships, ground vehicles, tanks, etc., and have been developed since the 1950s and 1960s (Jenn 2005). In weather radar applications, RCS is one of the most important considerations in the practical world. The electromagnetic characteristics of RCS make it very challenging to take multiple reflections into account from different debris objects while the co-polarized and cross-polarized radar returns are measured. Here, RCS is applied for modeling individual tornadic debris scatterer, but without the

consideration of multiple reflections. Therefore, the RCS modeling will be starting from the importance of electromagnetic theory and simulation for individual scatterers in anticipation of multiple scattering capabilities in radar detection in the future.

Polarimetric radar variables build the bridge between the received radar signal and polarimetric RCS values. Polarimetric radar features both horizontal and vertical operations to transmit and receive signals (Doviak et al. 2000). Polarimetric radar variables referred to the covariance matrix C (e.g. $\langle S_{hv}S_{hh}^* \rangle$ or $\langle S_{hh}S_{vv}^* \rangle$) can be calculated through the measurement of combinations of co-polarization and cross-polarization of the complexed radar signals received. Radar reflectivity factor (Z_{hh} , Z_{vv}), differential reflectivity (Z_{DR}), co-polar cross-correlation coefficient (ρ_{HV}), backscatter differential phase (δ_{dp}), and the linear (L_{DR}) and circular depolarization ratio are all calculated by polarimetric radar variables. In terms of polarimetric RCS values, the amplitudes of co-polarization and cross-polarization can be calculated by formulating RCS for different debris objects. Therefore, the significance of polarimetric RCS modeling is that it generates predictions by emulating radar returns.

The tornadic debris signature (TDS) observed by weather radar has shown negative differential reflectivity (Z_{DR}) and low co-polar cross-correlation coefficient (ρ_{HV}) (Ryzhkov et al. 2005; Kumjian and Ryzhkov 2008; Bodine et al. 2013, Palmer et al. 2011; Schultz et al. 2012a, b;

Bluestein et al. 2007; Snyder and Bluestein 2014) at different radar frequencies and a high horizontal radar reflectivity factor (Ryzhkov et al. 2002, 2005). These variables, when combined with debris polarimetric scattering characteristics, are poorly understood due to the complexity associated with the variety of sizes, orientation, geometry and material compositions of tornadic debris. As such, debris polarimetric scattering characteristics may vary with different radar frequencies. The features of tornadic debris make it possible to distinguish electromagnetic scattering characteristics from hydrometeors. Thus, debris from tornadoes exhibits unique characteristics such as rotation, frequency dependence, centrifuging velocity, wind field and debris loading. For example, the estimate error on debris centrifuging and debris-influenced radial velocity fields (e.g., Dowell et al. 2005), and the difference between dual-pol fields tornadic and non-tornadic storms with different dynamics and thermodynamics of the near-storm environment (e.g., Crowe et al. 2012), are still under investigation. The relationships between debris characteristics and polarimetric variables are therefore unknown. In other words, it is not understood how the size, concentration, and shape of different debris scatter affect polarimetric variables.

There are questions still unanswered. For example, “What debris types and characteristics lead to observed polarimetric scattering signatures?”

and “What types of debris can be reasonably approximated in a computationally-efficient way for the purposes of this research?”

If a relationship between debris characteristics and polarimetric radar variables can be investigated, it may be possible to develop new debris classification algorithms using polarimetric radar at multiple frequencies.

It is well known that weather radars have the advantage of monitoring a large area in real time and often provide qualitative measurements. However, the conversion of the radar measurement into meteorological quantities of the target is not unique. The radar simulator used in this study is able to distinguish between the different contributions of polarimetric data on the received echoes.

Polarimetric data have the potential to provide information on clouds, and the particle size, shape, and ice density of precipitate (Zrníc and Ryzhkov 1999). Simulation of weather radar signals can be based on physical models for backscattering of distributed targets (e.g., Capsoni and D’Amico 1998), which are related to the electromagnetic field. By developing the physically-based radar simulator LES model, time-series data can be produced. The dual polarimetry is able to perform hydrometeor classifications (Straka et al. 2000; Park et al. 2009) and therefore improve tornado detection.

As one part of the complete tornado debris study, the simulator is developed and able to generate realistic, three dimensional modeling and

time series data (Cheong et al. 2008). The function of the simulator is to emulate radar return signals by generating the time series data in a finite volume by employing Monte Carlo integration. The randomly oriented scattering pieces consist of two parts: one is background driven by the wind field generated from a Large Eddy Simulation (LES) model; and the other is vortex driven, moving scattering debris around.

The overall simulator process is indicated in Figure 1.1. In the radar coordinated system, the z axis is denoted by the radar direction. The simulator calculates the Euler rotation angles ($\alpha \in [-180^\circ, +180^\circ]$ and $\beta \in [-90^\circ, +90^\circ]$) as the orientation angles of each object. Taking advantage of the coordinate transformation equation $S=T^{-1}(\gamma) S_{\text{local}}(\alpha, \beta) T(\gamma)$, the scattering matrix $S_{\text{local}}(\alpha, \beta)= \begin{bmatrix} S_{hh} & S_{hv} \\ S_{vh} & S_{vv} \end{bmatrix}$ can be transformed through the polarimetric transformation to contribute radar I/Q data. Thus, each dataset has an amplitude range of all polarizations relating to the local position and radar direction.

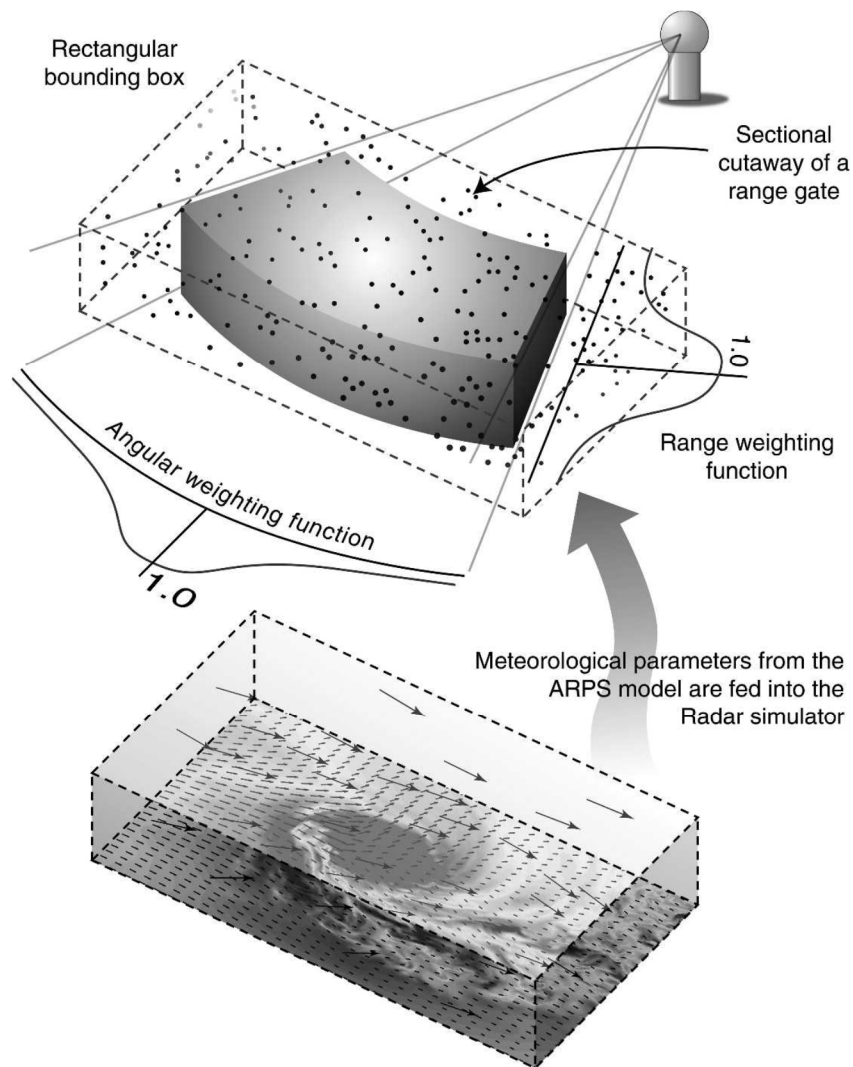


Figure 1.1: Conceptual diagram of the time series radar simulator. Each point scatterer represents a discrete position from which the transmit pulse is reflected. Meteorological parameters from the Advanced Regional Prediction (ARPS) model are used to derive the reflectivity and velocity of each discrete scatterer. All reflected echoes are integrated to obtain the composite returned signal. As the number of point increases, the

composite returned signal approximates well that which would be expected from volume scattering (Cheong 2008).

As indicated in Figure 1.1, the simulator emulates the radar return signal in terms of the parameters associated with rotation, orientation, frequency, wind field, velocity, position, etc. These radar parameters include transmit power, antenna gain, band frequency, location, atmospheric field, etc. In terms of electromagnetic scattering characteristics, RCS modeling is focused on the polarization, rotation, geometry, size, and material properties of each object. Therefore, RCS modeling is one of the more important aspects for better understanding polarimetric radar signatures. Furthermore, the scattering characteristics of RCS modeling, which include orientation angle (α , β), polarization (amplitude and phase), and debris type, can be shared with the simulator through an existing interface between them. RCS modeling for many objects requires a massive amount of theoretical derivation and simulation, and the simulator is therefore an efficient way to emulate the thousands of scatterers with the unique RCS signatures of each object indexed into the wind field generated from LES. Thus, building a library of RCS databases is necessary. Providing the RCS databases to the simulator makes it possible to generate realistic, three-dimensional dynamic polarimetric scattering radar I/Q data. The final goal of RCS modeling is to contribute

to a GPU-accelerated polarimetric radar time-series simulator that is necessary to further the study of tornadic debris.

The most common and important debris types are vegetation. A defining characteristic of debris scatterers is their geometric complexities, which impact the theoretic analysis and computational strategy. The electrical size and object geometry are crucial factors in determining which technique is suitable.

Electrically small particles, such as sand, dust, and raindrops, are modeled as spheroids in Rayleigh and Mie scattering regions using the T-matrix method (Mishcheko et al. 2000; Bodine 2014).

For objects with electrically large diameters, such as cylindrical structures, twigs, straight branches, iron rods, etc., go to the object classification with electrically large diameters of cylindrical structures.

For objects that have a large electrical size, are flat, and either penetrable or non-penetrable plate-like structures, such as leaves, endcaps to cylinders, roof shingles, flat siding, metal plates, wood board, drywall, foam insulation, and other building materials, go to the object classification with a large electrical size of plate-like structures.

The plate-like and cylindrical objects are proposed to contribute to RCS modeling of tornado debris types. The overall goals are to understand the target signatures both physically and phenomenologically, using technology for controlling and measuring RCS to develop a geometric

RCS modeling database which is achieved by emulating the realistic debris objects, and, finally, to develop the radar polarimetric algorithm.

This dissertation will introduce the processes and efforts being made to advance RCS modeling of plate-like and cylindrical objects. In particular, this study has made an achievement by developing an RCS library, which will contribute to the field of tornado debris study.

Chapter 2 includes an overview of a complete RCS modeling of this tornadic debris study, including theory, simulation, and measurement. The critical part of theoretic analysis associated with techniques is the geometry of the target. Many techniques have been developed to provide realistic results. They can be based on exact methods such as integral equations (IE), method of moments (MoM), finite-difference time-domain (FDTD), and finite element method (FEM), among others.

Physical Optics (PO) and extension of PO methods are chosen from the overall techniques discussed, and is predominantly used in the rest of the dissertation. The HFSS (High Frequency Structural Simulator) modeling package associated with FEM is discussed in detail. The FEKO simulation tool referred by MoM is also introduced. GO (Geometrical optics) is commonly used for large optical objects. They all have drawbacks in terms of theoretical analysis, calculating complexity, simulation time, accuracy of data, and electrical size of objects. The motivation for future

work comes from the validation of analytical results and simulation data in comparison to verified measurements.

In Chapter 3, PO-based calculations of the RCS of plate-like objects are presented. This chapter will introduce the calculation of rectangular thin sheets, rectangular thick plates, circular sheets, and plate-like debris objects based on the literature (Sarabandi 1987; Jenn 2005; Balanis 2012). Both rectangular- and circular- shaped- objects are compared with metal (non-penetrable) and dielectric (penetrable) cases. In addition, general derivations of objects for both rectangular and circular plates are provided. These include rectangular thin sheet approximations (penetrable) from Senior and Sarabandi (1987), rectangular plate (non-penetrable) from publications (Jenn 2005), and multi-layered reflection coefficient calculations from previous research (Sections 5.5.2.D and 11.3.2 in Balanis 2012). Calculations for circular plates (penetrable and non-penetrable) and rectangular plates (penetrable) are derived by hand. Furthermore, plots based on comparisons between HFSS and analytical results (MATLAB) for relatively small and large objects are presented.

In Chapter 4, PO-based calculations of the RCS of cylindrical objects are presented. Starting from infinitely long cylindrical broadside analysis in addition to endcaps, the finite cylindrical object modeling is derived. Plots based on comparisons between HFSS and analytical results (MATLAB) for relatively small and large cylinder objects are provided.

In Chapter 5, a leaf library and wood board study are presented as examples for realistic tornadic debris applications. This chapter will discuss the radar coordinate transformation system using the transformation matrix T with $P=Tp$, where p is a vector in the “radar” system and P is a vector in the “local” system. 3D analytical results of a single leaf for all polarization under the radar coordinate transformation system are provided at 2.8 GHz and 10 GHz frequency, respectively. For comparison, FEKO simulations are provided by the same size used for the analysis of leaves. Finally, the square dry and wet wood board study from research (Bodine et al. 2016) is summarized by utilizing two different methods: thin sheet approximation (Senior and Sarabandi 1987) and reflection coefficient computation for multi-layer structures (Balanis 2012). These methods are used for calculating RCS mean value of wood board.

Finally, the research questions are answered, and conclusions are presented in Chapter 6.

Chapter 2

Background

Tornadic debris scatters include a wide range of sizes, geometry, material properties, and orientations that must be accounted for in the production of electromagnetic scattering characteristics. Scatterers could include small particles like sand or rain-drops, or include large objects like plywood boards, roof tiles, or tree trunks, twigs and branches. Based on documented tornado debris storm observations, tornadic debris features polarimetric characteristics that are very different from hydrometeors.

Radar cross-sections σ are the areas intercepting the amount of power that, when scattered isotropically, produces at the receiver a density equal to the density scattered by the actual target (Balanis 2012).

The formal definition of RCS is

$$\begin{aligned}\sigma &= \frac{\text{power reflected to receiver per unit solid angle}}{\text{incident power density}/4\pi} \\ &= \lim_{R \rightarrow \infty} 4\pi R^2 \frac{|E_s|^2}{|E_i|^2}\end{aligned}$$

where E_s and E_i denote the scattered and incident electric fields. In the far scattered field of the target $E_s \sim 1/R^2$, RCS is range independent.

The RCS of a target is a fictional area that describes the amount and/or strength of the object scattering of the incident EM wave.

The RCS is frequency-dependent to a high degree, and is also influenced by the size, shape, surface roughness, and material of the target (Knott 2006).

For convenience, it is better to specify the size of the object in terms of wavelength λ rather than in a physical unit (meters). For example, length = 1.1 meters with radius = 0.033 meters of a cylinder at 2.8 GHz can be described as 10λ by 0.3λ . The RCS of the cylinder will be calculated based on λ in that given frequency. This dimension expression is used through the rest of dissertation.

For electrically small objects, the RCS simulation tool most used is MATLAB. For a larger and more complex debris scatterer, for which the RCS cannot be modeled analytically and efficiently, measurements and finite simulations in HFSS are necessary. However, the computational efficiency in terms of time and complexity is one of the most important factors in the decision making process. If the dimension is much larger than the wavelength λ (for example, 1.5λ in length by 30λ in radius of a cylinder), then it may take several days to finish the modeling. This is the largest object that can be simulated through the fastest computer the lab supplies. It is not hard to understand that the computational cost of full-wave analysis is too high if the dimension is above 50λ by 50λ . Therefore, non-full wave techniques such as approximate optics methods are used for larger objects. GO, Geometrical Theory of Diffraction (GTD),

and Uniform Theory of Diffraction (UTD), among others, are very popular optics-like techniques that can better analyze larger objects which produce a tremendous amount of theoretical complexity.

Since the exact solutions to Maxwell's equations are known only for special geometries such as spheres, spheroids, or cylinders, approximate methods under certain conditions are required for a given target of arbitrary geometry. To illuminate electromagnetic scattering characteristics of different debris types, several techniques to compute the scattering of radiation can be applied for objects in association with geometry. PO, MoM, FEM, GTD, and GO will be described in detail in the following sections.

Other techniques may not meet the needs of modeling tornadic debris scatterers. For example, Discrete Dipole Approximation (DDA) computes the radiation of particles with an arbitrary shape and periodic structure with more accurate results; FDTD based on Maxwell's curl equations in the time domain, however, involves some errors (staircase or grid dispersion) that are not easy to implement, or involve too many configuration steps in getting a scattered field for RCS calculation and computational implementation.

A complete study of RCS includes three important parts: theory, simulation and measurement. Analytical simulation (MATLAB) based on

theory will be validated with the full-wave simulation (HFSS) throughout the dissertation. In the case of a two-layer plate with different media, FEKO simulation software is used to construct the two-layer structures. Plots are illustrated for comparison.

Efforts were made to start from the electromagnetic theory and simulate in HFSS (FEKO is used occasionally). When possible, the analytical results and simulation data, in which approximations and techniques are used, will be compared with measured RCS data. The goal is to establish the RCS library of different debris types at different wavelengths through measurement validation in order to supply this information into the radar simulator (Cheong et al. 2008, 2014), and emulate scattering characteristic from radar returns.

2.1 Measurements

Since the techniques above have limitations mostly based on the geometry of the target, validation through measurements is necessary. Especially, for complex arbitrary objects or poorly known objects, for which RCS cannot be modeled analytically and computational efficiently (when supplying into larger electromagnetic database, computational efficiency is one of the important factors to consider), the choice of RCS data is the measurement. On the other hand, it is necessary to compare measurements to RCS modeling to make it a practical application, and to

determine which one is the best method for which types of scatterers. Particularly, processes that improve the accuracy of measurements will be leading the way to new scientific research. For example, if the result of the measurement is more exact, then mathematical modeling is required to check and modify. Alternately, measurements also present some degree of error; analytical calculation can be used to validate a measurement.

Evaluation of theory and simulation is another motivation to take measurements since they are used to understand basic scattering phenomena. The evaluation depends on the comparisons between measurement and predictions (Knott 2006). There is always the need to test theory or verify predictions and this can usually be accomplished only by means of measurements made on the test range (Knott 2006).

Measurement accuracy, in other words, is strongly dependent upon the accuracy of the instrumentation chosen.

In other situations, for example, measurement is not practical, such as when the antennas are mounted on large objects like ships, aircraft, and large man-made satellites. Also, measurement on a special object requires extensive modification, which is very expensive for large objects.

RCS measurements are closely associated with the terminals of the transmitted or received antenna, and contain fundamental considerations such as range far-field facility requirements and conditions, polarization, coordinate transformation systems, instrumentation sensitivity, etc.

Polarization plays an important role in RCS measurements; however, the process of separating targets from the positioner and surrounding background is complex. The solution was developed by Ruck (1970). Dimension scaling and operational frequencies are also important to RCS measurements. The scaling technique is manageable during the measurements. Increasing the frequency requires a smaller-sized facility (Blacksmith 1965). Instrument sensitivity is a factor that can improve the accuracy of data with respect to the RCS measurement point of view. Alternately, the accuracy of analytical results in Chapter 4 will show how to obtain more accurate data by adding the endcaps to cylinders. For example, a power amplifier inside the pulse modulator (if used) will improve the sensitivity between 10-20 dB (Orbit/FR).

In addition, high resolution RCS measurement has been developed inside the anechoic chamber (Zhang et al. 2010). The problem of antenna coupling can be solved by the disposition of the transmitting antenna and receiving antenna. The wave method (continuous or not), frequency domain response or time-domain response, absorbing form, and technical function (inverse fast Fourier transform) used will all affect the accuracy of measurements taken.

Past studies indicated that a short cylinder has a higher monostatic RCS than a long cylinder with the same maximum dimension which

defines a bounding box as the limiting factor in far-field measurements since it must fit within the measurement facility's quiet zone.

A monostatic radar system uses the same antenna as the transmitter and receiver. A bistatic radar system consists of transmitting and receiving antennas located separately at large distances. In practice, the monostatic RCS measurement setup is 5° apart from the transmitting antenna and receiving antenna, which is viewed as quasi-bistatic, namely, the transmitter and receiver are slightly separated but still appear to be the same location as viewed from the target (Knott 2006).

Basically, two scans were made during the measurement, one with the antenna polarized with E polarization and the other with H polarization. The incident angle α ranges from 0-90 degrees and β from -90 to +90 degrees in each measurement scan, in steps, in the radar coordinate system, and in the anechoic chamber. The steps are chosen to cooperate with the radar emulator. Measurements will be conducted with calibration spheres through network analyzer-based instrumentation.

2.2 Full-wave simulations

Theoretically, full wave analysis can be used to solve Maxwell's equations without any simplifications and assumptions. The electromagnetic E and H fields defined by the equations are time-variant and frequency-dependent. Unlike quasi-static analysis where the

Maxwell's equations are modified first with assumptions, in which the electromagnetic fields are supposed to be time-invariant and frequency-independent, full wave analysis is suitable for dealing with electrically small objects (physical size is below $1/6 \lambda$, $1/10 \lambda$ or even below 0.01λ). One of the most famous simulation solvers is Ansoft SpiceLink (Q2D/Q3D).

Full-wave analysis is best described in contrast to static and quasi-static methods, for its propagating speed in the media is the speed of light. Full-wave analysis is often used to analyze electrically large objects whose physical sizes are much larger compared to wavelength λ . Dimensions of objects range between 0.01λ and 50λ . This indicates that full-wave methods solve the problems at high frequency (GHz). Some famous full-wave simulation solvers are: Ansoft HFSS, and CST Microwave Studio.

2.2.1 Finite element method and HFSS modeling

The FEM is a numerical technique. The advantage of FEM is that it is able to solve the Maxwell's equations on an unstructured mesh that accounts for all the geometric detail of the object. FEM is able to generate sparse matrices results that are capable of applying a wide range of matrix-based solvers. Finite element solvers always define derivative coupling terms in Maxwell's equations to be finite. FEM is used typically as a tetrahedral mesh element contained in the model. HFSS as a finite element simulation solver is originally based on FEM which is directly developed

from scattering wave equations. It applies PMLs (perfectly matched layers), upon which the impinging incident is completely transmitted with minimal reflections (Jenn 2005). PMLs are a common grid termination technique in which a grid is bounded by a layer of absorbing material. HFSS processes a discretized volume in the computational domain (free space), which makes it suitable for a wide range of geometry and object materials in terms of frequency and direction. It is an asymptotic solver option. The PMLs must be placed at least one quarter of a wavelength from the scattering body inside PMLs to get more accurate results. HFSS is a more accurate approach for simulating polarimetric RCS modeling.

Since Faraday's Law and the displacement current become significant at high frequencies, the computational expense of the HFSS simulation must be investigated to obtain accurate results in terms of physical size of the object.

Here, HFSS simulation is compared with MATLAB modeling for RCS analysis for different debris types, since most of the debris sizes are within a suitable range for HFSS.

2.2.2 MoM-based method

MoM is a numerical and frequency domain method. It is based on Maxwell Harmonic (Phasor) Equations. The advantage of MoM is that it can be applied to arbitrary bodies. It solves the matrix equations typically. The size of the matrix is proportional to the electrical size of the object.

The electrical current can be expressed as a series of unknown coefficient and basis functions. The selection of basis functions is very important because they should be mathematically easier to implement, and are consistent with the electrical current. The basis functions can be chosen typically from pulses, triangles, sinusoids, δ functions etc. and used as testing functions. The current is obtained from the matrix form $\mathbf{V}=\mathbf{Z}\mathbf{I}$, where \mathbf{Z} represents the matrix with units of ohms and \mathbf{V} represents excitation vector with the units of volts. The scattered E field can be obtained through the radiation integral. The MoM technique is a power tool that provides a rigorous solution for the induced current density on a body (Harrington 1961), but requires longer computational time when dealing with large matrices resulting from larger objects. The FEKO simulation tool is a commercial application of a MoM- based simulation solver, and prefers triangle and wire settings as the mesh solution. Frequency range must be set before meshes can be automatically generated. Electric material properties of the media are considered in all cases with the exception of infinite layer. A finer mesh is required for more accurate results.

2.3 Analytical approaches

2.3.1 PO

PO provides an estimate for the unknown currents and gives relatively accurate results for electrically large bodies (Jenn 2005). The approximation becomes more accurate as the wavelength approaches zero, i.e., at high frequencies. Therefore, this is also called a high frequency approximation.

The shortcoming of PO is that the current flowing in the shadow region drops to zero, and is nonzero in reality at the shadow boundary. For an electrically large surface and near the specular direction, the error can be omitted. Other problems with PO include the infinite PEC surface and finite surface. For example, a reflection field is generated only when $\theta_r = \theta_i$ and is zero elsewhere for an infinite PEC surface; but if the surface is finite, PO gives the reflected field in finite beam widths. Edge scattering is also not taken into account. The mathematical model for edge diffraction combined with PO creates another method called physical theory of diffraction (PTD).

PO is a current integral-based technique and is used for the RCS in the far zone from the observation point. Current flowing on the surface combines with the magnetic vector potential and electric vector potential, and the radiated electrical and magnetic field at the observation point can be derived based on this current.

PO approximation is used to model flat, electrically large objects such as the resistive thin sheet (leaf) and plate-like objects (endcaps for metal and dielectric cylinders, wood board etc.) in the rest of the dissertation.

2.3.2 GO

GO is the most common ray tracing theory (optics-like method) and has been used for centuries. It describes the reflection and refraction at the interface between two media. It is suitable for larger objects. However, similar to other theories, it has its own limitations and assumptions. The ray sources are far away from the reflection surface and radii of scattering curvature from the media are much larger than the wavelength of the incident TEM wave. The incident wave direction is illustrated along the normal to the eikonal surface. In a homogeneous medium, the ray travels in straight lines. The polarization of the traveling wave will not change after reflection if the medium is isotropic. Energy (or power) is conserved in a flux tube. GO shares some similarities with PO, which requires the specular presentation on large surface areas. Edge scattering effect is not taken into account. When edge diffraction from an analytical model is combined with GO, it becomes another method called GTD. Again, GO has several problems. For the infinite PEC surface, GO agrees with PO, which gives zero beam width except when $\theta_r = \theta_i$. However, GO still gives the same solution for finite surfaces. Again, in the shadow region,

GO shows zero fields, which is the same shortcoming observed of PO. If the size is much larger than the wavelength (above 50x50 wavelengths), then the computational cost of the full-wave methods is too high, and non-full-wave methods such as GO or GTD should be used instead. For sizes above 50λ , approximate optics-like methods (GO, GTD, UTD, etc.) are suitable.

2.3.3 GTD

The GTD is a ray tracing technique that considers the edge diffraction, but it introduces a large amount of complexity in math for plate-like and cylindrical objects. It still suffers some shortcomings as an extension of the GO method. A ray arriving at the observation point is not located in the same place as the first ray. It is possible that there is no scattered field at the observation point without a reflected ray coming back after significant diffraction, giving the sharp discontinuity of the scattered field strength. In practice, this is not true because the field is still continuous. Even the surface reflection and edge diffraction do not give a complete scattering due to a complex body, especially with corners and tips. In this situation, the diffraction coefficient is relatively difficult to derive.

2.4 Summary

Different techniques are evaluated in this dissertation based on the geometry and size of debris types, complexity of theoretical derivation,

and computational cost. Because MoM and GTD consider edge effect, they will give more accurate results, especially for objects with corners and edges; but they also introduce a large amount of mathematical verification. As for GO, it is too imprecise for small objects in terms of wavelength and small debris types (small leaves, grass, rods etc.). The advantages and disadvantages of these methods were evaluated. PO was determined to be the best method for representing plate-like objects from thin sheets (leaves, endcaps), and thicker wood board towards the tornadic debris study. Since the goal of this study is to emulate the radar returns with integration and uncertainty of actual debris types, RCS modeling of individual scatter may not be very accurate. Even though PO is not as accurate as the MoM and GTD, it is sufficient to build a complete RCS library.

The analytical process using PO involves more complicated mathematical derivation, especially for dielectric objects such as endcaps of dielectric cylinders, leaves, wood boards or other lossy flat surface material. However, this process is necessary to achieve more accurate results by comparing full wave simulation, and through validation of the measurements. In turn, it helps us to better understand the fundamental theory.

Chapter 3

PO-based calculations of the RCS of plate-like objects

3.1 Literature review

The paper “Measuring and modeling the backscattering cross section of a leaf”, Senior and Sarabandi’s research on the application of RCS calculations for resistive thin sheets developed an RCS modeling of a leaf (1987). Resistive “sheets” are called infinitesimally thin penetrable plates with thickness $t \ll \lambda$. (Jenn 2005). A conductive sheet only supports magnetic currents for $J_s = 0$, whereas a resistive sheet only supports electric currents for $J_{ms} = 0$. The complex resistivity is specified by the moisture content of the leaf. The RCS is related to the leaf moisture content by the quantity R . The dielectric property ϵ (complex relative permittivity) plays an important role in the scattering characteristic of many types of vegetation. A leaf can be viewed as a resistive sheet which an electric current sheet whose strength is proportional to the local tangential electric field (Harrington and Mautz 1975) by a single quantity R . Starting from the infinite sheet by applying Maxwell’s equations and discontinuing boundary conditions to get the reflection coefficients for E and H polarizations, PO approximation is then used to integrate the induced surface current and is “truncated” to a finite rectangular dimension (4 cm x 6 cm). Further, modeling a leaf includes dielectric

property and certain parameters to be set up, including the moisture content, relative permittivity, relative permeability, thickness, and resistivity calculations. Finally, monostatic RCS can be formulated based on the scattered far-field amplitude generated.

Beyond RCS modeling of a leaf, one of the resistive sheets used is silvered mylar sheets, a resistive film for a very thin layer-“window tinting” which is applied to automobiles.

Sheets can also be extended to strips or plates of arbitrary shapes which multiply diffracted field appear for finite edges of strip (or plate). (Herman 1987) The GTD technique is involved in the diffraction solution instead of the PO method. Mutual edge effects dominate in the strip’s geometry. Non-optical behavior of the field exists the second edge after diffraction from the first one. The uniform diffraction coefficient is calculated from the surface current on the oblique incidence half plane, of which the boundary condition is satisfied. For a perfectly conducting case, UTD was applied. (Kouyoumjian 1974) The application of modeling strip is an extension of modeling a leaf for plate-like objects. Obviously, the edge effect and multi-diffraction give rise to more advanced techniques (GTD, UTD) and mathematical difficulty.

3.2 Motivation for detailed analysis

According to electrical size in terms of λ , the RCS modeling of debris type is divided into three different regimes: (a) $D \ll \lambda$ lies in the Rayleigh region, where D is the diameter of the object and is suitable for modeling sand and dust; (b) $D \approx \lambda$ lies away from the Rayleigh region and beyond the optical region for medium-size objects, and is suitable for modeling leaves and twigs. Both specular reflection scattering and polarization behavior demonstrate in this region; (c) $D \gg \lambda$ lies closely to the optical region for larger objects and is suitable for modeling tree branches and roof shingles. Specular reflection scattering mainly demonstrated in this region.

By identifying different regimes, dust and sand can be modeled as electrically small spheroids using the T-matrix method (Mishcheko 2000; Bodine 2014), but this is not suitable for PO. Mostly flat and electrically large-diameter plate-like objects such as leaves, tree branches, endcaps for cylinders, wood boards, drywall, foam, metal plates, and other housing materials are suitable for PO.

3.2.1 Circular vs. rectangular

Both circular and rectangular plates can be setup by two different paths with integrations and differentiation to calculate a radiation field; detailed analysis is in following sections. If both shapes are required to have a finite geometry, the upper and lower limit of a radiation integral is a fixed number called a “truncated” current. PO method is suitable for

both rectangular and circular geometries. The radiation field can be obtained by integrating the induced current on the surface. For convenience, the cylindrical coordinate system is used to set up geometry for RCS of the circular plate calculation. Similarly, the Cartesian coordinate system facilitates the RCS calculation for rectangular plates.

3.2.2 Metal vs. dielectric (penetrable vs. non-penetrable)

Mathematically, the electric behavior of metal plates is very close to perfect electrical conducting (PEC) plates, and is much easier to derive in comparison to dielectric plates. Instead of calculating the current from RCS calculations, the surface impedance concept is introduced and defined as the relationship between tangential components of E field and H field, $\eta_s = E_{\text{tan}} / H_{\text{tan}}, Z_s = \eta_s / \eta_0$; this is normal to free space on surface S. Surface impedance is approximate to simplify the RCS calculations for complex objects represented by both rectangular and circular plates. Surface impedance approximation is an extension of PO, which is modified based on the surface equivalence principle where the impedance boundary condition (IBC) is applied. Surface impedance can be complex and a function of an incident angle; it is not necessary for there to be a “real” physical impedance. Although surface impedance is an approximation, it is a quite useful technique with the most accurate results at the normal incident angle.

For metal plates, assume that there are no magnetic currents $\eta_s = 0 \rightarrow E_{\tan} = 0$. For dielectric plates, there is an additional term magnetic current added in the far-field radiation integral. For TM polarization, the difference from the PEC plate has the extra term-magnetic current added. Obviously, there is a loss in the radiation integral resulting in a loss within the radiation field.

3.2.3 Thick plates vs. thin plates

By calculating the reflection coefficient on each boundary, it is possible to solve multilayered structures. The impedance on the right side of a single layer onto the first boundary is embedded within the calculation of the reflection coefficient in front of the second boundary. Therefore, the calculation of the reflection coefficient in the first interface leads to the total reflection coefficient of the single layer. The same rule is applied for multiple-layer structures through impedance calculations inside each layer, which calculate the reflection coefficient in front of the next boundary. Finally, the recursive process is formulated in Balanis's research (Sections 5.5.2.D in Balanis 2012) to calculate the overall reflection coefficient in the first interface for multi-layer structures.

3.2.4 Electrically small vs. electrically-large objects

PO approximation provides an estimate for the unknown currents with relatively accurate results for electrically large bodies (Jenn 2005). When

determining the accuracy of the PO method, the electrical size should be carefully considered. The limitation of PO is that the edge diffraction effects are not taken into account. Other techniques such as GTD consider the edge effect, eliminating this limitation to improve the accuracy. However, considering the edge effect induces a large amount of derivation complexity in math.

3.3 Generic derivation for metal (non-penetrable) objects- rectangular and circular

The basic procedure of calculating RCS consists of differential or integral equation and boundary conditions. Figure 3.1 shows the basic geometry setup for the source and target.

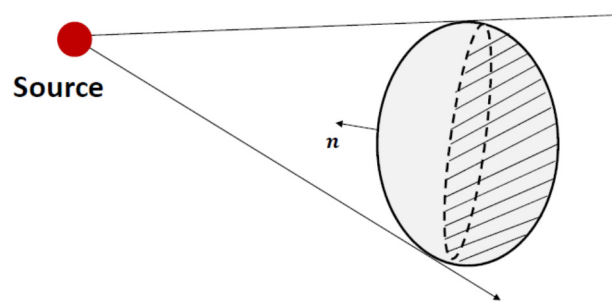


Figure 3.1: Illustration of setup for the source and target.

(<http://www.eecs.umich.edu/RADLAB/html/techreports/RL681.pdf>)

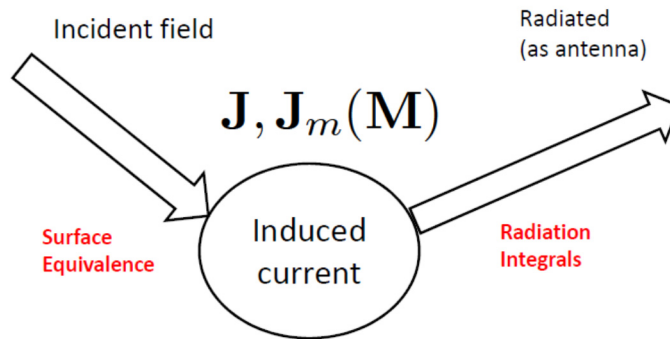


Figure 3.2: Procedure of RCS estimation.

(<http://dspace.mit.edu/bitstream/handle/1721.1/61254/701906470.pdf>)

After the induced current generated through the incident field is transmitted, the radiation field can be obtained by integrating this current. The current must radiate in an unbounded homogenous medium. The observation point can be anywhere.

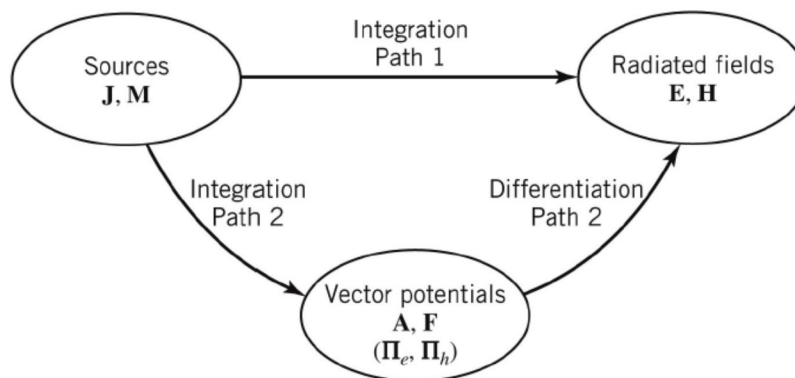


Figure 6-1
© John Wiley & Sons, Inc. All rights reserved.

Figure 3.3: Block diagram for computing radiated fields from electric and magnetic sources. (Source: C.A. Balanis, *Antenna Theory: Analysis and Design*. 3rd Edition, Copyright 2005, John Wiley & Sons, Inc.)

There are two paths to get the radiated field. The first path is to use the approximation in the radiation integral to get the radiation field.

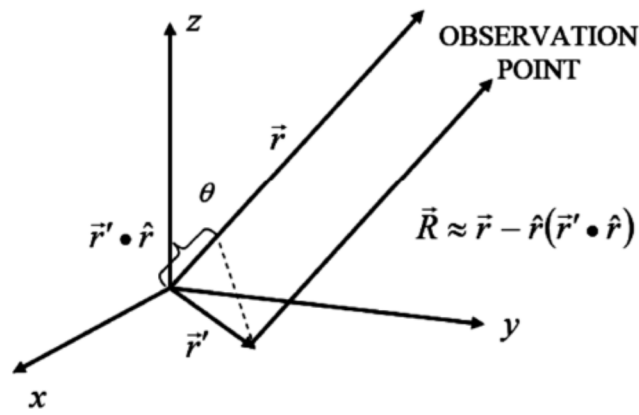


Figure 3.4: Target far-field geometry approximation

(<http://faculty.nps.edu/jenn/EC4630/TheoremsandConceptsV2.pdf>)

$$R = |\vec{r} - \vec{r}'| \approx r - \hat{r} \cdot \vec{r}' \quad (3.1)$$

$$\hat{r} = \hat{x}u + \hat{y}v + \hat{z}w \quad (3.2)$$

Because the observation point in RCS calculation is assumed in the far field, only the current flowing on the object in reality is of interest. The distance R can be viewed approximately parallel to the direction of radiation.

u, v, w are the direction cosine described as:

$$u = \cos \alpha_x = \sin \theta \cos \phi, v = \cos \alpha_y = \sin \theta \sin \phi, \quad (3.3)$$

Using the path 1 integration and (3.1), the radiation E field is:

$$\vec{E}(\vec{r}) = \frac{-j\omega\mu}{4\pi} \left(\frac{e^{-jkr}}{r} \right) \iiint_v \left[\vec{J}(\vec{r}') - \hat{r}(\vec{J}(\vec{r}') \cdot \hat{r}) + \frac{\vec{J}_m(\vec{r}') \times \hat{r}}{\eta} \right] e^{jk\vec{r}' \cdot \hat{r}} dv' \quad (3.4)$$

The electrical tangential component in terms of spherical coordinate system can be obtained as:

$$E_\theta(P) = \frac{-jk\eta}{4\pi} \left(\frac{e^{-jkr}}{r} \right) \iiint_v \left[\vec{J}(\vec{r}') \cdot \hat{\theta} + \frac{\vec{J}_m(\vec{r}') \cdot \hat{\phi}}{\eta} \right] e^{jk\vec{r}' \cdot \hat{r}} dv' \quad (3.5)$$

$$E_\phi(P) = \frac{-jk\eta}{4\pi} \left(\frac{e^{-jkr}}{r} \right) \iiint_v \left[\vec{J}(\vec{r}') \cdot \hat{\phi} - \frac{\vec{J}_m(\vec{r}') \cdot \hat{\theta}}{\eta} \right] e^{jk\vec{r}' \cdot \hat{r}} dv' \quad (3.6)$$

where $g = \vec{r}' \cdot \hat{r} = x'u + y'v + z'w$, the total field at the observation point is

$$\vec{E}(P) = E_\theta(P)\hat{\theta} + E_\phi(P)\hat{\phi} \quad (3.7)$$

3.3.1 Generic derivation for metal (non-penetrable)-perfect conducting rectangular plates

PO is used to derive the RCS of a perfect conducting rectangular plate in the x-y plane; the incident wave is arbitrarily polarized. (Jenn 2005)

$$\vec{E}_i = (E_{0\theta}\hat{\theta} + E_{0\phi}\hat{\phi})e^{-jk_i \cdot \vec{r}} \quad (3.8)$$

The observation point at $P(x, y, z) = P(r, \theta, \phi)$ to get the PO current is:

$$\vec{H}_i = \frac{\hat{k}_i \times \vec{E}_i}{\eta_0} = \frac{-\hat{r}_i \times (E_{0\theta}\hat{\theta} + E_{0\phi}\hat{\phi})e^{-jk_i \cdot \vec{r}'}}{\eta_0} = -(E_{0\theta}\hat{\phi} - E_{0\phi}\hat{\theta}) \frac{e^{-jk_i \cdot \vec{r}'}}{\eta_0} \quad (3.9)$$

$$\text{Then, } \vec{J}_s \approx 2\hat{n} \times \vec{H}_i = -2\hat{z} \times (E_{0\theta}\hat{\phi} - E_{0\phi}\hat{\theta}) \frac{e^{-jk_i \cdot \vec{r}'}}{\eta_0} \quad (3.10)$$

The final expression for the PO current is

$$\vec{J}_s \approx -\frac{2e^{jkh}}{\eta_0} \left[\underbrace{\hat{x}(E_{0\theta} \cos \phi - E_{0\phi} \cos \theta \sin \phi)}_{J_{sx}} + \underbrace{\hat{y}(E_{0\theta} \sin \phi + E_{0\phi} \cos \theta \cos \phi)}_{J_{sy}} \right] \quad (3.11)$$

The θ component of the scattered field is

$$E_\theta(P) = -\frac{jk\eta_0}{4\pi} \left(\frac{e^{-jkr}}{r} \right) \iint_S \frac{2e^{jkh}}{\eta_0} (J_{sx}\hat{x} + J_{sy}\hat{y}) \cdot \hat{\theta} e^{jkg} dx' dy' \quad (3.12)$$

$$\text{where } h \equiv \hat{k}_i \cdot \vec{r}' = x'u_i + y'v_i + z'w_i \quad (3.13)$$

$$g = \hat{k} \cdot \vec{r}' = x'u + y'v + z'w \quad (3.14)$$

$$\text{For monostatic: } u = u_i, v = v_i, w = w_i, \theta = \theta_i, \phi = \phi_i, g = h \quad (3.15)$$

$$E_{\theta}(P) = -\frac{jk}{2\pi} \left(\frac{e^{-jkr}}{r} \right) \int_{-a/2}^{a/2} \int_{-b/2}^{b/2} (J_{sx}\hat{x} + J_{sy}\hat{y}) \cdot \hat{\theta} e^{j2kg} dx' dy' \quad (3.16)$$

$$\text{For TM incidence wave: } E_{0\theta} = 1, E_{0\phi} = 0 \quad (3.17)$$

$$E_{\theta}(P) = -\frac{jk}{2\pi r} e^{-jkr} \cos \theta \int_{-a/2}^{a/2} e^{j2x'u} dx' \int_{-b/2}^{b/2} e^{j2y'v} dy' \quad (3.18)$$

$$E_{\theta}(P) = -\frac{jkab}{2\pi r} e^{-jkr} \cos \theta \sin c(kau) \sin c(kbv) \quad (3.19)$$

Applying RCS definition:

$$\sigma = \lim_{r \rightarrow \infty} 4\pi r^2 \frac{|E_{\theta}(P)|^2}{|E_{0\theta}|^2} = \frac{4\pi A^2}{\lambda^2} \cos^2 \theta \sin^2 c(kau) \sin^2 c(kbv) \quad (3.20)$$

$$\sigma = \frac{4\pi A^2}{\lambda^2} \text{ at } \theta = 0^\circ \text{ for normal incidence.} \quad (3.21)$$

3.3.2 Generic derivation for metal (non-penetrable)-perfect conducting circular plates

Assuming a surface circular plate of radius a lies in the x-y plane, the geometry setup is similar to Figure 3.4. A TM polarized plane wave is incident on the plane from the direction (θ, ϕ) , and the wave is propagating towards the origin $\vec{H}_i = \hat{\phi} H_0 e^{-j\vec{k}_i \cdot \vec{r}}$, $\hat{k}_i = -\hat{r}$. Again, the physical optics approximation technique is used with these assumptions:

$$\hat{r} = \hat{x}u + \hat{y}v + \hat{z}w \quad u = \sin \theta \cos \phi, \quad v = \sin \theta \sin \phi, \quad w = \cos \theta, \quad (3.22)$$

$$-\hat{k}_i \cdot \vec{r}' = \rho' \sin \theta \cos(\phi - \phi') \quad -\vec{k}_i \cdot \vec{r}' = k\rho' \sin \theta \cos(\phi - \phi') \quad (3.23)$$

$$\vec{J}_s = \begin{cases} 2\hat{n} \times \vec{H}_i & \text{illuminated portion} \\ 0 & \text{shadowed portion} \end{cases} \quad (3.24)$$

$$\vec{J}_s = -2H_0(\hat{x} \cos \phi + \hat{y} \sin \phi) e^{jk\rho' \sin \theta \cos(\phi - \phi')} \quad (3.25)$$

Applying the component of electric field tangential to sphere at radius r (Jenn 2005):

$$E_\theta(x, y, z) = \frac{-jk\eta}{4\pi r} e^{-jkr} \iiint_V \left[\vec{J} \cdot \hat{\theta} + \frac{1}{\eta} \vec{J}_m \cdot \hat{\phi} \right] e^{jk\vec{r}' \cdot \hat{r}} dv' \quad (3.26)$$

Since PEC circular plate $\vec{J}_m = 0$, the $E_\theta(x, y, z)$ becomes

$$E_\theta(\theta, \phi) = \frac{-jk\eta}{4\pi r} e^{-jkr} \iint_S \vec{J} \cdot \hat{\theta} \bullet e^{jk\vec{r}' \cdot \hat{r}} dv' \quad (3.27)$$

and the final result becomes

$$E_\theta(\theta, \phi) = \frac{j\eta a H_0 \cos \theta}{2r \sin \theta} e^{-jkr} J_1(2ka \sin \theta) \quad (3.28)$$

$$\text{When } \theta = 0, \quad E_\theta(\theta, \phi) = \frac{jk\eta H_0 a^2}{2r} e^{-jkr} \quad (3.29)$$

the final RCS becomes

$$\begin{aligned} \sigma(\theta, \phi) &= \lim_{r \rightarrow \infty} 4\pi r^2 \frac{|E_s|^2}{|E_i|^2} = \lim_{r \rightarrow \infty} 4\pi r^2 \frac{|E_\theta(\theta)|^2}{|\eta H_i|^2} \\ &= \frac{\pi a^2 \cos^2 \theta J_1^2(2ka \sin \theta) |j|^2}{\sin^2 \theta} \end{aligned} \quad (3.30)$$

$$\text{for } \theta = 0, \quad \sigma(0) = \pi k^2 a^4 |j|^2 \quad (3.31)$$

Due to the duality theorem, the magnitude is opposite by applying the

$$H_0 \rightarrow -E_0$$

$$H_\theta(\theta, \phi) = \frac{-jaE_0 \cos \theta}{\eta 2r \sin \theta} e^{-jkr} J_1(2ka \sin \theta) \quad (3.32)$$

The RCS for TE mode

$$\sigma(\theta, \phi) = \frac{\pi a^2 \cos^2 \theta J_1^2(2ka \sin \theta) |-j|^2}{\sin^2 \theta} \quad (3.33)$$

$$\sigma(\theta, \phi) = \frac{\pi a^2 \cos^2 \theta J_1^2(2ka \sin \theta) |-je^{jkl \cos \theta}|^2}{\sin^2 \theta} \quad (3.34)$$

Phase shift $e^{jkl \cos \theta}$ is applied to the RCS formula of a perfect circular plate. Formulation (3.34) is used for conducting cylinder endcap in Chapter 4.

3.3.3 Simulation vs. analytical results-conducting circular

plates

Circular plates with a thickness of 0.001 wavelengths (λ), 0.1 wavelengths (λ), and greater than one wavelength in diameter detour from the Rayleigh region; the analytical results of conducting circular thin sheets and plates are in good agreement with HFSS. Some examples of the comparison between HFSS simulation and MATLAB are demonstrated here.

Metal thin sheet (0.0001 ($\sim 0.001 \lambda$) meters) is very similar to a perfect conducting plate (0.01 ($\sim 0.1 \lambda$) meters), as the incident angle is less than 40 degrees for HFSS except the incident angle is close to 90 degrees(edge) with different thickness. Analytical results for metal sheets and plates are the same. These differences indicate that edge effect has a contribution to RCS in HFSS simulation while it is ignored by PO.

3.3.3.1 Small (radius $< 0.5 \lambda$) conducting circular plates

For thickness at 0.0001 ($\sim 0.001 \lambda$) meters:

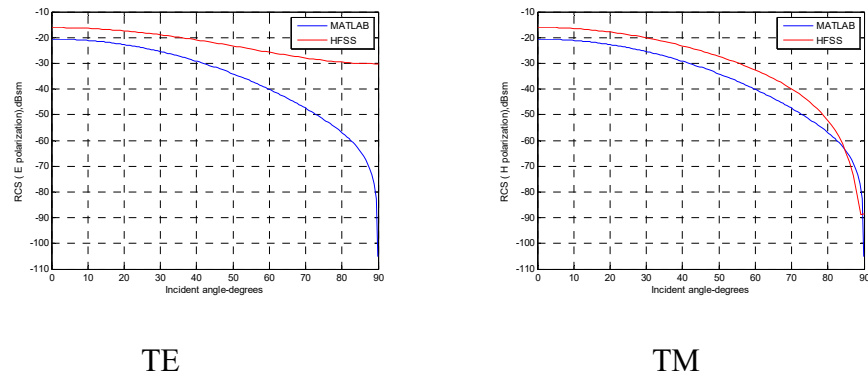
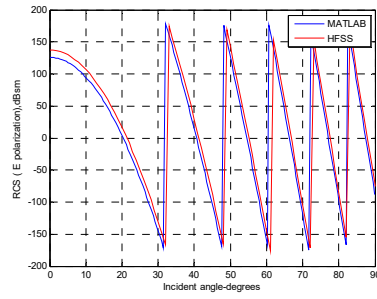
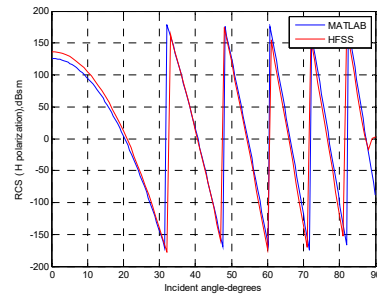


Figure 3.5: Amplitude comparison for TE and TM mode in MATLAB and HFSS (offset 0.0001 ($\sim 0.001 \lambda$) meters in thickness by 0.03 ($\sim 0.27 \lambda$) meters in radius for a metal thin sheet ($\epsilon_r = 10^6$) located in half of $L = 0.6$ ($\sim 6 \lambda$) meters). Amplitudes show a few dB differences for TE and TM.



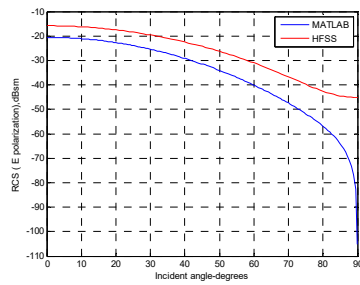
TE



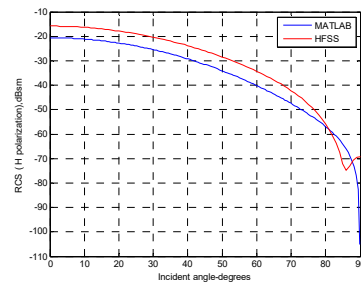
TM

Figure 3.6: Phase comparison for TE and TM mode in MATLAB and HFSS (offset 0.0001 ($\sim 0.001 \lambda$) meters in thickness by 0.03 ($\sim 0.27 \lambda$) meters in radius for a metal thin sheet ($= 10^6$) located in half of $L = 0.6$ ($\sim 6 \lambda$) meters). The phase matches well for both TE and TM.

For the same size with thickness at 0.01 ($\sim 0.1 \lambda$) meters:

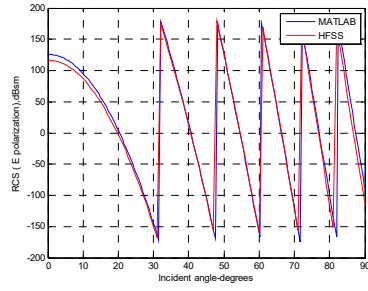


TE

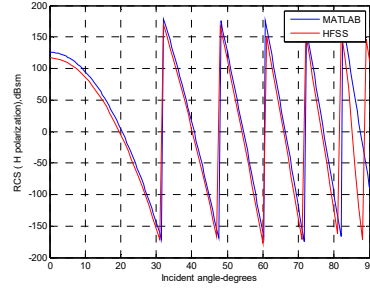


TM

Figure 3.7: Amplitude comparison for TE and TM mode in MATLAB and HFSS (offset 0.01 ($\sim 0.1 \lambda$) meters in thickness by 0.03 ($\sim 0.27 \lambda$) meters in radius for a perfect conducting plate located in half of $L = 0.6$ ($\sim 6 \lambda$) meters). Amplitudes show a few dB differences for both TE and TM.



TE

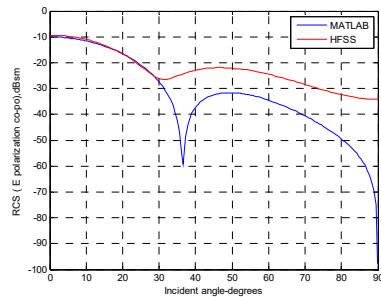


TM

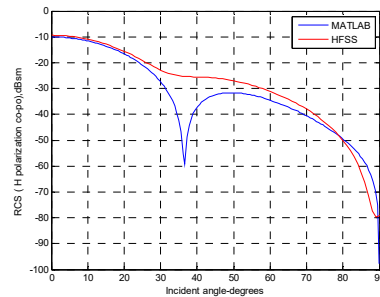
Figure 3.8: Phase comparison for TE and TM mode in MATLAB and HFSS (offset 0.01 ($\sim 0.1 \lambda$) meters in thickness by 0.03 ($\sim 0.27 \lambda$) meters in radius for a perfect conducting plate located in half of $L = 0.6$ ($\sim 6 \lambda$) meters). The phase matches well for TE, and mismatches as the incident angle is close to 90 degrees for TM.

3.3.3.2 Larger (radius $\geq 0.5 \lambda$) conducting circular plates

Metal thin sheet $\epsilon_r = 10^6$ for thickness at 0.00011 ($\sim 0.001 \lambda$) meters:



TE



TM

Figure 3.9: Amplitude comparison for TE and TM mode in MATLAB and HFSS (0.00011 ($\sim 0.001 \lambda$) meters in length by 0.055 ($\sim 0.5 \lambda$) meters in

radius at $\epsilon_r = 10^6$ for a metal thin sheet at half of $L = 0.11$ ($\sim 1 \lambda$) meters).

Amplitudes overlap at 0 degrees for both TE and TM.

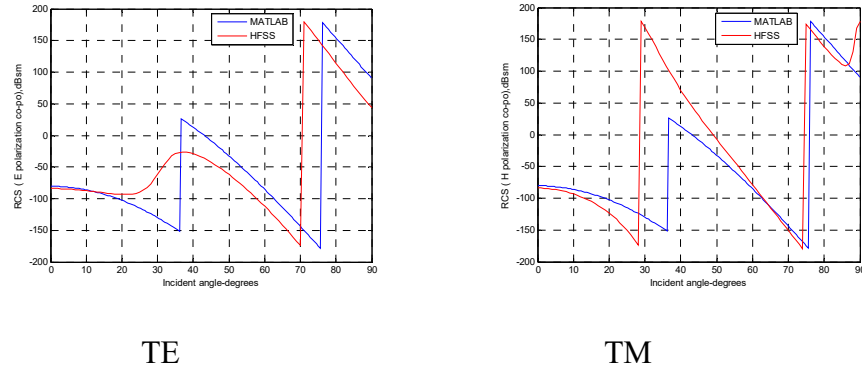


Figure 3.10: Phase comparison for TE and TM mode in MATLAB and HFSS (0.00011 ($\sim 0.001 \lambda$) meters in length by 0.055 ($\sim 0.5 \lambda$) meters in radius at $\epsilon_r = 10^6$ for a metal thin sheet with endcap located at half of $L = 0.11$ ($\sim 1 \lambda$) meters). The phase matches closely for both TE and TM.

For thickness at 0.0001 ($\sim 0.001 \lambda$) meters:

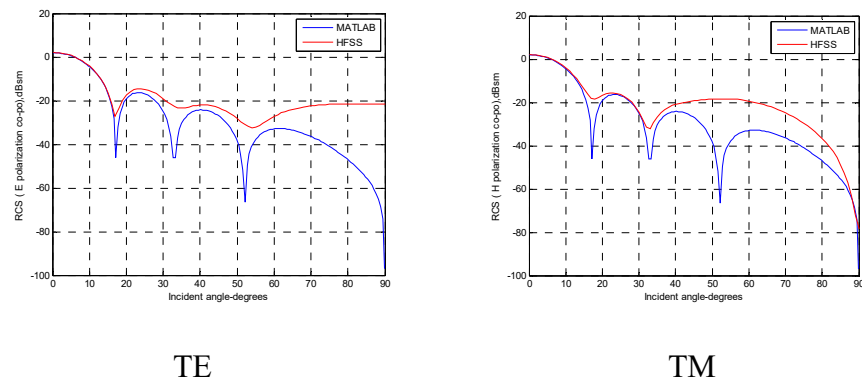


Figure 3.11: Amplitude comparison for TE and TM mode in MATLAB and HFSS (offset 0.0001 ($\sim 0.001 \lambda$) meters in thickness by 0.11 ($\sim 1 \lambda$) meters in radius for a metal ($\epsilon_r = 10^6$) thin sheet located in half of $L =$

1.1 ($\sim 10 \lambda$) meters). Amplitudes match well as the incident angle is less than 30 degrees for both TE and TM.

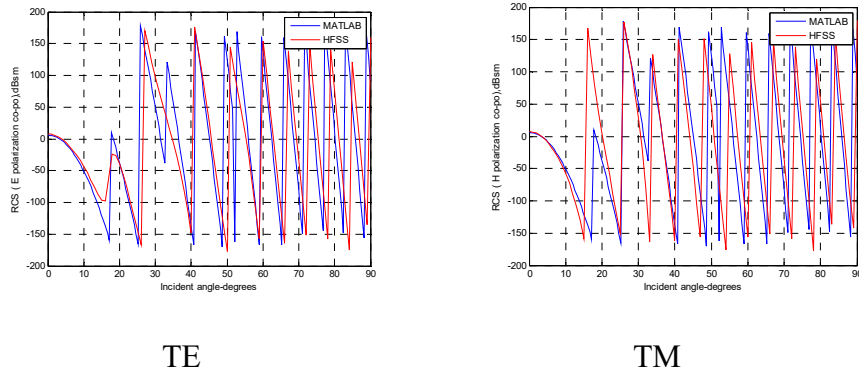


Figure 3.12: Phase comparison for TE and TM mode in MATLAB and HFSS (offset 0.0001 ($\sim 0.001 \lambda$) meters in thickness by 0.11 ($\sim 1 \lambda$) meters in radius for a metal ($\epsilon_r = 10^6$) thin sheet located in half of $L = 1.1$ ($\sim 10 \lambda$) meters). The phase shows a little mismatch for both TE and TM.

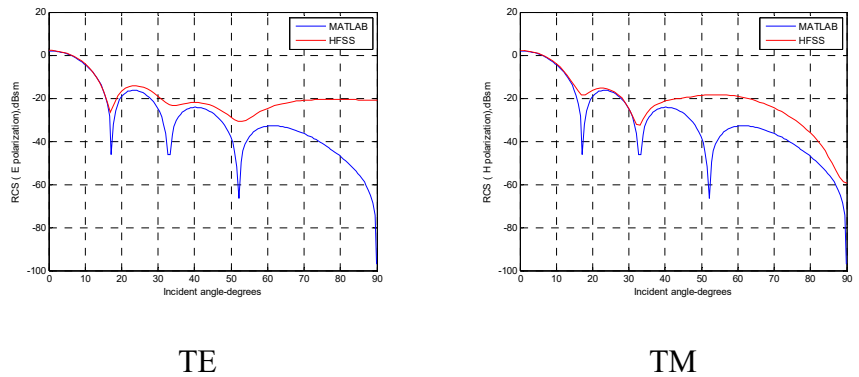


Figure 3.13: Amplitude comparison for TE and TM mode in MATLAB and HFSS (offset 0.001 ($\sim 0.01 \lambda$) meters in thickness by 0.11 ($\sim 1 \lambda$) meters in radius for a conducting thin plate located in half of $L = 1.1$ ($\sim 10 \lambda$) meters).

meters). Amplitudes match well as the incident angle is less than 30 degrees for both TE and TM.

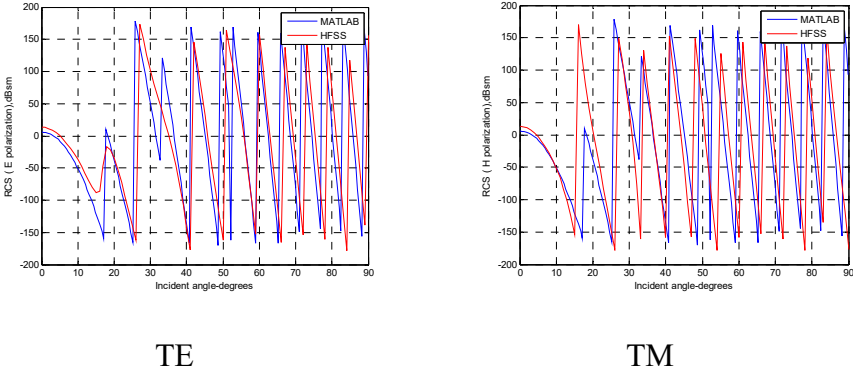


Figure 3.14: Phase comparison for TE and TM mode in MATLAB and HFSS (offset 0.001 ($\sim 0.01 \lambda$) meters in thickness by 0.11 ($\sim 1 \lambda$) meters in radius for a conducting thin sheet located in half of $L = 1.1$ ($\sim 10 \lambda$) meters). The phase shows a little mismatch for both TE and TM.

For the same size as Figure 3.13 with thickness at 0.01 ($\sim 0.1 \lambda$) meters:

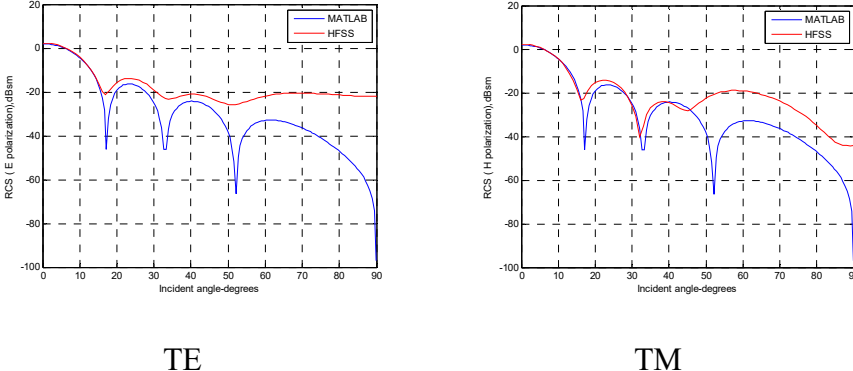


Figure 3.15: Amplitude comparison for TE and TM mode in MATLAB and HFSS (offset 0.01 ($\sim 0.1 \lambda$) meters in thickness by 0.11 ($\sim 1 \lambda$) meters in radius for a conducting thick plate located in half of $L = 1.1$ ($\sim 10 \lambda$) meters).

meters). Amplitudes match well as the incident angle is less than 20 degrees for both TE and TM.

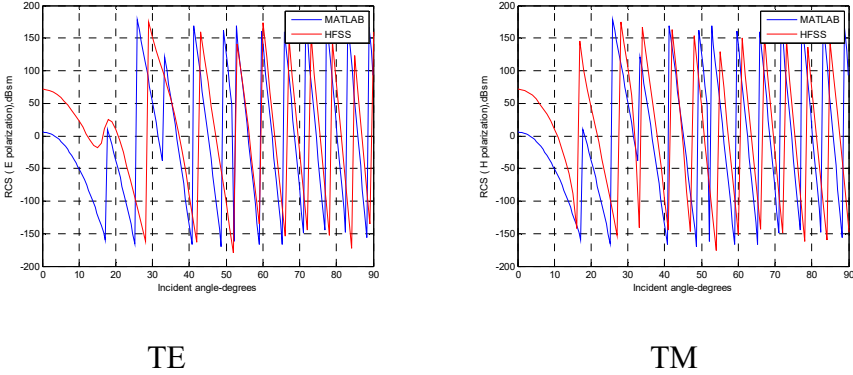


Figure 3.16: Phase comparison for TE and TM mode in MATLAB and HFSS (offset 0.01 ($\sim 0.1 \lambda$) meters in thickness by 0.11 ($\sim 1 \lambda$) meters in radius for a conducting thick plate located in half of $L = 1.1$ ($\sim 10 \lambda$) meters). Slight phase mismatch for TE and TM is observed.

For thickness at 0.0001 ($\sim 0.001 \lambda$) meters:

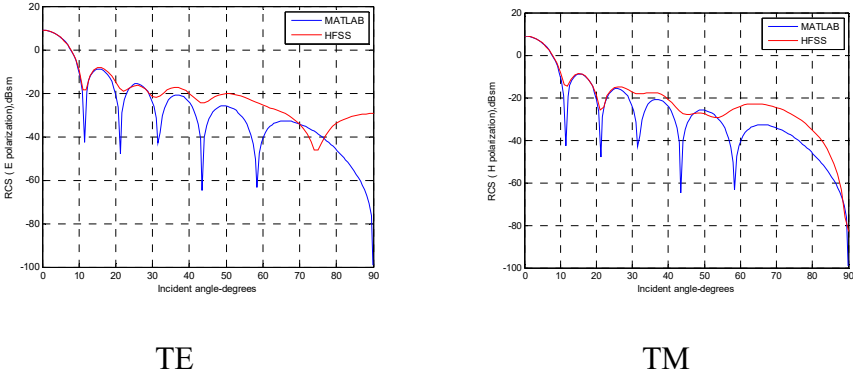


Figure 3.17: Amplitude comparison for TE and TM mode in MATLAB and HFSS (offset 0.0001 ($\sim 0.001 \lambda$) meters in thickness by 0.165 ($\sim 1.5 \lambda$) meters in radius for a metal thin sheet located in half of $L = 3.3$ ($\sim 30 \lambda$)

meters). Amplitudes match well as the incident angle is less than 30 degrees for both TE and TM.

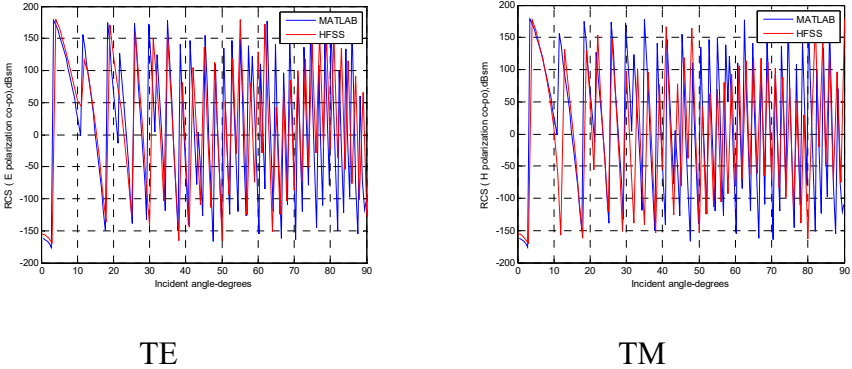


Figure 3.18: Phase comparison for TE and TM mode in MATLAB and HFSS (offset 0.0001 (~0.001 λ) meters in thickness by 0.165 (~1.5 λ) meters in radius for a metal thin plate located in half of $L = 3.3$ (~30 λ) meters). The phase matches well for both TE and TM.

For thickness at 0.0001 (~0.001 λ) meters:

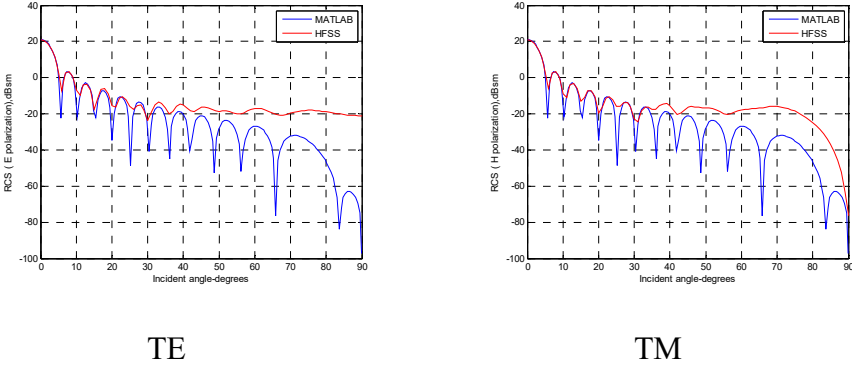
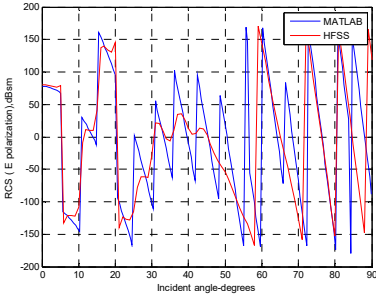
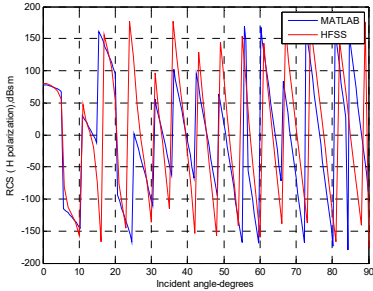


Figure 3.19: Amplitude comparison for TE and TM mode in MATLAB and HFSS (offset 0.0001 (~0.001 λ) meters in thickness by 0.33 (~3 λ) meters in radius for a perfect conducting thin sheet located in half of $L =$

0.8 ($\sim 8 \lambda$) meters). Amplitudes match well as the incident angle is less than 30 degrees for both TE and TM. This plate is relatively large in size and takes 1 hour for HFSS to simulate.



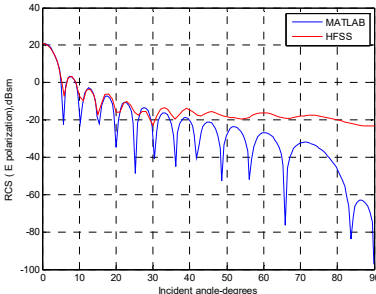
TE



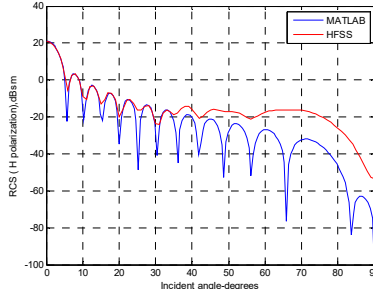
TM

Figure 3.20: Phase comparison for TE and TM mode in MATLAB and HFSS (offset 0.0001 ($\sim 0.001 \lambda$) meters in thickness by 0.33 ($\sim 3 \lambda$) meters in radius for a perfect conducting thin sheet located in half of $L = 0.8$ ($\sim 8 \lambda$) meters). The phase matches closely for both TE and TM. This plate is relatively large in size and takes 1 hour for HFSS to simulate.

For the same size as Figure 3.19 with the thickness at 0.001 ($\sim 0.1 \lambda$) meters:



TE



TM

Figure 3.21: Amplitude comparison for TE and TM mode in MATLAB and HFSS (offset 0.001 ($\sim 0.01 \lambda$) meters in thickness by 0.33 ($\sim 3 \lambda$) meters in radius for a perfect conducting thin sheet located in half of $L = 0.8$ ($\sim 8 \lambda$) meters). Amplitudes match well as the incident angle is less than 30 degrees for both TE and TM. This plate is relatively large in size and takes 1 hour for HFSS to simulate.

Phase term is the same as Figure 3.20.

For the same size with the thickness at 0.01 ($\sim 0.1 \lambda$) meters:

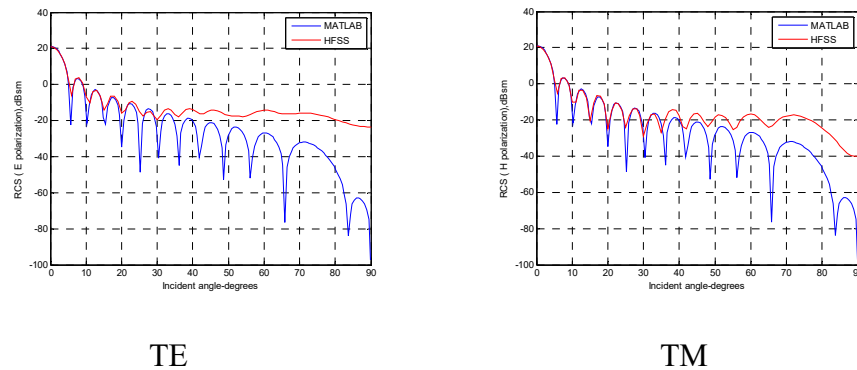


Figure 3.22: Amplitude comparison for TE and TM mode in MATLAB and HFSS (offset 0.01 ($\sim 0.1 \lambda$) meters in thickness by 0.33 ($\sim 3 \lambda$) meters in radius for a perfect conducting plate located in half of $L = 0.8$ ($\sim 8 \lambda$) meters). Amplitudes match well as the incident angle is less than 30 degrees for both TE and TM. This plate is relatively large in size and takes 1 hour for HFSS to simulate.

Phase term is the same as Figure 3.20.

3.3.4 Simulation vs. analytical results – conducting rectangular

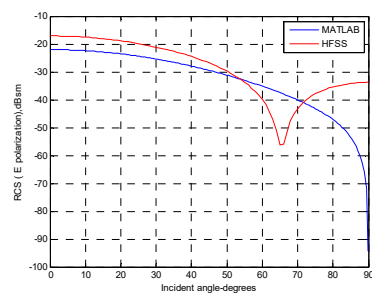
plates

Rectangular plates with a thickness 0.01 wavelength (λ), 0.1 wavelength (λ), or with a length greater than one wavelength on each side, move away from the Rayleigh region and produce better results. Here, some examples of the comparison between HFSS simulation and MATLAB are demonstrated.

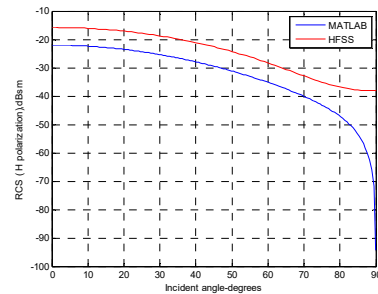
Metal thin plate (0.001 ($\sim 0.01 \lambda$) meters) has very similar amplitude as metal conducting plate (0.01 ($\sim 0.1 \lambda$) meters) as suggested by the incident angle, which is less than 50 degrees in HFSS simulation, but they have different amplitudes as incident angles are close to 90 degrees (edge) in HFSS simulation.

3.3.4.1 Small ($a, b < 1 \lambda$) conducting rectangular plates

For thickness at 0.01 ($\sim 0.1 \lambda$) meters, 0.001 ($\sim 0.01 \lambda$) meters: The phase is not accurate for this size.



TE



TM

Figure 3.23: Amplitude comparison for TE and TM mode in MATLAB and HFSS (offset 0.01 ($\sim 0.1 \lambda$) meters in thickness for a metal rectangular

plate at $a = 0.04$ ($\sim 0.4 \lambda$) meters, $b = 0.06$ ($\sim 0.6 \lambda$) meters located at origin). A few dB differences in amplitude are observed for both TE and TM.

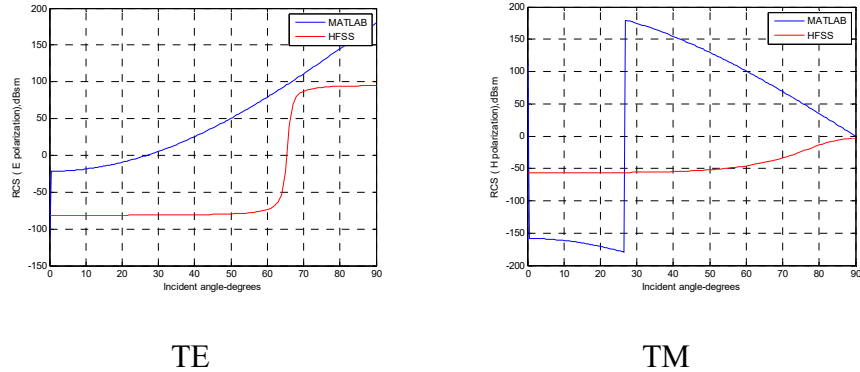


Figure 3.24: Phase comparison for TE and TM mode in MATLAB and HFSS (offset 0.01 ($\sim 0.1 \lambda$) meters in thickness for a metal rectangular plate at $a = 0.04$ ($\sim 0.4 \lambda$) meters, $b = 0.06$ ($\sim 0.6 \lambda$) meters located at origin). The phase mismatch is observed for both TE and TM.

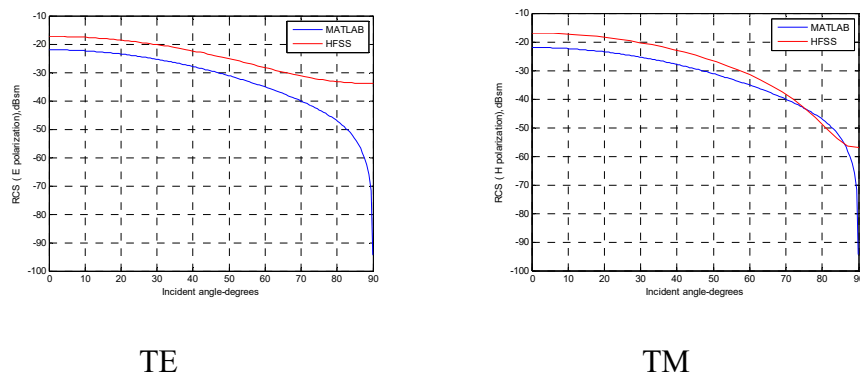


Figure 3.25: Amplitude comparison for TE and TM mode in MATLAB and HFSS (offset 0.001 ($\sim 0.01 \lambda$) meters in thickness for a metal rectangular thin plate at $a = 0.04$ ($\sim 0.4 \lambda$) meters, $b = 0.06$ ($\sim 0.6 \lambda$) meters

located at origin). A few dB differences in amplitude are observed for both TE and TM.

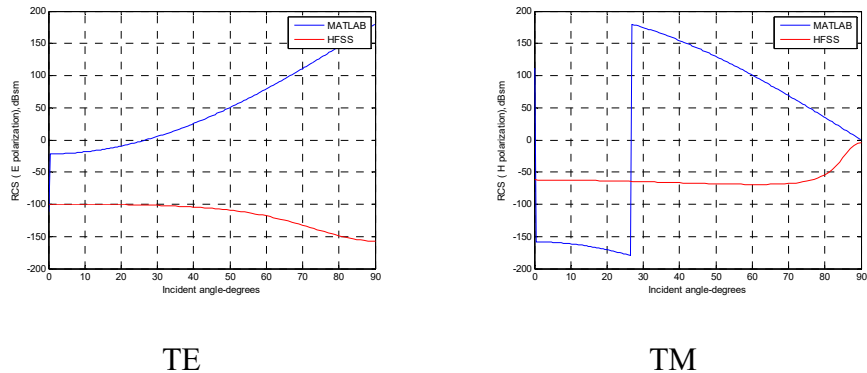


Figure 3.26: Phase comparison for TE and TM mode in MATLAB and HFSS (offset 0.001 ($\sim 0.01 \lambda$) meters in thickness for a metal rectangular thin plate at $a = 0.04$ ($\sim 0.4 \lambda$) meters, $b = 0.06$ ($\sim 0.6 \lambda$) meters located at origin). The phase mismatch is observed for both TE and TM.

3.3.4.2 Large ($a, b \geq 1 \lambda$) conducting rectangular plates

For thickness at 0.01 ($\sim 0.1 \lambda$) meters:

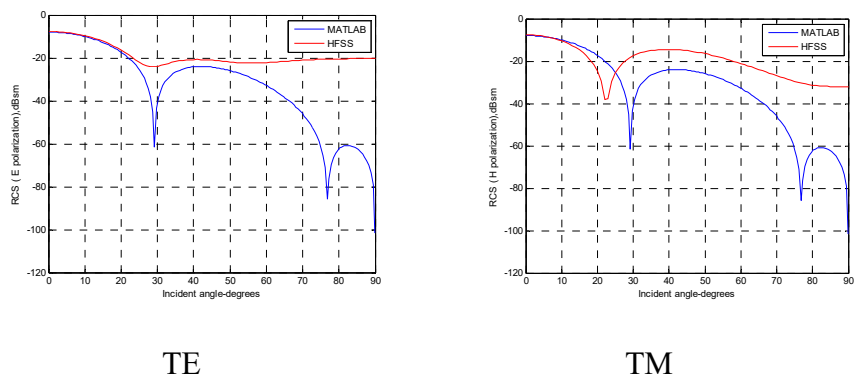


Figure 3.27: Amplitude comparison for TE and TM mode in MATLAB and HFSS (offset 0.01 ($\sim 0.1 \lambda$) meters in thickness for a metal rectangular

plate at $a = 0.11$ ($\sim 1 \lambda$) meters, $b = 0.11$ ($\sim 1 \lambda$) meters located at origin). They match well as the incident angle is less than 30 degrees for both TE and TM.

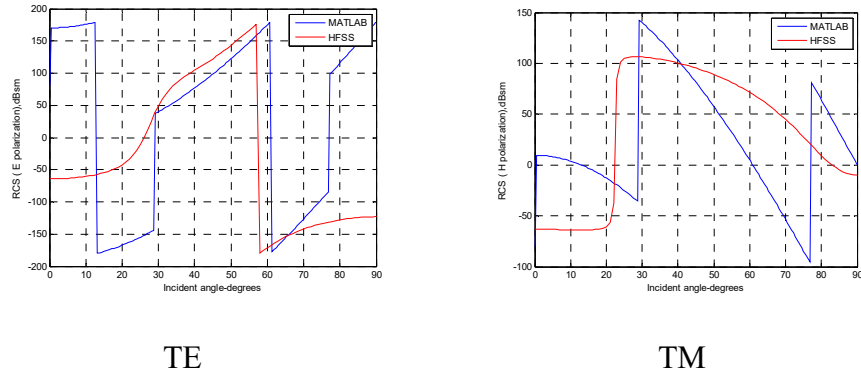


Figure 3.28: Phase comparison for TE and TM mode in MATLAB and HFSS (offset 0.01 ($\sim 0.1 \lambda$) meters in thickness for a metal rectangular plate at $a = 0.11$ ($\sim 1 \lambda$) meters, $b = 0.11$ ($\sim 1 \lambda$) meters located at origin). The phase does not match well for both TE and TM.

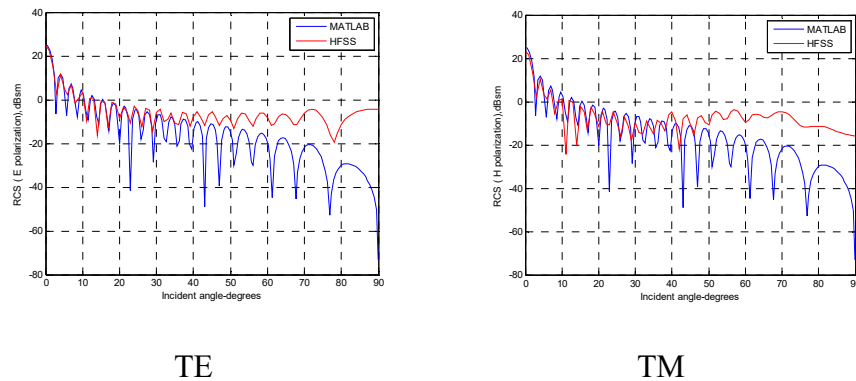


Figure 3.29: Amplitude comparison for TE and TM mode in MATLAB and HFSS (offset 0.01 ($\sim 0.1 \lambda$) meters in thickness for a metal rectangular plate at $a = 1.1$ ($\sim 10 \lambda$) meters, $b = 0.5$ ($\sim 5 \lambda$) meters located at origin).

Amplitudes are in good agreement with HFSS as the incident angle is less than 40 degrees for both TE and TM.

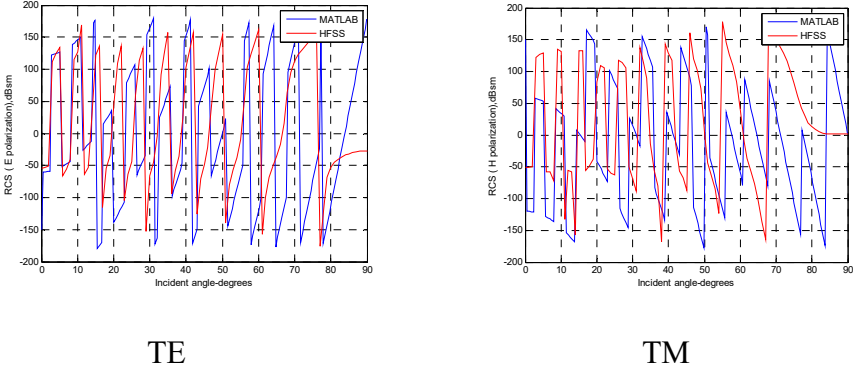


Figure 3.30: Phase comparison for TE and TM mode in MATLAB and HFSS (offset 0.01 (~0.1 λ) meters in thickness for a metal rectangular plate at $a = 1.1$ (~10 λ) meters, $b = 0.5$ (~5 λ) meters located at origin). The phase matches closely for both TE and TM.

3.4 Generic derivation for penetrable objects- rectangular and circular plates

3.4.1 Thin sheet approximation - rectangular

As mentioned earlier, a leaf can be viewed as a resistive thin sheet for a common scatter type in the study of tornadic debris. The derivation of resistive thin sheet follows.

The moisture content of Mg is used to define water content as a fraction in the leaf to the total weight. In our simulation, $Mg = 0.7$. The dielectric constant at 2.8 GHz and room temperature ($T = 22$ °C) (Senior and Sarabandi 1987) is:

$$\varepsilon' = 3.95 \exp(2.79 Mg) - 2.25 \quad (3.33)$$

$$\varepsilon'' = 2.69 \exp(2.15 Mg) - 2.68 \quad (3.34)$$

The complex relative permittivity is $\varepsilon = \varepsilon' - j \varepsilon''$. A leaf can be modeled as an infinite resistive sheet with a thickness τ (mm) and resistivity R. The expressions of τ and R are given by the following

$$\tau = 0.032 Mg^2 + 0.091 Mg + 0.075 \quad (3.35)$$

$$R = \frac{-iZ}{k\tau(\varepsilon - 1)} \quad (3.36)$$

where Z ($= 1/Y$) is the intrinsic impedance and k is the propagation constant of the surrounding free space medium (Harrington 1975). E polarization is based on the incident electric vector perpendicular to the xy plane, and is given as follows (Senior and Sarabandi 1987):

$$\vec{E}^i = \hat{z} e^{ik(x \sin \theta_0 - y \cos \theta_0)} \quad (|\theta_0| \leq \pi/2) \quad (3.37)$$

implying that,

$$\vec{H}^i = -Y(\hat{x} \cos \theta_0 + \hat{y} \sin \theta_0) e^{ik(x \sin \theta_0 - y \cos \theta_0)} \quad (3.38)$$

The reflected and the transmitted electric vector can be written as

$$\vec{E}^r = -\hat{z} \Gamma_E e^{ik(x \sin \theta_0 + y \cos \theta_0)} \quad (3.39)$$

$$\vec{E}^t = \hat{z} T_E e^{ik(x \sin \theta_0 - y \cos \theta_0)} \quad (3.40)$$

The boundary conditions are $[\hat{n} \times \vec{E}]^{\pm} = 0$ where $[\]^{\pm}$ represents the discontinuity across the sheet and $\hat{n} \times (\hat{n} \times \vec{E}) = -R\vec{J}$, where $\vec{J} = [\hat{n} \times \vec{H}]^{\pm}$ is the total electric current.

By applying the boundary conditions, reflection and transmission coefficient constants Γ_E and T_E can be obtained:

$$\Gamma_E = \left(1 + \frac{2R}{Z} \cos \theta_0\right)^{-1} \quad (3.41)$$

$$T_E = \frac{2R}{Z} \cos \theta_0 \Gamma_E \quad (3.42)$$

The current density is $\vec{J} = \hat{z}J_z$ where $J_z = \Gamma_E J_z^{pc}$,

$$J_z = 2Y \cos \theta_0 \Gamma_E e^{ik_x \sin \theta_0} \quad (3.43)$$

Superscript pc denotes the perfect conducting sheet for E polarization and $\Gamma_E=1$ for a perfectly conducting case.

Similarly, for H polarization in which the incident magnetic vector is perpendicular to the plane of incidence, the reflection and transmission coefficients Γ_H and T_H are derived as

$$\Gamma_H = \left(1 + \frac{2R}{Z} \sec \theta_0\right)^{-1} \quad (3.44)$$

$$T_H = \frac{2R}{Z} \sec \theta_0 \Gamma_H \quad (3.45)$$

The current density is $\vec{J} = \hat{x}J_x$, where $J_x = 2\Gamma_H e^{ik_x \sin \theta_0}$, $J_x = \Gamma_H J_x^{pc}$ (3.46)

Surface current J_z and J_x come from the definition of physical optics approximation,

$$\vec{J}_s = \begin{cases} 2\hat{n}\times\vec{H}_i & \text{illuminated portion} \\ 0 & \text{shadowed portion} \end{cases} \quad (3.47)$$

Where \vec{H}_i denotes incident magnetic field intensity at the surface, and \hat{n} denotes the local surface normal unit vector if the surface is PEC.

Similarly, superscript pc denotes the perfect conducting sheet for H polarization, and $\Gamma_H=1$ for a perfectly conducting case.

Then the infinite sheet is truncated to a rectangular 4 cm x 6 cm finite dimension area. By using the physical optics approximation which integrates the surface current J_z and J_x on an infinite sheet, the scattered electric Hertz vector is in the form of

$$\vec{\pi}(\vec{r}) = \hat{z} \frac{iZ}{4\pi k} \int_{-a/2}^{a/2} \int_{-b/2}^{b/2} J_x(x', z') \frac{e^{ik|\vec{r}-\vec{r}'|}}{|\vec{r}-\vec{r}'|} dx' dz' \quad (3.48)$$

$$\text{where } \vec{r} = r(-\hat{x} \sin \theta + \hat{y} \cos \theta) \text{ and } \vec{r}' = \hat{x}x' + \hat{z}z' \quad (3.49)$$

In the far field, the Hertz vector becomes

$$\vec{\pi}(\vec{r}) = \hat{z} \frac{e^{ikr}}{kr} \frac{i}{2\pi} ab \cos \theta_0 \Gamma_E \frac{\sin X}{X} \quad (3.50)$$

$$\begin{aligned} X &= \frac{ka}{2} (\sin \theta + \sin \theta_0) \\ X &= ka \sin \theta_0 \end{aligned} \quad (3.51)$$

with the scattered electric field obtained from the Hertz vector

$$\vec{E}^s = \hat{z} \frac{e^{ikr}}{kr} S(\theta, \theta_0) \quad (3.52)$$

The derivation of the monostatic amplitude and RCS can be calculated as below.

$$\text{The far-field cross section } \sigma \text{ is equal to } \quad \sigma = \frac{\lambda^2}{\pi} |S|^2 \quad (3.53)$$

where S is the far-field amplitude

$$S(\theta, \theta_0) = \frac{i}{2\pi} k^2 ab \cos \theta_0 \Gamma_E \frac{\sin X}{X} \quad (3.54)$$

For monostatic E polarization,

$$S_E(\theta, \theta_0) = \frac{i}{\lambda} 2\sqrt{\pi} ab \cos \theta_0 \Gamma_E \frac{\sin X}{X} \quad (3.55)$$

For monostatic H polarization,

$$S_H(\theta, \theta_0) = -\frac{i}{\lambda} 2\sqrt{\pi} ab \cos \theta_0 \Gamma_H \frac{\sin X}{X} \quad (3.56)$$

$$\sigma_E = \frac{\lambda^2}{\pi} |S_E|^2 = 4\pi \left| \frac{ab}{\lambda} \cos \theta_0 \Gamma_E \frac{\sin X}{X} \right|^2 \quad (3.57)$$

$$\sigma_H = \frac{\lambda^2}{\pi} |S_H|^2 = 4\pi \left| \frac{ab}{\lambda} \cos \theta_0 \Gamma_H \frac{\sin X}{X} \right|^2 \quad (3.58)$$

3.4.2 Multi-layered approach for thicker plates-rectangular

The goal is to figure out the reflection coefficient calculation toward the multi-layered approach of oblique-wave incidence; the idea was to start from the calculation of the reflection coefficient at the boundary of a single slab layer for normal incidence. Two sets of formulations can be used to solve the problem at normal incidence. First, the reflection coefficient is calculated on the first boundary by definition. The

impedance on the right side of first boundary is embedded in the calculation of the reflection coefficient of the second boundary. Therefore, the reflection coefficient in the front of the first interface will be the total reflection coefficient of the single slab (wood board, for example (5-67c, Banalis 2012)). Another set of formulation is carried out to calculate the reflection coefficient individually on each boundary (5-67d, Banalis 2012). The two sets of formulation for a single slab layer are related to each other by the further deriving of one to the other:

$$\begin{aligned}\Gamma_{in}(z = -d^-) &= \frac{Z_{in}(z = -d^+) - \eta_1}{Z_{in}(z = -d^+) + \eta_1} \\ &= \frac{\eta_2 \left[(\eta_3 + \eta_2) + (\eta_3 - \eta_2) e^{-j2\beta_2 d} \right] - \eta_1 \left[(\eta_3 + \eta_2) - (\eta_3 - \eta_2) e^{-j2\beta_2 d} \right]}{\eta_2 \left[(\eta_3 + \eta_2) + (\eta_3 - \eta_2) e^{-j2\beta_2 d} \right] + \eta_1 \left[(\eta_3 + \eta_2) - (\eta_3 - \eta_2) e^{-j2\beta_2 d} \right]}\end{aligned}$$

(Banalis 5-67c) (3.59)

This formula can also be further derived to

$$\Gamma_{in}(z = -d^-) = \frac{\Gamma_{12} + \Gamma_{23} e^{-j2\beta_2 d}}{1 + \Gamma_{12} \Gamma_{23} e^{-j2\beta_2 d}} \quad \text{(Banalis 5-67d)} \quad (3.60)$$

The recursive process is introduced by Balanis (2012) for an oblique incidence of the multilayered approach. It is easy to get confused when implementing the recursive formula. Recursive process is a very common technique in computer science, and it can be anything. Recursive process is an efficient approach for calculating the total reflection coefficient,

either with a single layer or multiple layers considering several parts, which include thickness, refraction angle inside the slab (can be complex for lossy material), phase term, Brewster's angle, etc.

The concept of reflection coefficient calculation in the front of first planar interface of a single layer for a normal incidence helps us understand the physical meaning of reflection and refraction coefficients before matching them into the recursive formulation. By verifying the overall components from the recursive process, the overall reflection and transmission coefficients of the recursive process for perpendicular (horizontal) and parallel (vertical) polarization for multi-layer structures are:

Perpendicular (Horizontal) TE polarization

$$\Gamma_{\perp} = \frac{E_{\perp}^r}{E_{\perp}^i} = \frac{B_0}{A_0} \quad T_{\perp} = \frac{E_{\perp}^t}{E_{\perp}^i} = \frac{1}{A_0} \quad (3.61)$$

Parallel (Vertical) TM polarization

$$\Gamma_{\parallel} = \frac{E_{\parallel}^r}{E_{\parallel}^i} = \frac{D_0}{C_0} \quad T_{\parallel} = \frac{E_{\parallel}^t}{E_{\parallel}^i} = \frac{1}{D_0} \quad (3.62)$$

Then, A_0 , B_0 , C_0 , D_0 can be found through the following recursive formula

$$A_j = \frac{e^{\psi_j}}{2} [A_{j+1}(1+Y_{j+1}) + B_{j+1}(1-Y_{j+1})] \quad (3.63)$$

$$B_j = \frac{e^{-\psi_j}}{2} [A_{j+1}(1-Y_{j+1}) + B_{j+1}(1+Y_{j+1})] \quad (3.64)$$

$$C_j = \frac{e^{\psi_j}}{2} [C_{j+1}(1+Z_{j+1}) + D_{j+1}(1-Z_{j+1})] \quad (3.65)$$

$$D_j = \frac{e^{-\psi_j}}{2} [C_{j+1}(1-Z_{j+1}) + D_{j+1}(1+Z_{j+1})] \quad (3.66)$$

where $A_{N+1} = C_{N+1} = 1$

$$B_{N+1} = D_{N+1} = 0 \quad (3.67)$$

$$Y_{j+1} = \frac{\cos \theta_{j+1}}{\cos \theta_j} \sqrt{\frac{\varepsilon_{j+1}(1-j \tan \delta_{j+1})\mu_j}{\varepsilon_j(1-j \tan \delta_j)\mu_{j+1}}} \quad (3.68)$$

$$Z_{j+1} = \frac{\cos \theta_{j+1}}{\cos \theta_j} \sqrt{\frac{\varepsilon_j(1-j \tan \delta_j)\mu_{j+1}}{\varepsilon_{j+1}(1-j \tan \delta_{j+1})\mu_j}} \quad (3.69)$$

$$\psi_j = d_j \gamma_j \cos \theta_j \quad (3.70)$$

$$\gamma_j = \pm \sqrt{j\omega\mu_j(\sigma_j + j\omega\varepsilon_j)} \quad (3.71)$$

θ_j = complex angle of refraction in the j^{th} layer

d_0 is the distance from the first interface as the reference to the calculation of the reflection and transmission coefficients.

Now, consider the surface impedance-loaded plate, TM polarization using the physical optics approximation. The electric current is given by equation (2.40, Jenn 2005) with $E_{0\phi}=0$:

$$\vec{J}_s \approx 2\hat{n} \times \vec{H}_i = -2E_{0\theta} \hat{z} \times \hat{\phi} \frac{e^{-jk_i \cdot \vec{r}'}}{\eta_0} = 2E_{0\theta} \hat{\rho} \frac{e^{-jk_i \cdot \vec{r}'}}{\eta_0} \quad (3.72)$$

There is also a magnetic current on the surface:

$$\vec{J}_{ms} = -\eta_s \hat{n} \times \vec{J}_s = -2\eta_s E_{0\theta} \hat{z} \times \hat{\rho} \frac{e^{-jk_i \cdot \vec{r}'}}{\eta_0} = -2\eta_s E_{0\theta} \hat{\phi} \frac{e^{-jk_i \cdot \vec{r}'}}{\eta_0} \quad (3.73)$$

The far-field radiation integral has two terms: the electric current terms are the same as the PEC plate, and the magnetic current terms are as follows:

$$\begin{aligned} E_\theta(P) &= \frac{-jk\eta}{4\pi r} e^{-jkr} \iint_s (\vec{J} \cdot \hat{\theta} + \frac{\vec{J}_{ms} \cdot \hat{\phi}}{\eta_0}) e^{jkg} dx' dy' \\ &= \frac{-jkE_{0\theta}}{2\pi r} e^{-jkr} \iint_s (\hat{\rho} \cdot \hat{\theta} - \frac{\eta_s \hat{\phi} \cdot \hat{\phi}}{\eta_0}) e^{j2kg} dx' dy' \end{aligned} \quad (3.74)$$

Separable integral results

$$\begin{aligned} E_\theta(P) &= \frac{-jkE_{0\theta}}{2\pi r} e^{-jkr} (\cos\theta - Z_s) \int_{-a/2}^{a/2} e^{j2x'u} dx' \int_{-b/2}^{b/2} e^{j2y'v} dy' \\ &= \frac{-jkE_{0\theta}ab}{2\pi r} e^{-jkr} (\cos\theta - Z_s) \sin c(kau) \sin c(kbv) \end{aligned} \quad (3.75)$$

$$\sigma_{\theta\theta} = \frac{4\pi ab}{\lambda^2} |\cos\theta(1 - Z_s / \cos\theta) \sin c(kau) \sin c(kbv)|^2 \quad (3.76)$$

Starting with the Fresnel reflection coefficient for TM polarization

$$\Gamma_{TM} = \frac{\eta_s \cos \theta_t - \eta_0 \cos \theta_i}{\eta_s \cos \theta_t + \eta_0 \cos \theta_i} \approx \frac{Z_s - \cos \theta}{Z_s + \cos \theta} = -\frac{\cos \theta - Z_s}{Z_s + \cos \theta} \approx -(1 - Z_s / \cos \theta) \quad (3.77)$$

under the condition $\theta_t = \theta, \cos \theta_t \approx 1, Z_s \ll \cos \theta$

$$\sigma(\theta, \theta) \approx \sigma_{PEC} |\Gamma_{TM}|^2 \quad (3.78)$$

$$\text{where } \sigma_{PEC} = \frac{4\pi A^2}{\lambda^2} \cos^2 \theta \sin^2 c(kau) \sin^2 c(kbv)$$

$$\text{Similarly, for TE polarization } \sigma(\phi, \phi) \approx \sigma_{PEC} |\Gamma_{TE}|^2 \quad (3.79)$$

S_E, S_H are the far-field amplitudes.

For E polarization

$$S_E = -j \frac{2\sqrt{\pi}}{\lambda} ab \Gamma_E \cos \theta \sin c(kau) \sin c(kbv) \quad (3.80)$$

$$\text{For H polarization } S_H = j \frac{2\sqrt{\pi}}{\lambda} ab \Gamma_H \cos \theta \sin c(kau) \sin c(kbv) \quad (3.81)$$

Γ_E and Γ_H are the same as (3.61) and (3.62).

3.4.3 Generic derivation of penetrable (non-metal) circular plates

3.4.3.1 Surface impedance circular plates (non-metal)

Assume a circular plate of a radius lies in the x-y plane. A TM polarized plane wave is incident on the plane from the direction (θ, ϕ) , and the wave is propagating towards the origin $\vec{H}_i = \hat{\phi} H_0 e^{-jk_i \vec{r}}, \hat{k}_i = -\hat{r}$ again, then the physical optics approximation technique with the assumptions

and a PO modification based on IBC (impedance boundary condition) is applied.

$$-\hat{k}_i \cdot \vec{r}' = \rho' \sin \theta \cos(\phi - \phi') \quad -\vec{k}_i \cdot \vec{r}' = k\rho' \sin \theta \cos(\phi - \phi') \quad (3.82)$$

$$\hat{r} = \hat{x}u + \hat{y}v + \hat{z}w \quad u = \sin \theta \cos \phi, \quad v = \sin \theta \sin \phi, \quad w = \cos \theta, \quad (3.83)$$

$$\vec{J}_s = \begin{cases} 2\hat{n} \times \vec{H}_i & \text{illuminated portion} \\ 0 & \text{shadowed portion} \end{cases} \quad (3.84)$$

and the same \vec{J}_s as the PEC plate

$$\vec{J}_s = -2H_0(\hat{x} \cos \phi + \hat{y} \sin \phi) e^{jk\rho' \sin \theta \cos(\phi - \phi')} \quad (3.85)$$

There is also a magnetic current on the surface

$$\vec{J}_{ms} = -\eta_s \hat{n} \times \vec{J}_s = 2\eta_s \hat{z} \times \hat{\rho} H_0 e^{jk\rho' \sin \theta \cos(\phi - \phi')} \quad (3.86)$$

The component of electric field tangential to sphere at radius r is below (Jenn 2005):

$$E_\theta(x, y, z) = \frac{-jk\eta}{4\pi r} e^{-jkr} \iiint_V \left[\vec{J} \cdot \hat{\theta} + \frac{1}{\eta} \vec{J}_m \cdot \hat{\phi} \right] e^{jk\vec{r}' \cdot \hat{r}} dv' \quad (3.87)$$

In this case, the far-field radiation integral has two components. The electric current term \vec{J}_s is the same as PEC circular plate; the second term is the magnetic current \vec{J}_{ms} , and the $E_\theta(x, y, z)$ becomes

$$E_\theta(\theta, \phi) = \frac{-jk\eta}{4\pi r} e^{-jkr} \iint_S \left(\vec{J} \cdot \hat{\theta} + \frac{\vec{J}_{ms} \cdot \hat{\phi}}{\eta_0} \right) e^{jk\vec{r}' \cdot \hat{r}} ds \quad (3.88)$$

The final result becomes

$$E_\theta(\theta, \phi) = \frac{-j\eta_0 a H_0}{2r \sin \theta} \left(-\cos \theta + \frac{\eta_s}{\eta_0} \right) e^{-jkr} J_1(2ka \sin \theta) \quad (3.89)$$

$$\text{when } \theta = 0, \quad E_{\theta}(\theta, \phi) = \frac{-jk\eta_0 H_0 a^2}{2r} \left(-1 + \frac{\eta_s}{\eta_0}\right) e^{-jkr} \quad (3.90)$$

The final RCS for TM mode becomes

$$\begin{aligned} \sigma(\theta, \phi) &= \lim_{r \rightarrow \infty} 4\pi r^2 \frac{|E_s|^2}{|E_i|^2} = \lim_{r \rightarrow \infty} 4\pi r^2 \frac{|E_{\theta}(\theta)|^2}{|\eta H_i|^2} \\ &= \frac{\pi a^2 \left(-\cos \theta + \frac{\eta_s}{\eta_0}\right)^2 J_1^2(2ka \sin \theta) |j|^2}{\sin^2 \theta} \end{aligned} \quad (3.91)$$

$$\text{for } \theta = 0, \quad \sigma(0) = \pi k^2 a^4 \left(-1 + \frac{\eta_s}{\eta_0}\right)^2 |j|^2 \quad (3.92)$$

$$\text{where } Z_s = \frac{\eta_s}{\eta_0} = \frac{n_1}{n_2}, \quad (3.93)$$

n_1 and n_2 are the refractive index of the surrounding medium and the inside of a cylinder.

Due to the duality theorem, the magnitude is opposite by applying the

$$H_0 \rightarrow -E_0, E_0 \rightarrow H_0$$

$$H_{\theta}(\theta, \phi) = \frac{jaE_0}{\eta_0 2r \sin \theta} \left(-\cos \theta + \frac{\eta_s}{\eta_0}\right) e^{-jkr} J_1(2ka \sin \theta) \quad (3.94)$$

$$\text{when } \theta = 0, \quad H_{\theta}(\theta, \phi) = \frac{jka^2 E_0}{\eta_0 2r} \left(-1 + \frac{\eta_s}{\eta_0}\right) e^{-jkr} \quad (3.95)$$

The final RCS for TE mode is

$$\sigma(\theta, \phi) = \frac{\pi a^2 \left(-\cos \theta + \frac{\eta_s}{\eta_0}\right)^2 J_1^2(2ka \sin \theta) |j|^2}{\sin^2 \theta} \quad (3.96)$$

A phase shift $e^{jkl \cos \theta}$ is added to the amplitude of RCS of endcaps for far-field. This formula is used for dielectric cylinder endcap in Chapter 4.

3.4.3.2 General non-metal circular plates (sheets)

Since the Fresnel reflection coefficient for TM polarization is

$$\Gamma_{TM} = \frac{\eta_s \cos \theta_t - \eta_0 \cos \theta_i}{\eta_s \cos \theta_t + \eta_0 \cos \theta_i} \approx \frac{Z_s - \cos \theta}{Z_s + \cos \theta} \approx Z_s - \cos \theta \approx -(1 - Z_s' \cos \theta) \quad (3.97)$$

under the condition $\theta_t = \theta, \cos \theta_t \approx 1, Z_s \ll \cos \theta$

compared to conducting circular plate (3.34), non-metal circular can be

obtained approximately via:

$$\sigma(\theta, \theta) \approx \sigma_{PEC} |\Gamma_{TM}|^2 \quad (3.98)$$

$$\sigma(\phi, \phi) \approx \sigma_{PEC} |\Gamma_{TE}|^2 \quad (3.99)$$

The conducting circular plate formula (3.34) is used to derive the non-metal circular plate. The non-metal circular plate formula is derived as

$$\sigma(\theta, \phi) = \frac{\pi a^2 \cos^2 \theta J_1^2(2ka \sin \theta) | -je^{jkL \cos \theta} |^2}{\sin^2 \theta} |\Gamma|^2 \quad (3.100)$$

Γ_{TE} and Γ_{TH} can be obtained from (3.61-3.71).

The non-metal circular thin sheet Γ_{TE} and Γ_{TH} are the same as (3.41) and (3.44)

3.4.3.3 Simulation vs. analytical results for non-metal circular plates

Amplitudes for all selected sizes are in good agreement with HFSS as the incident angle is less than 40 degrees for TM; amplitudes are in good agreement with HFSS for TE. There is a little phase mismatch for TE and TM.

3.4.3.3.1 Small (radius $< 0.5 \lambda$) non-metal circular sheets

For thickness at 0.0001 ($\sim 0.001 \lambda$) meters:

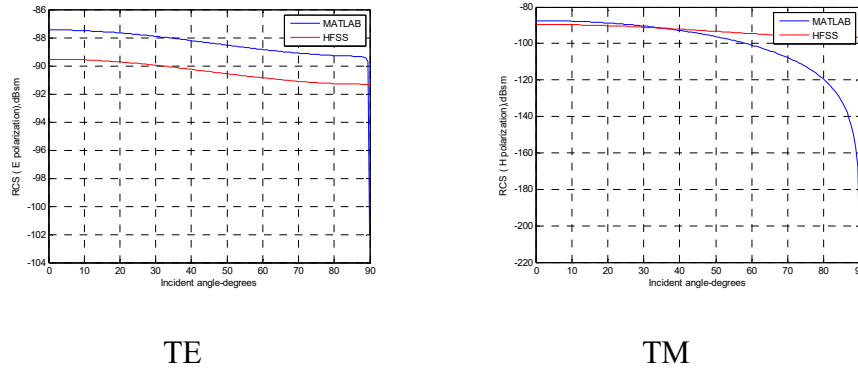


Figure 3.31: Amplitude comparison for TE and TM mode in MATLAB and HFSS (offset 0.0001 ($\sim 0.001 \lambda$) meters in thickness by 0.011 ($\sim 0.1 \lambda$) meters in radius $\epsilon_r = 2.15$ for a thin sheet located in half of $L = 1.1$ ($\sim 10 \lambda$) meters). Amplitudes show a few dB differences for TE with HFSS, and match closely with HFSS as the incident angle is less than 40 degrees for TM.

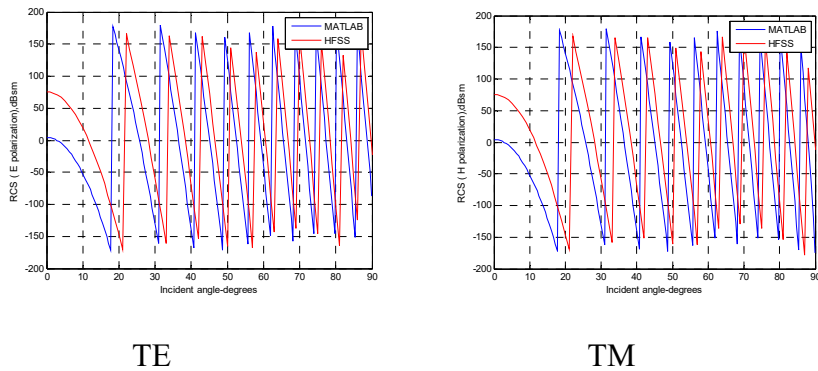


Figure 3.32: Phase comparison for TE and TM mode in MATLAB and HFSS (offset 0.0001 ($\sim 0.001 \lambda$) meters in thickness by 0.011 ($\sim 0.1 \lambda$)

meters in radius dielectric $\epsilon_r = 2.15$ for a thin sheet located in half of $L = 1.1$ ($\sim 10 \lambda$) meters). The phase shows a little mismatch for TE and TM.

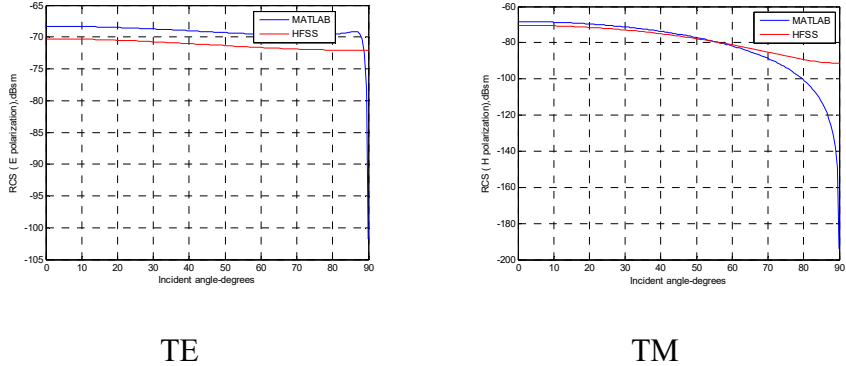


Figure 3.33: Amplitude comparison for TE and TM mode in MATLAB and HFSS (offset 0.0001 ($\sim 0.001 \lambda$) meters in thickness by 0.011 ($\sim 0.1 \lambda$) meters in radius $\epsilon_r = 10-5j$ for a thin sheet located in half of $L = 1.1$ ($\sim 10 \lambda$) meters). Amplitudes show a few dB differences for TE with HFSS, and match closely with HFSS as the incident angle is less than 60 degrees for TM.

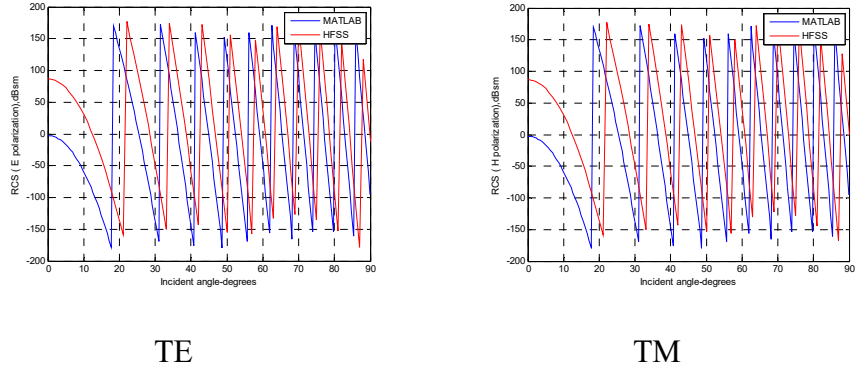


Figure 3.34: Phase comparison for TE and TM mode in MATLAB and HFSS (offset 0.0001 ($\sim 0.001 \lambda$) meters in thickness by 0.011 ($\sim 0.1 \lambda$) meters in radius $\epsilon_r = 10-5j$ for a thin sheet located in half of $L = 1.1$ ($\sim 10 \lambda$) meters). Amplitudes show a few dB differences for TE with HFSS, and match closely with HFSS as the incident angle is less than 60 degrees for TM.

meters in radius dielectric $\epsilon_r = 10-5j$ for a thin sheet located in half of $L = 1.1$ ($\sim 10 \lambda$) meters). The phase shows a little mismatch for TE and TM.

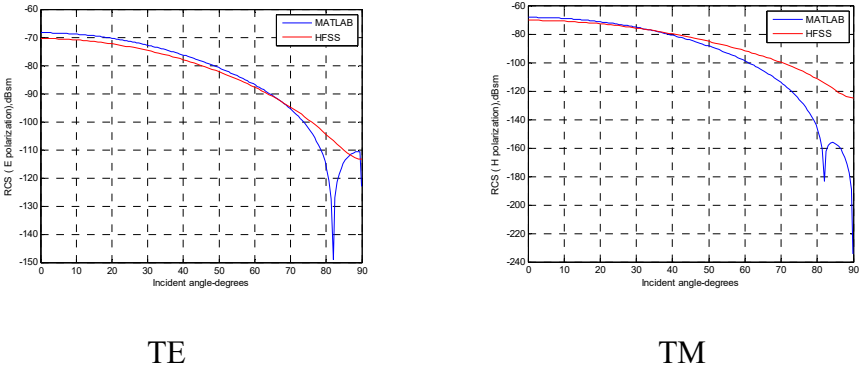


Figure 3.35: Amplitude comparison for TE and TM mode in MATLAB and HFSS (offset 0.0001 ($\sim 0.001 \lambda$) meters in thickness by 0.033 ($\sim 0.3 \lambda$) meters in radius $\epsilon_r = 2.15$ (wood) for a thin sheet located in half of $L = 3.3$ ($\sim 30 \lambda$) meters). Amplitude matches closely with HFSS as the incident angle is less than 70 degrees for TE, and is less than 40 degrees for TM.

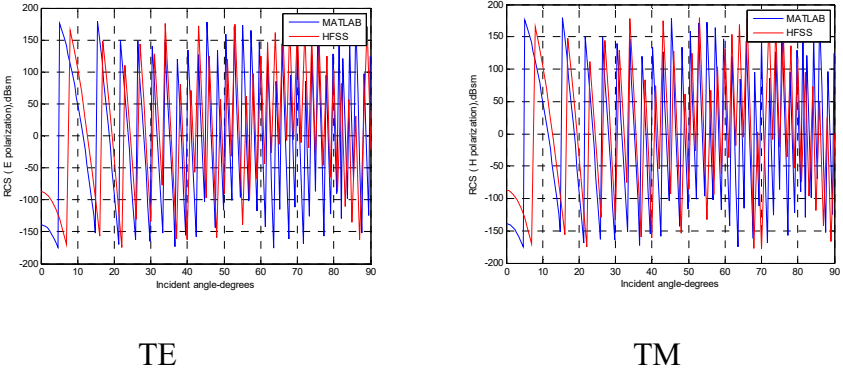


Figure 3.36: Phase comparison for TE and TM mode in MATLAB and HFSS (offset 0.0001 ($\sim 0.001 \lambda$) meters in thickness by 0.033 ($\sim 0.3 \lambda$) meters in radius $\epsilon_r = 2.15$ for a thin sheet located in half of $L = 3.3$ ($\sim 30 \lambda$)

meters). The phase shows a little mismatch, as the incident angle is less than 20 degrees for both TE and TM.

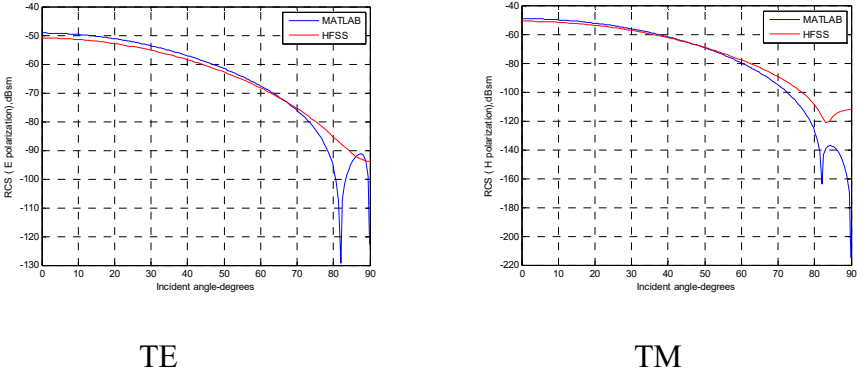


Figure 3.37: Amplitude comparison for TE and TM mode in MATLAB and HFSS (offset 0.0001 ($\sim 0.001 \lambda$) meters in thickness by 0.033 ($\sim 0.3 \lambda$) meters in radius $\epsilon_r = 10-5j$ for a thin sheet located in half of $L = 3.3$ ($\sim 30 \lambda$) meters). Amplitudes show to be very close as the incident angle is less than 70 degrees for TE, and is less than 60 degrees for TM.

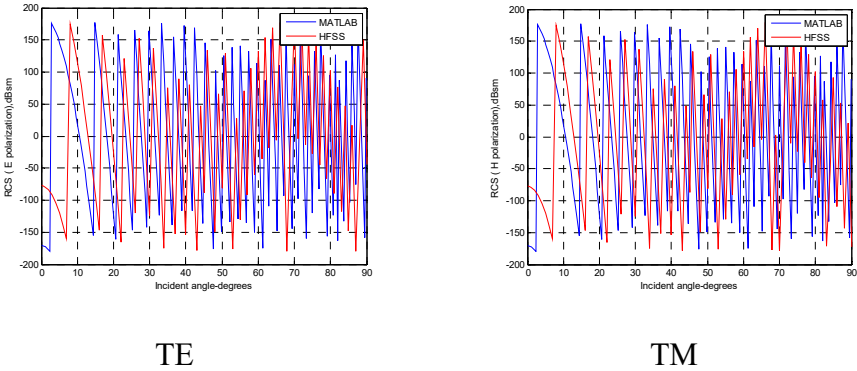
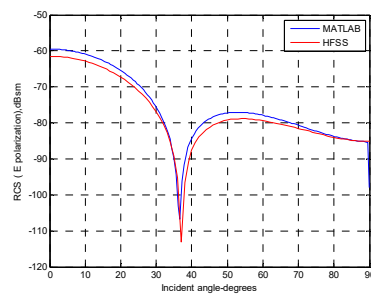


Figure 3.38: Phase comparison for TE and TM mode in MATLAB and HFSS (offset 0.0001 ($\sim 0.001 \lambda$) meters in thickness by 0.033 ($\sim 0.3 \lambda$) meters in radius $\epsilon_r = 10-5j$ for a thin sheet located in half of $L = 3.3$ ($\sim 30 \lambda$) meters).

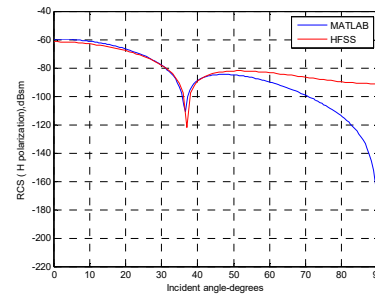
λ) meters). The phase has a little mismatch, as the incident angle is less than 20 degrees for both TE and TM.

3.4.3.3.2 Larger (radius $> 0.5 \lambda$) non-metal circular sheets

For thickness at 0.0001 ($\sim 0.001 \lambda$) meters with $\epsilon_r = 2.15$ and $10^{-5}j$ for different sizes:

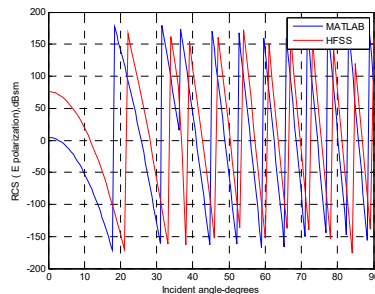


TE

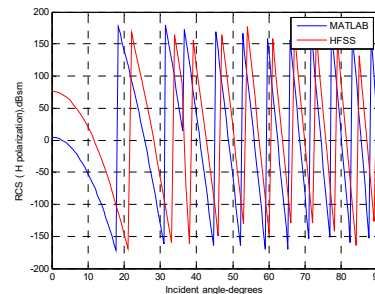


TM

Figure 3.39: Amplitude comparison for TE and TM mode in MATLAB and HFSS (offset 0.0001 ($\sim 0.001 \lambda$) meters in thickness by 0.055 ($\sim 0.5 \lambda$) meters in radius $\epsilon_r = 2.15$ for a thin sheet located in half of $L = 1.1$ ($\sim 10 \lambda$) meters). Amplitude for TE is in good agreement with HFSS and matches well for TM with HFSS as the incident angle is less than 40 degrees.



TE



TM

Figure 3.40: Phase comparison for TE and TM mode in MATLAB and HFSS (offset 0.0001 ($\sim 0.001 \lambda$) meters in thickness by 0.055 ($\sim 0.5 \lambda$) meters in radius $\epsilon_r = 2.15$ for a thin sheet located in half of $L = 1.1$ ($\sim 10 \lambda$) meters). The phase shows a little mismatch for both TE and TM.

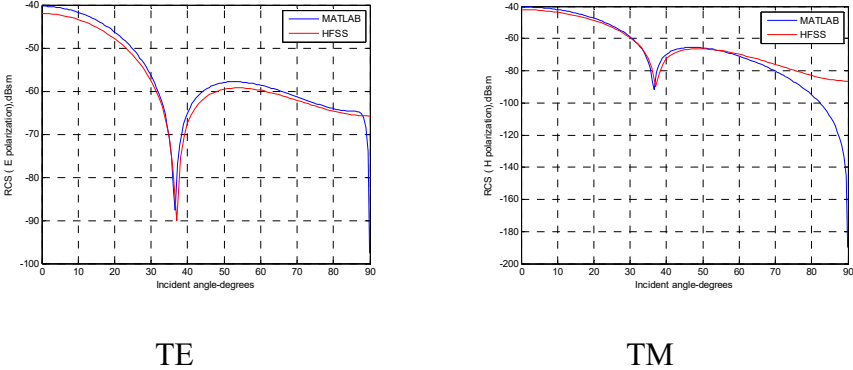


Figure 3.41: Amplitude comparison for TE and TM mode in MATLAB and HFSS (offset 0.0001 ($\sim 0.001 \lambda$) meters in thickness by 0.055 ($\sim 0.5 \lambda$) meters in radius $\epsilon_r = 10-5j$ for a thin sheet located in half of $L = 1.1$ ($\sim 10 \lambda$) meters). Amplitude is in good agreement for TE with HFSS and matches well for TM with HFSS as the incident angle is less than 60 degrees.

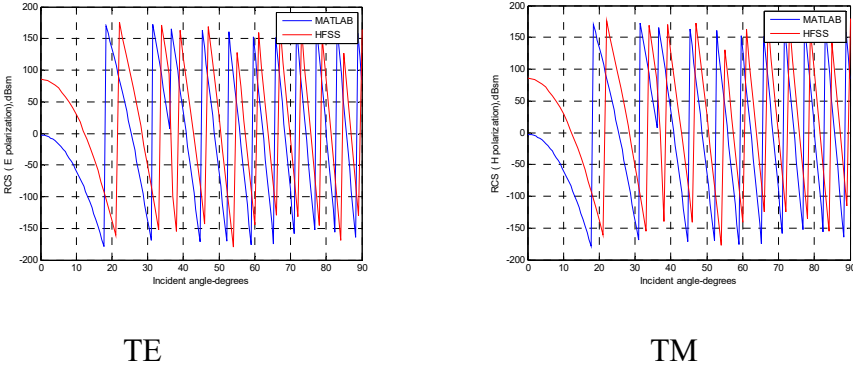


Figure 3.42: Phase comparison for TE and TM mode in MATLAB and HFSS (offset 0.0001 ($\sim 0.001 \lambda$) meters in thickness by 0.055 ($\sim 0.5 \lambda$) meters in radius $\epsilon_r = 10-5j$ for a thin sheet located in half of $L = 1.1$ ($\sim 10 \lambda$) meters). The phase shows a little mismatch for both TE and TM.

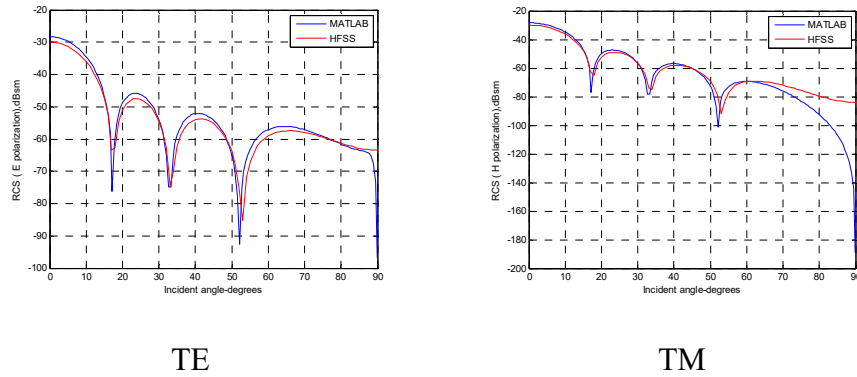


Figure 3.43: Amplitude comparison for TE and TM mode in MATLAB and HFSS (offset 0.0001 ($\sim 0.001 \lambda$) meters in thickness by 0.11 ($\sim 1 \lambda$) meters in radius $\epsilon_r = 10-5j$ for a thin sheet located in half of $L = 1.1$ ($\sim 10 \lambda$) meters). Amplitudes for TE are in good agreement with HFSS and match well for TM with HFSS as the incident angle is less than 60 degrees.

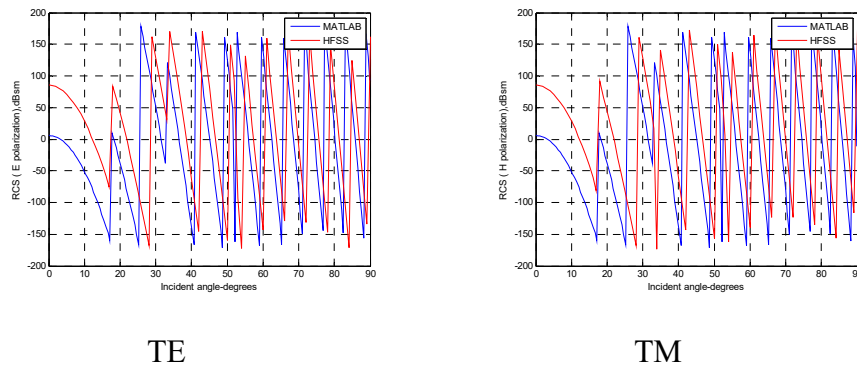
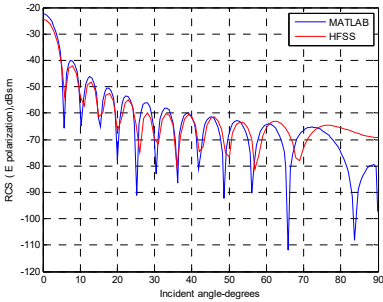
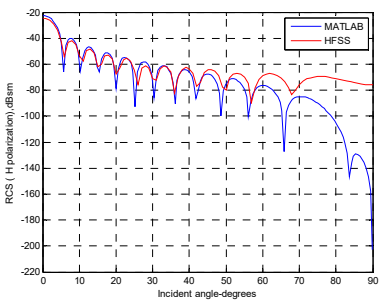


Figure 3.44: Phase comparison for TE and TM mode in MATLAB and HFSS (offset 0.0001 (~0.001 λ) meters in thickness by 0.11 (~1 λ) meters in radius $\epsilon_r = 10-5j$ for a thin sheet located in half of $L = 1.1$ (~10 λ) meters). The phase shows a little mismatch for both TE and TM.

Dielectric thin sheet $\epsilon_r = 2.15$ for thickness at 0.0002 (~0.002 λ) meters:

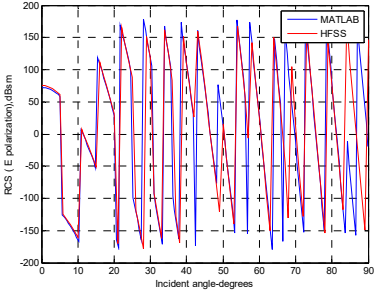


TE

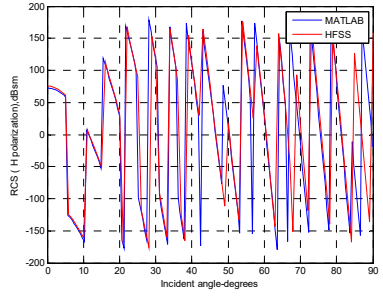


TM

Figure 3.45: Amplitude comparison for TE and TM mode in MATLAB and HFSS (0.0002 (~0.002 λ) meters in length by 0.33 (~3 λ) meters in radius at $\epsilon_r = 2.15$ for a dielectric thin sheet at $L = 1.1$ (~10 λ) meters). Amplitudes are almost in good agreement except at 80- 90 degrees for TE and TM.



TE

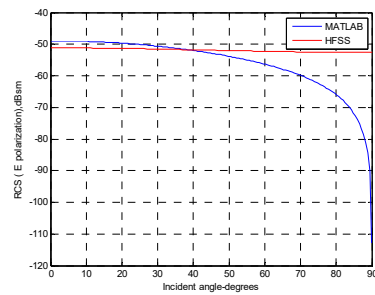


TM

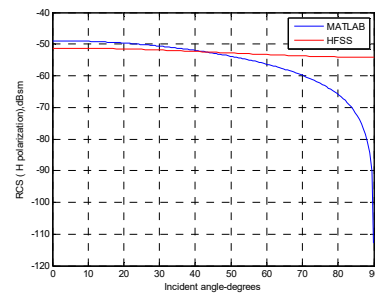
Figure 3.46: Phase comparison for TE and TM mode in MATLAB and HFSS (0.0002 ($\sim 0.002 \lambda$) meters in length by 0.33 ($\sim 3 \lambda$) meters in radius at $\epsilon_r = 2.15$ for a dielectric thin sheet at $L = 1.1$ ($\sim 10 \lambda$) meters). The phase is in good agreement with HFSS for both TE and TM.

3.4.3.3.3 Small (radius $< 0.5 \lambda$) non-metal circular thicker plates

For $\epsilon_r = 2.15$, thickness at 0.01 ($\sim 0.1 \lambda$) meters:

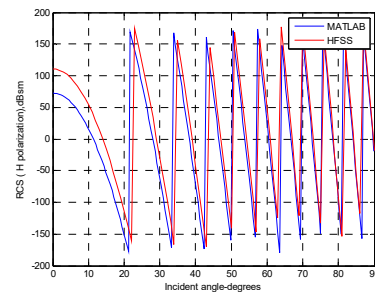
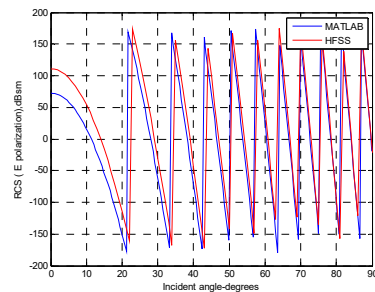


TE



TM

Figure 3.47: Amplitude comparison for TE and TM mode in MATLAB and HFSS (offset 0.01 ($\sim 0.1 \lambda$) meters in thickness by 0.011 ($\sim 0.1 \lambda$) meters in radius $\epsilon_r = 2.15$ for a thicker plate located in half of $L = 1.1$ ($\sim 10 \lambda$) meters). Amplitudes for TE and TM are close as the incident angle is less than 40 degrees.

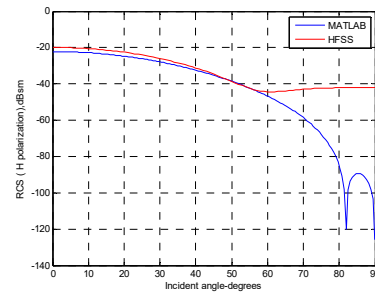
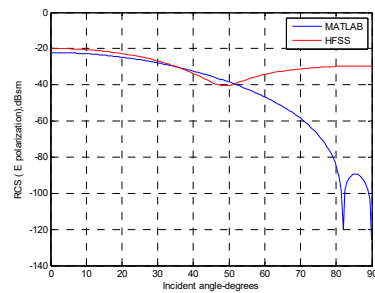


TE

TM

Figure 3.48: Phase comparison for TE and TM mode in MATLAB and HFSS (offset 0.01 (~0.1 λ) meters in thickness by 0.011 (~0.1 λ) meters in radius $\epsilon_r = 2.15$ for a thicker plate located in half of $L = 1.1$ (~10 λ) meters). The phase shows a little mismatch, as the incident angle is less than 50 degrees for both TE and TM.

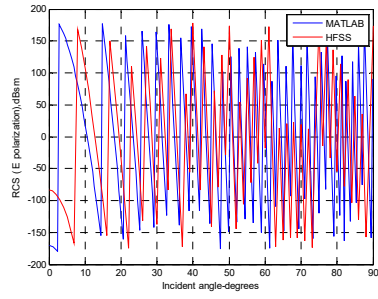
For $\epsilon_r = 10-5j$, thickness at 0.01 (~0.1 λ) meters:



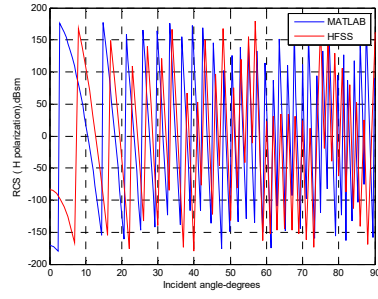
TE

TM

Figure 3.49: Amplitude comparison for TE and TM mode in MATLAB and HFSS (offset 0.01 (~0.1 λ) meters in thickness by 0.033 (~0.3 λ) meters in radius $\epsilon_r = 10-5j$ for a thin plate located in half of $L = 3.3$ (~30 λ) meters). Amplitudes for TE and TM match well as the incident angle is less than 40 degrees.



TE

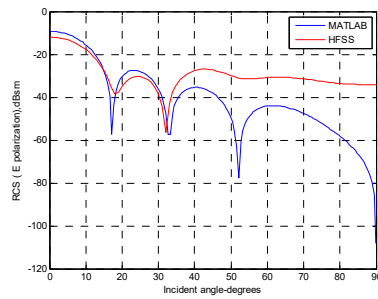


TM

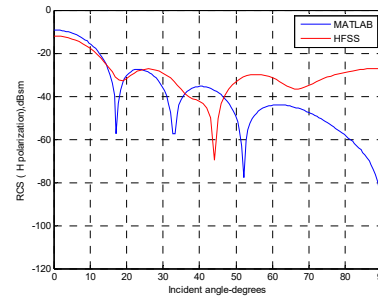
Figure 3.50: Phase comparison for TE and TM mode in MATLAB and HFSS (offset 0.01 ($\sim 0.1 \lambda$) meters in thickness by 0.033 ($\sim 0.3 \lambda$) meters in radius $\epsilon_r = 10 - 5j$ for a thin plate located in half of $L = 3.3$ ($\sim 30 \lambda$) meters). The phase shows a little mismatch, as the incident angle is less than 40 degrees for both TE and TM.

3.4.3.3.4 Large (radius $> 0.5 \lambda$) circular non-metal thicker plates

For thickness at 0.1 ($\sim 1 \lambda$) meters:



TE



TM

Figure 3.51: Amplitude comparison for TE and TM mode in MATLAB and HFSS (offset 0.1 ($\sim 1 \lambda$) meters in thickness by 0.11 ($\sim 1 \lambda$) meters in

radius $\epsilon_r = 2.15$ for a thick plate located in half of $L = 1.1$ ($\sim 10 \lambda$) meters).

Amplitudes match closely as the incident angle is less than 30 degrees for

both TE and TM.

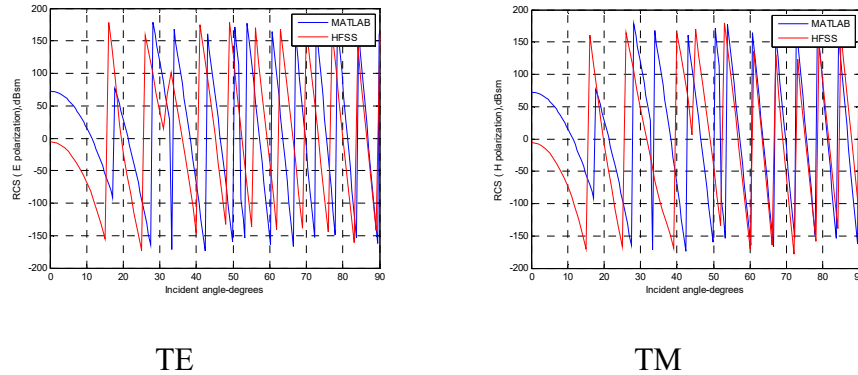


Figure 3.52: Phase comparison for TE and TM mode in MATLAB and

HFSS (offset 0.1 ($\sim 1 \lambda$) meters in thickness by 0.11 ($\sim 1 \lambda$) meters in radius

$\epsilon_r = 2.15$ for a thick plate located in half of $L = 1.1$ ($\sim 10 \lambda$) meters). The

phase matches well as incident angle is close to 90 degrees for TE and 60-

90 degrees for TM.

3.4.3.4 Simulation vs. analytical results for non-metal rectangular sheets

The amplitudes are in good agreement with HFSS for all plots. Phase

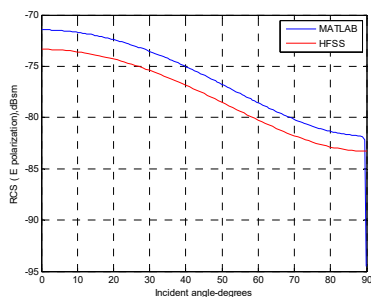
terms closely matched for TE and TM. The thickness is 0.0001 ($\sim 0.001 \lambda$)

or 0.0002 ($\sim 0.002 \lambda$) meters at $\epsilon_r = 2.15$, $\epsilon_r = 34.56 - 12.34j$, $\epsilon_r = 10 - 5j$ for

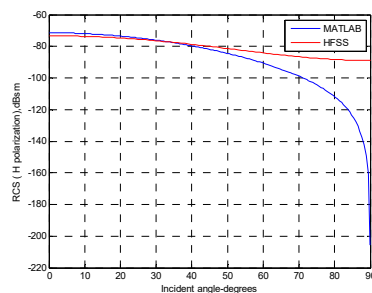
different sizes.

3.4.3.4.1 Small ($a, b < 1 \lambda$) non-metal rectangular thin sheets

For thickness at 0.0001 ($\sim 0.001 \lambda$) meters at $\epsilon_r = 2.15$:

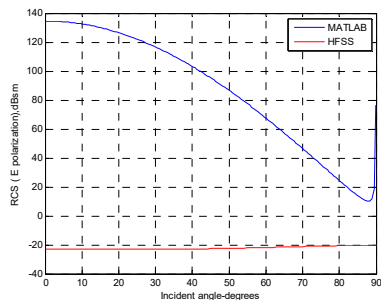


TE

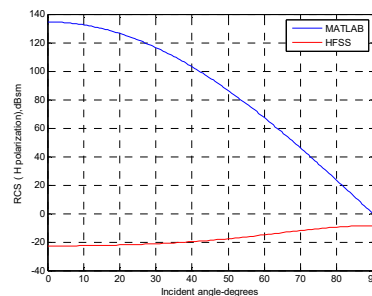


TM

Figure 3.53: Amplitude comparison for TE and TM mode in MATLAB and HFSS (offset 0.0001 ($\sim 0.001 \lambda$) meters in thickness by 0.04 ($\sim 0.4 \lambda$) meters by 0.06 ($\sim 0.6 \lambda$) meters $\epsilon_r = 2.15$ for a rectangular thin sheet located at origin). Amplitude matches well for TM as the incident angle is less than 40 degrees. Amplitude has a few dB differences from 0-90 degrees for TE.



TE



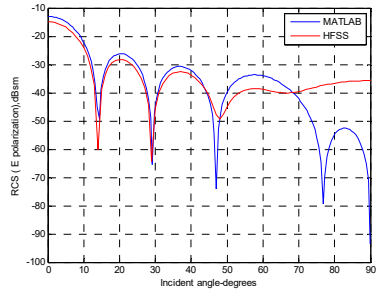
TM

Figure 3.54: Phase comparison for TE and TM mode in MATLAB and HFSS (offset 0.0001 ($\sim 0.001 \lambda$) meters in thickness by 0.04 ($\sim 0.4 \lambda$)

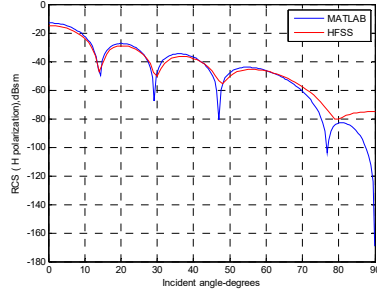
meters by 0.06 ($\sim 0.6 \lambda$) meters $\epsilon_r = 2.15$ for a rectangular thin sheet located at origin). The phase shows a big gap for both TE and TM.

3.4.3.4.2 Large (a, b > 1 λ) non-metal rectangular thin sheets

For thickness 0.0002 ($\sim 0.002 \lambda$) meters at $\epsilon_r = 34.56-12.34j$, $\epsilon_r = 10-5j$:

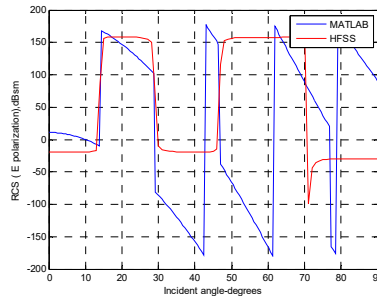


TE

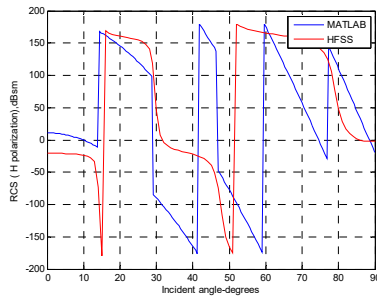


TM

Figure 3.55: Amplitude comparison for TE and TM mode in MATLAB and HFSS (offset 0.0002 ($\sim 0.002 \lambda$) meters in thickness by 0.22 ($\sim 2 \lambda$) meters by 0.14 ($\sim 1.27 \lambda$) meters $\epsilon_r = 34.56-12.34j$ (leaf) for a rectangular sheet located at origin). Amplitudes match well as the incident angle is less than 50 degrees for both TE and TM.



TE



TM

Figure 3.56: Phase comparison for TE and TM mode in MATLAB and HFSS (offset 0.0002 ($\sim 0.002 \lambda$) meters in thickness by 0.22 ($\sim 2 \lambda$) meters by 0.14 ($\sim 1.27 \lambda$) meters $\epsilon_r = 34.56 - 12.34j$ (leaf) for a rectangular sheet located at origin). The phase matches closely to both TE and TM.

Same size for thickness at 0.0001 ($\sim 0.001 \lambda$) meters at $\epsilon_r = 2.15$:

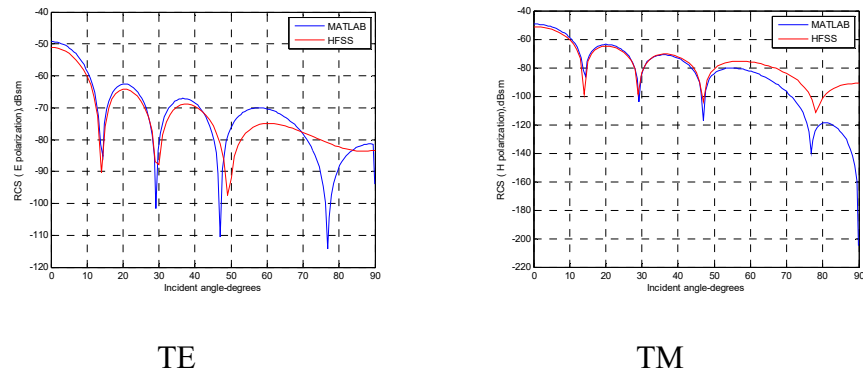


Figure 3.57: Amplitude comparison for TE and TM mode in MATLAB and HFSS (offset 0.0001 ($\sim 0.001 \lambda$) meters in thickness by 0.22 ($\sim 2 \lambda$) meters by 0.14 ($\sim 1.27 \lambda$) meters $\epsilon_r = 2.15$ for a rectangular sheet located at origin). Amplitudes match closely as the incident angle is less than 50 degrees for both TE and TM.

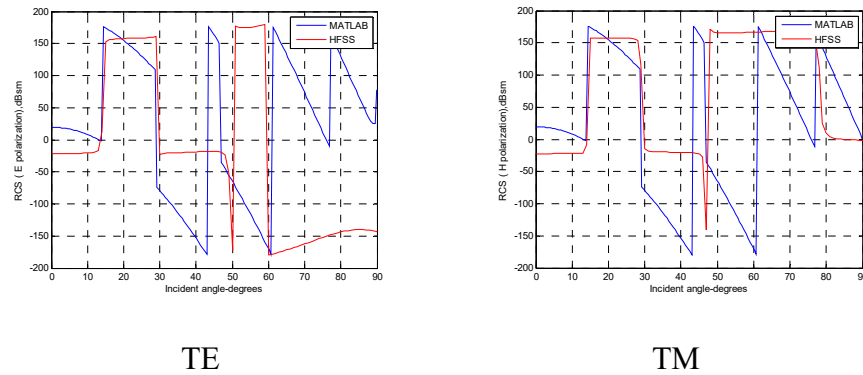


Figure 3.58: Phase comparison for TE and TM mode in MATLAB and HFSS (offset 0.0001 ($\sim 0.001 \lambda$) meters in thickness by 0.22 ($\sim 2 \lambda$) meters by 0.14 ($\sim 1.27 \lambda$) meters $\epsilon_r = 2.15$ a rectangular sheet located at origin). The phase matches closely to both TE and TM.

Same size for thickness at 0.0001 ($\sim 0.001 \lambda$) meters at $\epsilon_r = 10-5j$:

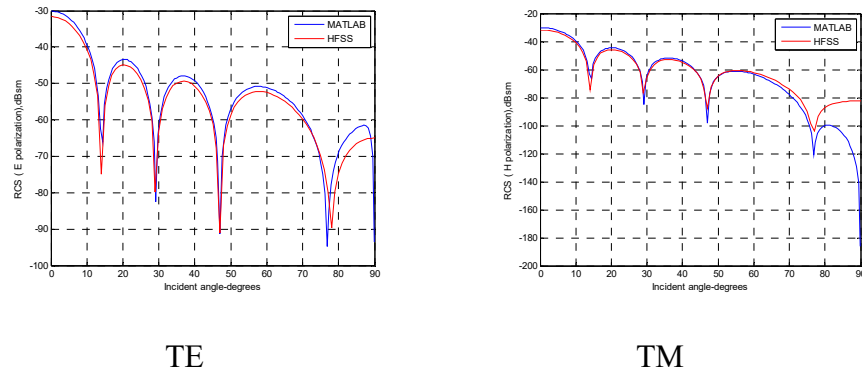


Figure 3.59: Amplitude comparison for TE and TM mode in MATLAB and HFSS (offset 0.0001 ($\sim 0.001 \lambda$) meters in thickness by 0.22 ($\sim 2 \lambda$) meters by 0.14 ($\sim 1.27 \lambda$) meters $\epsilon_r = 10-5j$ for a rectangular sheet located at origin). Amplitudes match closely as the incident angle is less than 70 degrees for both TE and TM.

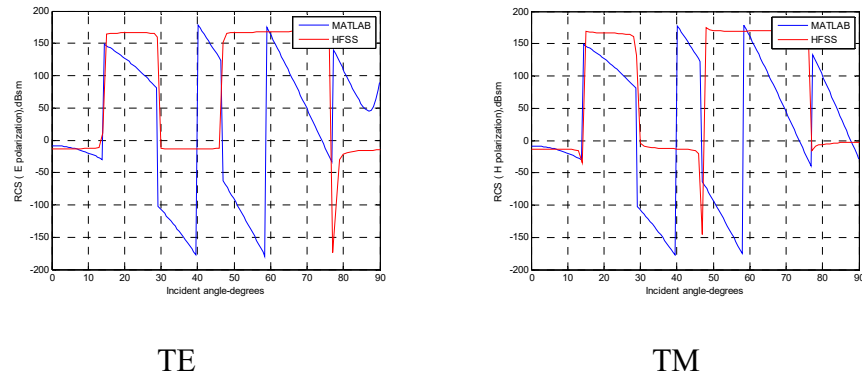
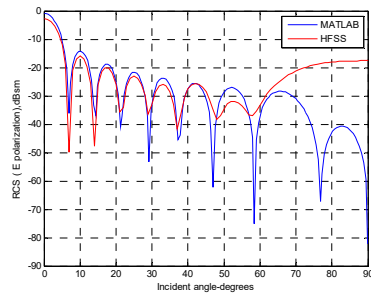
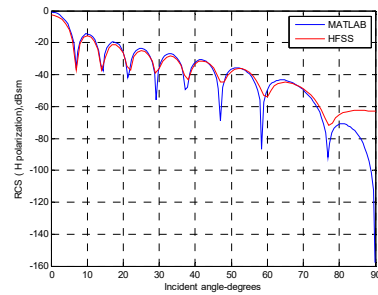


Figure 3.60: Phase comparison for TE and TM mode in MATLAB and HFSS (offset 0.0001 ($\sim 0.001 \lambda$) meters in thickness by 0.22 ($\sim 2 \lambda$) meters by 0.14 ($\sim 1.27 \lambda$) meters $\epsilon_r = 10-5j$ for a rectangular sheet located at origin). The phase matches closely to both TE and TM.

Size double for thickness at 0.0002 ($\sim 0.002 \lambda$) meters at $\epsilon_r = 34.56-12.34j$:

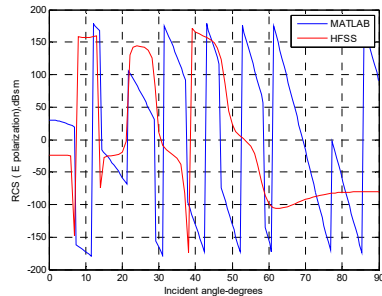


TE

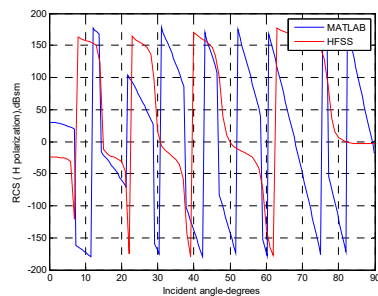


TM

Figure 3.61: Amplitude comparison for TE and TM mode in MATLAB and HFSS (offset 0.0002 ($\sim 0.002 \lambda$) meters in thickness by 0.44 ($\sim 4 \lambda$) meters by 0.28 ($\sim 2.54 \lambda$) meters $\epsilon_r = 34.56-12.34j$ (leaf) for a rectangular sheet located at origin). Amplitudes match closely as the incident angle is less than 50 degrees for TE, and less than 70 degrees for TM.



TE



TM

Figure 3.62: Phase comparison for TE and TM mode in MATLAB and HFSS (offset 0.0002 ($\sim 0.002 \lambda$) meters in thickness by 0.44 ($\sim 4 \lambda$) meters by 0.28 ($\sim 2.54 \lambda$) meters $\epsilon_r = 34.56 - 12.34j$ (leaf) for a rectangular sheet located at origin). The phase matches closely to both TE and TM.

3.4.3.5 Simulation vs. analytical results for rectangular thicker plates

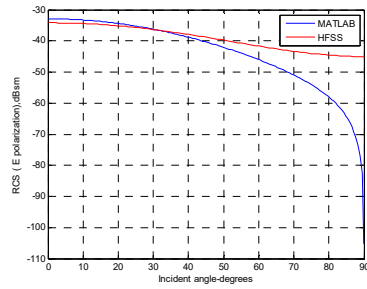
The recursive formulation mentioned above is used to get the rectangular plates at oblique incidence for 1 and 2 layers. FEKO is used to simulate 2 layers with different media for comparison with analytical results.

3.4.3.5.1 One layer non-metal rectangular plates

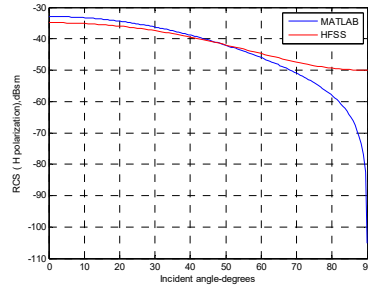
The amplitudes are in good agreement with HFSS for all plots. Phase terms are closely matched to TE and TM. The thickness is 0.01 ($\sim 0.1 \lambda$) meters, 0.02 ($\sim 0.2 \lambda$) meters, 0.001 ($\sim 0.01 \lambda$) meters, or 0.1 ($\sim 1 \lambda$) meters at $\epsilon_r = 2.15$, $\epsilon_r = 10 - 5j$ for different sizes.

3.4.3.5.1.1 Small ($a, b < 1 \lambda$) non-metal plates

For thickness 0.01 ($\sim 0.1 \lambda$) meters at $\epsilon_r = 2.15$:

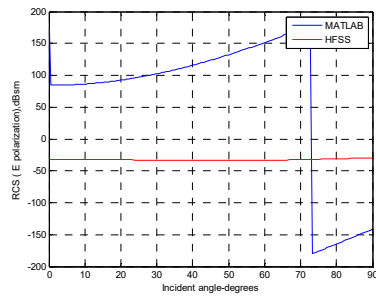


TE

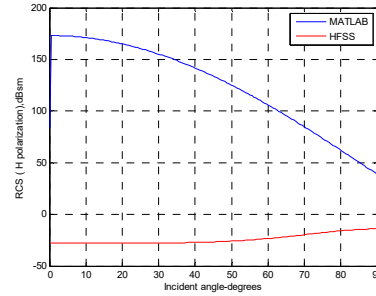


TM

Figure 3.63: Amplitude comparison for TE and TM mode in MATLAB and HFSS (offset 0.01 ($\sim 0.1 \lambda$) meters in thickness by 0.04 ($\sim 0.4 \lambda$) meters by 0.06 ($\sim 0.6 \lambda$) meters $\epsilon_r = 2.15$ for a rectangular thick plate located at origin). Amplitudes match closely as the incident angle is less than 40 degrees for both TE and TM.



TE



TM

Figure 3.64: Phase comparison for TE and TM mode in MATLAB and HFSS (offset 0.01 ($\sim 0.1 \lambda$) meters in thickness by 0.04 ($\sim 0.4 \lambda$) meters by 0.06 ($\sim 0.6 \lambda$) meters $\epsilon_r = 2.15$ for a rectangular thick plate located at origin). The phase shows a big gap for both TE and TM.

Same size for thickness 0.02 (~0.2 λ) meters at ε_r = 2.15:

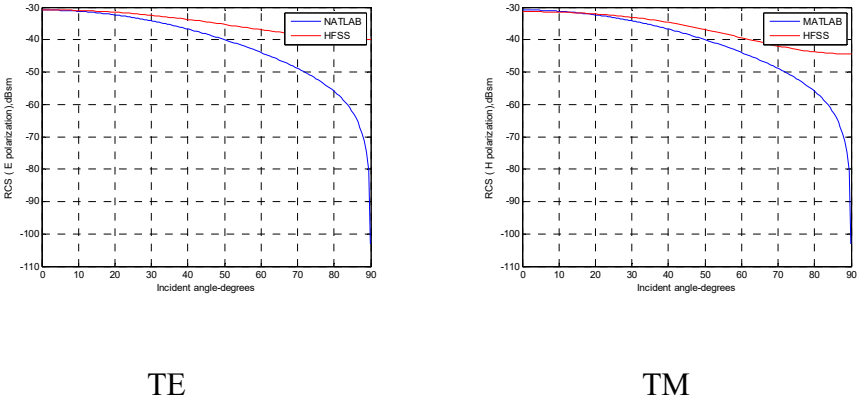


Figure 3.65: Amplitude comparison for TE and TM mode in MATLAB and HFSS (offset 0.02 (~0.2 λ) meters in thickness by 0.04 (~0.4 λ) meters by 0.06 (~0.6 λ) meters ε_r = 2.15 for a rectangular thicker plate located at origin). Amplitudes match closely as the incident angle is less than 20 degrees for both TE and TM.

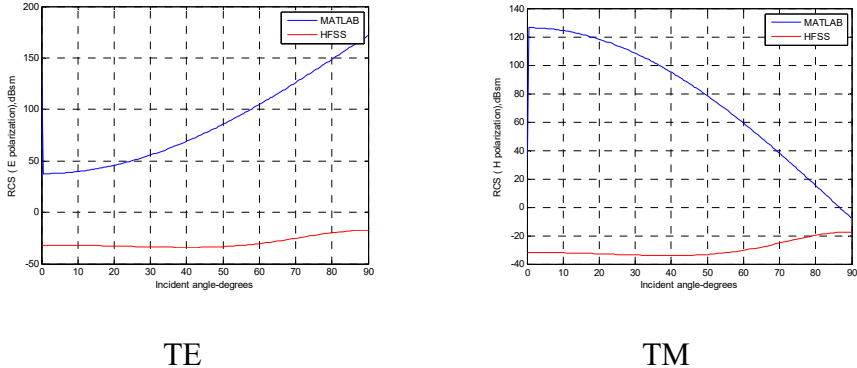
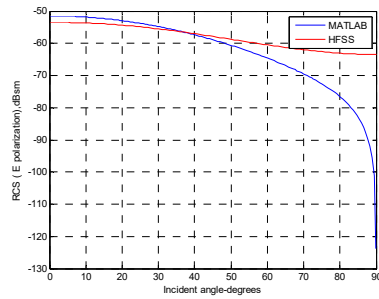


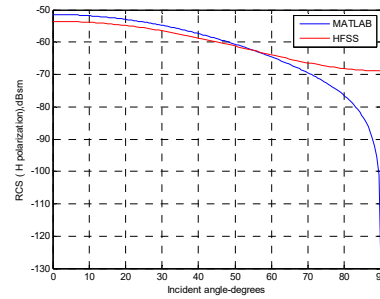
Figure 3.66: Phase comparison for TE and TM mode in MATLAB and HFSS (offset 0.02 (~0.2 λ) meters in thickness by 0.04 (~0.4 λ) meters by 0.06 (~0.6 λ) meters ε_r = 2.15 for a rectangular thicker plate located at origin). Phases match closely as the incident angle is less than 20 degrees for both TE and TM.

0.06 ($\sim 0.6 \lambda$) meters $\epsilon_r = 2.15$ for a rectangular thick plate located at origin). The phase shows a big gap for both TE and TM.

Same size for thickness 0.001 ($\sim 0.01 \lambda$) meters at $\epsilon_r = 2.15$:

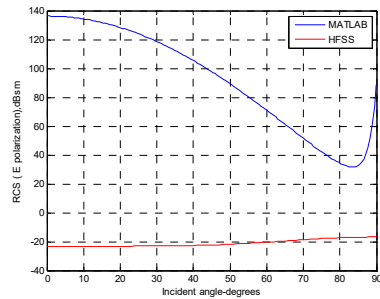


TE

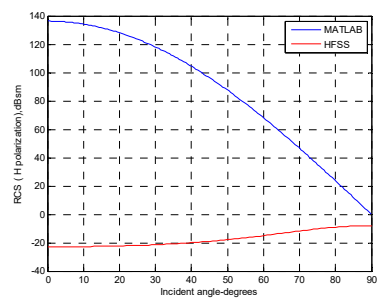


TM

Figure 3.67: Amplitude comparison for TE and TM mode in MATLAB and HFSS (offset 0.001 ($\sim 0.01 \lambda$) meters in thickness by 0.04 ($\sim 0.4 \lambda$) meters by 0.06 ($\sim 0.6 \lambda$) meters $\epsilon_r = 2.15$ for a rectangular thin plate located at origin). Amplitudes match closely as the incident angle is less than 40 degrees for both TE and TM.



TE

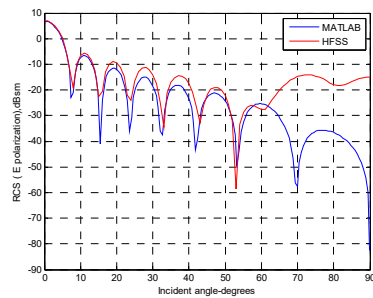


TM

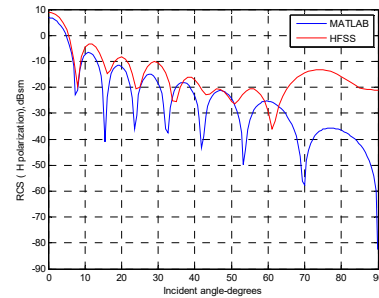
Figure 3.68: Phase comparison for TE and TM mode in MATLAB and HFSS (offset 0.001 ($\sim 0.01 \lambda$) meters in thickness by 0.04 ($\sim 0.4 \lambda$) meters by 0.06 ($\sim 0.6 \lambda$) meters $\epsilon_r = 2.15$ for a rectangular thin plate located at origin). The phase shows a large gap for both TE and TM.

3.4.3.5.1.2 Large ($a, b > 1 \lambda$) non-metal thicker plates

For thickness 0.1 ($\sim 1 \lambda$) meters at $\epsilon_r = 2.15$:

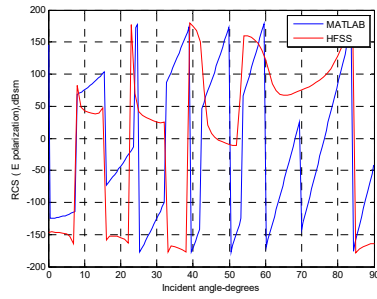


TE

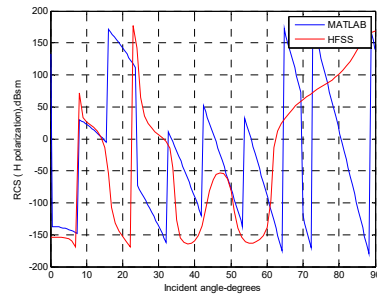


TM

Figure 3.69: Amplitude comparison for TE and TM mode in MATLAB and HFSS (offset 0.1 ($\sim 1 \lambda$) meters in thickness by 0.4 ($\sim 3.64 \lambda$) meters by 0.6 ($\sim 5.45 \lambda$) meters $\epsilon_r = 2.15$ for a rectangular thick plate located at origin). Amplitudes match closely as the incident angle is less than 40 degrees for both TE and TM.



TE

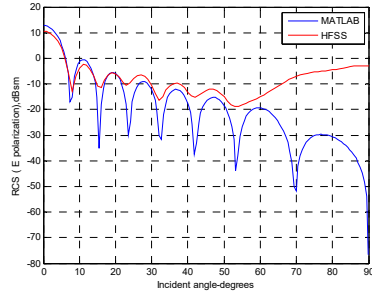


TM

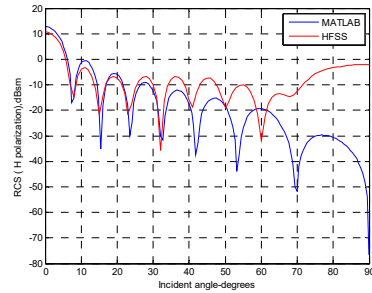
Figure 3.70: Phase comparison for TE and TM mode in MATLAB and HFSS (offset 0.1 ($\sim 1 \lambda$) meters in thickness by 0.4 ($\sim 3.64 \lambda$) meters by 0.6 ($\sim 5.45 \lambda$) meters $\epsilon_r = 2.15$ for a rectangular thick plate located at origin).

The phase matches closely to TE and TM.

For thickness 0.1 ($\sim 1 \lambda$) meters at $\epsilon_r = 10-5j$:

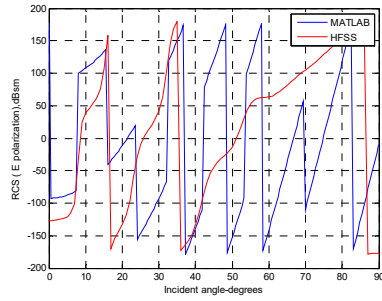


TE

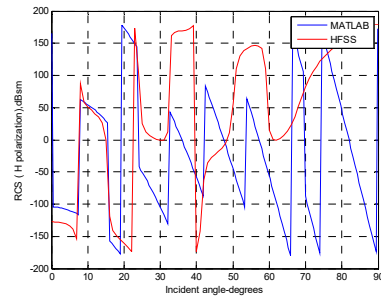


TM

Figure 3.71: Amplitude comparison for TE and TM mode in MATLAB and HFSS (offset 0.1 ($\sim 1 \lambda$) meters in thickness by 0.4 ($\sim 3.64 \lambda$) meters by 0.6 ($\sim 5.45 \lambda$) meters $\epsilon_r = 10-5j$ for a rectangular thick plate located at origin). Amplitudes match closely as the incident angle is less than 30 degrees.



TE

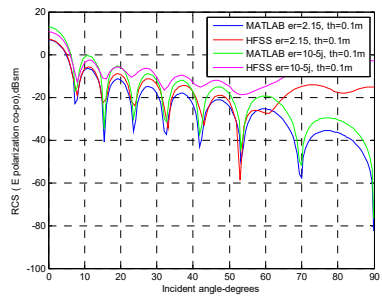


TM

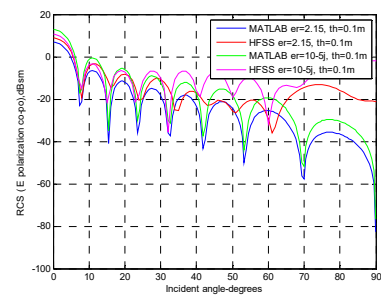
Figure 3.72: Phase comparison for TE and TM mode in MATLAB and HFSS (offset 0.1 ($\sim 1 \lambda$) meters in thickness by 0.4 ($\sim 3.64 \lambda$) meters by 0.6 ($\sim 5.45 \lambda$) meters $\epsilon_r = 10-5j$ for a rectangular thick plate located at origin).

The phase matches closely to TE and TM.

Compare the two:



TE



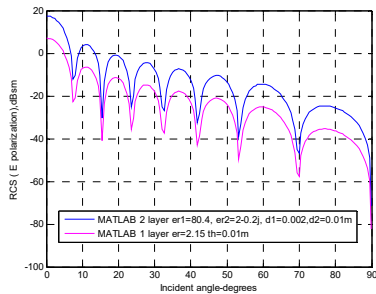
TM

Figure 3.73: Amplitude comparison for TE and TM mode in MATLAB and HFSS (offset 0.1 ($\sim 1 \lambda$) meters in thickness by 0.4 ($\sim 3.64 \lambda$) meters by 0.6 ($\sim 5.45 \lambda$) meters $\epsilon_r = 2.15$ and $\epsilon_r = 10-5j$ for a rectangular thick plate located at origin). Resistance R at $\epsilon_r = 2.15$ is greater than resistance R at $\epsilon_r = 10-5j$, amplitudes for both analytical and HFSS are lower than $\epsilon_r =$

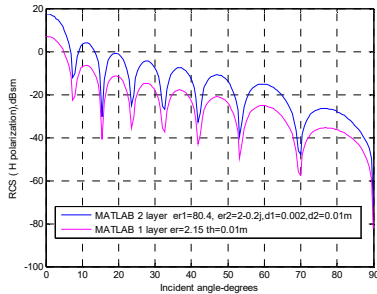
10-5j, which is consistent with previous research (Jenn 2005). Lower scattering amplitude for higher R accounts for more transmission and less reflection in the material.

3.4.3.5.2 Multi-layer (two layers) rectangular thicker plates

Assume the first layer is water, $\epsilon_r = 80.4$, and the thickness is 0.002 (~0.02 λ) meters. The second layer is wood board $\epsilon_r = 2-0.2j$, and the thickness is 0.01 (~0.1 λ) meters. 2 layer plates with a water layer on the top increases by 10 dB, and 5 dB more than 1 layer wood board, respectively.



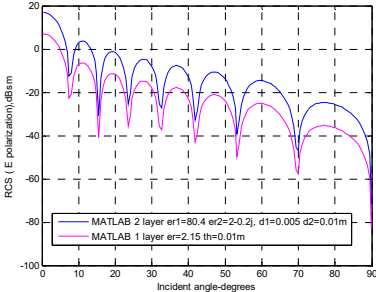
TE



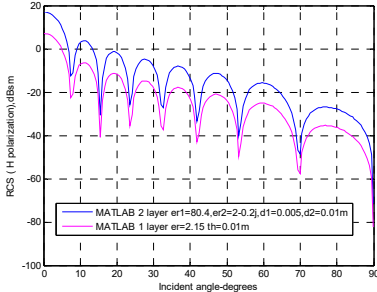
TM

Figure 3.74: Amplitude comparison for TE and TM mode in MATLAB and HFSS (water with $\epsilon_r = 80.4$, thickness 0.002 (~0.02 λ) meters on the top of wood board $\epsilon_r = 2.15$, 0.01 (~0.1 λ) meters in thickness for 0.4 (~3.64 λ) meters by 0.6 (~5.45 λ) meters rectangular 2-layer thick plate in comparison to 1 layer of the same size wood board $\epsilon_r = 2.15$, 0.01 (~0.1 λ) meters in thickness, located at origin). The amplitude of two-layer water-

coated wood board increases by 10 dB when compared to 1-layer wood board.

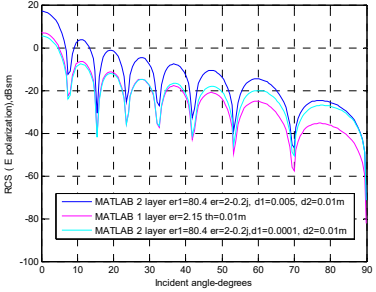


TE

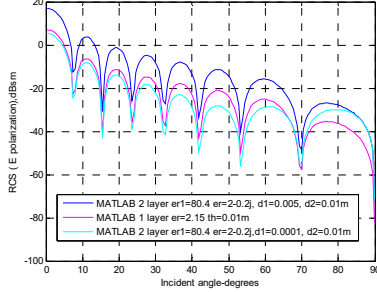


TM

Figure 3.75: Amplitude comparison for TE and TM mode in MATLAB and HFSS (water with $\epsilon_r = 80.4$, thickness 0.005 ($\sim 0.05 \lambda$) meters on the top of wood board $\epsilon_r = 2.15$, 0.01 ($\sim 0.1 \lambda$) meters in thickness by 0.4 ($\sim 3.64 \lambda$) meters by 0.6 ($\sim 5.45 \lambda$) meters rectangular 2-layer thick plate in comparison to 1 layer of the same size wood board $\epsilon_r = 2.15$, 0.01 ($\sim 0.1 \lambda$) meters in thickness, located at origin). The amplitude of two-layer water-coated wood board increases by 10 dB when compared to 1-layer wood board.



TE



TM

Figure 3.76: Amplitude comparison for TE and TM mode in MATLAB and HFSS (water with $\epsilon_r = 80.4$, thickness 0.005 ($\sim 0.05 \lambda$) meters, 0.0001 ($\sim 0.001 \lambda$) meters, respectively, on the top of wood board $\epsilon_r = 2.15$, 0.01 ($\sim 0.1 \lambda$) meters in thickness by 0.4 ($\sim 3.64 \lambda$) meters by 0.6 ($\sim 5.45 \lambda$) meters of rectangular 2-layer thick plate in comparison to 1 layer of the same size wood board $\epsilon_r = 2.15$, 0.01 ($\sim 0.1 \lambda$) meters in thickness, located at origin). Wood board coated with a thicker layer of water increases 10 dB more than 1-layer wood board. Wood board coated with a thin sheet layer of water shows some variation from 0-90 degrees.

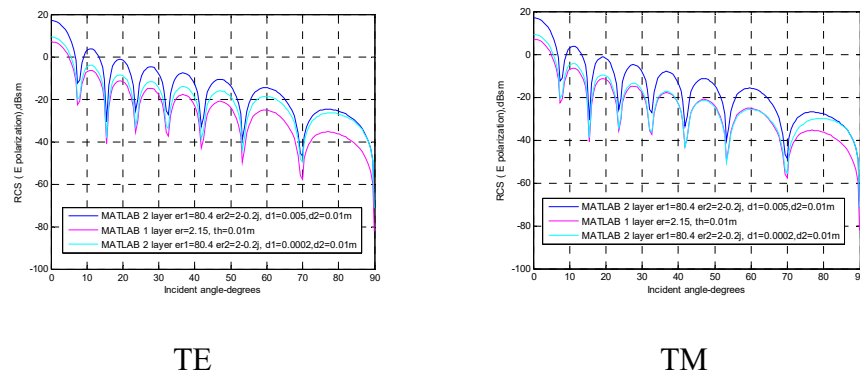


Figure 3.77: Amplitude comparison for TE and TM mode in MATLAB and HFSS (water with $\epsilon_r = 80.4$, thickness 0.005 ($\sim 0.05 \lambda$) meters, 0.0002 ($\sim 0.002 \lambda$) meters, respectively, on the top of wood board $\epsilon_r = 2.15$, 0.01 ($\sim 0.1 \lambda$) meters in thickness by 0.4 ($\sim 3.64 \lambda$) meters by 0.6 ($\sim 5.45 \lambda$) meters rectangular 2-layer thick plate in comparison to 1 layer of the same size wood board $\epsilon_r = 2.15$, 0.01 ($\sim 0.1 \lambda$) meters in thickness, located at

origin). Wood board coated with a thicker layer of water increases by 10 dB when compared to 1-layer wood board. Wood board coated with a thin sheet layer of water shows some variation from 0-90 degrees.

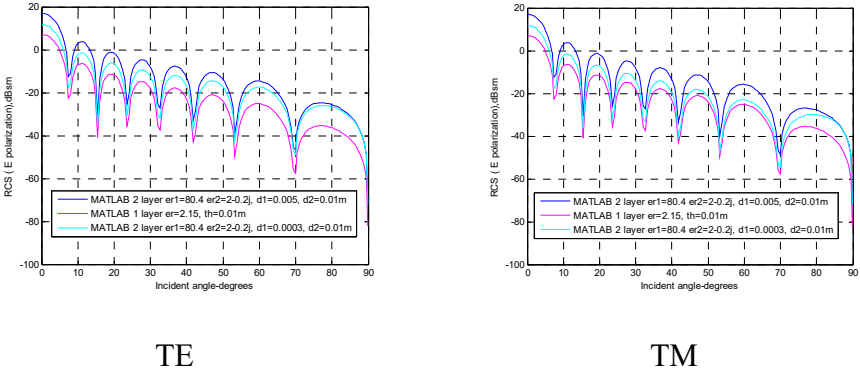
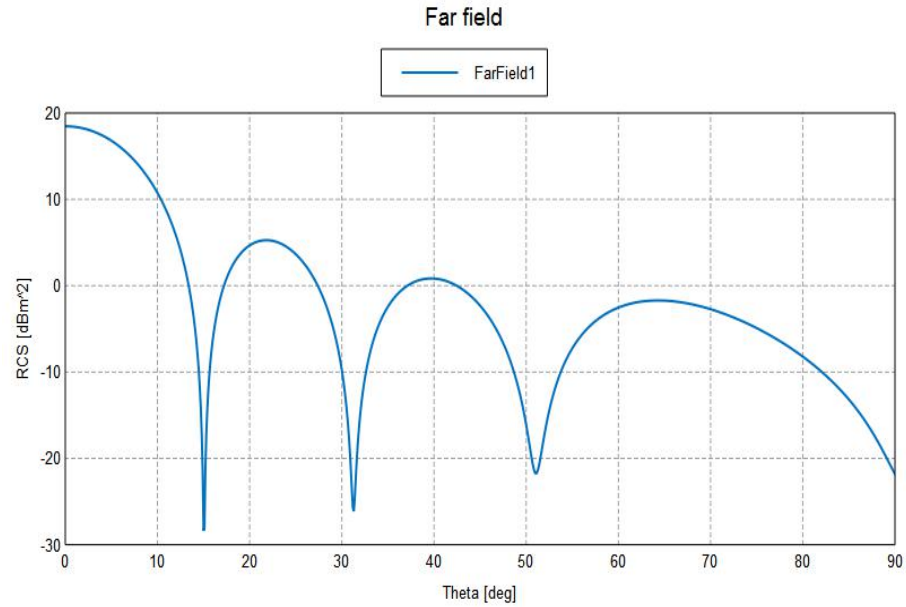


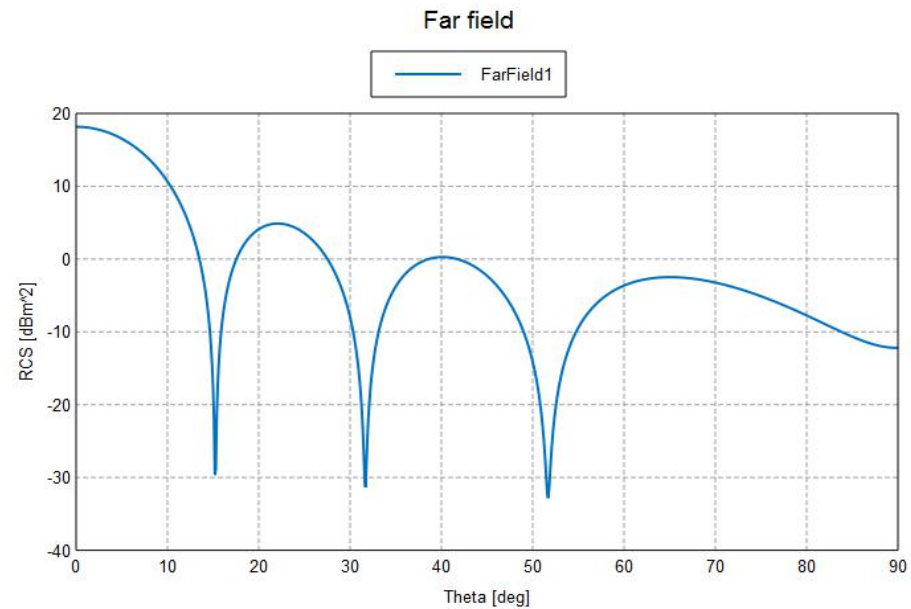
Figure 3.78: Amplitude comparison for TE and TM mode in MATLAB and HFSS (2-layers of water with $\epsilon_r = 80.4$, thickness 0.005 ($\sim 0.05 \lambda$) meters, 0.0003 ($\sim 0.003 \lambda$) meters, respectively, on the top of wood board $\epsilon_r = 2.15$, 0.01 ($\sim 0.1 \lambda$) meters in thickness by 0.4 ($\sim 3.64 \lambda$) meters by 0.6 ($\sim 5.45 \lambda$) meters of rectangular thick plate in comparison to 1 layer of the same size wood board, located at origin). Water coated in 2 layers increases by 10 dB, and 5 dB when compared to 1-layer wood board, respectively.

The plots show that with 2 layers of water $\epsilon_{r1} = 80.4$ on the top of wood board $\epsilon_{r2} = 2.15$, the amplitudes go up more than 1 layer of wood board because $\epsilon_{r1} > \epsilon_{r2}$, and the resistance of water R_1 is less than wood board R_2 . The plots also show that the amplitude will go up unless the

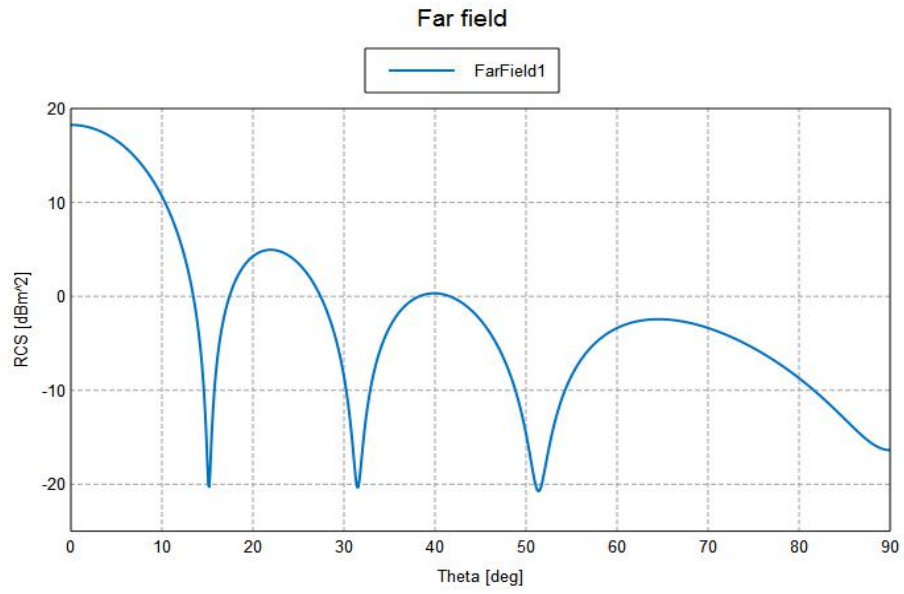
thickness of water is less than 0.0003 (~0.003 λ) meters (sheet range). This is probably because the water sheet is more penetrable than a thicker plate.



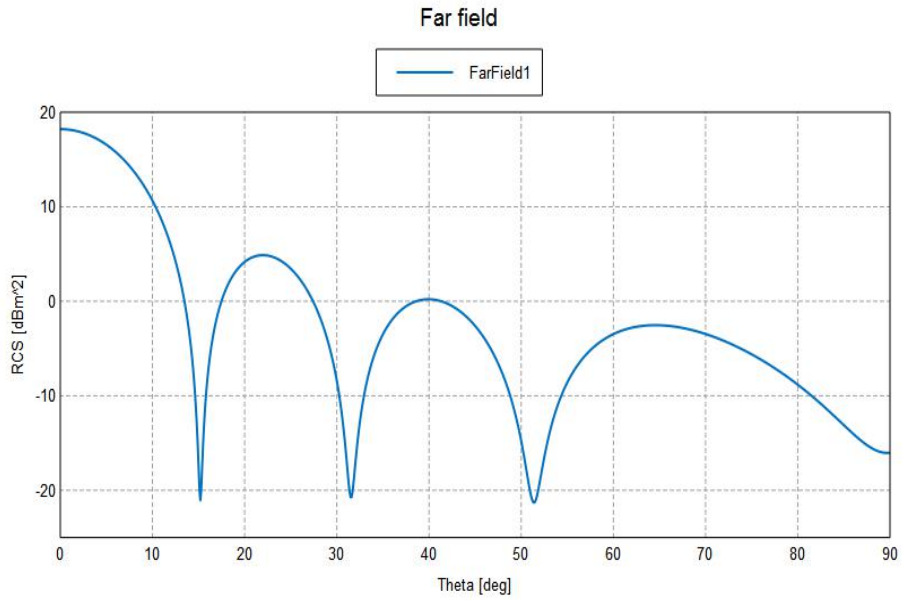
1 RCS [dBm²] (Frequency = 2.8 GHz; Plane Wave Theta = 0 deg; Plane Wave Phi = 0 deg; Phi = 0 deg) - 2 layer 0.01-0.01-0.4 by 0.6 rectangular



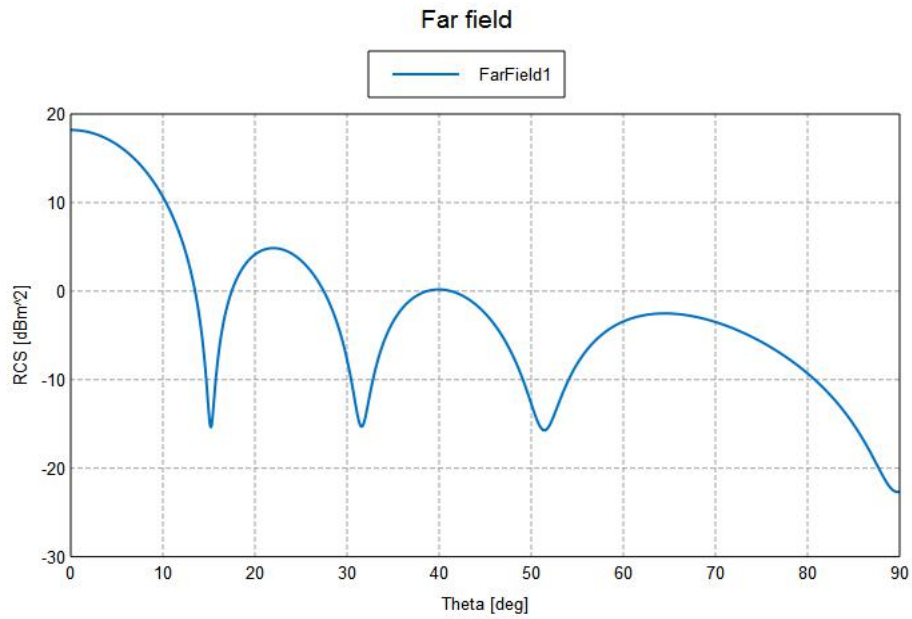
2] (Frequency = 2.8 GHz; Plane Wave Theta = 0 deg; Plane Wave Phi = 0 deg; Phi = 0 deg) - 2 layer 0.005-0.01-0.4 by 0.6



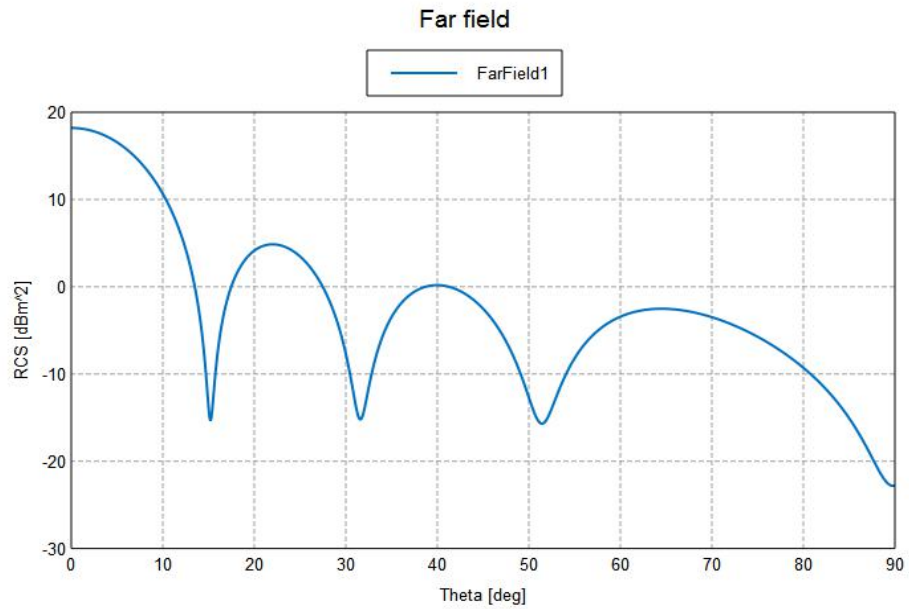
2] (Frequency = 2.8 GHz; Plane Wave Theta = 0 deg; Plane Wave Phi = 0 deg; Phi = 0 deg) - 2 layer 0.002-0.01-0.4by 0.6



3] (Frequency = 2.8 GHz; Plane Wave Theta = 0 deg; Plane Wave Phi = 0 deg; Phi = 0 deg) - 2 layer 0.0003-0.01-0.4by 0.6 rectangular



] (Frequency = 2.8 GHz; Plane Wave Theta = 0 deg; Plane Wave Phi = 0 deg; Phi = 0 deg) - 2 layer 0.0002-0.01-0.4by 0.6



] (Frequency = 2.8 GHz; Plane Wave Theta = 0 deg; Plane Wave Phi = 0 deg; Phi = 0 deg) - 2 layer 0.0001-0.01-0.4by 0.6

Figure 3.79: RCS FEKO plots for 2 layers with different water coating thicknesses at 0.01 ($\sim 0.1 \lambda$) meters, 0.005 ($\sim 0.05 \lambda$) meters, 0.002 ($\sim 0.02 \lambda$)

meters, 0.0003 ($\sim 0.003 \lambda$) meters, 0.0002 ($\sim 0.002 \lambda$) meters, 0.0001 ($\sim 0.001 \lambda$) meters on top of wood board with a thickness of 0.01 ($\sim 0.1 \lambda$) meters. FEKO plots are very similar to analytical results for two layers.

Since HFSS has no function to construct two overlapping layers with different mediums, the FEKO application software was used to generate the plots in order to compare with analytical results. FEKO is limited to a thickness on the top layer of less than 0.0003 ($\sim 0.003 \lambda$) meters by testing.

3.5 The errors and limitations

The circular plates with at least 1 wavelength in diameter show more accuracy by PO. The rectangular plates with at least 1 wavelength on each side show more accuracy and amplitudes begin to oscillate. The phase term especially shows little to no accuracy at small sizes. A better understanding of the limitation of theory and HFSS by validation with measurements is still necessary. Therefore, detailed comparisons with measurements and the demand for calibration are necessary in future work.

The limitation for electrically-small objects is that the current at the edge remarkably affects the scattered field when the PO method is applied. PO is more accurate for an electrically large object at a high frequency. The error will be observed by the cases such as metal vs. non-metal, and thick vs. thin through HFSS vs. MATLAB in the following sections. This

limitation is extended to endcap on the finite cylindrical objects detailed in Chapter 4.

All plots show the errors as close to 90 degrees. There are two reasons: for this: first, PO method ignores the edge effect; and second, more accurate results occur as the incident angle approaches the normal incidence for non-metal rectangular and circular plates under the certain conditions $\theta_i = \theta, \cos \theta_i \approx 1, Z_s \ll \cos \theta$ resulting from the surface impedance restrictions. Most of the plots, when compared to HFSS, show that more accurate results are obtained when the incident angle is less than 40 degrees. This is in agreement with surface impedance limitations.

3.5.1 Metal vs. non-metal – PO vs. simulations

3.5.1.1 Metal vs. non-metal for circular plates

Non-metal material has dielectric constant considered as lossy material; therefore, reduced reflection and increased transmission are expected as energy loss in the media than metal plates. For an electrically small plate, the errors of PO become obvious and comparisons to analytical results with HFSS simulations do not match well.

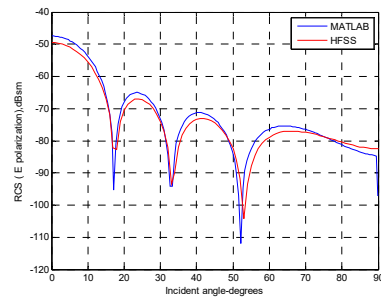
As shown in Section 3.3.3, the MATLAB vs. HFSS results for conducting sheets and plates further confirm that the errors shown on the edges are omitted by PO. The limitation of PO is that more accurate

oscillating results are observed for plates with a larger radius (1.5λ vs. 0.1λ).

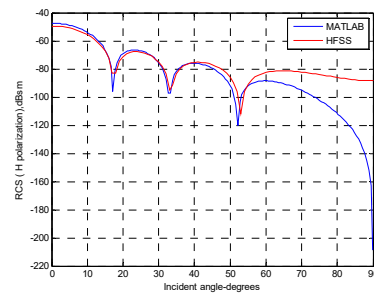
The results reveal another phenomenon, which is that the RCS of a conducting plate is the same as a conducting sheet. This fact is confirmed by existing research (Jenn 2005).

One example: PO (MATLAB) vs. simulation (HFSS) of non-metal amplitude and phase at $\epsilon_r = 2.15$ with 0.0001 ($\sim 0.001 \lambda$) meters, 0.001 (0.01λ) meters, 0.01 ($\sim 0.1 \lambda$) meters of 3 different thicknesses at 0.11 ($\sim 1 \lambda$) meters in radius, produce a difference roughly 20 dB in amplitude for different ϵ_r . Amplitude in metal is about 10 dB greater when compared to non-metal.

For thickness at 0.0001 ($\sim 0.001 \lambda$) meters $\epsilon_r = 2.15$:



TE



TM

Figure 3.80: Amplitude comparison for TE and TM mode in MATLAB and HFSS (offset 0.0001 ($\sim 0.001 \lambda$) meters in thickness by 0.11 ($\sim 1 \lambda$) meters in radius $\epsilon_r = 2.15$ for a thin sheet located in half of $L = 1.1$ ($\sim 10 \lambda$)

meters). Amplitude for TE is in good agreement with HFSS, and matches well for TM as the incident angle is less than 60 degrees.

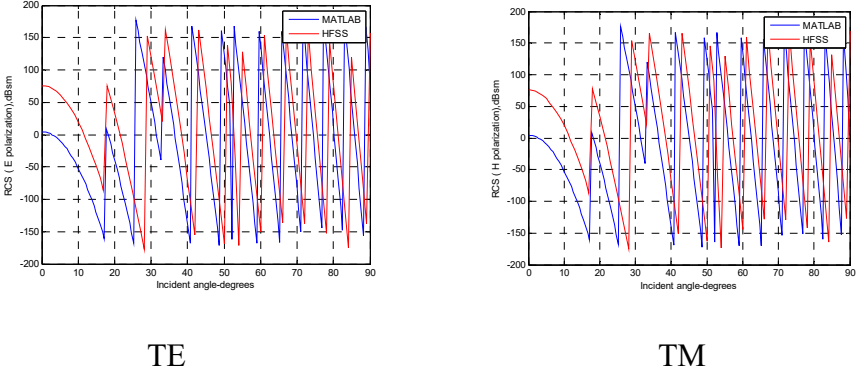


Figure 3.81: Phase comparison for TE and TM mode in MATLAB and HFSS (offset 0.0001 (~0.001 λ) meters in thickness by 0.11 (~1 λ) meters in radius $\epsilon_r = 2.15$ for a thin sheet located in half of $L = 1.1$ (~10 λ) meters). The phase shows a little mismatch for both TE and TM.

For thickness at 0.001 (~0.01 λ) meters $\epsilon_r = 2.15$:

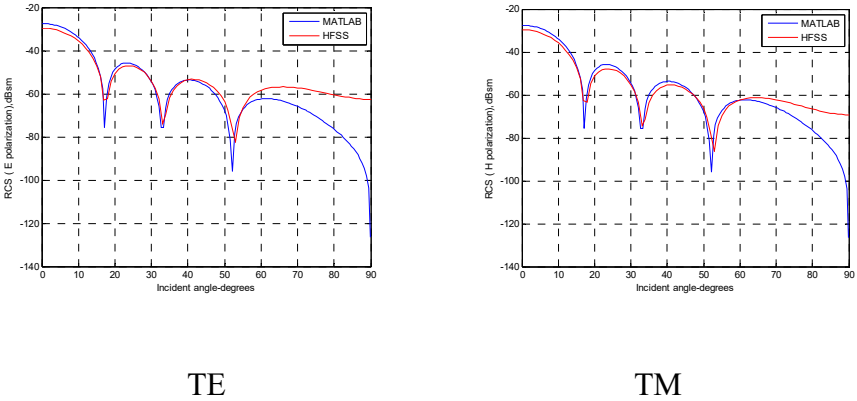
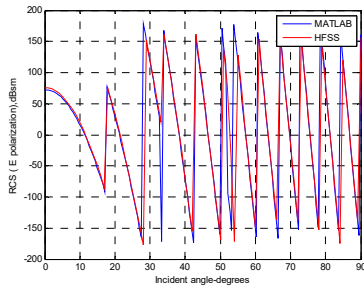
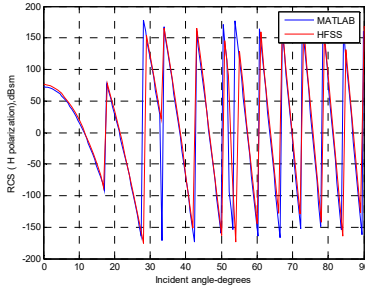


Figure 3.82: Amplitude comparison for TE and TM mode in MATLAB and HFSS (offset 0.001 (~0.01 λ) meters in thickness by 0.11 (~1 λ)

meters in radius $\epsilon_r = 2.15$ for a thin plate located in half of $L = 1.1$ ($\sim 10 \lambda$) meters). Amplitudes match well as the incident angle is less than 50 degrees for both TE and TM.



TE

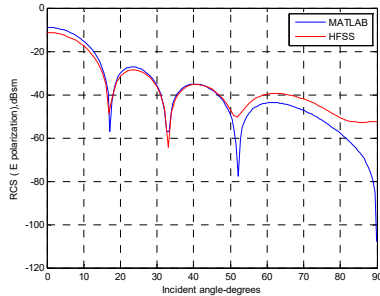


TM

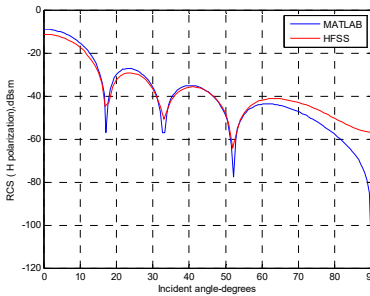
Figure 3.83: Phase comparison for TE and TM mode in MATLAB and HFSS (offset 0.001 ($\sim 0.01 \lambda$) meters in thickness by 0.11 ($\sim 1 \lambda$) meters in radius $\epsilon_r = 2.15$ for a thin plate located in half of $L = 1.1$ ($\sim 10 \lambda$) meters).

The phase matches well to both TE and TM.

For thickness at 0.01 ($\sim 0.1 \lambda$) meters $\epsilon_r = 2.15$:



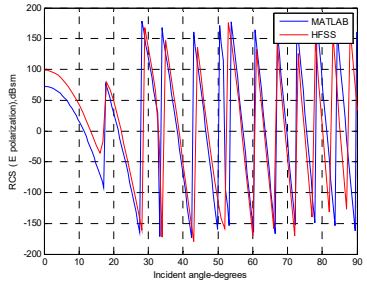
TE



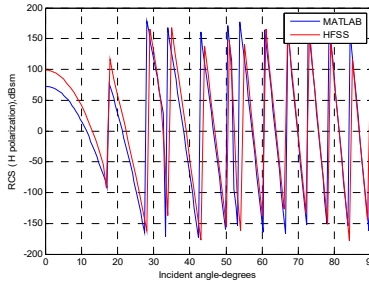
TM

Figure 3.84: Amplitude comparison for TE and TM mode in MATLAB and HFSS (offset 0.01 ($\sim 0.1 \lambda$) meters in thickness by 0.11 ($\sim 1 \lambda$) meters

in radius $\epsilon_r = 2.15$ for a thick plate located in half of $L = 1.1$ ($\sim 10 \lambda$ meters). Amplitudes match well as the incident angle is less than 50 degrees for both TE and TM.



TE

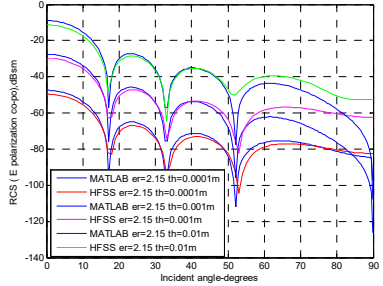


TM

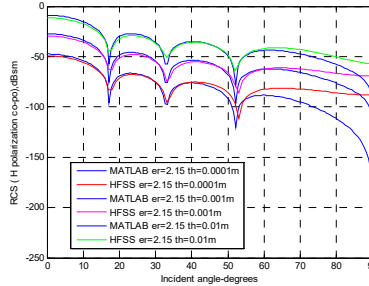
Figure 3.85: Phase comparison for TE and TM mode in MATLAB and HFSS (offset 0.01 ($\sim 0.1 \lambda$) meters in thickness by 0.11 ($\sim 1 \lambda$) meters in radius $\epsilon_r = 2.15$ for a thick plate located in half of $L = 1.1$ ($\sim 10 \lambda$) meters).

The phase matches well as the incident angle is between 60-90 degrees for both TE and TM.

Compare all of 3 different thicknesses:



TE



TM

Figure 3.86: Amplitude comparison for TE and TM mode in MATLAB and HFSS (offset 0.0001 ($\sim 0.001 \lambda$), 0.001 ($\sim 0.01 \lambda$), and 0.01 ($\sim 0.1 \lambda$) meters in 3 different thicknesses by 0.11 ($\sim 1 \lambda$) meters in radius $\epsilon_r = 2.15$ for plates located in half of $L = 1.1$ ($\sim 10 \lambda$) meters). Each thickness produces roughly 20 dB of amplitude difference. Because there is more transmission and less reflection in thinner plates, a thinner thickness corresponds to lower amplitude.

The following figures compare metal case in section 3.3.3: Figure 3.15 has the same thickness 0.01 ($\sim 0.1 \lambda$) meters, while Figure 3.13 has a thickness of 0.001 ($\sim 0.01 \lambda$) meters:

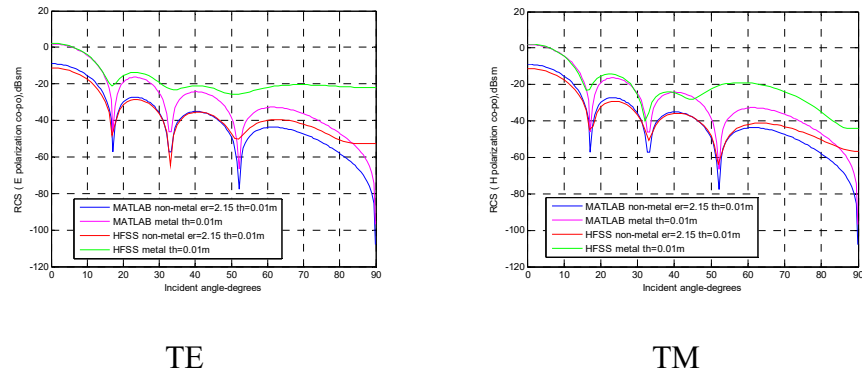
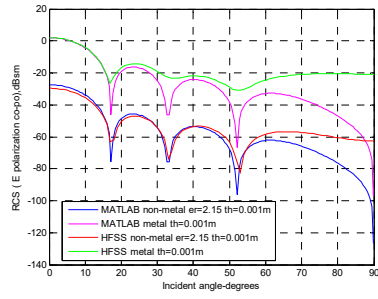
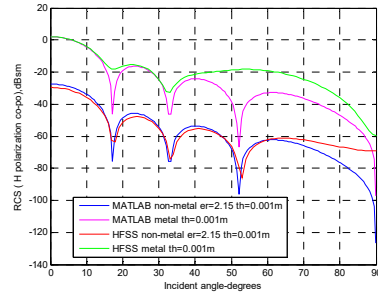


Figure 3.87: Amplitude comparison for TE and TM mode in MATLAB and HFSS (offset 0.01 ($\sim 0.1 \lambda$) meters in thickness by 0.11 ($\sim 1 \lambda$) meters in radius for metal and non-metal $\epsilon_r = 2.15$ for thick plates located in half of $L = 1.1$ ($\sim 10 \lambda$) meters). Amplitude in metal is about 10 dB greater than non-metal due to more reflection and less transmission in the metal plate.



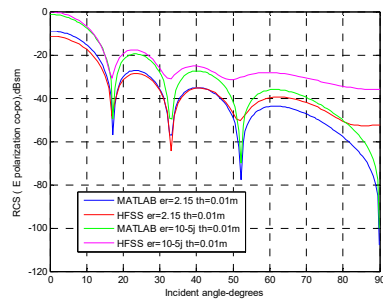
TE



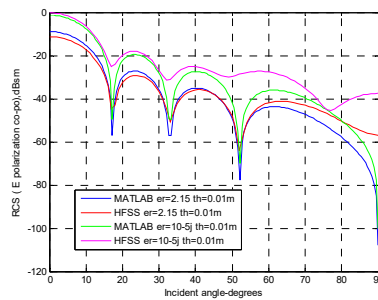
TM

Figure 3.88: Amplitude comparison for TE and TM mode in MATLAB and HFSS (offset 0.001 ($\sim 0.01 \lambda$) meters in thickness by 0.11 ($\sim 1 \lambda$) meters in radius for metal and non-metal $\epsilon_r = 2.15$ for thick plates located in half of $L = 1.1$ ($\sim 10 \lambda$) meters). Amplitude in metal is about 30 dB greater than non-metal due to more reflection and less transmission in the metal plate.

For the same thickness (0.01 ($\sim 0.1 \lambda$) meters or 0.001 ($\sim 0.01 \lambda$) meters) with different $\epsilon_r = 2.15$ and $\epsilon_r = 10-5j$:



TE



TM

Figure 3.89: Amplitude comparison for TE and TM mode in MATLAB and HFSS (offset 0.01 ($\sim 0.1 \lambda$) meters in thickness by 0.11 ($\sim 1 \lambda$) meters

in radius for $\epsilon_r = 2.15$ and $\epsilon_r = 10-5j$ for a thick plate located in half of $L = 1.1$ ($\sim 10 \lambda$) meters). There is about 10 dB difference in amplitude for different ϵ_r . The higher the resistance R for $\epsilon_r = 2.15$, the lower the amplitude.

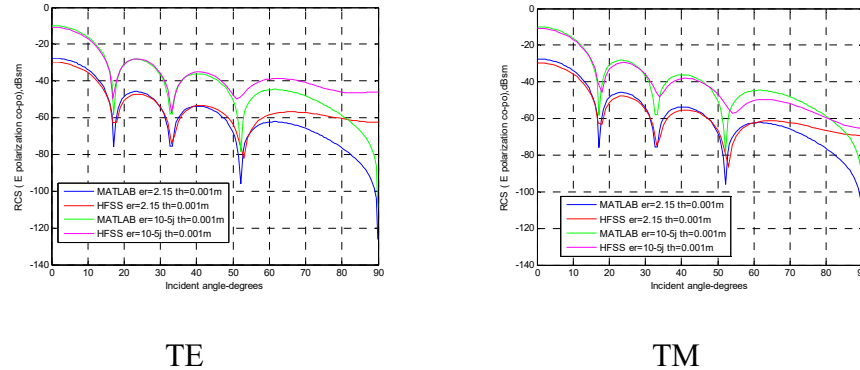


Figure 3.90: Amplitude comparison for TE and TM mode in MATLAB and HFSS (offset 0.001 ($\sim 0.01 \lambda$) meters in thickness by 0.11 ($\sim 1 \lambda$) meters in radius for $\epsilon_r = 2.15$ and $\epsilon_r = 10-5j$ for a thick plate located in half of $L = 1.1$ ($\sim 10 \lambda$) meters). An approximate 20 dB differences in amplitude for different ϵ_r are observed. The higher the resistance at $\epsilon_r = 2.15$, the lower the amplitude.

3.5.1.2 Metal vs. non-metal for rectangular plates

The following is a comparison of two different sizes for non-metal-rectangular plates at $\epsilon_r = 2.15$ or $\epsilon_r = 10-5j$ vs. metal rectangular plates with the same thickness at 0.01 ($\sim 0.1 \lambda$) meters. The amplitudes are in

good agreement with HFSS for all plots. Phase terms are closely matched to both TE and TM.

For metal rectangular plate at thickness 0.01 ($\sim 0.1 \lambda$) meters:

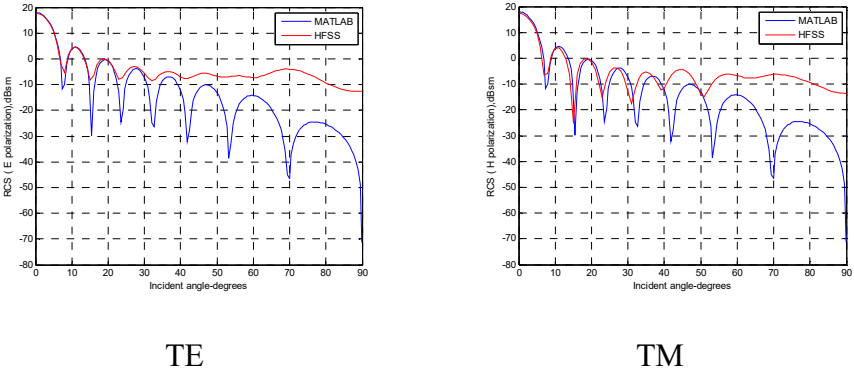


Figure 3.91: Amplitude comparison for TE and TM mode in MATLAB and HFSS (offset 0.01 ($\sim 0.1 \lambda$) meters in thickness for a metal rectangular plate at $a = 0.4$ ($\sim 4 \lambda$) meters, $b = 0.6$ ($\sim 6 \lambda$) meters). Amplitudes match well as the incident angle is less than 30 degrees for both TE and TM.

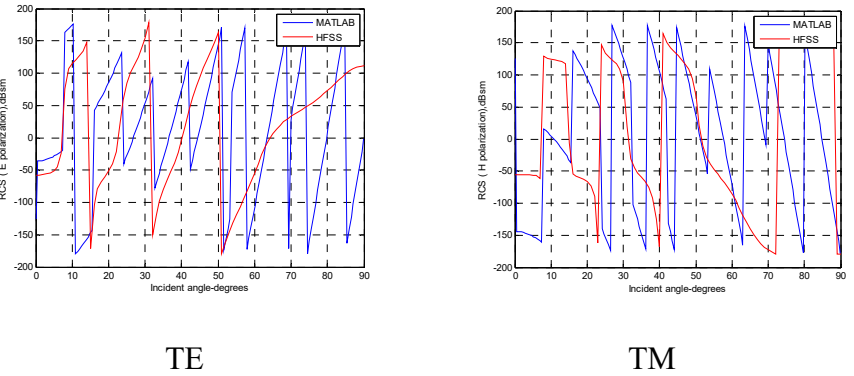


Figure 3.92: Phase comparison for TE and TM mode in MATLAB and HFSS (offset 0.01 ($\sim 0.1 \lambda$) meters in thickness for a metal rectangular

plate at $a = 0.4$ ($\sim 4 \lambda$) meters, $b = 0.6$ ($\sim 6 \lambda$) meters). The phase matches closely for both TE and TM.

For non-metal rectangular plate at 0.01 ($\sim 0.1 \lambda$) meters at $\epsilon_r = 2.15$:

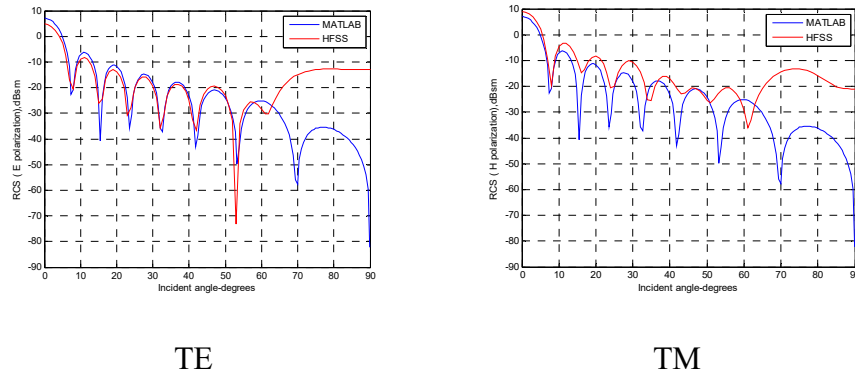


Figure 3.93: Amplitude comparison for TE and TM mode in MATLAB and HFSS (offset 0.01 ($\sim 0.1 \lambda$) meters in thickness by 0.4 ($\sim 3.64 \lambda$) meters by 0.6 ($\sim 5.45 \lambda$) meters $\epsilon_r = 2.15$ for a rectangular thick plate located at origin). Amplitudes match well as the incident angle is less than 50 degrees for TE, and closely matches to TM.

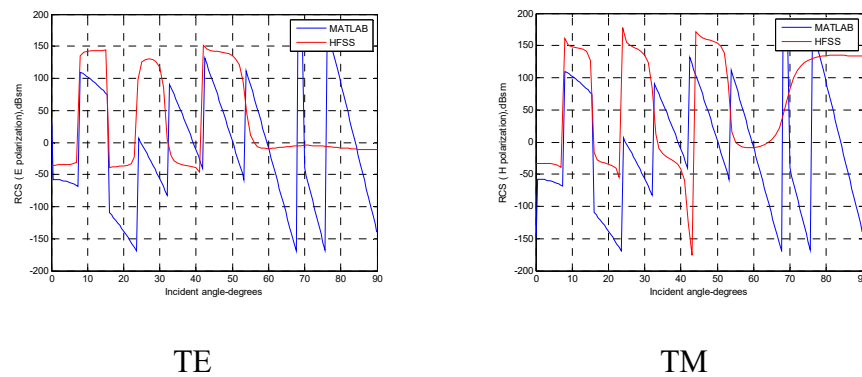


Figure 3.94: Phase comparison for TE and TM mode in MATLAB and HFSS (offset 0.01 ($\sim 0.1 \lambda$) meters in thickness by 0.4 ($\sim 3.64 \lambda$) meters by

0.6 ($\sim 5.45 \lambda$) meters $\epsilon_r = 2.15$ for a rectangular thick plate located at origin). The phase matches closely to both TE and TM.

In a comparison of metal to non-metal plates at the same thicknesses $\epsilon_r = 2.15$:

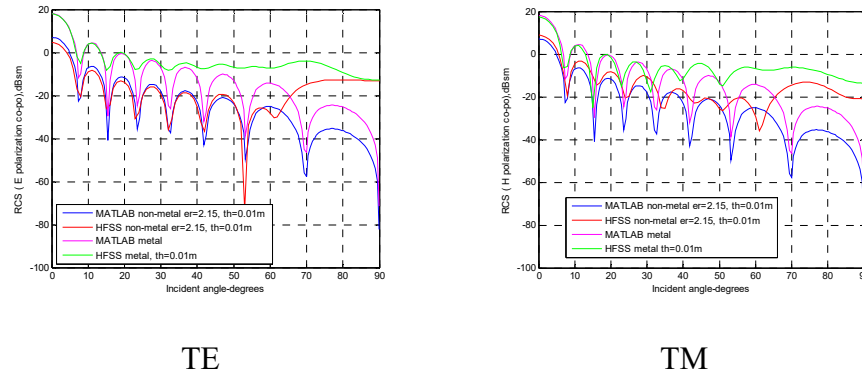
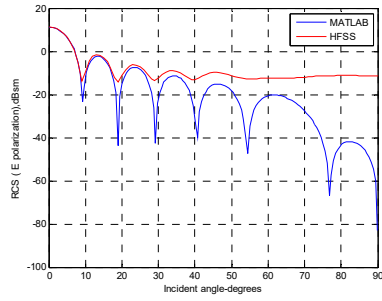
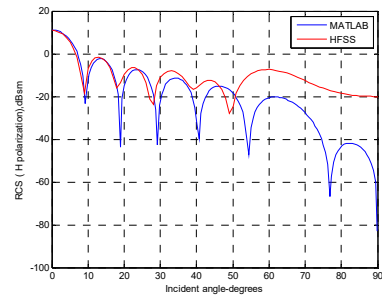


Figure 3.95: Amplitude comparison for TE and TM mode in MATLAB and HFSS (offset 0.01 ($\sim 0.1 \lambda$) meters in thickness by 0.4 ($\sim 3.64 \lambda$) meters by 0.6 ($\sim 5.45 \lambda$) meters $\epsilon_r = 2.15$ for a metal rectangular thick plate at the same thickness located at origin). The amplitude for metal is 10 dB greater than non-metal as a consequence of more reflection and less transmission in metal.

For a different size metal rectangular plate with a thickness of 0.01 ($\sim 0.1 \lambda$) meters at $\epsilon_r = 10-5j$:

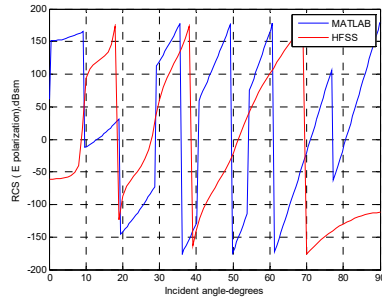


TE

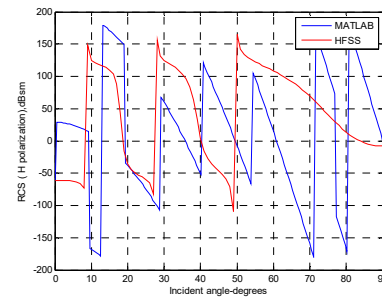


TM

Figure 3.96: Amplitude comparison for TE and TM mode in MATLAB and HFSS (offset 0.01 ($\sim 0.1 \lambda$) meters in thickness for a metal rectangular plate at $a = 0.33$ ($\sim 3 \lambda$) meters, $b = 0.33$ ($\sim 3 \lambda$) meters). Amplitudes are in good agreement with HFSS as the incident angle is less than 30 degrees for both TE and TM.



TE



TM

Figure 3.97: Phase comparison for TE and TM mode in MATLAB and HFSS (offset 0.01 ($\sim 0.1 \lambda$) meters in thickness for a metal rectangular plate at $a = 0.33$ ($\sim 3 \lambda$) meters, $b = 0.33$ ($\sim 3 \lambda$) meters). The phase matches closely to both TE and TM.

For the same size non-metal rectangular plate with a thickness of 0.01 (~0.1 λ) meters at $\epsilon_r = 10-5j$:

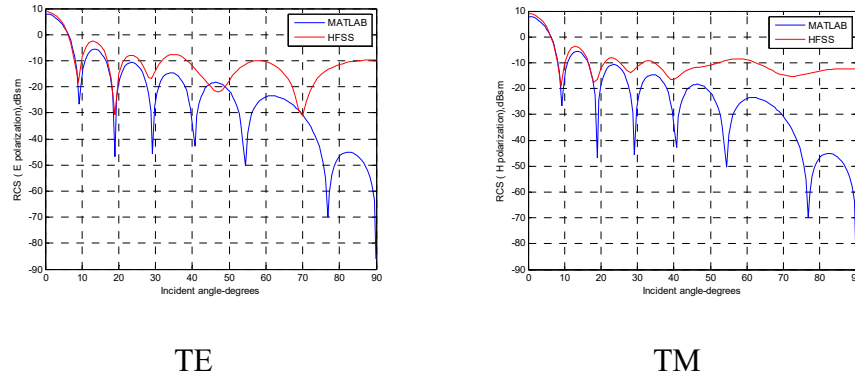


Figure 3.98: Amplitude comparison for TE and TM mode in MATLAB and HFSS (offset 0.01 (~0.1 λ) meters in thickness 0.33 (~3 λ) by 0.33 (~3 λ) meters at $\epsilon_r = 10-5j$ for a rectangular thick plate located at origin). Amplitudes are in good agreement with HFSS as the incident angle is less than 30 degrees for both TE and TM.

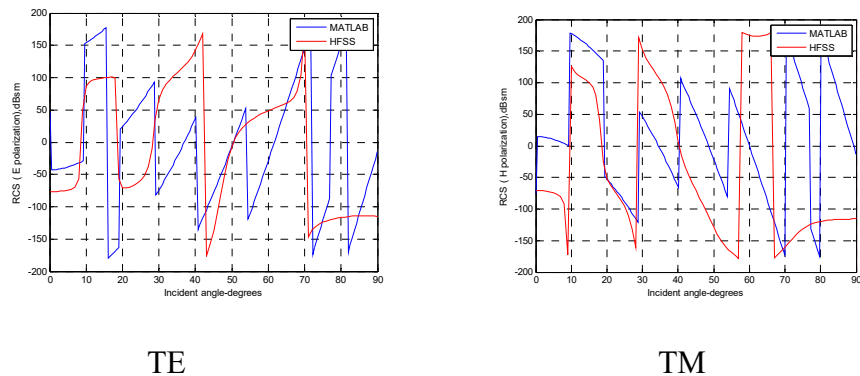


Figure 3.99: Phase comparison for TE and TM mode in MATLAB and HFSS (offset 0.01 (~0.1 λ) meters in thickness 0.33 (~3 λ) by 0.33 (~3 λ) meters at $\epsilon_r = 10-5j$ for a rectangular thick plate located at origin).

meters at $\epsilon_r = 10-5j$ for a rectangular thick plate located at origin). The phase matches closely to TE and TM.

To compare metal with non-metal plate at the same thicknesses $\epsilon_r = 10-5j$:

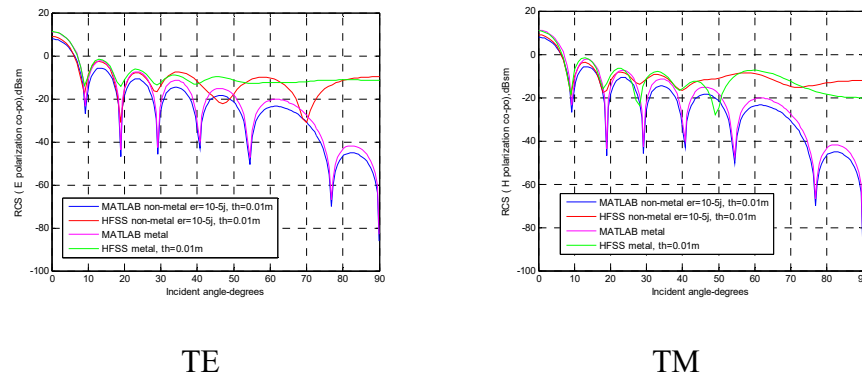


Figure 3.100: Amplitude comparison for TE and TM mode in MATLAB and HFSS (offset 0.01 ($\sim 0.1 \lambda$) meters in thickness 0.33 ($\sim 3 \lambda$) by 0.33 ($\sim 3 \lambda$) meters at $\epsilon_r = 10-5j$ for a metal rectangular thick plate located at origin). Amplitude in metal is higher than non-metal materials because of more reflection and less transmission in metal. Amplitude of a metal rectangular plate is close to a non-metal plate at a relative permittivity of 10-5j.

In this comparison of PO vs. simulation (metal vs. non-metal (wood $\epsilon_r = 2.15$)), again, errors are shown due to edge effect at angles close to 90 degrees for both metal and non-metal plates. Also, the RCS amplitudes of metal plates for both MATLAB and HFSS are higher than non-metal plates, as was expected. These phenomena are due to greater transmission and less reflection on non-metal plates. Examples for non-metal plates

with different thicknesses (0.0001 ($\sim 0.001 \lambda$) meters, 0.001 ($\sim 0.01 \lambda$) meters, and 0.01 ($\sim 0.1 \lambda$) meters) indicate that values of HFSS simulation and MATLAB are getting higher as thicknesses increase. This is due to the correlation to thinner plates, which provide less reflection and more penetration.

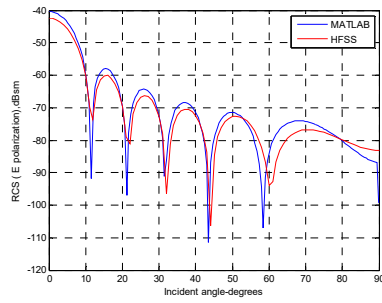
3.5.2 Thick vs. thin – PO vs. simulations

The results show that metal cases match well between HFSS and MATLAB for larger sizes. The amplitudes are in good agreement with HFSS as the incident angle is less than around 50 degrees for non-metal plots. Phase terms are closely matched to both TE and TM.

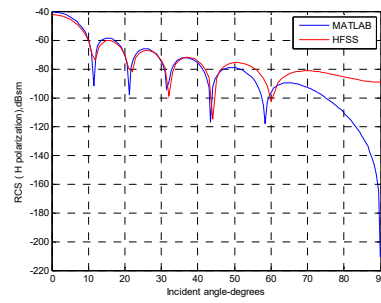
3.5.2.1 Thin vs. thick for circular non-metal plates

The following examples compare a dielectric thin sheet of three different thicknesses: thickness = 0.0001 ($\sim 0.001 \lambda$) meters at $\epsilon_r = 2.15$ by 0.165 ($\sim 1.5 \lambda$) meters in radius; the same size dielectric thin plate where thickness = 0.001 ($\sim 0.01 \lambda$) meters at $\epsilon_r = 2.15$; and the same size dielectric thick plate where thickness = 0.01 ($\sim 0.1 \lambda$) meters at $\epsilon_r = 2.15$. The resulting plots show that there are about 20 dB differences between each scale.

For a dielectric thin sheet with a thickness of 0.0001 ($\sim 0.001 \lambda$) meters at $\epsilon_r = 2.15$:

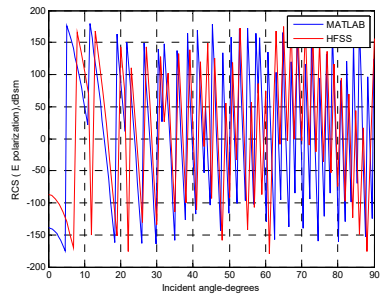


TE

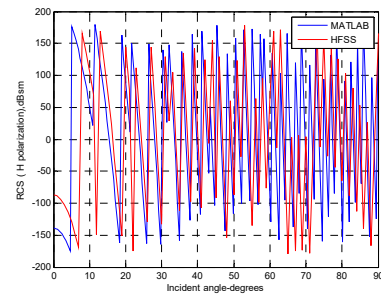


TM

Figure 3.101: Amplitude comparison for TE and TM mode in MATLAB and HFSS (offset 0.0001 ($\sim 0.001 \lambda$) meters in thickness by 0.165 ($\sim 1.5 \lambda$) meters in radius $\epsilon_r = 2.15$ for a thin sheet located in half of $L = 3.3$ ($\sim 30 \lambda$) meters). Amplitudes for TE and TM match closely as the incident angle is less than 50 degrees.



TE



TM

Figure 3.102: Phase comparison for TE and TM mode in MATLAB and HFSS (offset 0.0001 ($\sim 0.001 \lambda$) meters in thickness by 0.165 ($\sim 1.5 \lambda$) meters in radius $\epsilon_r = 2.15$ for a thin sheet located in half of $L = 3.3$ ($\sim 30 \lambda$) meters). The phase shows a little mismatch for TE and TM with an incident angle of less than 20 degrees.

For the same size dielectric thin plate with a thickness of 0.001 ($\sim 0.01 \lambda$) meters at $\epsilon_r = 2.15$:

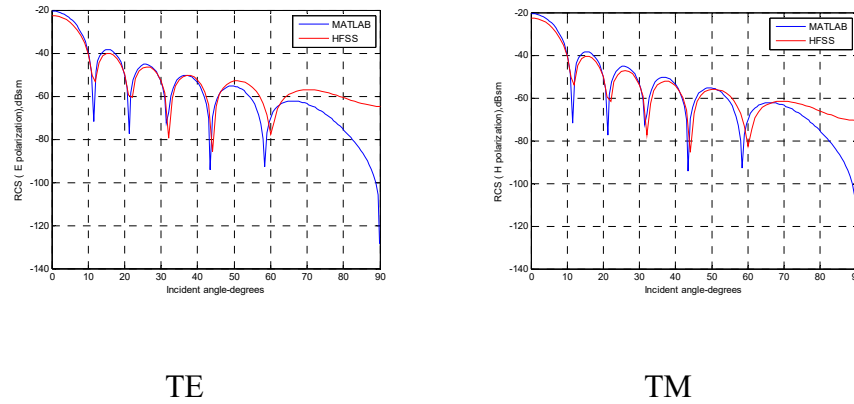


Figure 3.103: Amplitude comparison for TE and TM mode in MATLAB and HFSS (offset 0.001 ($\sim 0.01 \lambda$) meters in thickness by 0.165 ($\sim 1.5 \lambda$) meters in radius $\epsilon_r = 2.15$ for a thin plate located in half of $L = 3.3$ ($\sim 30 \lambda$) meters). Amplitudes are in good agreement with HFSS as the incident angle is less than 50 degrees for both TE and TM.

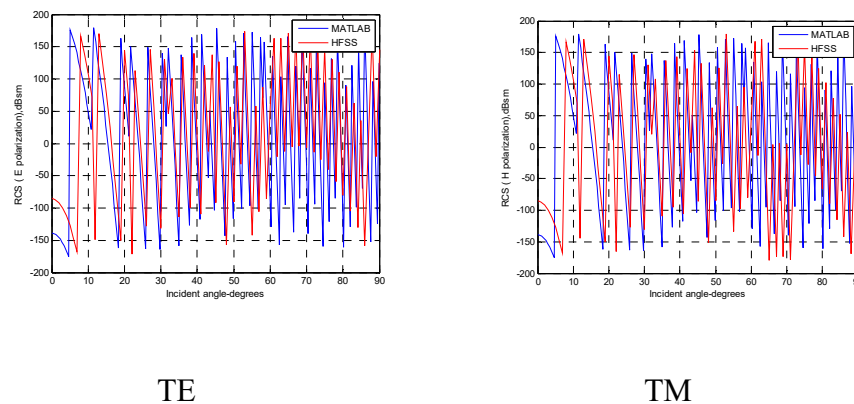


Figure 3.104: Phase comparison for TE and TM mode in MATLAB and HFSS (offset 0.001 ($\sim 0.01 \lambda$) meters in thickness by 0.165 ($\sim 1.5 \lambda$) meters in radius $\epsilon_r = 2.15$ for a thin plate located in half of $L = 3.3$ ($\sim 30 \lambda$) meters). The phase shows mismatch as the incident angle is less than 20 degrees.

For the same size dielectric plate with a thickness of 0.01 ($\sim 0.1 \lambda$) meters at $\epsilon_r = 2.15$:

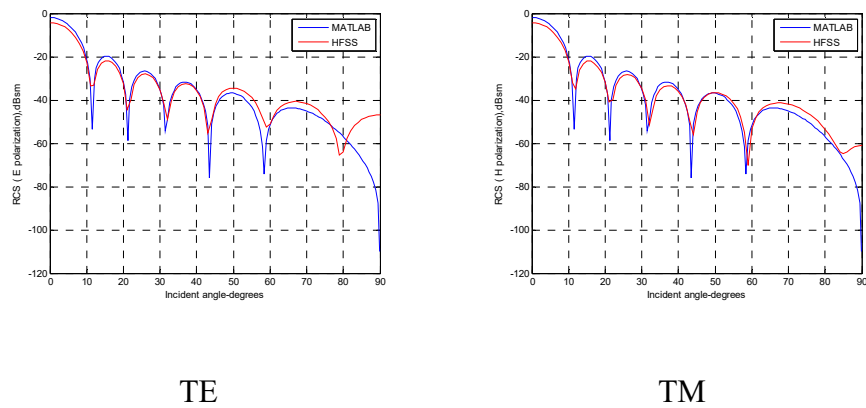
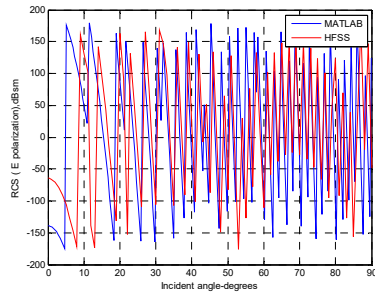
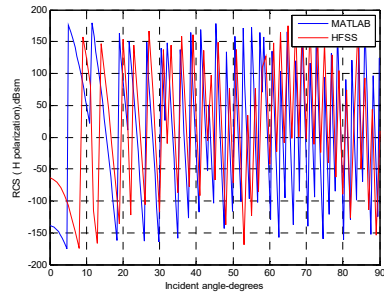


Figure 3.105: Amplitude comparison for TE and TM mode in MATLAB and HFSS (offset 0.01 ($\sim 0.1 \lambda$) meters in thickness by 0.165 ($\sim 1.5 \lambda$) meters in radius $\epsilon_r = 2.15$ for a thick plate located in half of $L = 3.3$ ($\sim 30 \lambda$) meters). Amplitudes are in good agreement with HFSS as the incident angle is less than 50 degrees for both TE and TM.



TE

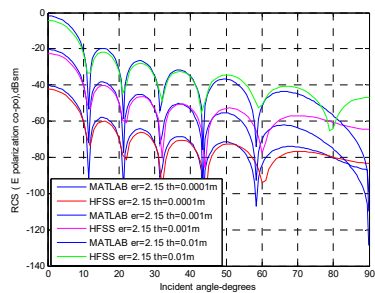


TM

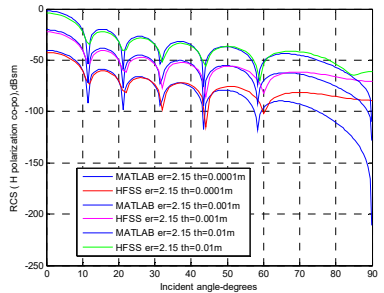
Figure 3.106: Phase comparison for TE and TM mode in MATLAB and HFSS (offset 0.01 ($\sim 0.1 \lambda$) meters in thickness by 0.165 ($\sim 1.5 \lambda$) meters in radius $\epsilon_r = 2.15$ for a thick plate located in half of $L = 3.3$ ($\sim 30 \lambda$) meters).

The phase shows mismatch as the incident angle is less than 20 degrees.

The following figures compare all three thicknesses:



TE



TM

Figure 3.107: Amplitude comparison for TE and TM mode in MATLAB and HFSS (offset 0.0001 ($\sim 0.001 \lambda$) meters, 0.001 ($\sim 0.01 \lambda$) meters, and 0.01 ($\sim 0.1 \lambda$) meters in thickness by 0.165 ($\sim 1.5 \lambda$) meters in radius $\epsilon_r = 2.15$ for a thin plate located in half of $L = 3.3$ ($\sim 30 \lambda$) meters). The plots

for both HFSS and the analytical results demonstrate that amplitude differs by about 20 dB as scales increase in thickness by multiples of ten.

Another set of examples compare three dielectric plates of varying thicknesses: dielectric thin sheet where thickness = 0.0001 (~0.001 λ) meters at $\epsilon_r = 10-5j$ by 0.165 (~1.5 λ) meters in radius; the same size dielectric thin plate where thickness = 0.001 (~0.01 λ) meters at $\epsilon_r = 10-5j$; and the same size dielectric thick plate where thickness = 0.01 (~0.1 λ) meters at $\epsilon_r = 10-5j$:

For dielectric thin sheet at thickness 0.0001 (~0.001 λ) meters at $\epsilon_r = 10-5j$:

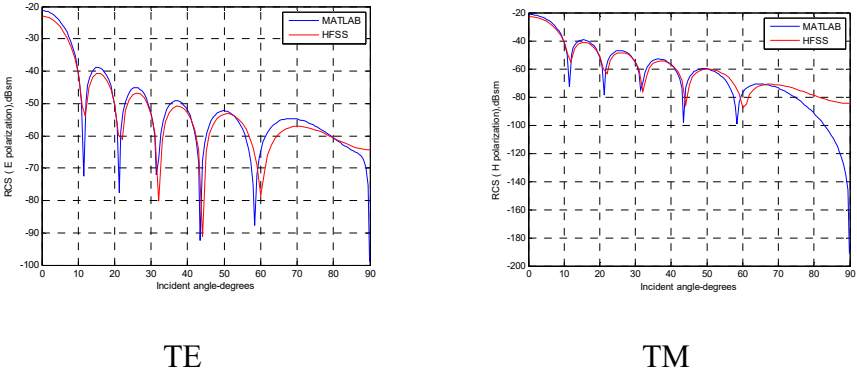
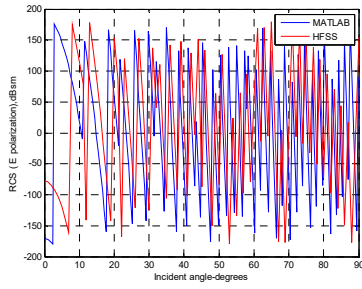
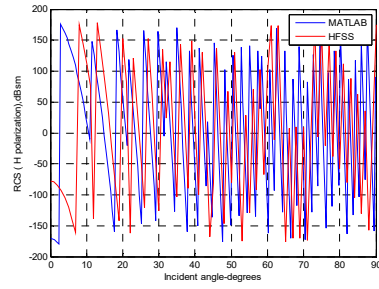


Figure 3.108: Amplitude comparison for TE and TM mode in MATLAB and HFSS (offset 0.0001 (~0.001 λ) meters in thickness by 0.165 (~1.5 λ) meters in radius $\epsilon_r = 10-5j$ for a thin sheet located in half of $L = 3.3$ (~30 λ) meters). Amplitudes are in good agreement with HFSS as the incident angle is less than 50 degrees for both TE and TM.



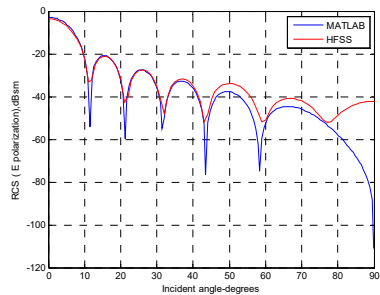
TE



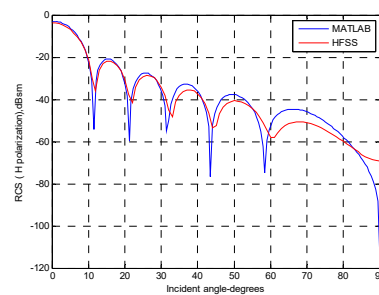
TM

Figure 3.109: Phase comparison for TE and TM mode in MATLAB and HFSS (offset 0.0001 ($\sim 0.001 \lambda$) meters in thickness by 0.165 ($\sim 1.5 \lambda$) meters in radius $\epsilon_r = 10-5j$ for a thin sheet located in half of $L = 3.3$ ($\sim 30 \lambda$) meters). The phase shows a little mismatch for TE and TM, as the incident angle is less than 20 degrees.

For a dielectric thin plate with a thickness 0.001 ($\sim 0.01 \lambda$) meters at $\epsilon_r = 10-5j$:



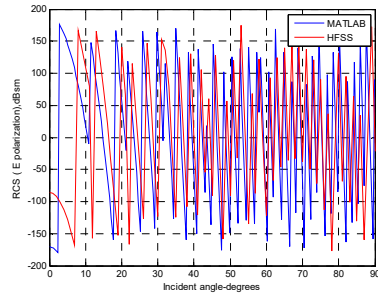
TE



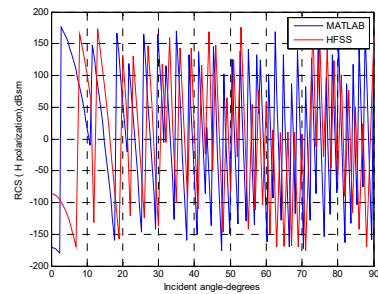
TM

Figure 3.110: Amplitude comparison for TE and TM mode in MATLAB and HFSS (offset 0.001 ($\sim 0.01 \lambda$) meters in thickness by 0.165 ($\sim 1.5 \lambda$) meters in radius $\epsilon_r = 10-5j$ for a thin plate located in half of $L = 3.3$ ($\sim 30 \lambda$) meters).

λ) meters). Amplitudes match well as the incident angle is less than 50 degrees for both TE and TM.



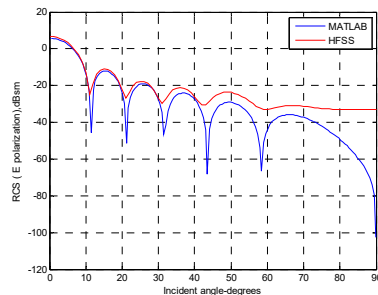
TE



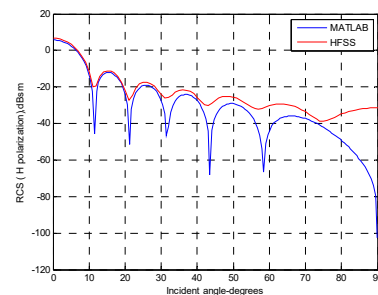
TM

Figure 3.111: Phase comparison for TE and TM mode in MATLAB and HFSS (offset 0.001 ($\sim 0.01 \lambda$) meters in thickness by 0.165 ($\sim 1.5 \lambda$) meters in radius $\epsilon_r = 10-5j$ for a thin plate located in half of $L = 3.3$ ($\sim 30 \lambda$) meters). The phase shows mismatch as the incident angle is less than 20 degrees.

For a dielectric thin plate with a thickness of 0.01 ($\sim 0.1 \lambda$) meters at $\epsilon_r = 10-5j$:



TE



TM

Figure 3.112: Amplitude comparison for TE and TM mode in MATLAB and HFSS (offset 0.01 (~0.1 λ) meters in thickness by 0.165 (~1.5 λ) meters in radius $\epsilon_r = 10-5j$ for a plate located in half of $L = 3.3$ (~30 λ) meters). Amplitudes match well as the incident angle is less than 30 degrees for both TE and TM.

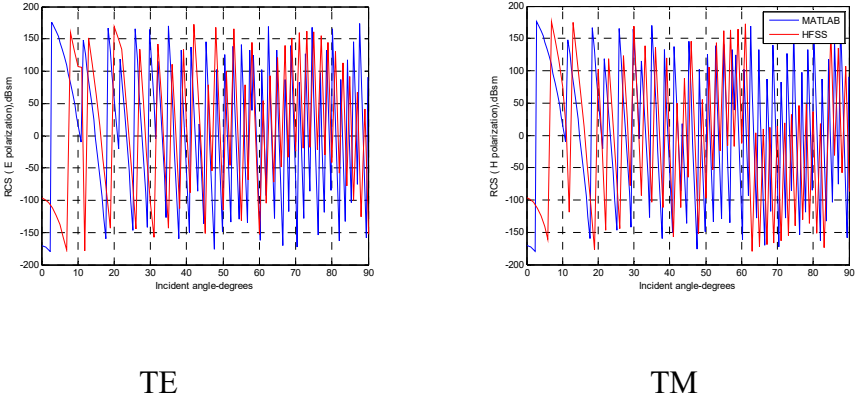
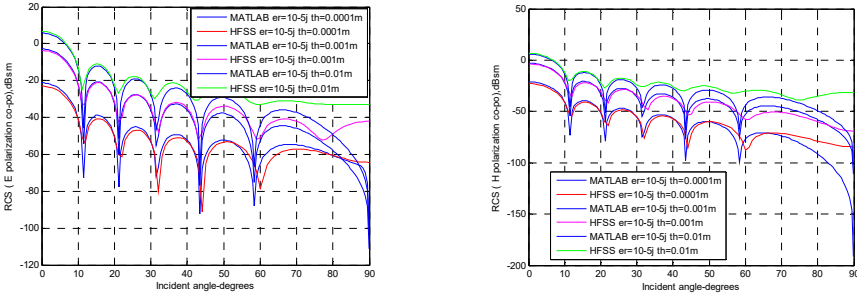


Figure 3.113: Phase comparison for TE and TM mode in MATLAB and HFSS (offset 0.01 (~0.1 λ) meters in thickness by 0.165 (~1.5 λ) meters in radius $\epsilon_r = 10-5j$ for a thin plate located in half of $L = 3.3$ (~30 λ) meters). The phase shows mismatch as the incident angle is less than 20 degrees.

The following figures compare all three different thicknesses:



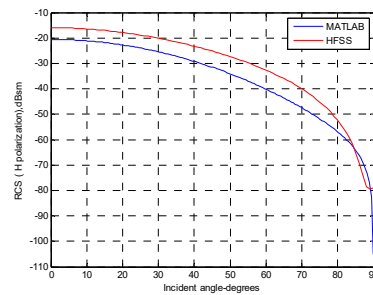
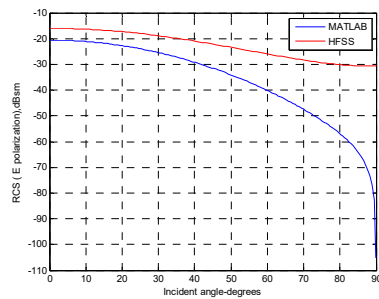
TE

TM

Figure 3.114: Amplitude comparison for TE and TM mode in MATLAB and HFSS (offset 0.0001 (~0.001 λ) meters, 0.001 (~0.01 λ) meters, and 0.01 (~0.1 λ) meters in 3 different thicknesses by 0.165 (~1.5 λ) meters in radius $\epsilon_r = 10-5j$ for plates located in half of $L = 3.3$ (~30 λ) meters). It appears that amplitude differs by about 10 dB when comparing thicknesses of 0.001 (~0.01 λ) meters and 0.01 (~0.1 λ) meters, and amplitude differs by about 20 dB when comparing thicknesses of 0.0001 (~0.001 λ) meters and 0.001 (~0.01 λ) meters.

3.5.2.2 Thin vs. thick for circular metal plates

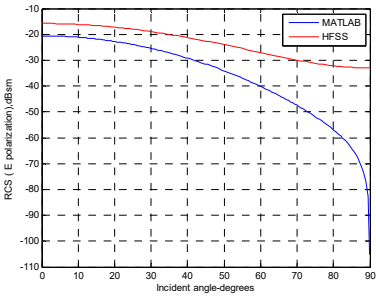
When comparing examples of a small circular plate with a radius of 0.03 (~0.3 λ) meters for different thickness, including 0.0003 (~0.003 λ) meters, 0.003 (~0.03 λ) meters, and 0.03 (~0.3 λ) meters located at origin, the amplitudes for different thickness are closer to one another. The phase terms are the same as those illustrated in Figure 3.8.



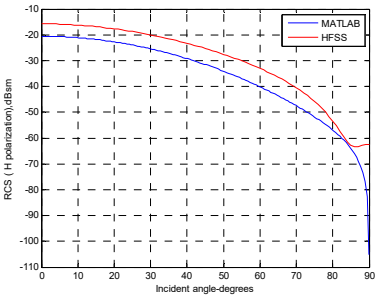
TE

TM

Figure 3.115: Amplitude comparison for TE and TM mode in MATLAB and HFSS (offset 0.0003 (~0.003 λ) meters in thickness by 0.03 (~0.3 λ) meters in radius for a conducting thin sheet located at origin). Amplitude differs by a few dB for both TE and TM.

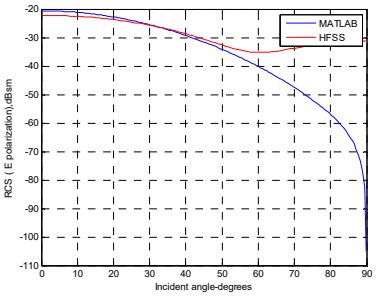


TE

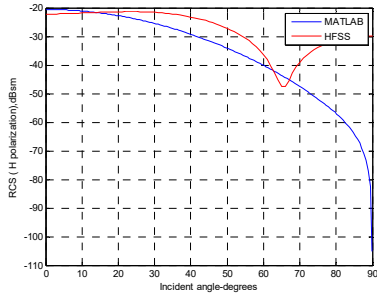


TM

Figure 3.116: Amplitude comparison for TE and TM mode in MATLAB and HFSS (offset 0.003 (~0.03 λ) meters in thickness by 0.03 (~0.3 λ) meters in radius for a conducting thin plate located at origin). Amplitude differs by a few dB for both TE and TM.



TE



TM

Figure 3.117: Amplitude comparison for TE and TM mode in MATLAB and HFSS (offset 0.03 ($\sim 0.3 \lambda$) meters in thickness by 0.03 ($\sim 0.3 \lambda$) meters in radius for a conducting thick plate located at origin). Amplitude matches well for TE as the incident angle is less than 40 degrees, and matches closely for TM as the incident angle is less than 20 degrees.

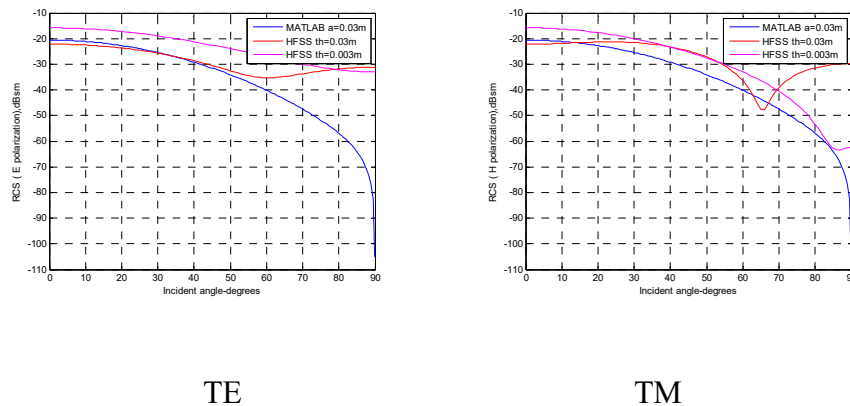
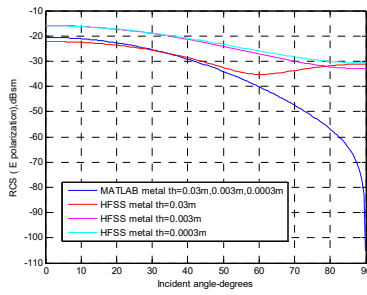
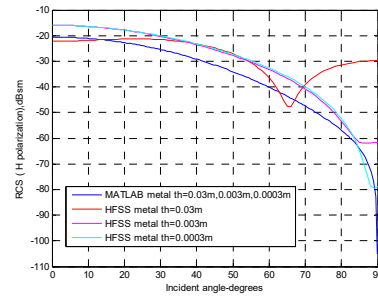


Figure 3.118: Amplitude comparison for TE and TM mode in MATLAB and HFSS (offset 0.03 ($\sim 0.3 \lambda$) meters and 0.003 ($\sim 0.03 \lambda$) meters in 2 different thicknesses by 0.03 ($\sim 0.3 \lambda$) meters in radius for a conducting thick plate located at origin). Amplitude is greater for thicker plates when compared to thinner plates as a consequence of more penetration in thinner plates.

The following figures compare all 3 different thicknesses:



TE

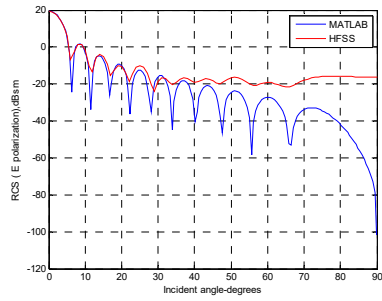


TM

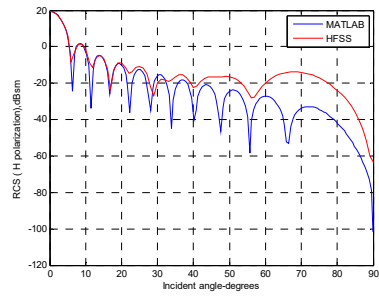
Figure 3.119: Amplitude comparison for TE and TM mode in MATLAB and HFSS (offset 0.03 ($\sim 0.3 \lambda$) meters, 0.003 ($\sim 0.03 \lambda$) meters, and 0.0003 ($\sim 0.003 \lambda$) meters in 3 different thicknesses by 0.03 ($\sim 0.3 \lambda$) meters in radius for a conducting thick plate located at origin). HFSS shows little difference for varying thickness.

When thickness increases, HFSS simulation is close to the analytical results for both TE and TM for a smaller circular plate at 0.03 ($\sim 0.3 \lambda$) meters in radius, but shows a small gap for other thicknesses. This is because HFSS is not suitable for electrically small objects.

In another example of a larger circular plate with a radius of 0.3 ($\sim 3 \lambda$) meters located at origin, and at different thicknesses from 0.0002 ($\sim 0.002 \lambda$) meters, 0.002 ($\sim 0.02 \lambda$) meters, and 0.02 ($\sim 0.2 \lambda$) meters, the phase terms are the same as those illustrated in Figure 3.20. Amplitudes match well as the incident angle is less than 30 degrees for both TE and TM.

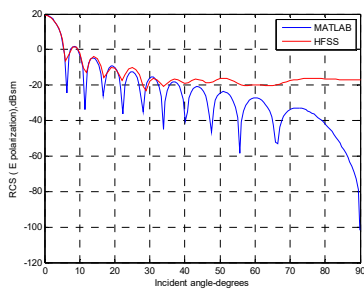


TE

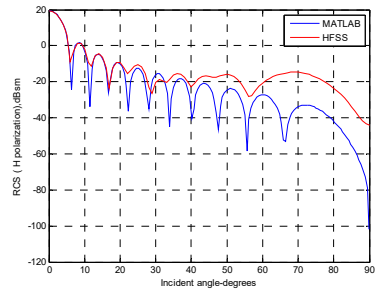


TM

Figure 3.120: Amplitude comparison for TE and TM mode in MATLAB and HFSS (offset 0.0002 ($\sim 0.002 \lambda$) meters in thickness by 0.3 ($\sim 3 \lambda$) meters in radius for a conducting thin sheet located at origin). Amplitudes match well as the incident angle is less than 30 degrees for both TE and TM.

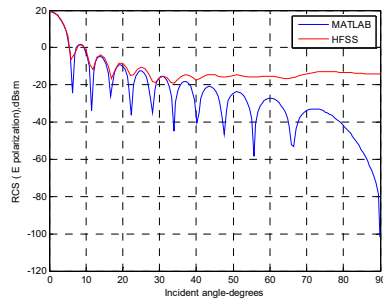


TE

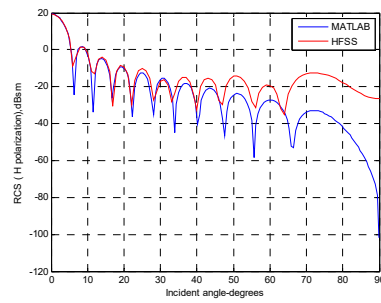


TM

Figure 3.121: Amplitude comparison for TE and TM mode in MATLAB and HFSS (offset 0.002 ($\sim 0.02 \lambda$) meters in thickness by 0.3 ($\sim 3 \lambda$) meters in radius for a conducting thin plate located at origin). Amplitudes match well as the incident angle is less than 30 degrees for both TE and TM.



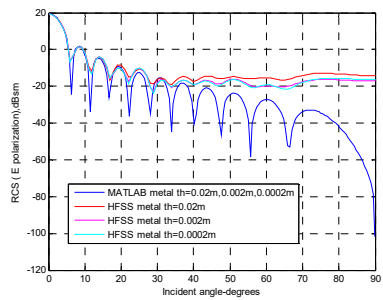
TE



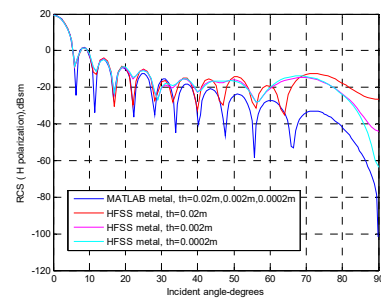
TM

Figure 3.122: Amplitude comparison for TE and TM mode in MATLAB and HFSS (offset 0.02 ($\sim 0.2 \lambda$) meters in thickness by 0.3 ($\sim 3 \lambda$) meters in radius for a conducting plate located at origin). Amplitudes match well as the incident angle is less than 30 degrees for both TE and TM.

The following figures compare all different thicknesses:



TE



TM

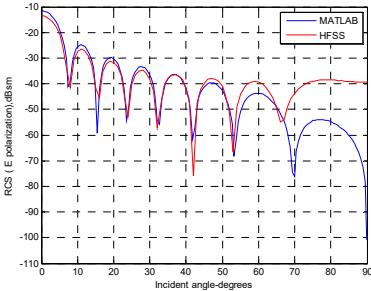
Figure 3.123: Amplitude comparison for TE and TM mode in MATLAB and HFSS (offset 0.02 ($\sim 0.2 \lambda$) meters, 0.002 ($\sim 0.02 \lambda$) meters, and 0.0002 ($\sim 0.002 \lambda$) meters in 3 different thicknesses by 0.3 ($\sim 3 \lambda$) meters in radius for conducting plates located at origin). Amplitudes match well for all

three thicknesses as the incident angle is less than 30 degrees for both TE and TM.

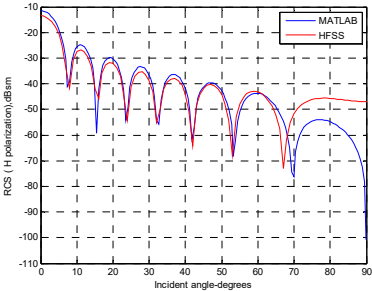
The plots shown above indicate that amplitudes for a conducting circular thicker plate are the same as a conducting sheet for several wavelengths in radius. This phenomenon is consistent with published research (Jenn 2005), and is due to the non-penetrative characteristic of PEC material. The analytical plots are almost the same as HFSS for a larger circular plate across all thicknesses at radius $0.3 (\sim 3 \lambda)$ meters. The errors are obvious as the incident angle is above 50 degrees.

3.5.2.3 Thin vs. thick for rectangular non-metal plates

For rectangular plates measuring $0.4 (\sim 3.64 \lambda)$ meters by $0.6 (\sim 5.45 \lambda)$ meters at $\epsilon_r = 2.15$ with thicknesses of $0.01 (\sim 0.1 \lambda)$ meters (Figure 3.93, Figure 3.94), $0.001 (\sim 0.01 \lambda)$ meters, and $0.0001 (\sim 0.001 \lambda)$ meters, amplitudes vary by about 20 dB for each scale change in thickness (ten times bigger from thin to thick) for both MATLAB and HFSS.



TE



TM

Figure 3.124: Amplitude comparison for TE and TM mode in MATLAB and HFSS (offset 0.001 ($\sim 0.01 \lambda$) meters in thickness by 0.4 ($\sim 3.64 \lambda$) meters by 0.6 ($\sim 5.45 \lambda$) meters $\epsilon_r = 2.15$ for a rectangular thin plate located at origin). Amplitudes match well as the incident angle is less than 50 degrees for both TE and TM.

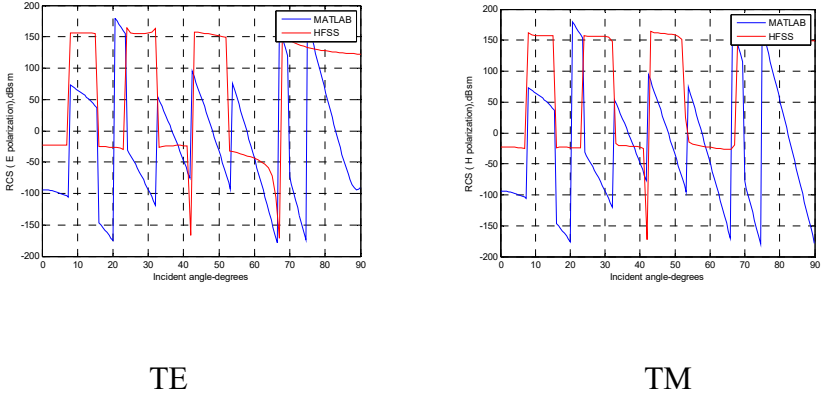


Figure 3.125: Phase comparison for TE and TM mode in MATLAB and HFSS (offset 0.001 ($\sim 0.01 \lambda$) meters in thickness by 0.4 ($\sim 3.64 \lambda$) meters by 0.6 ($\sim 5.45 \lambda$) meters $\epsilon_r = 2.15$ for a rectangular thin plate located at origin). The phase matches closely to both TE and TM.

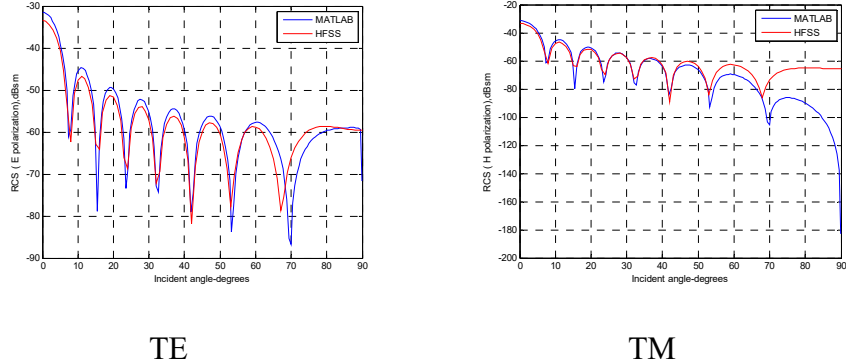
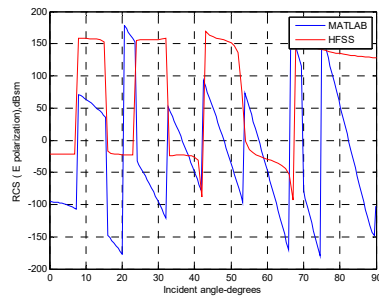
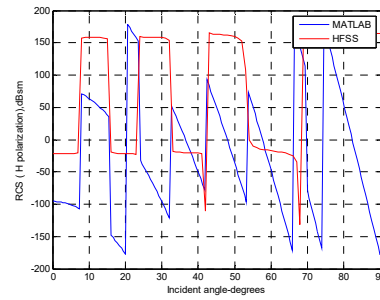


Figure 3.126: Amplitude comparison for TE and TM mode in MATLAB and HFSS (offset 0.0001 ($\sim 0.001 \lambda$) meters in thickness by 0.4 ($\sim 3.64 \lambda$) meters by 0.6 ($\sim 5.45 \lambda$) meters $\epsilon_r = 2.15$ for a rectangular thin sheet located at origin). Amplitudes match closely to both TE and TM as the incident angle is less than 50 degrees.



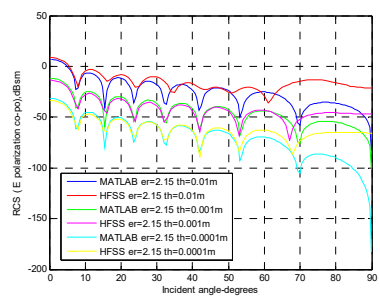
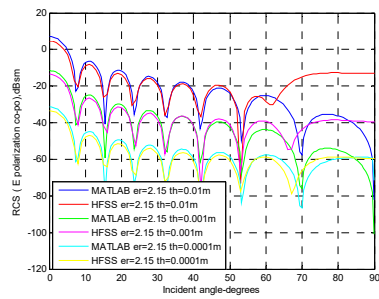
TE



TM

Figure 3.127: Phase comparison for TE and TM mode in MATLAB and HFSS (offset 0.0001 ($\sim 0.001 \lambda$) meters in thickness by 0.4 ($\sim 3.64 \lambda$) meters by 0.6 ($\sim 5.45 \lambda$) meters $\epsilon_r = 2.15$ for a rectangular thin sheet located at origin). The phase matches closely to both TE and TM.

The following figures compare all three different thicknesses:

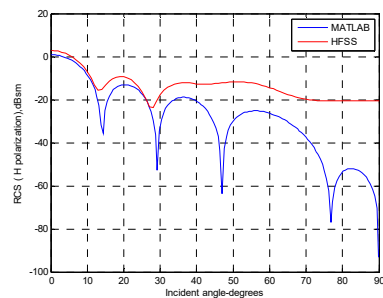
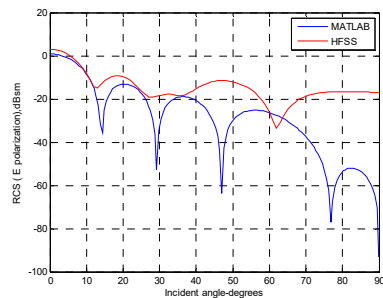


TE

TM

Figure 3.128: Amplitude comparison for TE and TM mode in MATLAB and HFSS (offset 0.0001 ($\sim 0.001 \lambda$) meters, 0.001 ($\sim 0.01 \lambda$) meters, and 0.01 ($\sim 0.1 \lambda$) meters in 3 different thicknesses by 0.4 ($\sim 3.64 \lambda$) meters by 0.6 ($\sim 5.45 \lambda$) meters $\epsilon_r = 2.15$ for rectangular plates located at origin). Amplitudes vary by about 20 dB for each scale change in thickness (ten times bigger from thin to thick) for both MATLAB and HFSS.

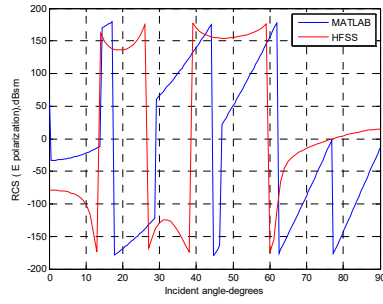
For different thicknesses at 0.01 ($\sim 0.1 \lambda$) meters $\epsilon_r = 10-5j$, amplitudes have less than 10 dB or 20 dB differences between two plates.



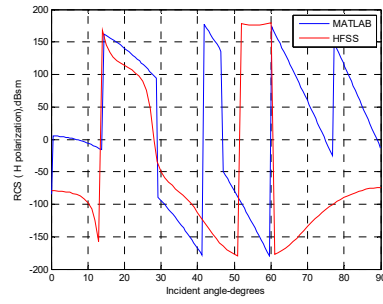
TE

TM

Figure 3.129: Amplitude comparison for TE and TM mode in MATLAB and HFSS (offset 0.01 ($\sim 0.1 \lambda$) meters in thickness by 0.22 ($\sim 2 \lambda$) meters by 0.22 ($\sim 2 \lambda$) meters $\epsilon_r = 10-5j$ for a rectangular thick plate located at origin). Amplitudes match closely as the incident angle is less than 30 degrees for both TE and TM.

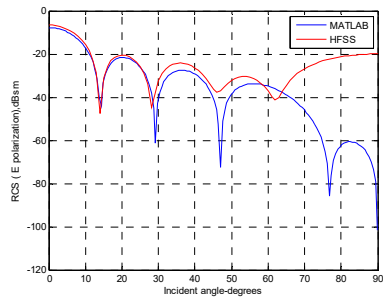


TE

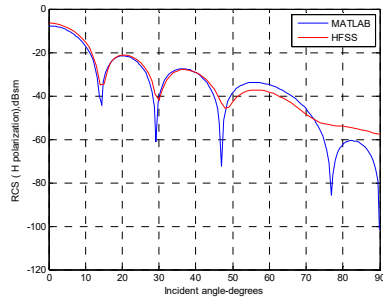


TM

Figure 3.130: Phase comparison for TE and TM mode in MATLAB and HFSS (offset 0.01 ($\sim 0.1 \lambda$) meters in thickness by 0.22 ($\sim 2 \lambda$) meters by 0.22 ($\sim 2 \lambda$) meters $\epsilon_r = 10-5j$ for a rectangular thick plate located at origin). The phase matches closely to both TE and TM.

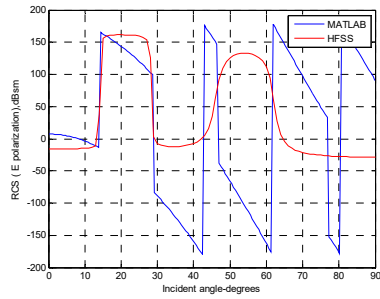


TE

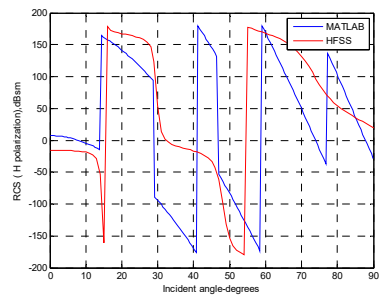


TM

Figure 3.131: Amplitude comparison for TE and TM mode in MATLAB and HFSS (offset 0.001 ($\sim 0.01 \lambda$) meters in thickness by 0.22 ($\sim 2 \lambda$) meters by 0.22 ($\sim 2 \lambda$) meters $\epsilon_r = 10-5j$ for a rectangular thin plate located at origin). Amplitudes match closely as the incident angle is less than 30 degrees for both TE and TM.



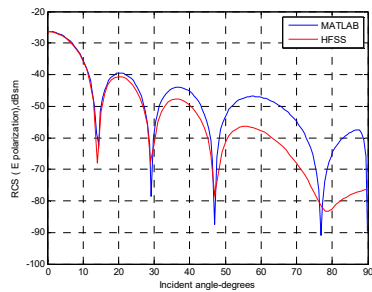
TE



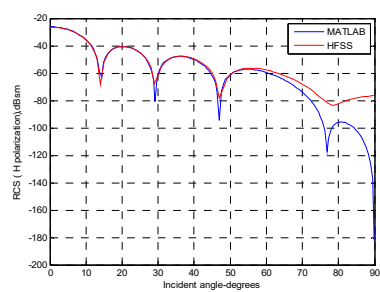
TM

Figure 3.132: Phase comparison for TE and TM mode in MATLAB and HFSS (offset 0.001 ($\sim 0.01 \lambda$) meters in thickness by 0.22 ($\sim 2 \lambda$) meters by 0.22 ($\sim 2 \lambda$) meters $\epsilon_r = 10 - 5j$ for a rectangular thin plate located at origin).

The phase matches closely to both TE and TM.

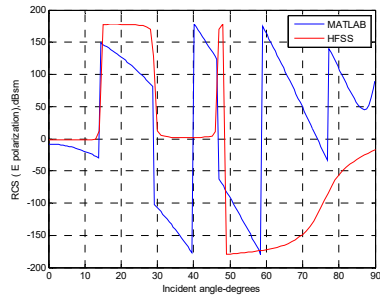


TE

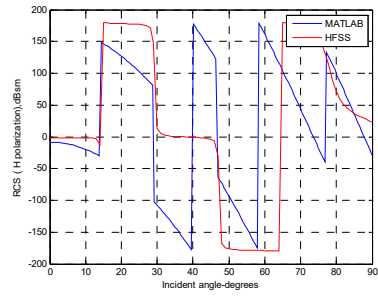


TM

Figure 3.133: Amplitude comparison for TE and TM mode in MATLAB and HFSS (offset 0.0001 ($\sim 0.001 \lambda$) meters in thickness by 0.22 ($\sim 2 \lambda$) meters by 0.22 ($\sim 2 \lambda$) meters $\epsilon_r = 10 - 5j$ for a rectangular sheet plate located at origin). Amplitudes match closely as the incident angle is less than 50 degrees for both TE and TM.



TE

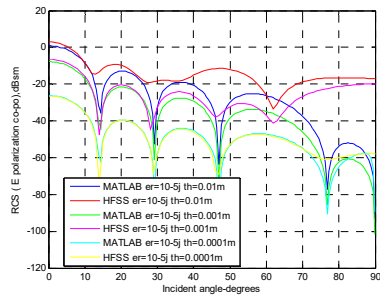


TM

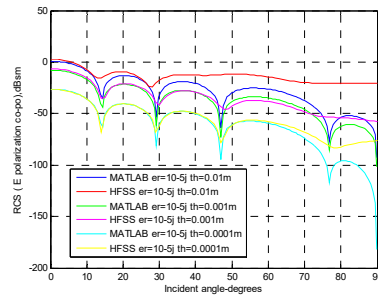
Figure 3.134: Phase comparison for TE and TM mode in MATLAB and HFSS (offset 0.0001 ($\sim 0.001 \lambda$) meters in thickness by 0.22 ($\sim 2 \lambda$) meters by 0.22 ($\sim 2 \lambda$) meters $\epsilon_r = 10-5j$ for a rectangular sheet located at origin).

The phase matches closely to both TE and TM.

The following figures compare all three different thicknesses:



TE



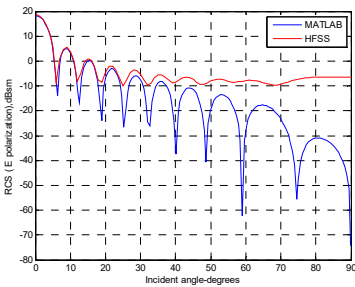
TM

Figure 3.135: Amplitude comparison for TE and TM mode in MATLAB and HFSS (offset 0.0001 ($\sim 0.001 \lambda$) meters, 0.001 ($\sim 0.01 \lambda$) meters, and 0.01 ($\sim 0.1 \lambda$) meters in 3 different thicknesses by 0.22 ($\sim 2 \lambda$) meters by 0.22 ($\sim 2 \lambda$) meters $\epsilon_r = 10-5j$ for a rectangular plate located at origin). Amplitudes have less than a 10 dB difference between two plates at 0.001

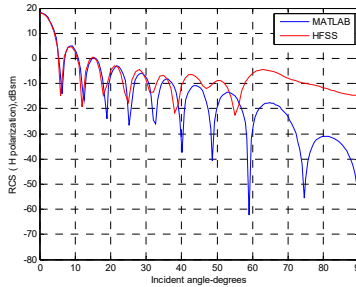
($\sim 0.01 \lambda$) meters and 0.01 ($\sim 0.1 \lambda$) meters thicknesses. The amplitude for a “sheet” at 0.0001 ($\sim 0.001 \lambda$) meters in thickness is 20 dB or 30 dB lower than the other two plates.

3.5.2.4 Thin vs. thick for rectangular metal plates

The following are examples of a metal rectangular plate with a thickness of 0.01 ($\sim 0.1 \lambda$) meters:

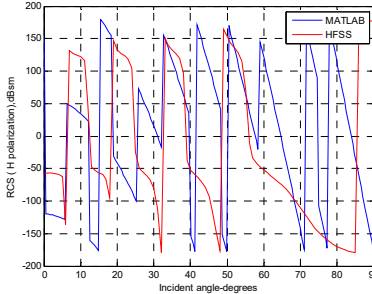
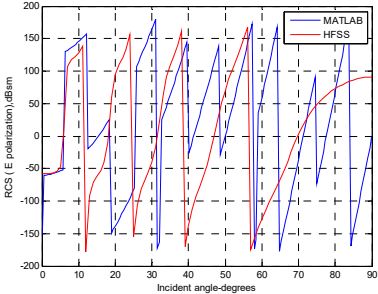


TE



TM

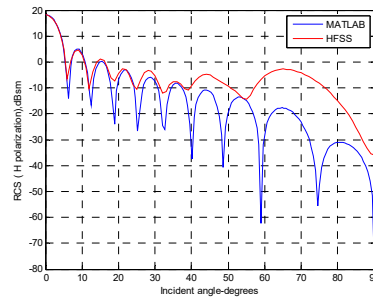
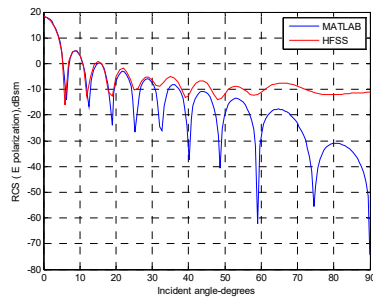
Figure 3.136: Amplitude comparison for TE and TM mode in MATLAB and HFSS (offset 0.01 ($\sim 0.1 \lambda$) meters in thickness for a metal rectangular plate at $a = 0.5 (\sim 5 \lambda)$ meters, $b = 0.5 (\sim 5 \lambda)$ meters). They match well as the incident angle is less than 30~40 degrees for both TE and TM.



TE

TM

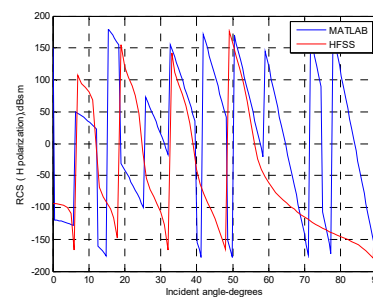
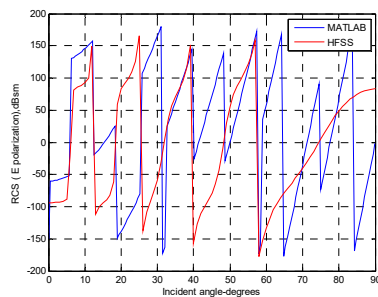
Figure 3.137: Phase comparison for TE and TM mode in MATLAB and HFSS (offset 0.01 (~0.1 λ) meters in thickness for a metal rectangular plate at $a = 0.5$ (~5 λ) meters, $b = 0.5$ (~5 λ) meters). The phase matches closely for both TE and TM.



TE

TM

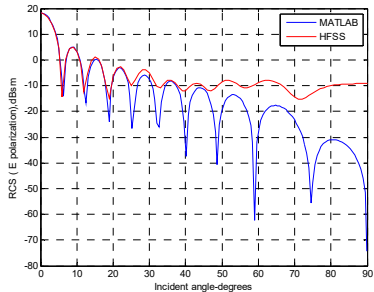
Figure 3.138: Amplitude comparison for TE and TM mode in MATLAB and HFSS (offset 0.001 (~0.01 λ) meters in thickness for a metal rectangular thin plate at $a = 0.5$ (~5 λ) meters, $b = 0.5$ (~5 λ) meters). Amplitudes match well as the incident angle is less than 40 degrees for both TE and TM.



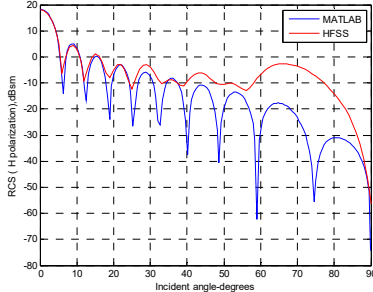
TE

TM

Figure 3.139: Phase comparison for TE and TM mode in MATLAB and HFSS (offset 0.001 ($\sim 0.01 \lambda$) meters in thickness for a metal rectangular thin plate at $a = 0.5 (\sim 5 \lambda)$ meters, $b = 0.5 (\sim 5 \lambda)$ meters). The phase matches closely for both TE and TM.

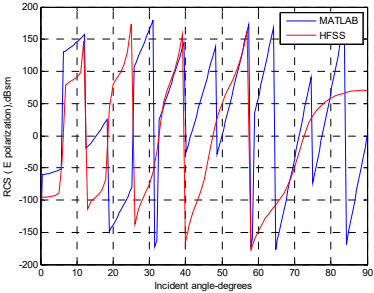


TE

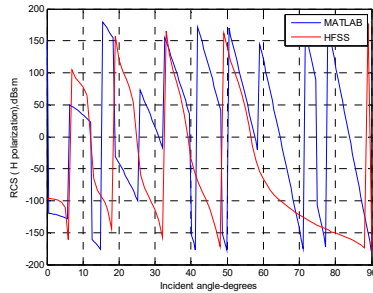


TM

Figure 3.140: Amplitude comparison for TE and TM mode in MATLAB and HFSS (offset 0.0001 ($\sim 0.001 \lambda$) meters in thickness for a metal rectangular thin sheet at $a = 0.5 (\sim 5 \lambda)$ meters, $b = 0.5 (\sim 5 \lambda)$ meters). Amplitudes match closely as the incident angle is less than 40 degrees for both TE and TM.



TE



TM

Figure 3.141: Phase comparison for TE and TM mode in MATLAB and HFSS (offset 0.0001 ($\sim 0.001 \lambda$) meters in thickness for a metal rectangular thin sheet at $a = 0.5$ ($\sim 5 \lambda$) meters, $b = 0.5$ ($\sim 5 \lambda$) meters). The phase matches closely for both TE and TM.

The following figures compare all three thicknesses:

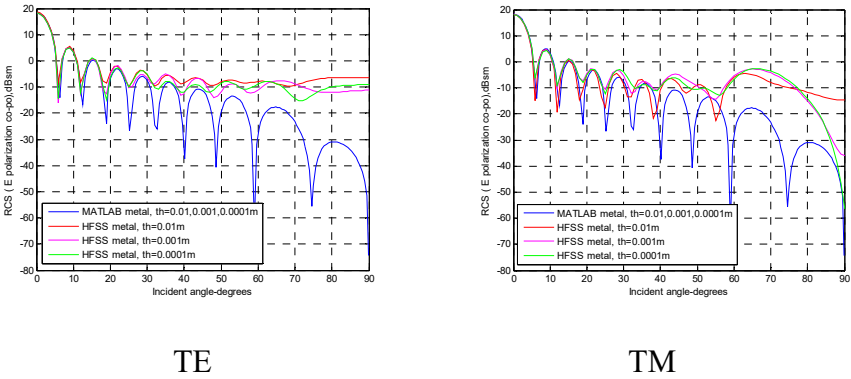


Figure 3.142: Amplitude comparison for TE and TM mode in MATLAB and HFSS (offset 0.0001 ($\sim 0.001 \lambda$) meters, 0.001 ($\sim 0.01 \lambda$) meters, and 0.01 ($\sim 0.1 \lambda$) meters in 3 different thicknesses by 0.5 ($\sim 5 \lambda$) meters by 0.5 ($\sim 5 \lambda$) meters for metal rectangular plates located at origin).

Analytical results for the amplitude and phase of metal did not change. Theoretically, $R \rightarrow 0$ for perfect conducting plates, as all incident waves are reflected. Resistance R of a plate is greater at $\epsilon_r = 2.15$ than resistance R at $\epsilon_r = 10-5j$; therefore, RCS is higher at $\epsilon_r = 10-5j$. This means that more energy is stored in non-metal plates for higher R at $\epsilon_r = 2.15$. RCS with both MATLAB and HFSS simulation changed when the thickness

increased from 0.0001 ($\sim 0.001 \lambda$) meters, 0.001 ($\sim 0.01 \lambda$) meters, and to 0.01 ($\sim 0.1 \lambda$) meters. Amplitudes changed by approximately 20 dB differences when the thicknesses increased from 0.0001 ($\sim 0.001 \lambda$) meters to 0.001 ($\sim 0.01 \lambda$) meters, and by approximately 10 dB when the thickness increased from 0.001 ($\sim 0.01 \lambda$) meters to 0.01 ($\sim 0.1 \lambda$) meters $\epsilon_r = 10-5j$ for non-metal plates.

Both thin and thicker plates show errors between 60 to 90 degrees, which confirms that the edge effect is ignored by PO.

3.6 Summary

For thin vs. thick plates, a difference of approximately 10 to 20 dB is observed as the thickness increases from 0.001λ to 0.1λ at 2.8 GHz for $\epsilon_r = 2.15$ or $\epsilon_r = 10-5j$. Analytical results are in good agreement with HFSS, which indicates that accuracy is sufficient. In general, as the thickness increases (no more than 0.01λ ($\sim 0.1 \lambda$) meters), the amplitude becomes higher for the same non-metal material. This is because sheet ($\sim 0.001 \lambda$) is more penetrable than plates ($\sim 0.1 \lambda$).

For metal vs. non-metal plates, the amplitude of metal is higher than non-metal. The differences (10 dB or 30 dB) between them depend on the relative permittivity of non-metal plates. This is because there is more reflection in metal plates when compared to non-metal plates. This fact can be extended to non-metal vs. non-metal with different relative

permittivity. The resistance of a plate at $\epsilon_r = 2.15$ is higher than it is at $\epsilon_r = 10-5j$, and the amplitude is lower by about 10 dB or 20 dB depending on the relative permittivity.

Surface impedance has restrictions: a) more accurate results appear as the incident angle approaches the normal; b) $Z_s \ll 1$; c) the surface is flat; and d) under the conditions $\theta_t = \theta, \cos \theta_t \approx 1, Z_s \ll \cos \theta$ is used to derive the reflection coefficient for non-metal plates. The analytical plots for all rectangular and circular non-metal plates in comparison to HFSS have demonstrated that more accurate results are observed when the incident angle is less than approximately 40 degrees, which is close to normal. These comparisons further confirmed the theoretical limitations described above.

In terms of computational efficiency, all small sizes for metal and non-metal plates take a few seconds to simulate for both MATLAB and HFSS simulation tools. However, the computational time may vary from size to size for large objects. For thicker large plates (thickness ≥ 0.1 ($\sim 10 \lambda$) meters, radius above 2 wavelengths), HFSS may take one to several hours. For example, for a circular plate at radius = 3λ , HFSS takes at least 30 minutes to get the solution resolved for a thickness of = 0.001 ($\sim 0.01 \lambda$) meters. In this case, using MATLAB for calculations is the best choice.

The same challenge will reappear for long and large radius cylinders in Chapter 4.

Finite cylindrical objects encounter challenges when “truncated” from infinite long cylinders. This requires the use of flat and electrically large surface plate-like endcaps by “truncating” equivalent surface current using PO. The broadside (curved surface) of a dielectric cylinder will be evaluated based on literature review (Wait 1955) in Chapter 4. The circular conducting and dielectric plates used in Chapter 3 will be added to cylinders in Chapter 4 to produce more accurate results for the scattering angle between 0-60 degrees. The challenges of modeling cylindrical objects are similar to those encountered modeling plate-like objects in PO-based approximation. The edge effect will introduce the error by PO on the edge between endcap and broadside.

Chapter 4

PO-based calculations of the RCS of cylindrical objects

4.1 Review of standard results and current

implementation of these standard results (PO)

Based on the literature for cylinder-based RCS, researchers have presented different implementation frameworks. For example,

- a. Most papers described electromagnetic scattering between two adjunct objects (Sarabandi 1994), multiple cylinder interaction (Elsherbeni 1992), or non-interaction multiple cylinders echo width (Henin 2007);
- b. The cylinders interact with rough surfaces (i.e. ground surface) (Chiu 1999; Karam 1988);
- c. Most literature presented the scattering features of infinite long cylinders (Liou 1972).

Most of the literature (or textbook) begins with infinite long cylinders which can be directly applied to the boundary conditions of the interface between two media. Therefore, RCS modeling on cylindrical objects is commonly calculated as infinitely long for 2D solutions. No directly analytical answer to RCS prediction for the finite cylinder is found, especially in penetrable media. The 3D far-field RCS implementation for finite dielectric solutions will be further formulated. Fortunately, a clue for

finite formulation on a single circular cylinder was discovered. The scattering of oblique electromagnetic plane waves on a single dielectric circular cylinder (Wait 1955) and a conducting circular cylinder (Balanis 2012) has been studied for many years, and is referenced often in literature. Both RCS formulations are performed by “truncating” the infinite dimension to finite geometry.

4.2 Motivation for detailed analysis

Currently, sand and dust are considered to be electrically small spherical objects, and are modeled as spheroids near the Rayleigh region using the T-matrix method (Mishcheko 2000). Raindrops near the Mie scattering region are modeled as prolate and oblate spheroidal objects with flat surfaces using T-matrix (Bodine 2014); this has also been studied extensively.

When $ka \ll 1$ electrically small objects lying in the Rayleigh region, PO is not suitable. Therefore, it is necessary to distinguish which method is best to use for cylinders of varying sizes that are very small ($0.01 (\lambda)$ wavelength to $0.1 (\lambda)$ in length, $0.0001 (\lambda)$ wavelength to $0.001 (\lambda)$ in radius). Conducting sphere calculations is an alternative way to replace the cylindrical objects in the Rayleigh region.

Away from the Rayleigh region, RCS modeling on cylindrical objects shows promise for representing electrically larger ($D > \lambda$) dimensions such

as stems, twigs and branches. Regardless, PO is not suitable for curved cylindrical broadside surfaces.

In electromagnetic theory, basic scattering fields are described from the Maxwell equations. When dealing with a cylinder or sphere, the Maxwell equations become more complicated in cylindrical and spherical coordinate systems when compared to Cartesian coordinate system. More specifically, the scattering field has to be involved in tackling the Henkel function, Bessel function, and any other polynomials to the second order for a curved surface.

The infinitely long conducting cylindrical formulation can be viewed as the starting point for understanding Maxwell's equations in the cylindrical coordinate system in order to set up the geometry for solving the dielectric cylinder problem. The formulation for a conducting circular cylinder from Balanis's book (section 11.5.3-11.5.4 in Chapter 11, 2002) is able to implement the RCS of cylindrical broadside. However, to obtain the RCS formulation of a single dielectric cylinder broadside, derivation by hand is necessary. Further, Maxwell's equations in the cylindrical coordinate system are used to verify the coefficients for TE and TM polarization first based on research (Wait 1955), and then used as a model solution. As such, RCS for finite dielectric cylinder broadside is formulated by the definition of RCS in the far-field. In addition, by "truncating" equivalent surface currents in the radiation integral, the RCS

modeling of circular plates (endcaps) can be derived for a metal cylinder. Furthermore, by applying the surface impedance principle of PO, the RCS modeling of circular plates (endcaps) can be derived for a dielectric cylinder as well (derived and demonstrated in Chapter 3). Edge diffractions are not taken into account by PO.

After the formulation was created, the electrical behavior for selected small-size dielectric cylinders was tested. It was found that oblate spheroid is another choice for small cylinders in the Rayleigh region using T-matrix (Bodine 2014) calculations. Even further, because cylinders with 1λ in length and radius are smaller than 0.5λ (which lies in the Mie region), the results found were not accurate.

4.2.1 Metal vs. Non-metal (dielectric) cylinders

Metal cylinders are also considered to be non-penetrable since most incident scattering is reflected from the conducting body with less refraction. Dielectric cylinders are considered to be penetrable media since dielectric properties cause the energy (stored) inside the cylinder body to be lost. Both cylinder RCS calculations are suitable to the length 1λ , and become more accurate as cylinder length increases.

4.2.2 Long vs. short cylinders

In this chapter, the analytical results are shown for comparison between HFSS and MATLAB for long (above 10λ in length) and thin (0.1λ to 1.5λ in radius) cylinders with and without endcaps, and thin sheet

results for short and fat cylinders. Based on the results for different cases described in this dissertation, a determination is made based on which technique is chosen. In most cases, PO is the best choice for electrically large, flat, cylindrical plate (endcaps) geometries.

Based on the comparison of simulation vs. analytical results, for thin cylinders longer than 5λ in length and above 0.3λ in radius, HFSS matches MATLAB well at the range from 60 to 90 degrees. The results still show a large gap for theta at the 0- to 60- degree range; endcaps for both metal and penetrable cylinders are added up to compensate for these technical deficiencies. The results with endcaps are much more accurate than those produced without endcaps. This further confirms that the analytical derivation by hand is correct. For dielectric circular plates (endcaps), PO is modified using the surface equivalent principle with IBC (impedance boundary condition), which is called the extension of PO. Both conducting and dielectric endcap formulations are derived and verified by adding them up to the broadside of corresponding cylinders. Since the centers of endcaps are displaced from the origin, a phase shift $e^{(j*k*l*\cos(\theta))}$ must be added to the amplitude of a RCS formulation for a plate located at half of the length (L) of the cylinder, centered at the origin as a target observed from far-field. The results show that they match pretty well at 0 degrees between HFSS simulation and MATLAB. They present even overlap from each other for some selected sizes of

cylinders. By testing circular plates at $\epsilon_r = 2.15$ and $\epsilon_r = 10-5j$ in Chapter 3, when the thickness > 0.01 ($\sim 0.1 \lambda$) meters for $\lambda = 0.11$ meters at frequency 2.8 GHz, a short cylinder with a radius that is at least the same as the thickness should be used instead. The thickness of 0.01 ($\sim 0.1 \lambda$) meters is a point that distinguishes the plate and the short dielectric cylinder.

4.3 Generic derivation for metal cylinders

4.3.1 Generic derivation for metal cylinders broadside

Assume a TM^z oblique incident plane wave traveling parallel to xz plane is incident upon a circular cylinder of a radius. (Balanis 2012)

$$E^i = E_0(\hat{a}_x \cos \theta_i + \hat{a}_z \sin \theta_i)e^{-j\beta x \sin \theta_i} e^{+j\beta z \cos \theta_i} \quad (4.1)$$

Using the transformation, the z component can be also expressed as

$$E_z^i = E_0 \sin \theta_i e^{+j\beta z \cos \theta_i} \sum_{n=-\infty}^{+\infty} j^{-n} J_n(\beta \rho \sin \theta_i) e^{jn\phi} \quad (4.2)$$

The z component of the scattered field can be written as

$$E_z^s = E_0 \sin \theta_s e^{-j\beta z \cos \theta_s} \sum_{n=-\infty}^{+\infty} C_n H_n^{(2)}(\beta \rho \sin \theta_s) \quad (4.3)$$

The tangential component of the incident electrical field and scattered field are decomposed into E_ρ^i and E_ϕ^i , E_ρ^s and E_ϕ^s , respectively. The boundary conditions in the cylindrical coordinate system are:

$$E_z^t(\rho = a, 0 \leq \theta_i, \theta_i = \theta_s, \phi = \pi) = E_z^i + E_z^s \quad (4.4)$$

$$E_\phi^t(\rho = a, 0 \leq \theta_i, \theta_i = \theta_s, \phi = \pi) = E_\phi^i + E_\phi^s \quad (4.5)$$

By applying the boundary above, the scattered field for TM^z can be written as

$$E_\rho^s = jE_0 \cos \theta_i e^{+j\beta z \cos \theta_i} \sum_{n=-\infty}^{+\infty} j^{-n} a_n H_n^{(2)'}(\beta \rho \sin \theta_i) e^{jn\phi} \quad (4.6)$$

$$E_\phi^s = jE_0 \frac{\cot \theta_i}{\beta \rho} e^{+j\beta z \cos \theta_i} \sum_{n=-\infty}^{+\infty} nj^{-n+1} a_n H_n^{(2)}(\beta \rho \sin \theta_i) e^{jn\phi} \quad (4.7)$$

$$E_\rho^s = E_0 \sin \theta_i e^{+j\beta z \cos \theta_i} \sum_{n=-\infty}^{+\infty} j^{-n} a_n H_n^{(2)}(\beta \rho \sin \theta_i) e^{jn\phi} \quad (4.8)$$

$$H_\rho^s = jE_0 \frac{e^{+j\beta z \cos \theta_i}}{\omega \mu \rho \sin \theta_i} \sum_{n=-\infty}^{+\infty} nj^{-n+1} a_n H_n^{(2)}(\beta \rho \sin \theta_i) e^{jn\phi} \quad (4.9)$$

$$H_z^s = 0 \quad (4.10)$$

$$H_\phi^s = -jE_0 \sqrt{\frac{\varepsilon}{\mu}} e^{+j\beta z \cos \theta_i} \sum_{n=-\infty}^{+\infty} j^{-n} a_n H_n^{(2)'}(\beta \rho \sin \theta_i) e^{jn\phi} \quad (4.11)$$

$$a_n = -\frac{J_n(\beta a \sin \theta_i)}{H_n^{(2)}(\beta a \sin \theta_i)} \quad , = \frac{\partial}{\partial(\beta \rho \sin \theta_i)} \quad (4.12)$$

Then, applying the far-zone Henkel function and its derivative

$$H_n^2(\alpha x) \stackrel{\alpha x \rightarrow \infty}{\cong} \sqrt{\frac{2j}{\pi \alpha x}} j^n e^{-j\alpha x} \quad (4.13)$$

$$H_n^{2'}(\alpha x) \stackrel{\alpha x \rightarrow \infty}{\cong} -\sqrt{\frac{2j}{\pi \alpha x}} j^{n+1} e^{-j\alpha x} \quad (4.14)$$

The two-dimensional target (also called scattering width) can be expressed

as σ_{2-D}

$$H_\phi^s \stackrel{\rho \rightarrow \infty}{\approx} -E_0 \sqrt{\frac{\varepsilon}{\mu}} \sqrt{\frac{2j}{\pi \beta \rho \sin \theta_i}} e^{+j\beta(z \cos \theta_i - \rho \sin \theta_i)} \sum_{n=0}^{+\infty} \varepsilon_n a_n \cos(n\phi) \quad (4.15)$$

$$\sigma_{2-D} = \lim_{\rho \rightarrow \infty} (2\pi\rho \frac{|H_\phi^s|^2}{|H^i|^2}) = \lim_{\rho \rightarrow \infty} \left[2\pi\rho \frac{\frac{|E_0|^2}{\eta^2} \left(\frac{2}{\pi\beta\rho \sin \theta_i}\right)}{\frac{|E_0|^2}{\eta^2}} \left| \sum_{n=-\infty}^{+\infty} a_n e^{jn\phi} \right|^2 \right]$$

$$\sigma_{2-D} = \frac{2\lambda}{\pi} \frac{1}{\sin \theta_i} \left| \sum_{n=0}^{+\infty} \varepsilon_n a_n \cos(n\phi) \right|^2 \quad (4.16)$$

where

$$a_n = -\frac{J_n(\beta a \sin \theta_i)}{H_n^{(2)}(\beta a \sin \theta_i)} \quad \varepsilon_n = \begin{cases} 1 & n=0 \\ 2 & n \neq 0 \end{cases} \quad (4.17)$$

The three-dimensional radar cross section for oblique incident wave refers to two-dimensional scattering width and can be expressed as

$$\sigma_{3-D} = \sigma_{2-D} \left\{ \frac{2l^2}{\lambda} \sin^2 \theta_{i,s} \left[\frac{\sin \left[\frac{\beta l}{2} (\cos \theta_i + \cos \theta_s) \right]}{\frac{\beta l}{2} (\cos \theta_i + \cos \theta_s)} \right]^2 \right\} \quad l \gg a$$

$$\sigma_{3-D} \cong \frac{4l^2}{\pi} \frac{\sin^2 \theta_s}{\sin \theta_i} \left| \sum_{n=0}^{\infty} \varepsilon_n a_n \cos(n\phi) \right|^2 \left[\frac{\sin \left[\frac{\beta l}{2} (\cos \theta_i + \cos \theta_s) \right]}{\frac{\beta l}{2} (\cos \theta_i + \cos \theta_s)} \right]^2 \quad (4.18)$$

Similarly, for the TE^z oblique incidence plane wave scattering by conducting circular cylinder, the scattered fields can be expressed by the given incident magnetic field for an oblique plane wave traveling parallel to the x-z plane

$$H^i = H_0(\hat{a}_x \cos \theta_i + \hat{a}_z \sin \theta_i) e^{-j\beta x \sin \theta_i} e^{+j\beta z \cos \theta_i} \quad (4.19)$$

$$E_\rho^s = -j \frac{H_0}{\omega \varepsilon \rho} \frac{e^{+j\beta z \cos \theta_i}}{\sin \theta_i} \times \sum_{n=-\infty}^{+\infty} n j^{-n+1} b_n H_n^{(2)'}(\beta \rho \sin \theta_i) e^{jn\phi} \quad (4.20)$$

Following the same procedure by applying the Maxwell equations and boundary conditions of a cylindrical coordinate system, the E and H field can be obtained as follows:

$$E_\phi^s = j H_0 \sqrt{\frac{\mu}{\varepsilon}} e^{+j\beta z \cos \theta_i} \times \sum_{n=-\infty}^{+\infty} j^{-n} b_n H_n^{(2)'}(\beta \rho \sin \theta_i) e^{jn\phi} \quad (4.21)$$

$$E_z^s = 0 \quad (4.22)$$

$$H_\rho^s = j H_0 \cos \theta_i e^{+j\beta z \cos \theta_i} \times \sum_{n=-\infty}^{+\infty} j^{-n} b_n H_n^{(2)'}(\beta \rho \sin \theta_i) e^{jn\phi} \quad (4.23)$$

$$H_\phi^s = j H_0 \frac{\cot \theta_i}{\beta \rho} e^{+j\beta z \cos \theta_i} \times \sum_{n=-\infty}^{+\infty} n j^{-n+1} b_n H_n^{(2)'}(\beta \rho \sin \theta_i) e^{jn\phi} \quad (4.24)$$

$$H_z^s = H_0 \sin \theta_i e^{+j\beta z \cos \theta_i} \times \sum_{n=-\infty}^{+\infty} j^{-n} b_n H_n^{(2)'}(\beta \rho \sin \theta_i) e^{jn\phi} \quad (4.25)$$

$$b_n = -\frac{J_n'(\beta a \sin \theta_i)}{H_n^{(2)'}(\beta a \sin \theta_i)} \quad ' = \frac{\partial}{\partial(\beta \rho \sin \theta_i)} \quad (4.26)$$

Then, apply the Hankel function and its derivative in the far-zone scattered field:

$$E_\phi^s \stackrel{\rho \rightarrow \infty}{\approx} H_0 \sqrt{\frac{\mu}{\varepsilon}} \sqrt{\frac{2j}{\pi \beta \rho \sin \theta_i}} e^{+j\beta(z \cos \theta_i - \rho \sin \theta_i)} \sum_{n=0}^{+\infty} \varepsilon_n b_n \cos(n\phi) \quad (4.27)$$

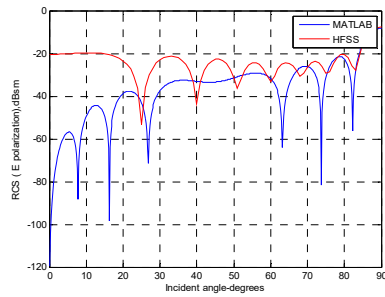
$$\sigma_{2-D} = \frac{2\lambda}{\pi} \frac{1}{\sin \theta_i} \left| \sum_{n=0}^{+\infty} \varepsilon_n b_n \cos(n\phi) \right|^2 \quad \varepsilon_n = \begin{cases} 1 & n=0 \\ 2 & n \neq 0 \end{cases} \quad (4.28)$$

$$\sigma_{3-D} \cong \frac{4l^2}{\pi} \sin \theta_i \left| \sum_{n=0}^{\infty} \varepsilon_n b_n \cos(n\phi) \right|^2 \left[\frac{\sin \left[\frac{\beta l}{2} (\cos \theta_i + \cos \theta_s) \right]}{\frac{\beta l}{2} (\cos \theta_i + \cos \theta_s)} \right]^2 \quad (4.29)$$

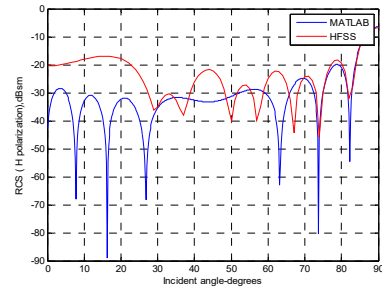
A phase shift $e^{-j\pi/2}$ is added to the broadside of cylinder RCS amplitude. This appears to agree with HFSS. A phase shift $e^{jkl \cos \theta}$ is added to the amplitude of RCS for endcaps.

4.3.2 Simulation vs. analytical results for metal large, thin cylinders with and without endcaps

Conducting cylinders without endcaps with a size > 0.4 ($\sim 3.64 \lambda$) meters in length and > 0.02 ($\sim 0.2 \lambda$) meters in radius have amplitudes that show big gaps at 0 degrees without endcaps, but are in good agreement with HFSS with endcaps. Phase shows the same.

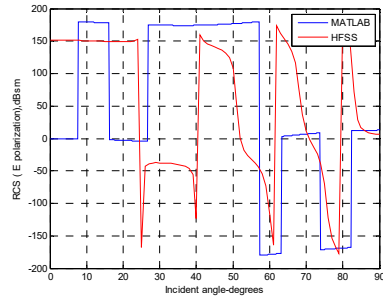


TE

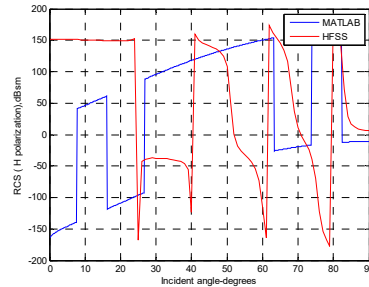


TM

Figure 4.1: Amplitude comparison for TE and TM mode in MATLAB and HFSS (0.4 (~3.64 λ) meters in length by 0.02 (~0.2 λ) meters in radius for a conducting cylinder without endcap). Amplitudes overlap at the peak of 90° for both TE and TM.



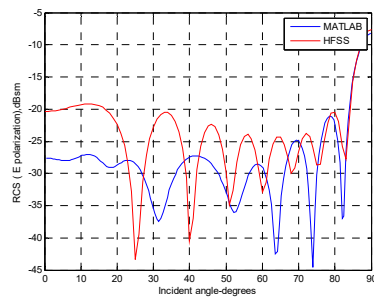
TE



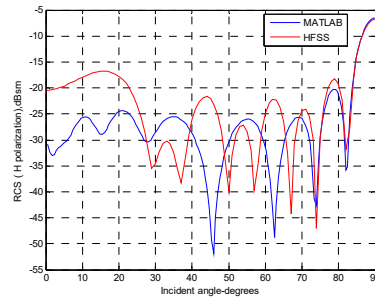
TM

Figure 4.2: Phase comparison for TE and TM mode in MATLAB and HFSS (0.4 (~3.64 λ) meters in length by 0.02 (~0.2 λ) meters in radius for a conducting cylinder without endcap). The phase shows mismatch for both TE and TM.

For the same size conducting cylinder with endcap:



TE



TM

Figure 4.3: Amplitude comparison for TE and TM mode in MATLAB and HFSS (0.4 ($\sim 3.64 \lambda$) meters in length by 0.02 ($\sim 0.2 \lambda$) meters in radius for a conducting cylinder with endcap). Amplitude increases 70 dB in TE at 0° . Amplitude increases 16 dB in TM at 0° .

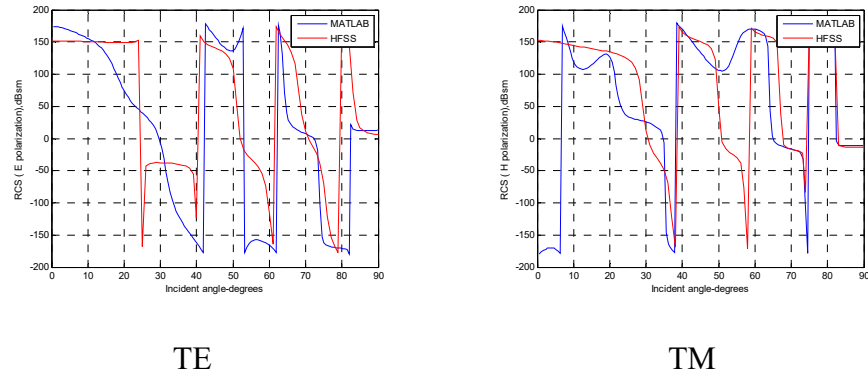


Figure 4.4: Phase comparison for TE and TM mode in MATLAB and HFSS (0.4 ($\sim 3.64 \lambda$) meters in length by 0.02 ($\sim 0.2 \lambda$) meters in radius for a conducting cylinder with endcap). The phase matches closely for both TE and TM.

For a conducting cylinder without endcap:

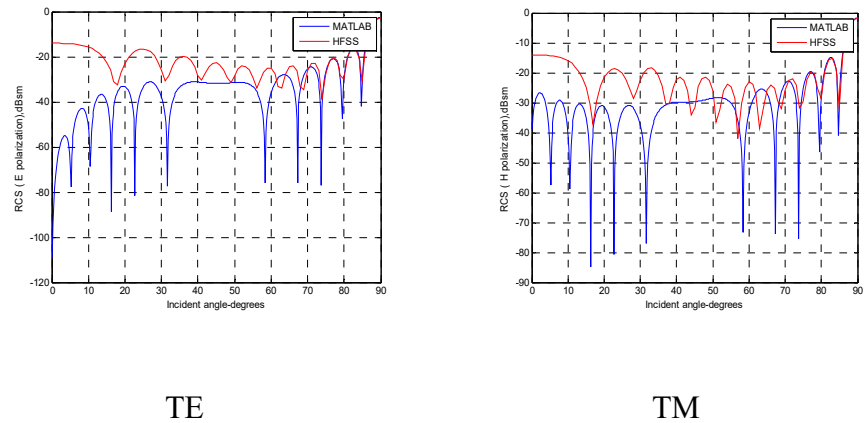
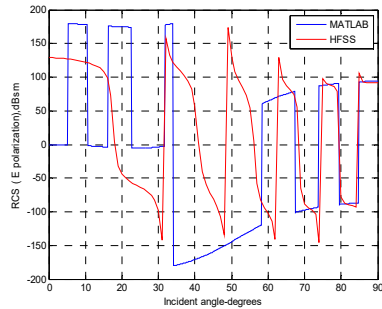
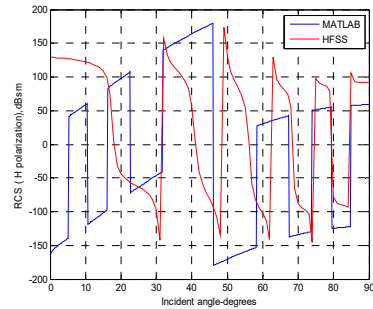


Figure 4.5: Amplitude comparison for TE and TM mode in MATLAB and HFSS (0.6 (~5.5 λ) meters in length by 0.03 (~0.3 λ) meters in radius for a conducting cylinder without endcap). Amplitudes overlap at the peak of 90° but show big gaps at 0° for both TE and TM.



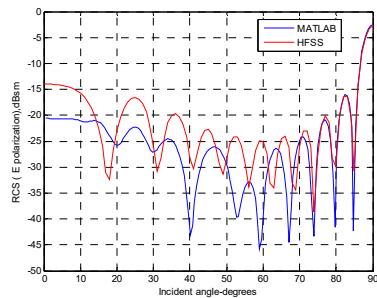
TE



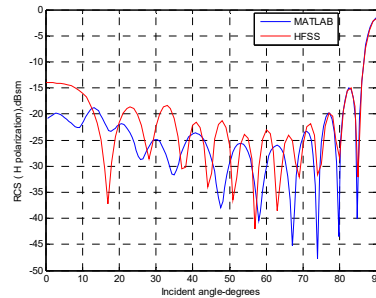
TM

Figure 4.6: Phase comparison for TE and TM mode in MATLAB and HFSS (0.6 (~5.5 λ) meters in length by 0.03 (~0.3 λ) meters in radius for a conducting cylinder without endcap). The phase shows mismatch between 0-60° for both TE and TM.

For the same size conducting cylinder with endcap:



TE



TM

Figure 4.7: Amplitude comparison for TE and TM mode in MATLAB and HFSS (0.6 (~5.5 λ) meters in length by 0.03 (~0.3 λ) meters in radius for a conducting cylinder with endcap). Amplitude increases 80 dB in TE at 0°. Amplitude increases 15 dB in TM at 0°.

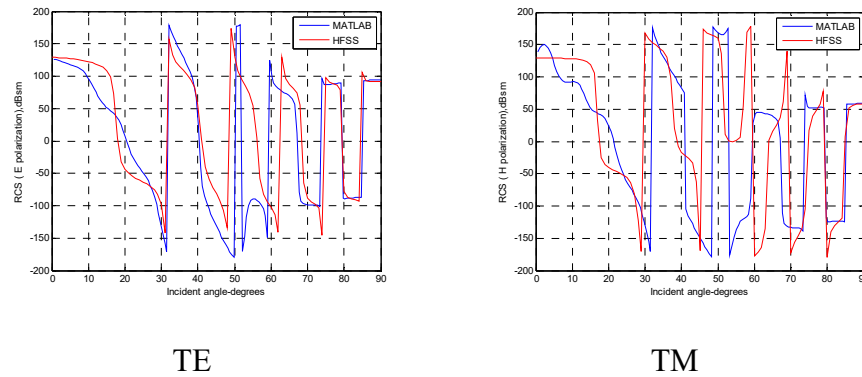


Figure 4.8: Phase comparison for TE and TM mode in MATLAB and HFSS (0.6 (~5.5 λ) meters in length by 0.03 (~0.3 λ) meters in radius for a conducting cylinder with endcap). The phase matches well in both TE and TM.

For a conducting cylinder without endcap:

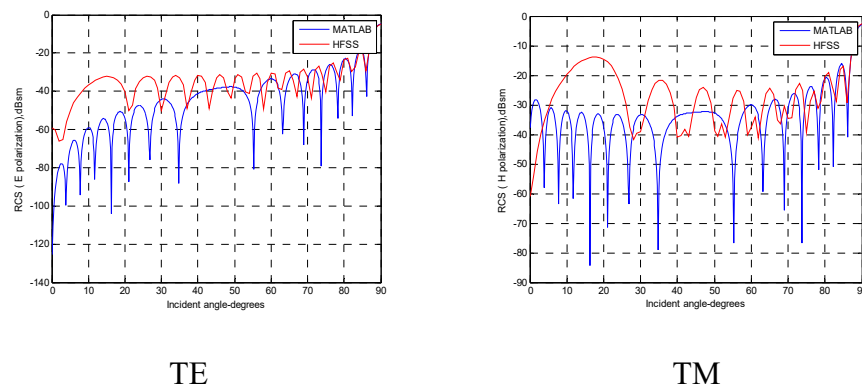


Figure 4.9: Amplitude comparison for TE and TM mode in MATLAB and HFSS (0.8 ($\sim 7.27 \lambda$) meters in length by 0.01 ($\sim 0.1 \lambda$) meters in radius for a conducting cylinder without endcap). Amplitudes overlap at the peak of 90° , but show big gaps at 0° for both TE and TM.

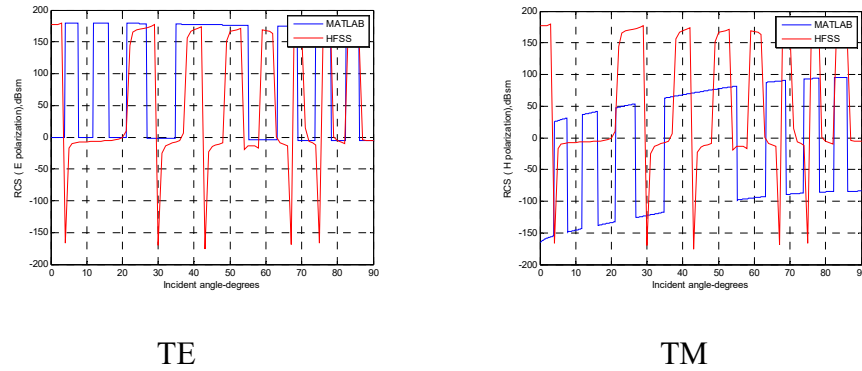


Figure 4.10: Phase comparison for TE and TM mode in MATLAB and HFSS (0.8 ($\sim 7.27 \lambda$) meters in length by 0.01 ($\sim 0.1 \lambda$) meters in radius for a conducting cylinder without endcap). The phase shows mismatch for TE and TM.

For the same size conducting cylinder with endcap:

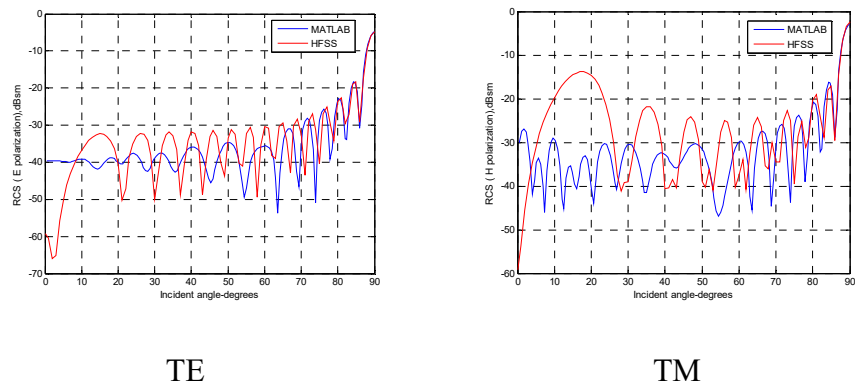


Figure 4.11: Amplitude comparison for TE and TM mode in MATLAB and HFSS (0.8 (~7.27 λ) meters in length by 0.01 (~0.1 λ) meters in radius for a conducting cylinder with endcap). Amplitude increases 50 dB in TE at 0°. Amplitude increases 5 dB in TM at 0°.

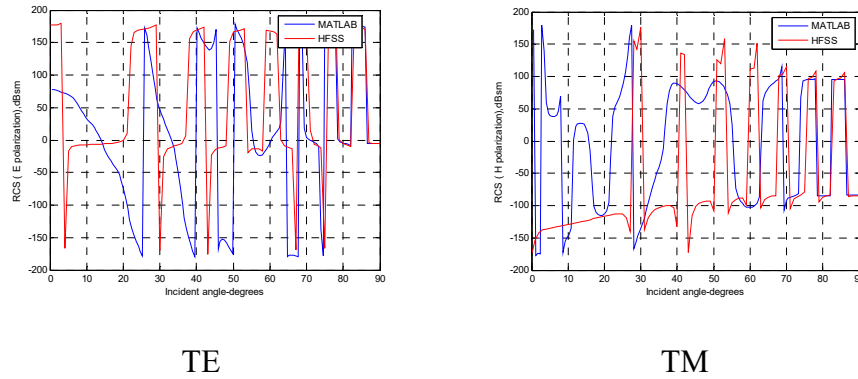


Figure 4.12: Phase comparison for TE and TM mode in MATLAB and HFSS (0.8 (~7.27 λ) meters in length by 0.01 (~0.1 λ) meters in radius for a conducting cylinder with endcap). The phase matches closely for both TE and TM.

For a conducting cylinder without endcap:

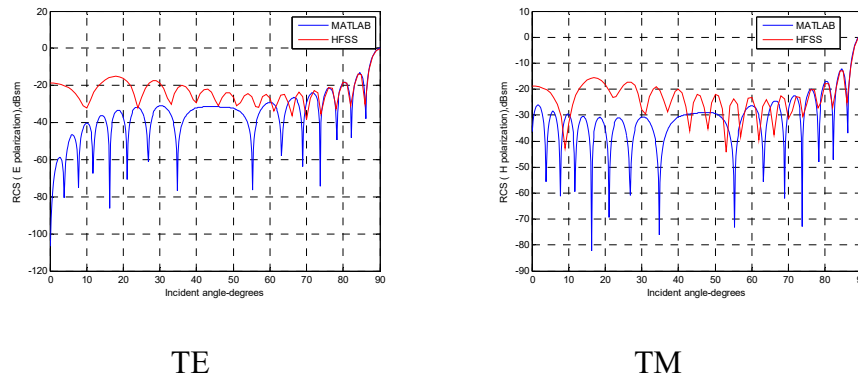


Figure 4.13: Amplitude comparison for TE and TM mode in MATLAB and HFSS (0.8 (~7.27 λ) meters in length by 0.03 (~0.3 λ) meters in radius for a conducting cylinder without endcap). Amplitudes overlap at the peak of 90°, but show big gaps at 0° for both TE and TM.

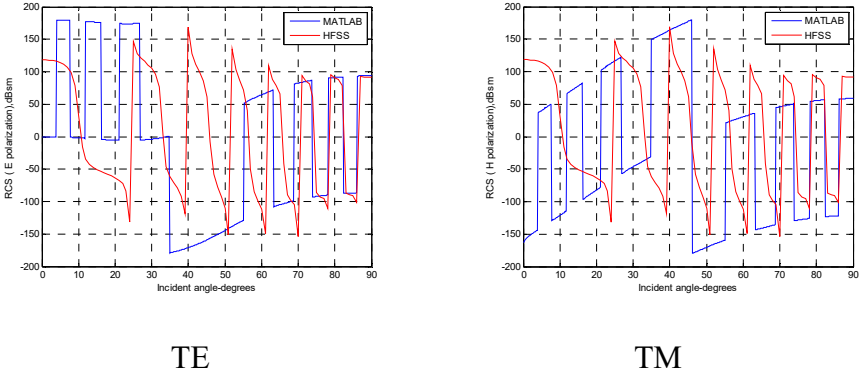


Figure 4.14: Phase comparison for TE and TM mode in MATLAB and HFSS (0.8 (~7.27 λ) meters in length by 0.03 (~0.3 λ) meters in radius for a conducting cylinder without endcap). The phase shows mismatch between 0-60° for both TE and TM.

For the same size conducting cylinder with endcap:

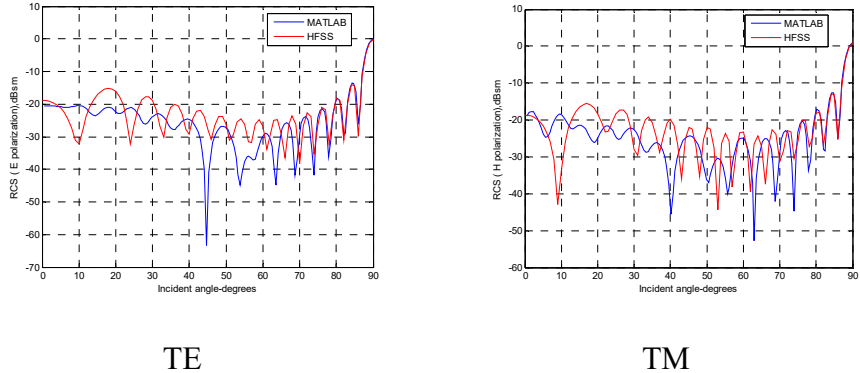
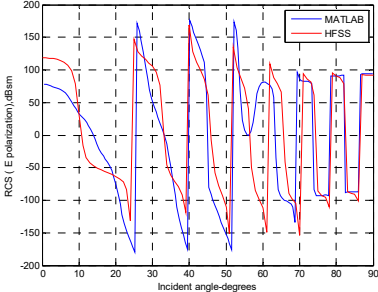
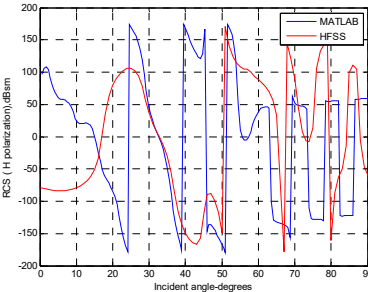


Figure 4.15: Amplitude comparison for TE and TM mode in MATLAB and HFSS (0.8 (~7.27 λ) meters in length by 0.03 (~0.3 λ) meters in radius for a conducting cylinder with endcap). Amplitudes match closely for both TE and TM.



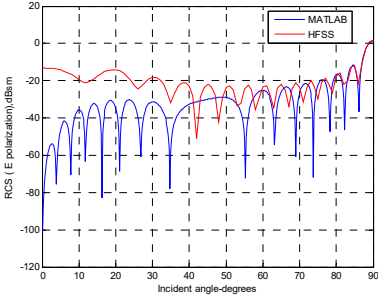
TE



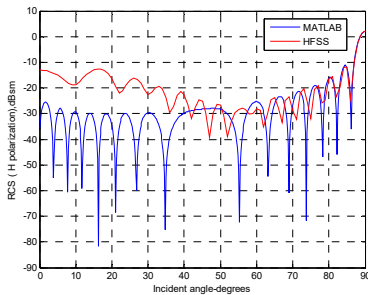
TM

Figure 4.16: Phase comparison for TE and TM mode in MATLAB and HFSS (0.8 (~7.27 λ) meters in length by 0.03 (~0.3 λ) meters in radius for a conducting cylinder with endcap). The phase matches well for TE, and matches closely for TM.

For a conducting cylinder without endcap:



TE



TM

Figure 4.17: Amplitude comparison for TE and TM mode in MATLAB and HFSS (0.8 (~7.27 λ) meters in length by 0.04 (~0.36 λ) meters in radius for a conducting cylinder without endcap). Big gaps are observed at 0° and overlap at 90° for both TE and TM.

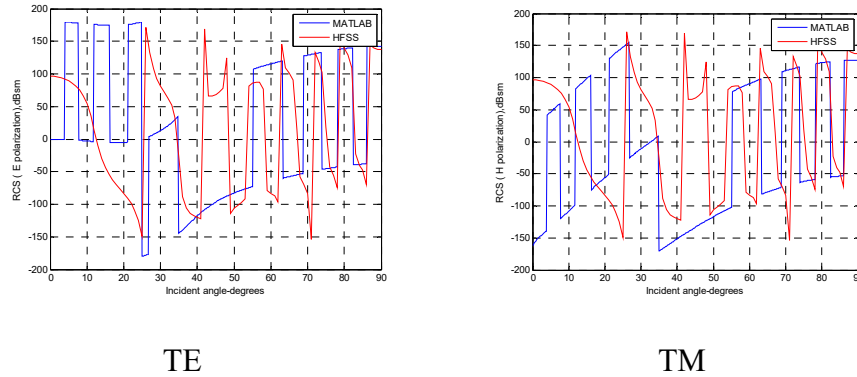


Figure 4.18: Phase comparison for TE and TM mode in MATLAB and HFSS (0.8 (~7.27 λ) meters in length by 0.04 (~0.36 λ) meters in radius for a conducting cylinder without endcap). The phase shows mismatch between 0-60°.

For the same size conducting cylinder with endcap:

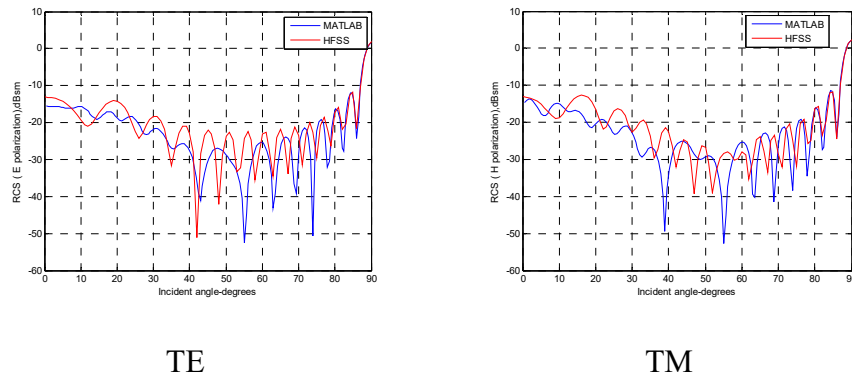
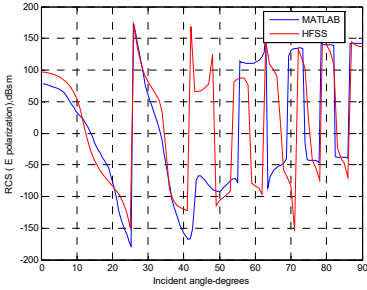
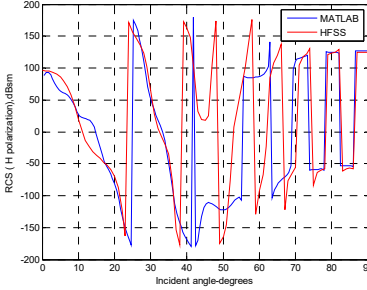


Figure 4.19: Amplitude comparison for TE and TM mode in MATLAB and HFSS (0.8 (~7.27 λ) meters in length by 0.04 (~0.36 λ) meters in radius for a conducting cylinder with endcap). Amplitudes match well for both TE and TM.



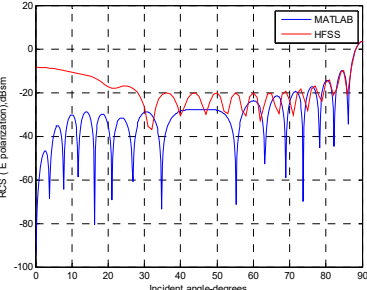
TE



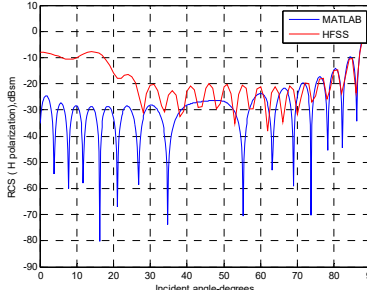
TM

Figure 4.20: Phase comparison for TE and TM mode in MATLAB and HFSS (0.8 (~7.27 λ) meters in length by 0.04 (~0.36 λ) meters in radius for a conducting cylinder with endcap). The phase matches well for both TE and TM.

For a conducting cylinder without endcap:

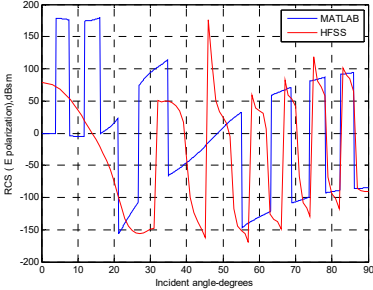


TE

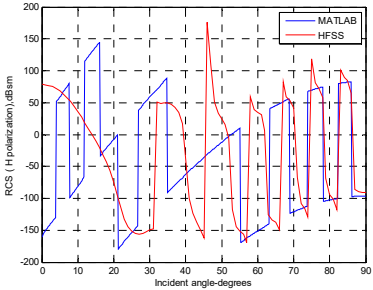


TM

Figure 4.21: Amplitude comparison for TE and TM mode in MATLAB and HFSS (0.8 (~7.27 λ) meters in length by 0.06 (~0.55 λ) meters in radius for a conducting cylinder without endcap). Amplitudes show big gaps at 0° and overlap at 90° for both TE and TM.



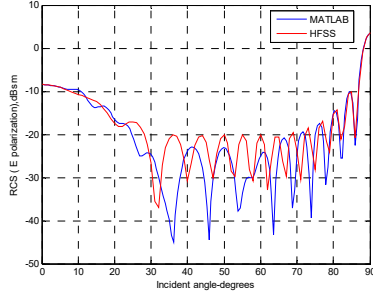
TE



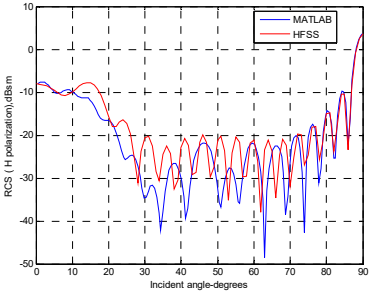
TM

Figure 4.22: Phase comparison for TE and TM mode in MATLAB and HFSS (0.8 (~7.27 λ) meters in length by 0.06 (~0.55 λ) meters in radius for a conducting cylinder without endcap). The phase shows mismatch between 0-60° for both TE and TM.

For the same size conducting cylinder with endcap:



TE



TM

Figure 4.23: Amplitude comparison for TE and TM mode in MATLAB and HFSS (0.8 (~7.27 λ) meters in length by 0.06 (~0.55 λ) meters in radius for a conducting cylinder with endcap). Amplitudes show good agreement with HFSS for both TE and TM.

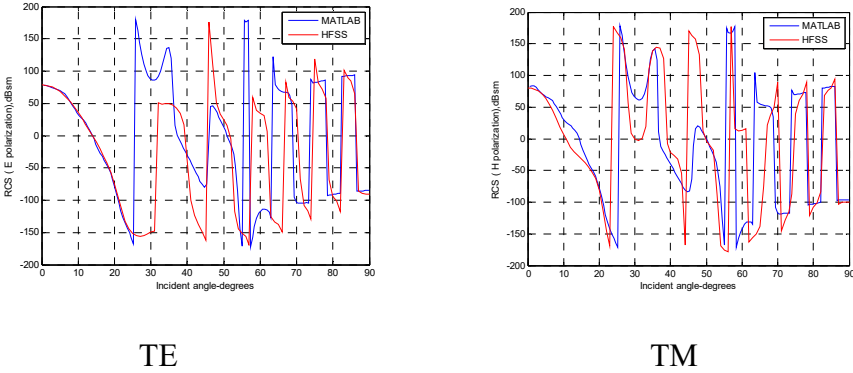


Figure 4.24: Phase comparison for TE and TM mode in MATLAB and HFSS (0.8 (~7.27 λ) meters in length by 0.06 (~0.55 λ) meters in radius for a conducting cylinder with endcap). The phase shows good agreement with HFSS for both TE and TM.

For a conducting cylinder without endcap:

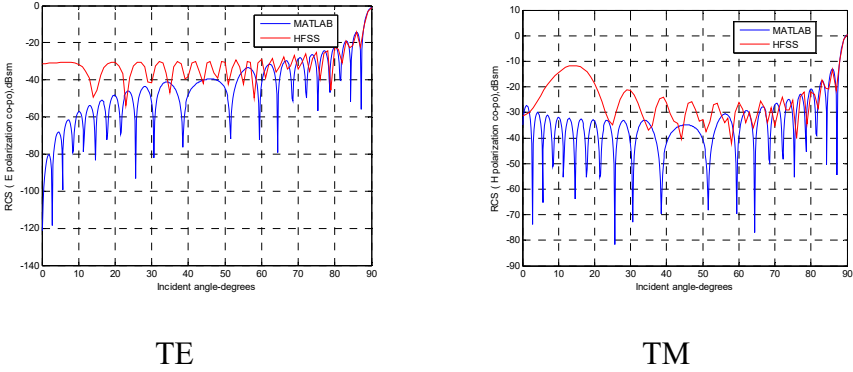


Figure 4.25: Amplitude comparison for TE and TM mode in MATLAB and HFSS (1.1 (~10 λ) meters in length by 0.011 (~0.1 λ) meters in radius for a conducting cylinder without endcap). Amplitudes show big gaps at 0° and overlap at 90° for both TE and TM.

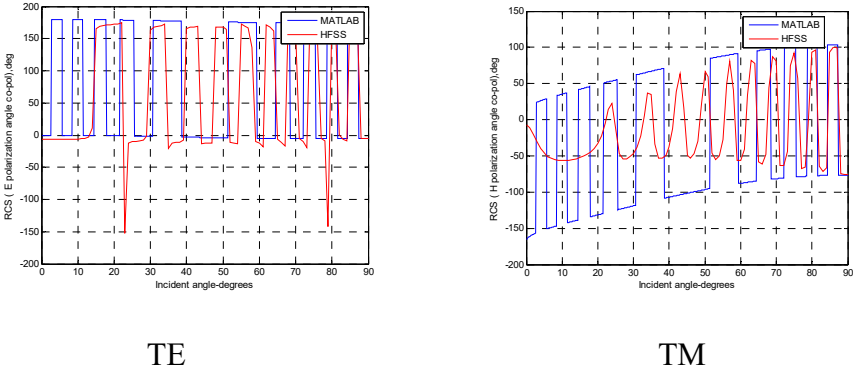


Figure 4.26: Phase comparison for TE and TM mode in MATLAB and HFSS (1.1 (~10 λ) meters in length by 0.011 (~0.1 λ) meters in radius for a conducting cylinder without endcap). The phase shows mismatch between 0-60° for both TE and TM.

For the same size conducting cylinder with endcap:

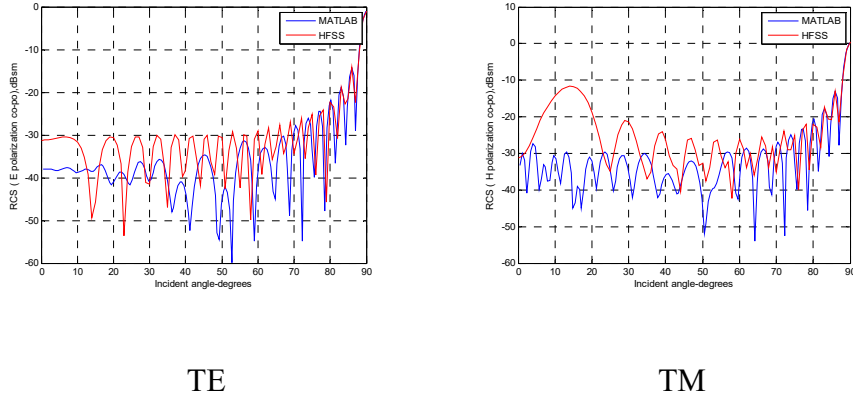


Figure 4.27: Amplitude comparison for TE and TM mode in MATLAB and HFSS (1.1 (~10 λ) meters in length by 0.011 (~0.1 λ) meters in radius for a conducting cylinder with endcap). Amplitudes have differences of less than 10 dB at 0° for both TE and TM.

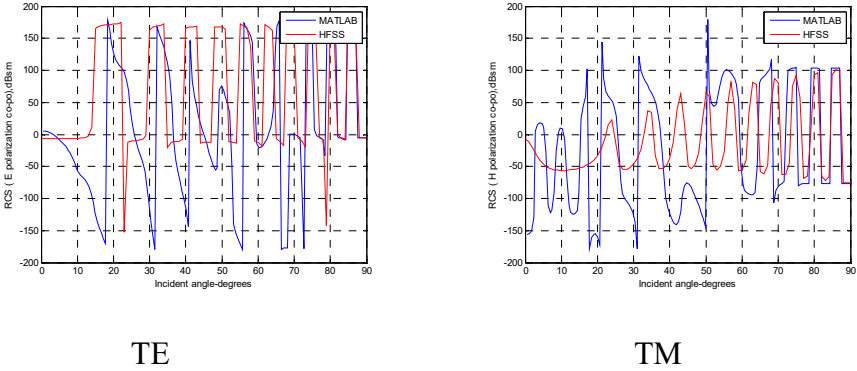


Figure 4.28: Phase comparison for TE and TM mode in MATLAB and HFSS (1.1 (~10 λ) meters in length by 0.011 (~0.1 λ) meters in radius for a conducting cylinder with endcap). The phase matches closely for both TE and TM.

For a conducting cylinder without endcap:

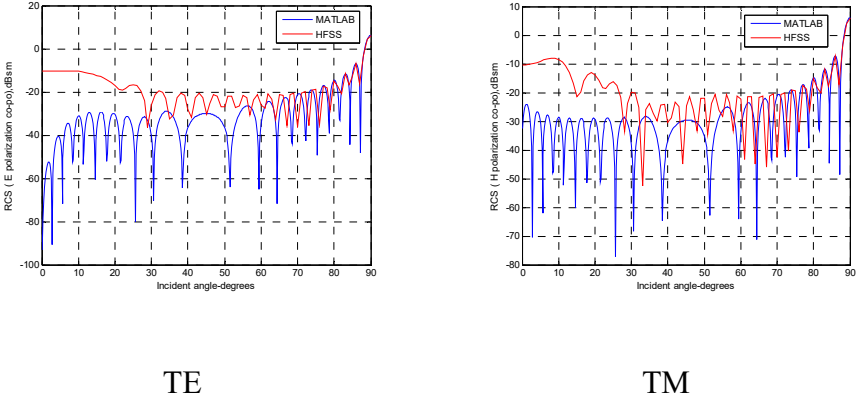


Figure 4.29: Amplitude comparison for TE and TM mode in MATLAB and HFSS (1.1 (~10 λ) meters in length by 0.055 (~0.5 λ) meters in radius for a conducting cylinder without endcap). Amplitudes show big gaps at 0° and overlap at 90° for both TE and TM.

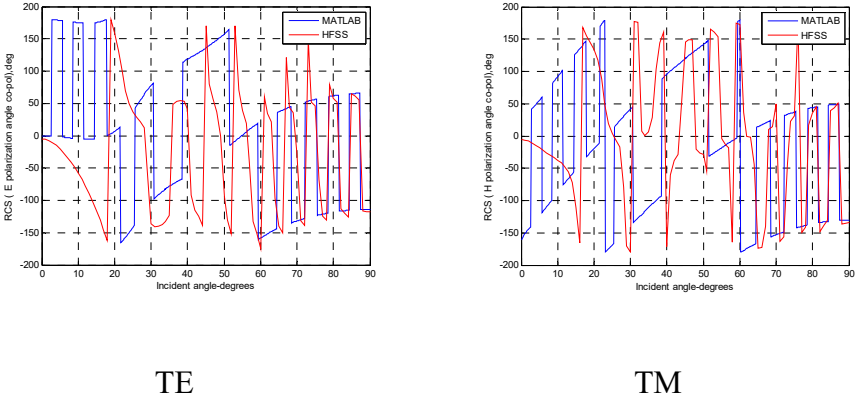


Figure 4.30: Phase comparison for TE and TM mode in MATLAB and HFSS (1.1 (~10 λ) meters in length by 0.055 (~0.5 λ) meters in radius for a conducting cylinder without endcap). The phase shows mismatch between 0-60° for both TE and TM.

For the same size conducting cylinder with endcap:

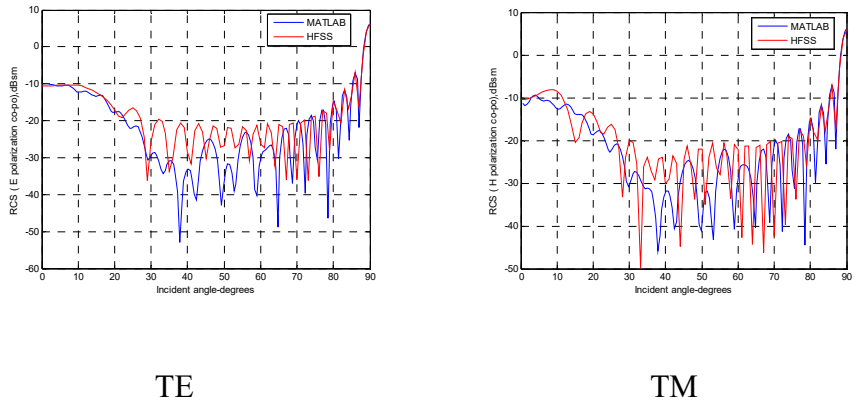
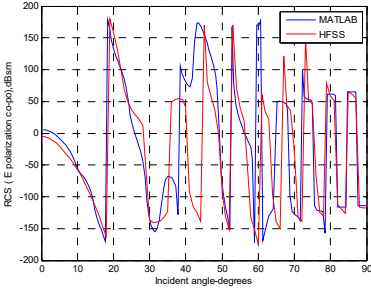
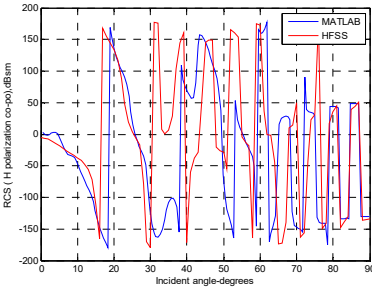


Figure 4.31: Amplitude comparison for TE and TM mode in MATLAB and HFSS (1.1 ($\sim 10 \lambda$) meters in length by 0.055 ($\sim 0.5 \lambda$) meters in radius for a conducting cylinder with endcap). Amplitudes show very few differences at 0° for both TE and TM.



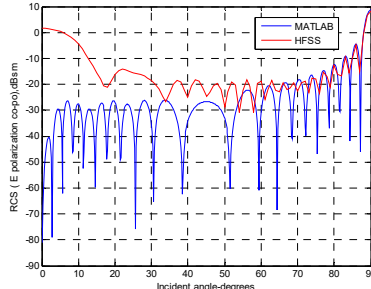
TE



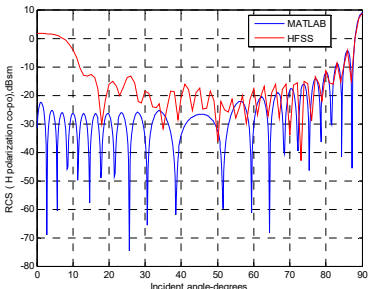
TM

Figure 4.32: Phase comparison for TE and TM mode in MATLAB and HFSS (1.1 ($\sim 10 \lambda$) meters in length by 0.055 ($\sim 0.5 \lambda$) meters in radius for a conducting cylinder with endcap). The phase is in good agreement with HFSS for both TE and TM.

For a conducting cylinder without endcap:



TE



TM

Figure 4.33: Amplitude comparison for TE and TM mode in MATLAB and HFSS (1.1 (~10 λ) meters in length by 0.11 (~1 λ) meters in radius for a conducting cylinder without endcap). Amplitudes show big gaps at 0° and overlap at 90° for both TE and TM.

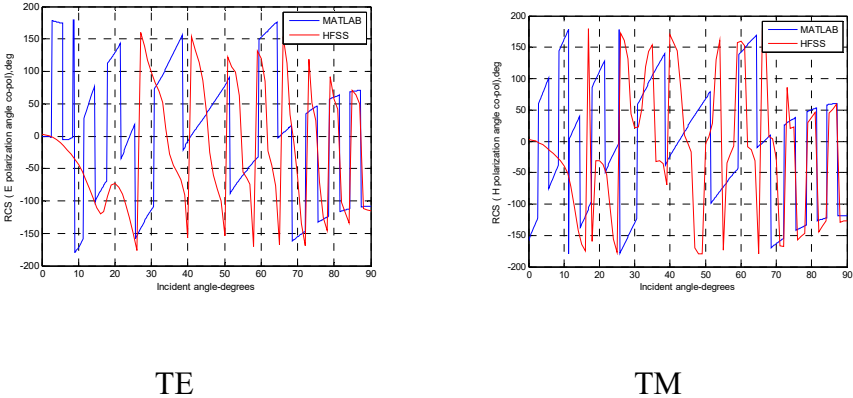


Figure 4.34: Phase comparison for TE and TM mode in MATLAB and HFSS (1.1 (~10 λ) meters in length by 0.11 (~1 λ) meters in radius for a conducting cylinder without endcap). The phase shows mismatch between 0-60° for both TE and TM.

For the same size conducting cylinder with endcap:

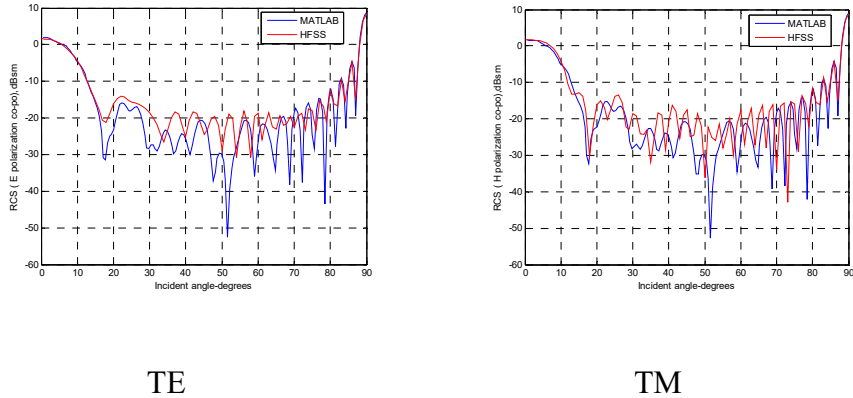


Figure 4.35: Amplitude comparison for TE and TM mode in MATLAB and HFSS (1.1 ($\sim 10 \lambda$) meters in length by 0.11 ($\sim 1 \lambda$) meters in radius for a conducting cylinder with endcap). Amplitudes almost overlap at 0° for both TE and TM.

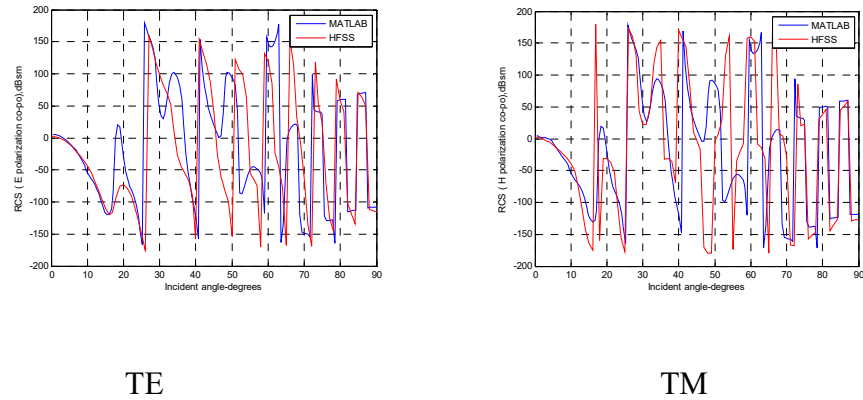


Figure 4.36: Phase comparison for TE and TM mode in MATLAB and HFSS (1.1 ($\sim 10 \lambda$) meters in length by 0.11 ($\sim 1 \lambda$) meters in radius for a conducting cylinder with endcap). The phase is in good agreement with HFSS for both TE and TM.

For a conducting cylinder without endcap:

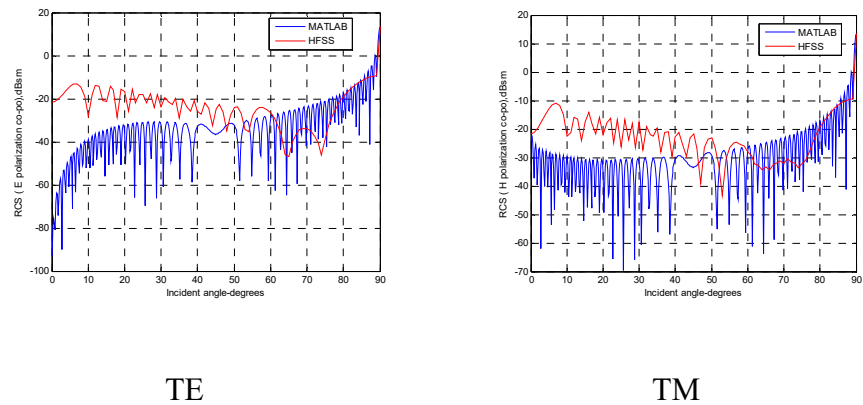


Figure 4.37: Amplitude comparison for TE and TM mode in MATLAB and HFSS (3.3 (~30 λ) meters in length by 0.033 (~0.3 λ) meters in radius for a conducting cylinder without endcap). Big gaps are shown at 0° for both TE and TM.

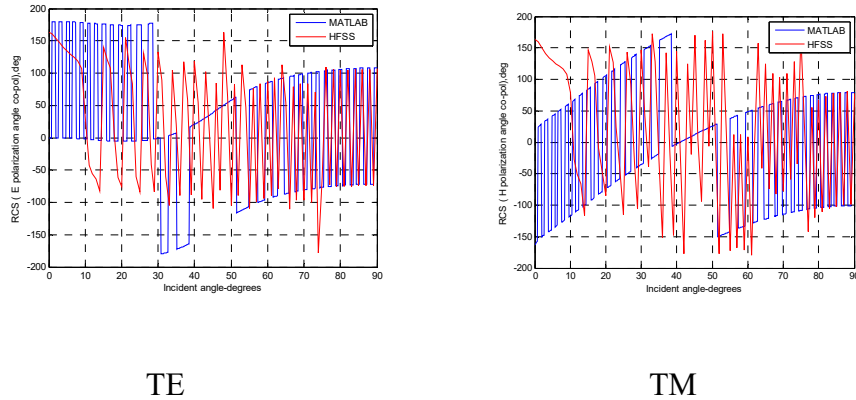


Figure 4.38: Phase comparison for TE and TM mode in MATLAB and HFSS (3.3 (~30 λ) meters in length by 0.033 (~0.3 λ) meters in radius for a conducting cylinder without endcap). The phase shows mismatch between 0-60° for both TE and TM.

For the same size conducting cylinder with endcap:

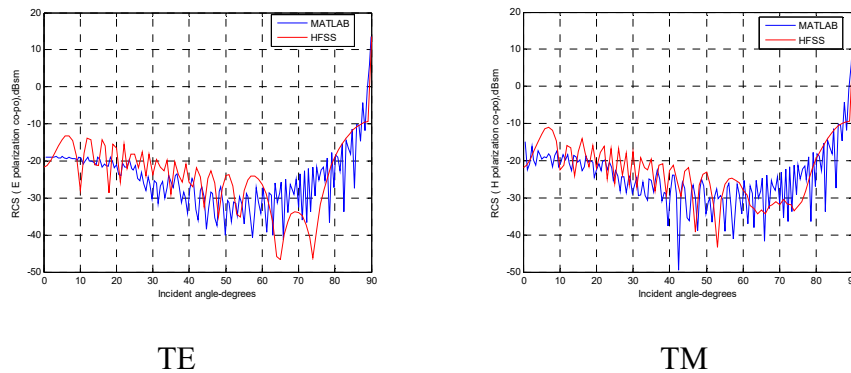
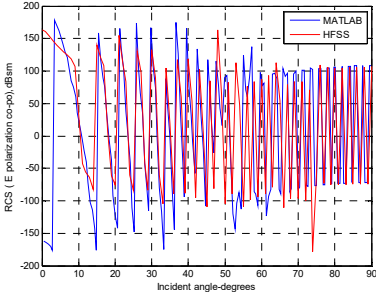
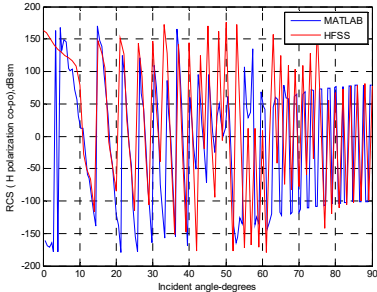


Figure 4.39: Amplitude comparison for TE and TM mode in MATLAB and HFSS (3.3 (~30 λ) meters in length by 0.033 (~0.3 λ) meters in radius for a conducting cylinder with endcap). Only a very slight amplitude difference is shown at 0° for both TE and TM.



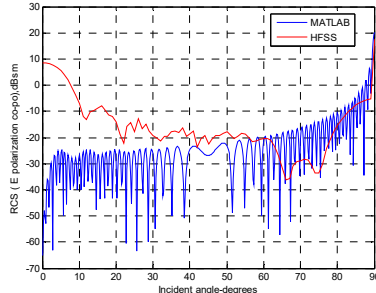
TE



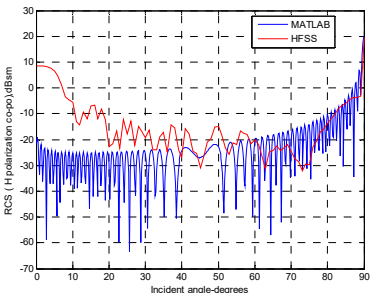
TM

Figure 4.40: Phase comparison for TE and TM mode in MATLAB and HFSS (3.3 (~30 λ) meters in length by 0.033 (~0.3 λ) meters in radius for a conducting cylinder with endcap). The phase is in good agreement with HFSS for both TE and TM.

For a conducting cylinder without endcap:



TE



TM

Figure 4.41: Amplitude comparison for TE and TM mode in MATLAB and HFSS (3.3 (~30 λ) meters in length by 0.165 (~1.5 λ) meters in radius for a conducting cylinder without endcap). Amplitudes overlap at the peak of 90°, but there are large gaps at 0° for both TE and TM.

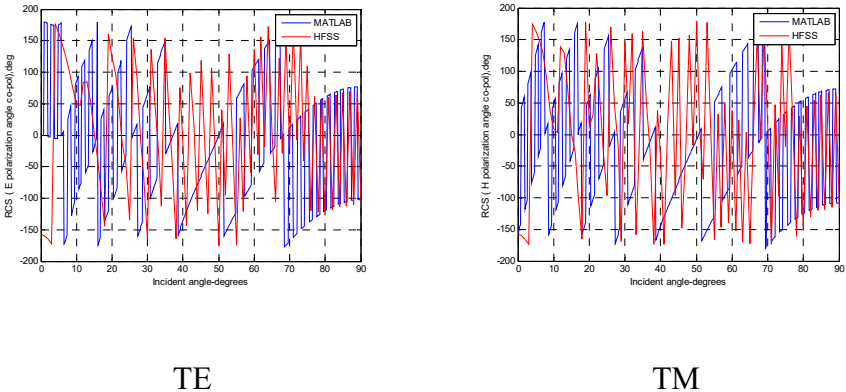


Figure 4.42: Phase comparison for TE and TM mode in MATLAB and HFSS (3.3 (~30 λ) meters in length by 0.165 (~1.5 λ) meters in radius for a conducting cylinder without endcap). The phase shows mismatch for both TE and TM.

For the same size conducting cylinder with endcap:

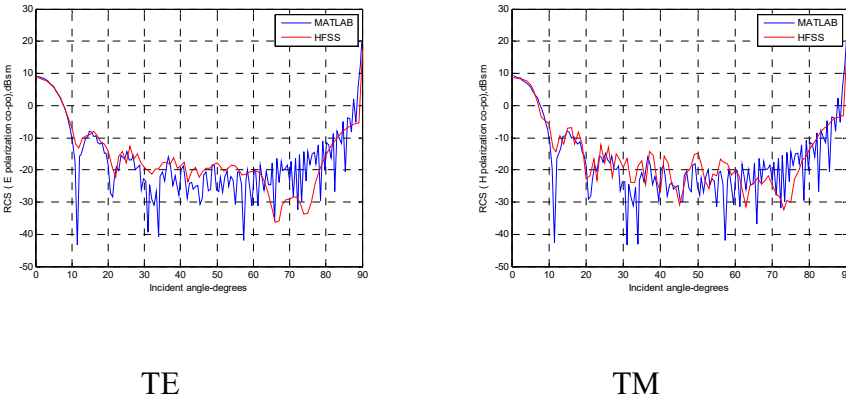


Figure 4.43: Amplitude comparison for TE and TM mode in MATLAB and HFSS (3.3 (~30 λ) meters in length by 0.165 (~1.5 λ) meters in radius for a conducting cylinder with endcap). Amplitudes overlap at 0° for both TE and TM.

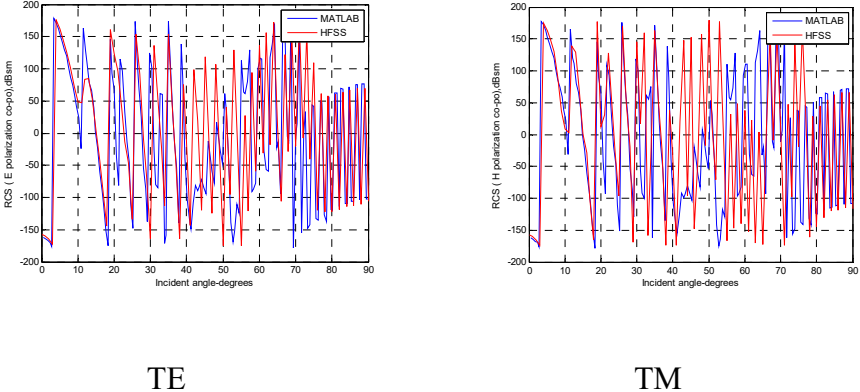


Figure 4.44: Phase comparison for TE and TM mode in MATLAB and HFSS (3.3 (~30 λ) meters in length by 0.165 (~1.5 λ) meters in radius for a conducting cylinder with endcap). The phase is in good agreement with HFSS for both TE and TM.

4.4 Generic derivation for dielectric cylinders

4.4.1 Generic derivation for dielectric cylinders broadside

If we assume an incident plane wave is scattering obliquely on the infinite circular dielectric cylinder, then the z component of electric field is given by (Wait 1955):

$$E_z^i = E_0 \sin \theta e^{i\beta_2 \rho \sin \theta \cos \phi} e^{-i\beta_2 z \cos \theta} e^{i\omega t} \tag{4.30}$$

The z component of the incident electric field can also be expressed as by applying the addition theorem

$$E_z^i = E_0 \sin \theta \sum_{n=-\infty}^{+\infty} i^n J_n(\lambda_2 \rho) F_n \quad (4.31)$$

The z component of scattered field of the surrounding medium can be written

$$E_z^s = \sum_{n=-\infty}^{+\infty} a_n^s H_n^{(2)}(\lambda_2 \rho) F_n \quad H_z^s = \sum_{n=-\infty}^{+\infty} b_n^s H_n^{(2)}(\lambda_2 \rho) F_n \quad (4.32)$$

The Hankel function of the second kind of order n guarantees that the cylinder behaves properly at infinity.

The z component of internal electric field is

$$E_z = \sum_{n=-\infty}^{+\infty} a_n J_n(\lambda_1 \rho) F_n \quad (4.33)$$

Where the Bessel function of the first kind of order n makes sure that the electric field is finite at the origin. It follows that the z component of incident and internal magnetic fields are

$$H_z^i = 0 \quad \text{for TM mode} \quad (4.34)$$

$$H_z = \sum_{n=-\infty}^{+\infty} b_n J_n(\lambda_1 \rho) F_n \quad (4.35)$$

where a_n^s and b_n^s specify the magnitude of TM and TE mode of the surrounding medium of the cylinder; a_n and b_n are the same except for the internal field.

$$F_n = e^{-in\phi} e^{-i\beta_2 z \cos\theta} e^{i\omega t} \quad (4.36)$$

$$\lambda_2 = \beta_2 \sin\theta \quad (4.37)$$

$$\lambda_1 = (\beta_1^2 - \beta_2^2 \cos^2\theta)^{1/2}, \text{ where } \beta_1 = (\varepsilon_1 \mu_1)^{1/2} \omega, \beta_2 = (\varepsilon_2 \mu_2)^{1/2} \omega \quad (4.38)$$

The tangential fields can be calculated based on the equations above from the Maxwell equations in cylindrical coordinate system, which assures the simplicity and convenience for the geometry of a cylinder.

$$E_\phi^i = \sum_{n=-\infty}^{+\infty} -\frac{hnE_0 \sin\theta i^n J_n(\lambda_2 \rho) F_n}{\rho \lambda_2^2} \quad (4.39)$$

$$E_\phi^s = \sum_{n=-\infty}^{+\infty} \left[-\frac{hna_n^s}{\rho \lambda_2^2} H_n^{(2)}(\lambda_2 \rho) + \frac{i\mu_2 \omega b_n^s}{\lambda_2} H_n^{(2)'}(\lambda_2 \rho) \right] F_n \quad (4.40)$$

$$E_\phi = \sum_{n=-\infty}^{+\infty} \left[-\frac{hna_n}{\rho \lambda_1^2} J_n(\lambda_1 \rho) + \frac{i\mu_1 \omega b_n}{\lambda_1} J_n'(\lambda_1 \rho) \right] F_n \quad (4.41)$$

$$H_\phi^i = \sum_{n=-\infty}^{+\infty} \frac{-i\beta_2^2 E_0 \sin\theta}{\mu_2 \omega \lambda_2} i^n J_n'(\lambda_2 \rho) F_n \quad (4.42)$$

$$H_\phi^s = \sum_{n=-\infty}^{+\infty} \left[-\frac{i\beta_2^2 a_n^s}{\mu_2 \omega \lambda_2} H_n^{(2)'}(\lambda_2 \rho) - \frac{nhb_n^s}{\lambda_2^2 \rho} H_n^{(2)}(\lambda_2 \rho) \right] F_n \quad (4.43)$$

$$H_\phi = \sum_{n=-\infty}^{+\infty} \left[-\frac{i\beta_1^2 a_n}{\mu_1 \omega \lambda_1} J_n'(\lambda_1 \rho) - \frac{nhb_n}{\lambda_1^2 \rho} J_n(\lambda_1 \rho) \right] F_n \quad (4.44)$$

The boundary equations are applied to the internal and external medium to get coefficients a_n , b_n , a_n^s , b_n^s .

$$H_z^i + H_z^s = H_z \text{ at } \rho = a, b_n \text{ can be calculated as } b_n = b_n^s \frac{H_n^{(2)}(v)}{J_n(u)} \quad (4.45)$$

$E_z^i + E_z^s = E_z$ at $\rho = a$, a_n can be calculated as

$$a_n = \left[E_0 \sin \theta^n J_n(v) + a_n^s H_n^{(2)}(v) \right] \frac{1}{J_n(u)} \quad (4.46)$$

$$\left. \begin{array}{l} E_\phi^i + E_\phi^s = E_\phi \\ H_\phi^i + H_\phi^s = H_\phi \end{array} \right\} \Rightarrow$$

$$a_n^s = E_0 \sin \theta^n \left[\frac{J_n(v)}{H_n^{(2)}(v)} - \frac{2i \left(\frac{H_n^{(2)'}(v)}{v H_n^{(2)}(v)} - \frac{K J_n'(u)}{u J_n(u)} \right)}{\pi v^2 [H_n^{(2)}(v)]^2 D} \right], \quad (4.47)$$

$$b_n^s = \frac{\beta_2}{\mu_2 \omega} E_0 \sin \theta^n \left[\frac{2}{\pi v^2} \left(\frac{1}{u^2} - \frac{1}{v^2} \right) \frac{n \cos \theta}{[H_n^{(2)}(v)]^2 D} \right] \quad (4.48)$$

where

$$D = \left(\frac{H_n^{(2)'}(v)}{v H_n^{(2)}(v)} - \frac{K J_n'(u)}{u J_n(u)} \right) \left(\frac{H_n^{(2)'}(v)}{v H_n^{(2)}(v)} - \frac{N^2 J_n'(u)}{K u J_n(u)} \right) - \left(\frac{1}{v^2} - \frac{1}{u^2} \right)^2 n^2 \cos^2 \theta \quad (4.49)$$

$$N^2 = \frac{\beta_1^2}{\beta_2^2} = \frac{\epsilon_1 \mu_1}{\epsilon_2 \mu_2}, \quad K = \frac{\mu_1}{\mu_2}, \quad u = \lambda_1 a = (\beta_1^2 - \beta_2^2 \cos^2 \theta)^{1/2} a, \quad (4.50)$$

$$v = \lambda_2 a = \beta_2 (\sin \theta) a, \quad (4.51)$$

Then, applying the far-zone Henkel function and its derivative

$$H_n^2(\alpha x) \stackrel{\alpha x \rightarrow \infty}{\cong} \sqrt{\frac{2j}{\pi \alpha x}} j^n e^{-j \alpha x} \quad (4.52)$$

$$H_n^{2'}(\alpha x) \cong -\sqrt{\frac{2j}{\pi\alpha x}} j^{n+1} e^{-j\alpha x} \quad (4.53)$$

$$\text{Let } a_n^{s'} = \frac{a_n^s}{E_0}, \quad b_n^{s'} = \frac{b_n^s}{E_0} \quad (4.54)$$

as $\rho \rightarrow \infty$, the terms in z component of both E and H scattered field become zero after derivation since it is in the denominator. As such, only the other term is taken into account.

$$|H_\phi^s|^2 = |\sqrt{j}|^2 \frac{2}{\pi\beta_2 \sin \theta \rho} \frac{\beta_2^4}{\mu_2^2 \omega^2 \lambda_2^2} \left| \sum_{n=-\infty}^{+\infty} j^n a_n^s e^{-jn\phi} \right|^2 \quad (4.55)$$

$$\sigma_{VV}^{2d} = \lim_{\rho \rightarrow \infty} \left(2\pi\rho \frac{|H_\phi^s|^2}{|H_0|^2} \right) = \lim_{\rho \rightarrow \infty} \left(2\pi\rho \frac{|H_\phi^s|^2}{|E_0|^2 / \eta_0^2} \right) = \lim_{\rho \rightarrow \infty} \left(2\pi\rho \eta_0^2 \frac{|H_\phi^s|^2}{|E_0|^2} \right)$$

$$\sigma_{VV}^{2d} = |\sqrt{j}|^2 \frac{2\lambda}{\pi \sin \theta} \left| \sum_{n=-\infty}^{\infty} a_n^{s''} j^n e^{-jn\phi} \right|^2 \quad (4.56)$$

$$a_n^{s''} = \frac{a_n^{s'}}{\sin \theta} = \frac{a_n^s}{E_0 \sin \theta} \quad b_n^{s''} = \frac{b_n^{s'}}{\sin \theta} = \frac{b_n^s}{E_0 \sin \theta} \quad (4.57)$$

From (11-139 Balanis 2012) and for monostatic, 3D RCS is reduced to

$$\sigma_{3-D} \cong \sigma_{2-D} \frac{2l^2}{\lambda} \sin^2 \theta \left[\frac{\sin(\beta l \cos \theta)}{\beta l \cos \theta} \right]^2 \quad (4.58)$$

3D co-pol TM mode RCS becomes

$$\sigma_{VV} = |\sqrt{j}|^2 \left| \sum_{n=-\infty}^{\infty} a_n^{s''} j^n \right|^2 \frac{4l^2}{\pi} \sin \theta \left[\frac{\sin(\beta l \cos \theta)}{\beta l \cos \theta} \right]^2 \quad (4.59)$$

The amplitude becomes

$$S_{VV} = \sqrt{\frac{4jl^2}{\pi}} \sin \theta \left(\sum_{n=-\infty}^{\infty} a_n^{s''} j^n \right) \frac{\sin(\beta l \cos \theta)}{\beta l \cos \theta} \quad (4.60)$$

For TM cross-pol, process is similar,

$$|E_\phi^s|^2 = |\sqrt{j}|^2 \frac{\mu_2^2 \omega^2}{\lambda_2^2} \frac{2}{\pi \lambda_2 \rho} \left| \sum_{n=-\infty}^{+\infty} j^n b_n^s e^{-in\phi} \right|^2 \quad (4.61)$$

$$\sigma_{VH}^{2d} = \lim_{\rho \rightarrow \infty} \left(2\pi\rho \frac{|E_\phi^s|^2}{|E_0|^2} \right) \quad (\phi = 0) \quad (4.62)$$

$$\sigma_{VH}^{2d} = \frac{4\mu_2^2 \omega^2}{\beta_2^3 \sin \theta} |\sqrt{j}|^2 \left| \sum_{n=-\infty}^{+\infty} j^n b_n^s \right|^2 \quad (\phi = 0) \quad (4.63)$$

3D cross-pol TM mode RCS becomes

$$\sigma_{VH} = |\sqrt{j}|^2 \left| \sum_{n=-\infty}^{\infty} b_n^s j^n \right|^2 \frac{8l^2 \mu_2^2 \omega^2}{\lambda \beta_2^3} \sin \theta \left[\frac{\sin(\beta l \cos \theta)}{\beta l \cos \theta} \right]^2 \quad (4.64)$$

$$S_{VH} = \sqrt{\frac{8jl^2 \mu_2^2 \omega^2}{\lambda \beta_2^3} \sin \theta} \left(\sum_{n=-\infty}^{\infty} b_n^s j^n \right) \frac{\sin(\beta l \cos \theta)}{\beta l \cos \theta} \quad (4.65)$$

For TE mode, due to the duality theorem by replacing E by H, H by -E,

μ by ε

$$\sigma_{HH}^{2d} = \lim_{\rho \rightarrow \infty} \left(2\pi\rho \frac{|-E_\phi^s|^2}{|E_0|^2} \right) = \lim_{\rho \rightarrow \infty} \left(2\pi\rho \frac{1}{\eta_0^2} \frac{|-E_\phi^s|^2}{|H_0|^2} \right) \quad (4.66)$$

The 2D RCS for co-pol TE mode is

$$\sigma_{HH}^{2d} = |\sqrt{j}|^2 \frac{2\lambda}{\pi \sin \theta} \left| \sum_{n=-\infty}^{\infty} a_n^s j^n \right|^2 \quad (4.67)$$

3D RCS becomes

$$\sigma_{HH} = \left| \sqrt{j} \right|^2 \left| - \sum_{n=-\infty}^{\infty} a_n^{s''} j^n \right|^2 \frac{4l^2}{\pi} \sin \theta \left[\frac{\sin(\beta l \cos \theta)}{\beta l \cos \theta} \right]^2 \quad (4.68)$$

$$S_{HH} = - \sqrt{\frac{4jl^2}{\pi} \sin \theta} \left(\sum_{n=-\infty}^{\infty} a_n^{s''} j^n \right) \frac{\sin(\beta l \cos \theta)}{\beta l \cos \theta} \quad (4.69)$$

Similarly, the cross-pol of TE mode is

$$\sigma_{HV}^{2d} = \lim_{\rho \rightarrow \infty} \left(2\pi\rho \frac{|H_\Phi^s|^2}{|H_0|^2} \right) \quad (4.70)$$

$$\sigma_{HV}^{2d} = \frac{4\varepsilon_2^2 \omega^2}{\beta_2^3 \sin \theta} \left| \sqrt{j} \right|^2 \left| \sum_{n=-\infty}^{+\infty} j^n b_n^{s''} \right|^2 \quad (\phi = 0) \quad (4.71)$$

$$\sigma_{HV} = \frac{4l^2 \varepsilon_2}{\mu_2 \pi} \sin \theta \left| \sqrt{j} \right|^2 \left| \sum_{n=-\infty}^{+\infty} j^n b_n^{s''} \right|^2 \quad (4.72)$$

$$S_{HV} = \sqrt{\frac{4jl^2 \varepsilon_2}{\mu_2 \pi} \sin \theta} \left(\sum_{n=-\infty}^{\infty} j^n b_n^{s''} \right) \frac{\sin(\beta l \cos \theta)}{\beta l \cos \theta} \quad (4.73)$$

In this case, TM cross-pol is not necessarily equal to the TE cross-pol.

A phase shift $e^{-j\pi/2}$ is added to the broadside of the cylinder RCS amplitude. This appears to be in good agreement with HFSS.

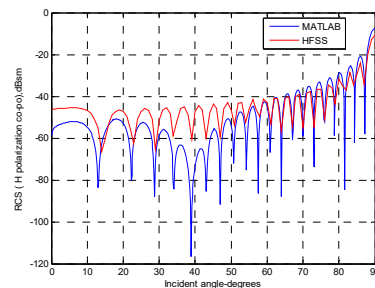
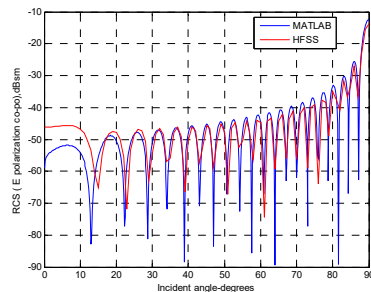
4.4.2 Generic derivation for dielectric cylinders endcaps

When adding the equations of surface impedance circular plate (3.4.3 section in Chapter 3) using an extension of PO approximation to the

broadside amplitude equations above, the complete finite dielectric cylinder model has been established. Furthermore, by observing the amplitudes at 0 degrees of the incident angle for both conducting and dielectric cylindrical broadside, the conducting and surface impedance circular plates are added to endcaps. All plots indicate that amplitudes increase dramatically with endcaps. Some plots show overlap at 0 degrees of the incident angle. The phase term for endcaps added at the half length (L) of a cylinder is used to match the phase in the same location of the cylinder simulated in HFSS when the RCS cylinder with an endcap is calculated in the far-field.

4.4.3 Simulation vs. analytical results for dielectric large, thin cylinders with and without endcaps

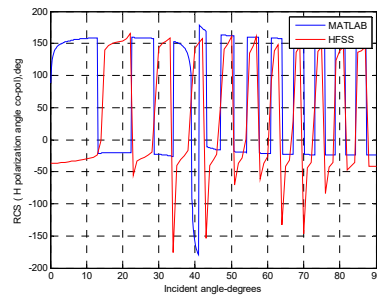
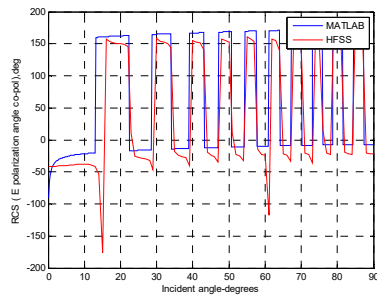
Dielectric cylinders at $\epsilon_r = 2.15$ without and with endcaps 1.1 ($\sim 10 \lambda$) meters in length by > 0.011 ($\sim 0.1 \lambda$) meters in radius have amplitudes showing big gaps at 0 degrees but are in good agreement with HFSS with endcaps. Phase shows the same.



TE

TM

Figure 4.45: Amplitude comparison for TE and TM mode in MATLAB and HFSS (1.1 (~10 λ) meters in length by 0.011 (~0.1 λ) meters in radius at $\epsilon_r = 2.15$ for a dielectric cylinder without endcap). Amplitudes have less than 20 dB differences at 0° for both TE and TM.

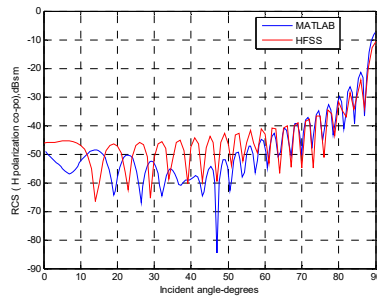
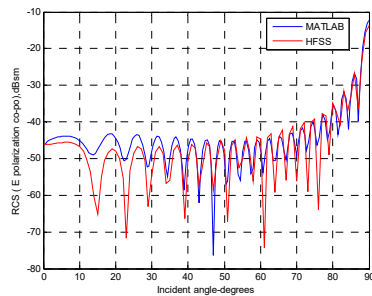


TE

TM

Figure 4.46: Phase comparison for TE and TM mode in MATLAB and HFSS (1.1 (~10 λ) meters in length by 0.011 (~0.1 λ) meters in radius at $\epsilon_r = 2.15$ for a dielectric cylinder without endcap). The phase shows mismatch for both TE and TM.

For the same size dielectric cylinder at $\epsilon_r = 2.15$ with endcap:



TE

TM

Figure 4.47: Amplitude comparison for TE and TM mode in MATLAB and HFSS (1.1 ($\sim 10 \lambda$) meters in length by 0.011 ($\sim 0.1 \lambda$) meters in radius at $\epsilon_r = 2.15$ for a dielectric cylinder with endcap). Amplitude almost overlaps at 0° for TE. Amplitude matches closely for TM.

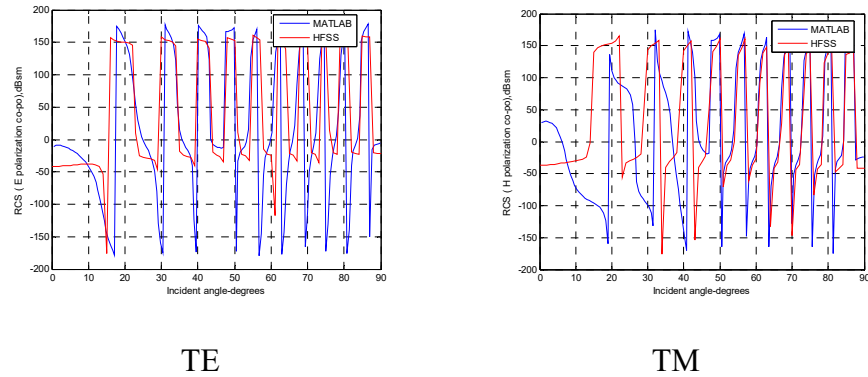


Figure 4.48: Phase comparison for TE and TM mode in MATLAB and HFSS (1.1 ($\sim 10 \lambda$) meters in length by 0.011 ($\sim 0.1 \lambda$) meters in radius at $\epsilon_r = 2.15$ for a dielectric cylinder with endcap). The phase is in good agreement with HFSS for both TE and TM.

For a dielectric cylinder at $\epsilon_r = 10-5j$ without endcap:

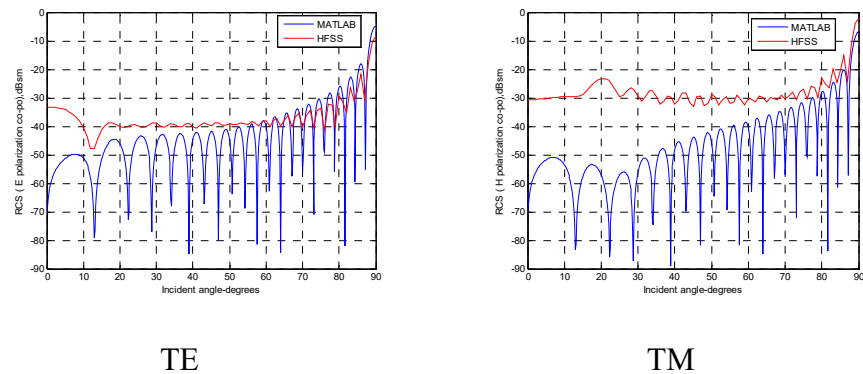


Figure 4.49: Amplitude comparison for TE and TM mode in MATLAB and HFSS (1.1 (~10 λ) meters in length by 0.011 (~0.1 λ) meters in radius at $\epsilon_r = 10-5j$ for a dielectric cylinder without endcap). Big gaps are observed at 0° for both TE and TM.

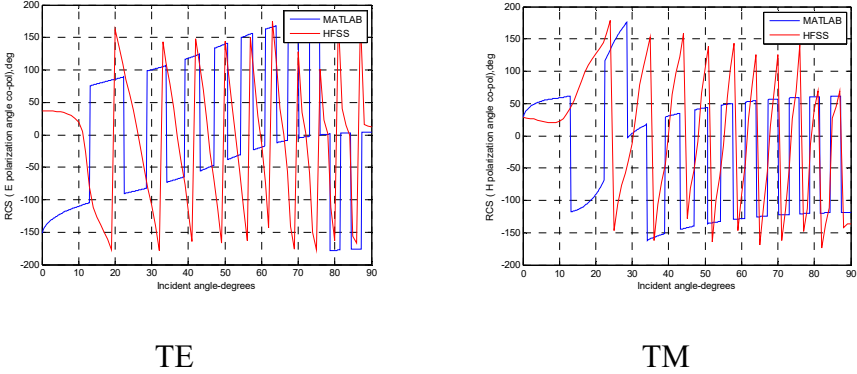


Figure 4.50: Phase comparison for TE and TM mode in MATLAB and HFSS (1.1 (~10 λ) meters in length by 0.011 (~0.1 λ) meters in radius at $\epsilon_r = 10-5j$ for a dielectric cylinder without endcap). The phase shows mismatch for both TE and TM.

For the same size dielectric cylinder at $\epsilon_r = 10-5j$ with endcap:

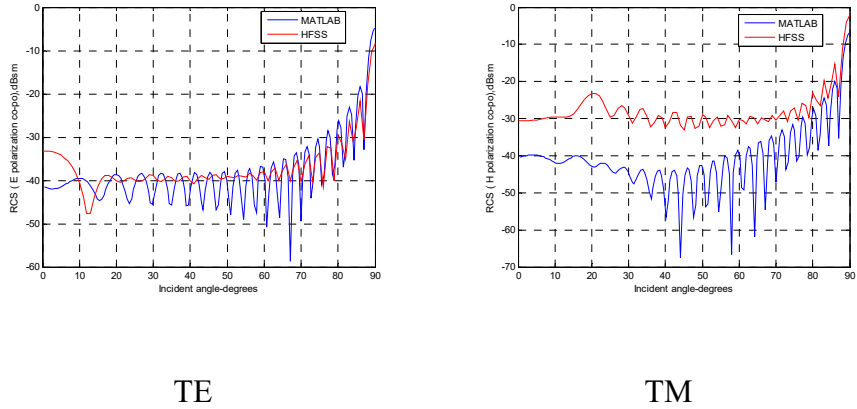


Figure 4.51: Amplitude comparison for TE and TM mode in MATLAB and HFSS (1.1 (~10 λ) meters in length by 0.011 (~0.1 λ) meters in radius at $\epsilon_r = 10-5j$ for a dielectric cylinder with endcap). Amplitude has less than 10 dB difference at 0° for TE. Amplitude has less than a 10 dB difference at 0° for TM.

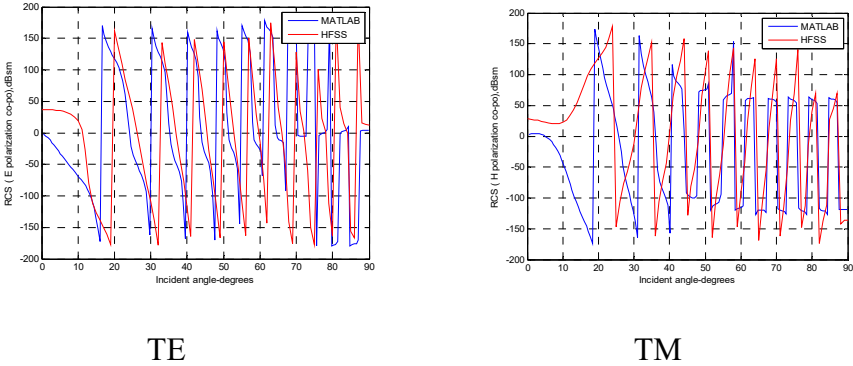


Figure 4.52: Phase comparison for TE and TM mode in MATLAB and HFSS (1.1 (~10 λ) meters in length by 0.011 (~0.1 λ) meters in radius at $\epsilon_r = 10-5j$ for a dielectric cylinder with endcap). The phase is in good agreement with HFSS for both TE and TM.

For a dielectric cylinder at $\epsilon_r = 2.15$ without endcap:

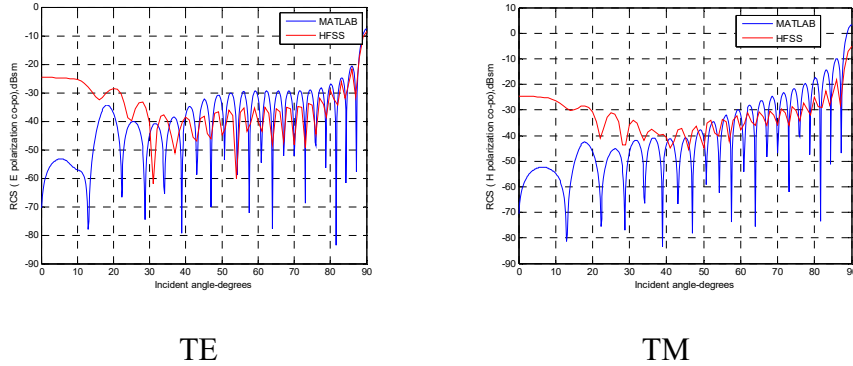


Figure 4.53: Amplitude comparison for TE and TM mode in MATLAB and HFSS (1.1 ($\sim 10 \lambda$) meters in length by 0.055 ($\sim 0.5 \lambda$) meters in radius at $\epsilon_r = 2.15$ for a dielectric cylinder without endcap). Big gaps are observed at 0° for both TE and TM.

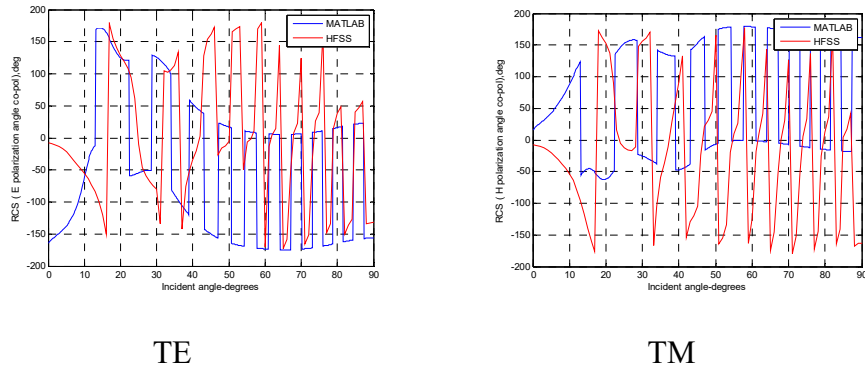


Figure 4.54: Phase comparison for TE and TM mode in MATLAB and HFSS (1.1 ($\sim 10 \lambda$) meters in length by 0.055 ($\sim 0.5 \lambda$) meters in radius at $\epsilon_r = 2.15$ for a dielectric cylinder without endcap). The phase shows mismatch for both TE and TM.

For the same size dielectric cylinder at $\epsilon_r = 2.15$ with endcap:

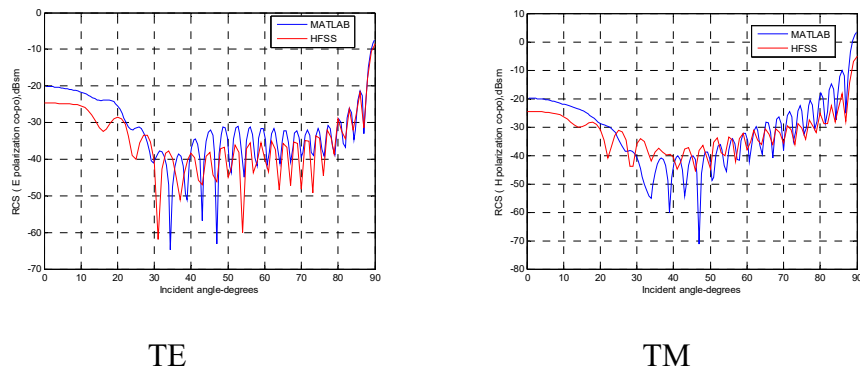


Figure 4.55: Amplitude comparison for TE and TM mode in MATLAB and HFSS (1.1 ($\sim 10 \lambda$) meters in length by 0.055 ($\sim 0.5 \lambda$) meters in radius at $\epsilon_r = 2.15$ for a dielectric cylinder with endcap). Amplitudes show a few dB differences for both TE and TM at 0° .

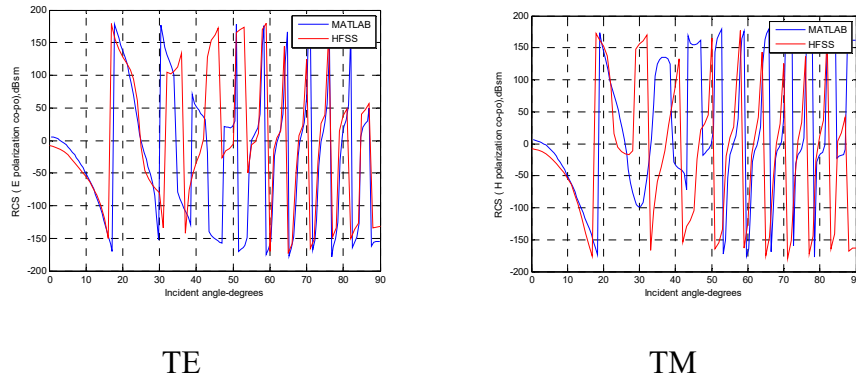


Figure 4.56: Phase comparison for TE and TM mode in MATLAB and HFSS (1.1 ($\sim 10 \lambda$) meters in length by 0.055 ($\sim 0.5 \lambda$) meters in radius at $\epsilon_r = 2.15$ for a dielectric cylinder with endcap). The phase is in good agreement with HFSS for both TE and TM.

For a dielectric cylinder at $\epsilon_r = 10-5j$ without endcap:

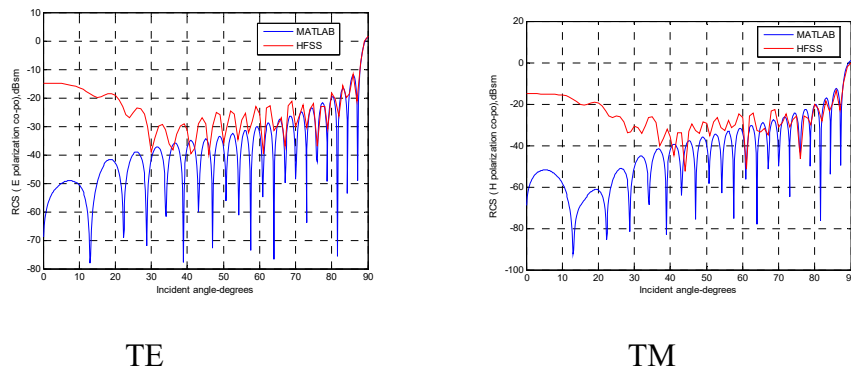


Figure 4.57: Amplitude comparison for TE and TM mode in MATLAB and HFSS (1.1 (~10 λ) meters in length by 0.055 (~0.5 λ) meters in radius at $\epsilon_r = 10-5j$ for a dielectric cylinder without endcap). Big gaps are observed at 0° for both TE and TM.

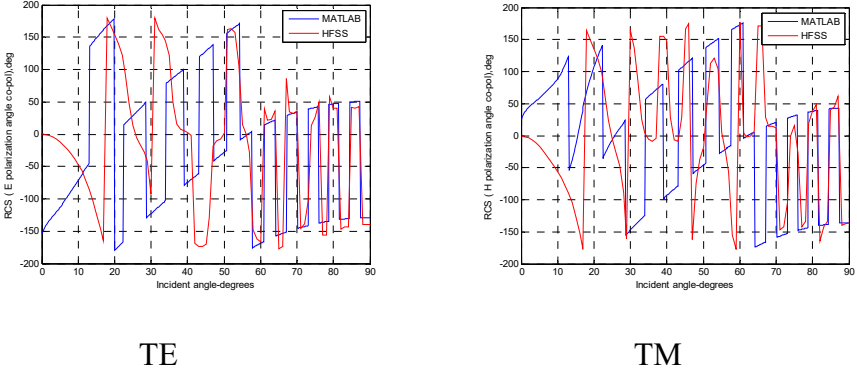


Figure 4.58: Phase comparison for TE and TM mode in MATLAB and HFSS (1.1 (~10 λ) meters in length by 0.055 (~0.5 λ) meters in radius at $\epsilon_r = 10-5j$ for a dielectric cylinder without endcap). The phase shows mismatch between 0-60° for both TE and TM.

For the same size dielectric cylinder at $\epsilon_r = 10-5j$ with endcap:

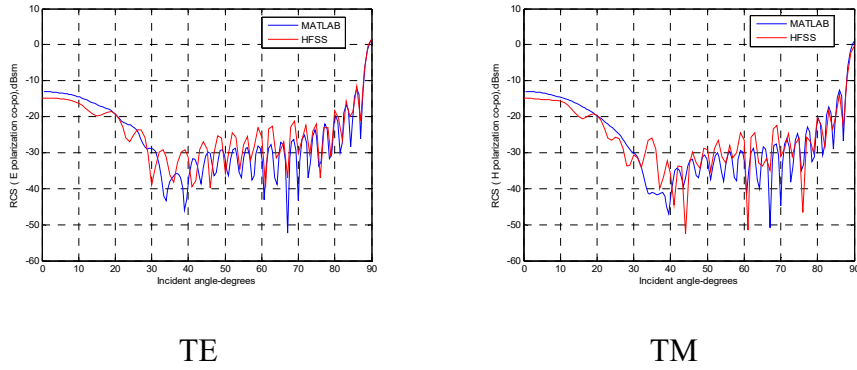


Figure 4.59: Amplitude comparison for TE and TM mode in MATLAB and HFSS (1.1 (~10 λ) meters in length by 0.055 (~0.5 λ) meters in radius at $\epsilon_r = 10-5j$ for a dielectric cylinder with endcap). A couple of dB differences are observed for both TE and TM.

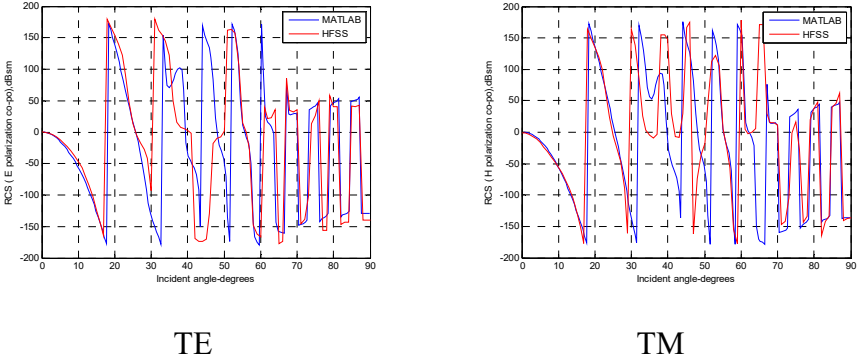


Figure 4.60: Phase comparison for TE and TM mode in MATLAB and HFSS (1.1 (~10 λ) meters in length by 0.055 (~0.5 λ) meters in radius at $\epsilon_r = 10-5j$ for a dielectric cylinder with endcap). The phase is in good agreement with HFSS for both TE and TM.

For a dielectric cylinder at $\epsilon_r = 2.15$ without endcap:

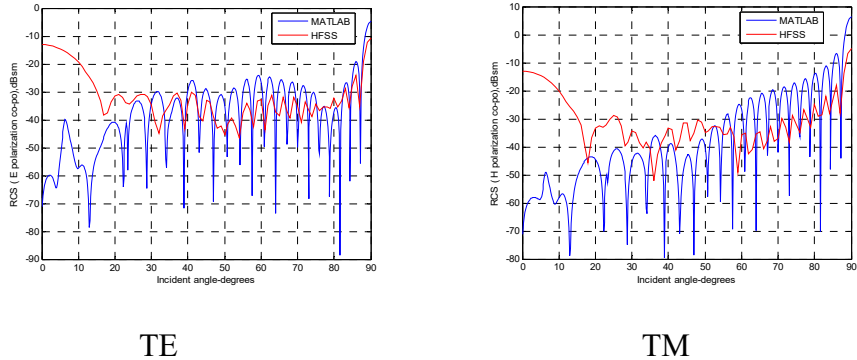


Figure 4.61: Amplitude comparison for TE and TM mode in MATLAB and HFSS (1.1 ($\sim 10 \lambda$) meters in length by 0.11 ($\sim 1 \lambda$) meters in radius at $\epsilon_r = 2.15$ for a dielectric cylinder without endcap). Big gaps are observed at 0° for both TE and TM.

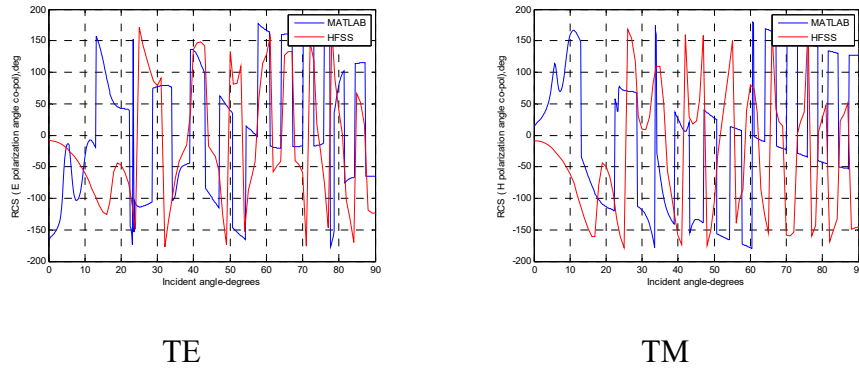


Figure 4.62: Phase comparison for TE and TM mode in MATLAB and HFSS (1.1 ($\sim 10 \lambda$) meters in length by 0.11 ($\sim 1 \lambda$) meters in radius at $\epsilon_r = 2.15$ for a dielectric cylinder without endcap). The phase shows mismatch for both TE and TM.

For the same size dielectric cylinder at $\epsilon_r = 2.15$ with endcap:

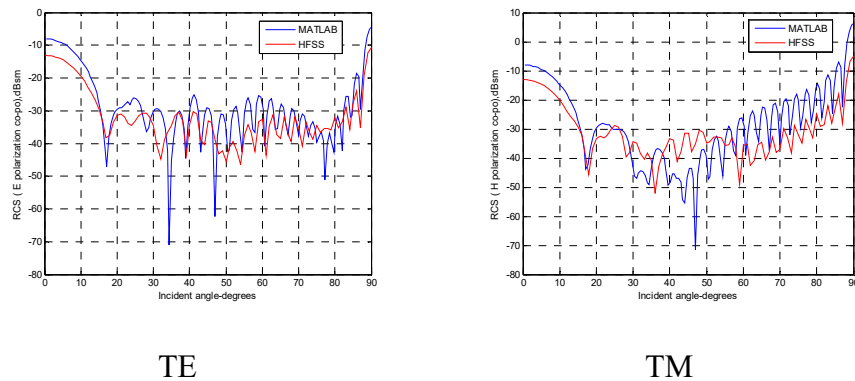


Figure 4.63: Amplitude comparison for TE and TM mode in MATLAB and HFSS (1.1 (~10 λ) meters in length by 0.11 (~1 λ) meters in radius at $\epsilon_r = 2.15$ for a dielectric cylinder with endcap). Amplitudes have less than 5 dB differences at 0° for both TE and TM.

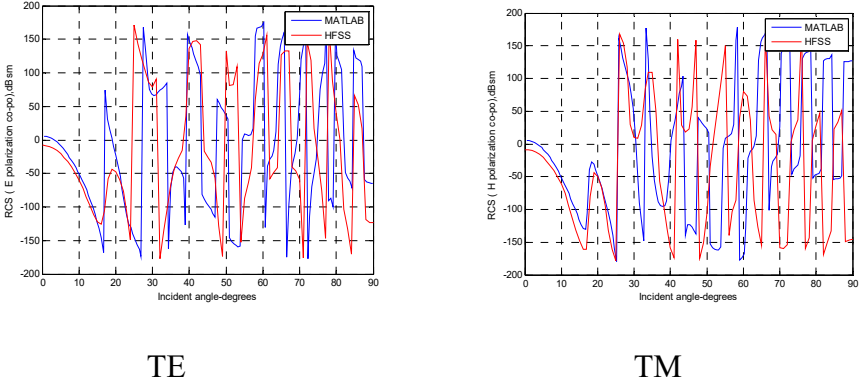


Figure 4.64: Phase comparison for TE and TM mode in MATLAB and HFSS (1.1 (~10 λ) meters in length by 0.11 (~1 λ) meters in radius at $\epsilon_r = 2.15$ for a dielectric cylinder with endcap). The phase is in good agreement with HFSS for both TE and TM.

For a dielectric cylinder at $\epsilon_r = 10-5j$ without endcap:

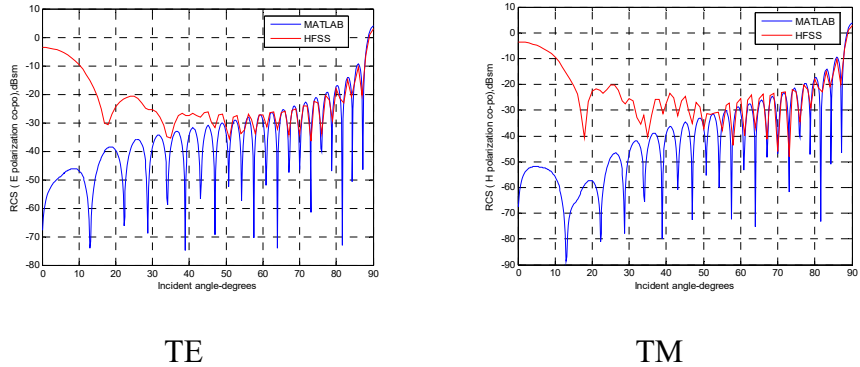


Figure 4.65: Amplitude comparison for TE and TM mode in MATLAB and HFSS (1.1 (~10 λ) meters in length by 0.11 (~1 λ) meters in radius at $\epsilon_r = 10-5j$ for a dielectric cylinder without endcap). Big gaps are observed at 0° for both TE and TM.

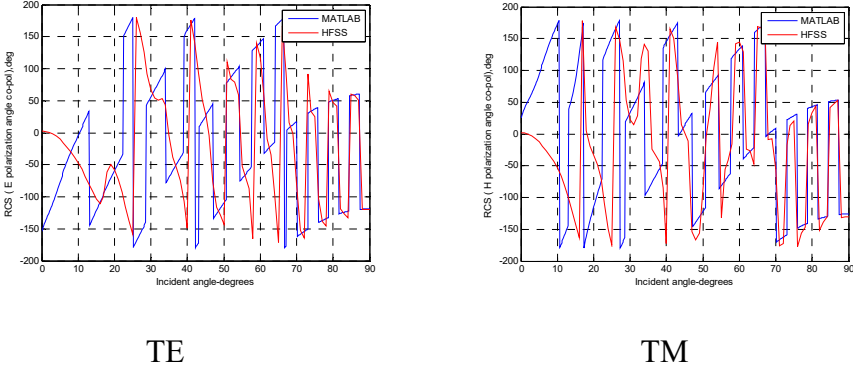


Figure 4.66: Phase comparison for TE and TM mode in MATLAB and HFSS (1.1 (~10 λ) meters in length by 0.11 (~1 λ) meters in radius at $\epsilon_r = 10-5j$ for a dielectric cylinder without endcap). The phase shows mismatch for both TE and TM.

For the same size dielectric cylinder at $\epsilon_r = 10-5j$ with endcap:

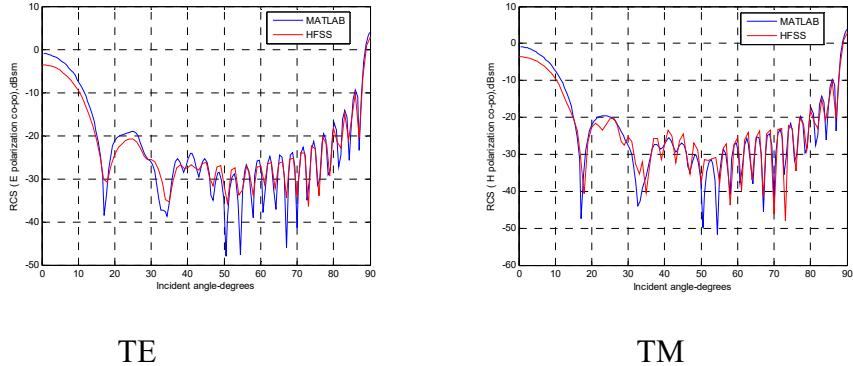


Figure 4.67: Amplitude comparison for TE and TM mode in MATLAB and HFSS (1.1 ($\sim 10 \lambda$) meters in length by 0.11 ($\sim 1 \lambda$) meters in radius at $\epsilon_r = 10-5j$ for a dielectric cylinder with endcap). Amplitudes are in good agreement with HFSS for both TE and TM.

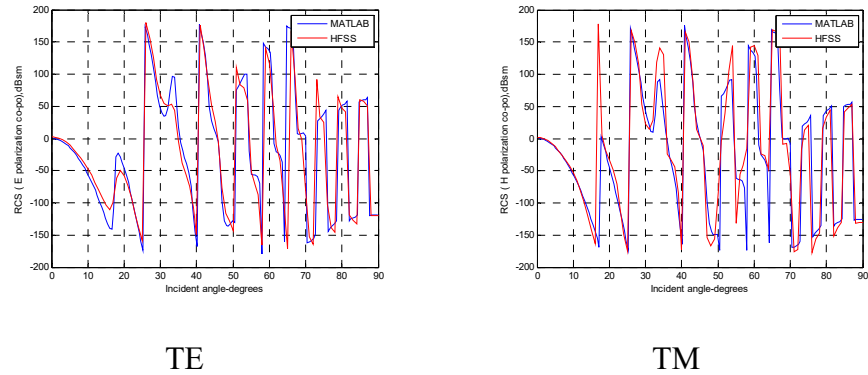


Figure 4.68: Amplitude comparison for TE and TM mode in MATLAB and HFSS (1.1 ($\sim 10 \lambda$) meters in length by 0.11 ($\sim 1 \lambda$) meters in radius at $\epsilon_r = 10-5j$ for a dielectric cylinder with endcap). Phase is in good agreement with HFSS for both TE and TM.

For a dielectric cylinder at $\epsilon_r = 2.15$ without endcap:

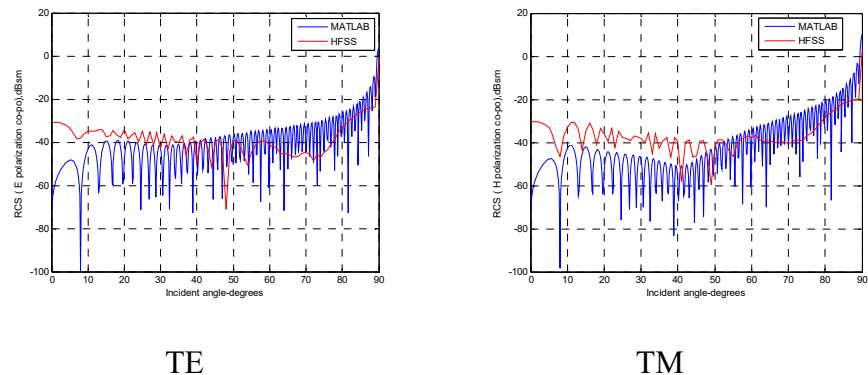


Figure 4.69: Amplitude comparison for TE and TM mode in MATLAB and HFSS (3.3 ($\sim 30 \lambda$) meters in length by 0.033 ($\sim 0.3 \lambda$) meters in radius at $\epsilon_r = 2.15$ for a dielectric cylinder without endcap). Big gaps are observed at 0° for both TE and TM.

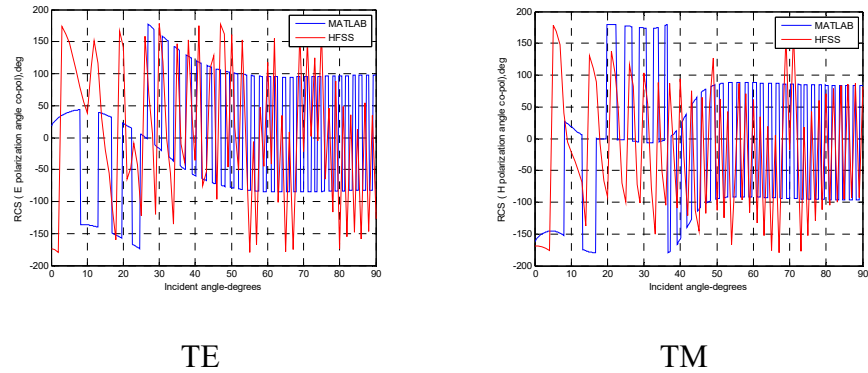


Figure 4.70: Phase comparison for TE and TM mode in MATLAB and HFSS (3.3 ($\sim 30 \lambda$) meters in length by 0.033 ($\sim 0.3 \lambda$) meters in radius at $\epsilon_r = 2.15$ for a dielectric cylinder without endcap). The phase shows mismatch for both TE and TM.

For the same size dielectric cylinder at $\epsilon_r = 2.15$ with endcap:

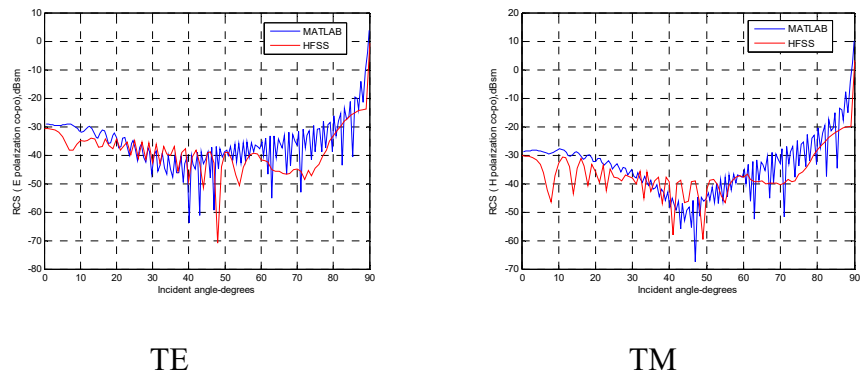


Figure 4.71: Amplitude comparison for TE and TM mode in MATLAB and HFSS (3.3 (~30 λ) meters in length by 0.033 (~0.3 λ) meters in radius at $\epsilon_r = 2.15$ for a dielectric cylinder with endcap). Only a few amplitude differences are observed at 0° for both TE and TM.

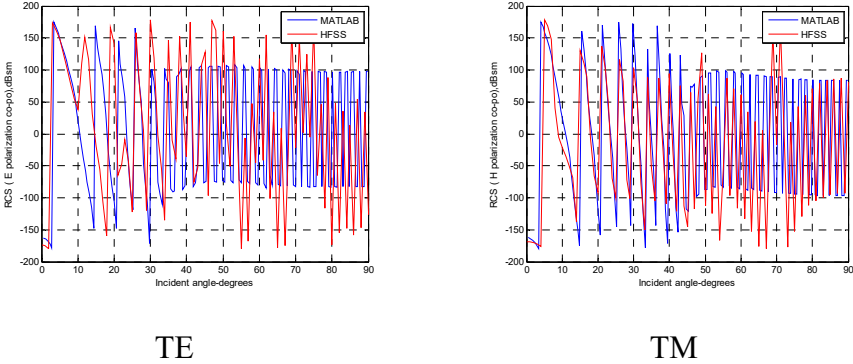


Figure 4.72: Phase comparison for TE and TM mode in MATLAB and HFSS (3.3 (~30 λ) meters in length by 0.033 (~0.3 λ) meters in radius at $\epsilon_r = 2.15$ for a dielectric cylinder with endcap). The phase is in good agreement with HFSS for both TE and TM.

For a dielectric cylinder at $\epsilon_r = 10-5j$ without endcap:

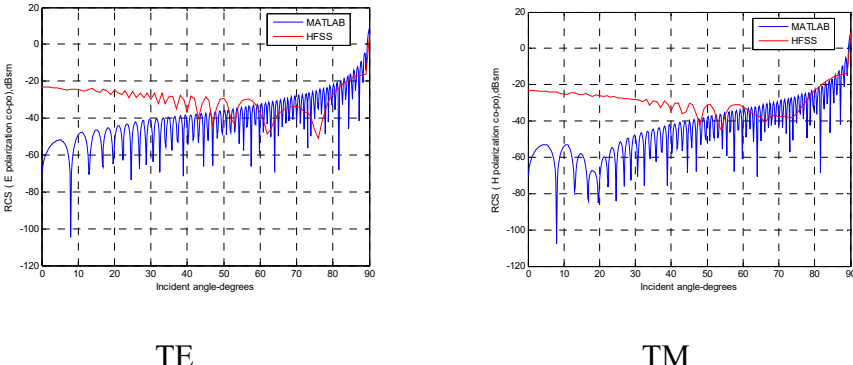


Figure 4.73: Amplitude comparison for TE and TM mode in MATLAB and HFSS (3.3 ($\sim 30 \lambda$) meters in length by 0.033 ($\sim 0.3 \lambda$) meters in radius at $\epsilon_r = 10-5j$ for a dielectric cylinder without endcap). Big gaps are observed at 0° for both TE and TM.

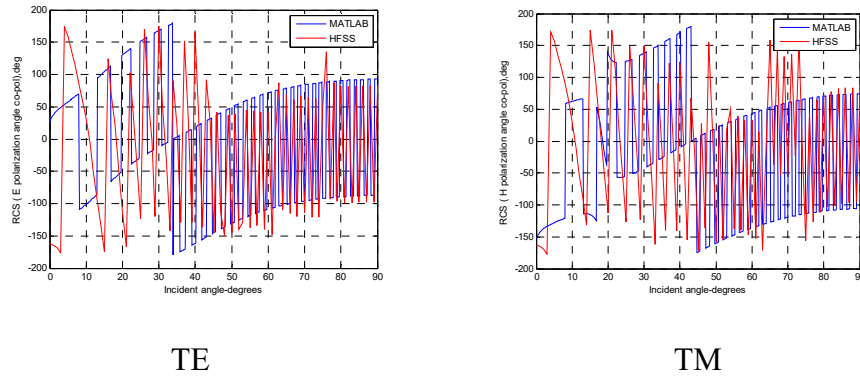


Figure 4.74: Phase comparison for TE and TM mode in MATLAB and HFSS (3.3 ($\sim 30 \lambda$) meters in length by 0.033 ($\sim 0.3 \lambda$) meters in radius at $\epsilon_r = 10-5j$ for a dielectric cylinder without endcap). The phase shows mismatch for both TE and TM.

For the same size dielectric cylinder at $\epsilon_r = 10-5j$ with endcap:

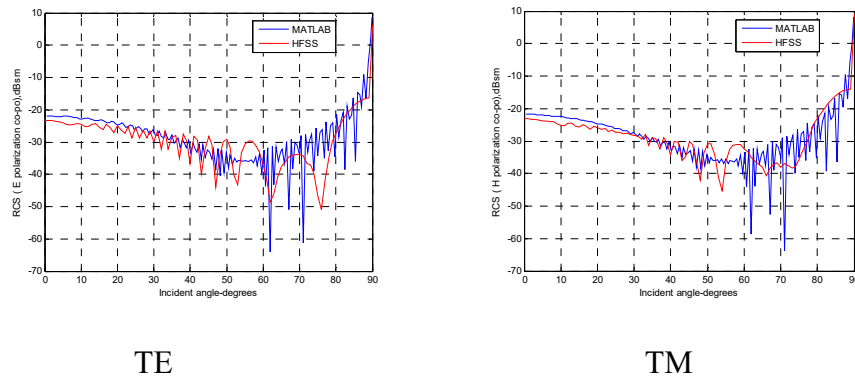


Figure 4.75: Amplitude comparison for TE and TM mode in MATLAB and HFSS (3.3 ($\sim 30 \lambda$) meters in length by 0.033 ($\sim 0.3 \lambda$) meters in radius at $\epsilon_r = 10-5j$ for a dielectric cylinder with endcap). Amplitudes have a very few dB difference at 0° for both TE and TM.

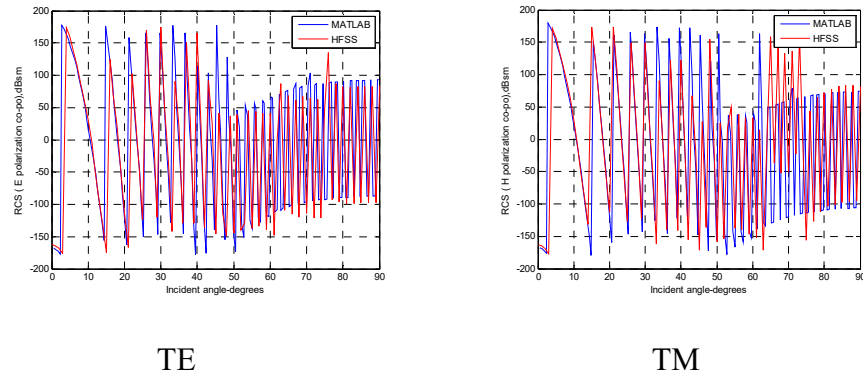


Figure 4.76: Phase comparison for TE and TM mode in MATLAB and HFSS (3.3 ($\sim 30 \lambda$) meters in length by 0.033 ($\sim 0.3 \lambda$) meters in radius at $\epsilon_r = 10-5j$ for a dielectric cylinder with endcap). The phase is in good agreement with HFSS for both TE and TM.

For a dielectric cylinder at $\epsilon_r = 2.15$ without endcap:

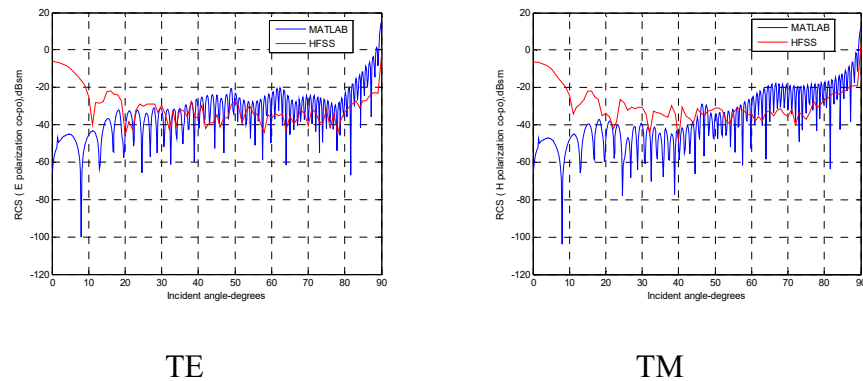


Figure 4.77: Amplitude comparison for TE and TM mode in MATLAB and HFSS (3.3 (~30 λ) meters in length by 0.165 (~1.5 λ) meters in radius at $\epsilon_r = 2.15$ for a dielectric cylinder without endcap). Big gaps are observed at 0° for both TE and TM.

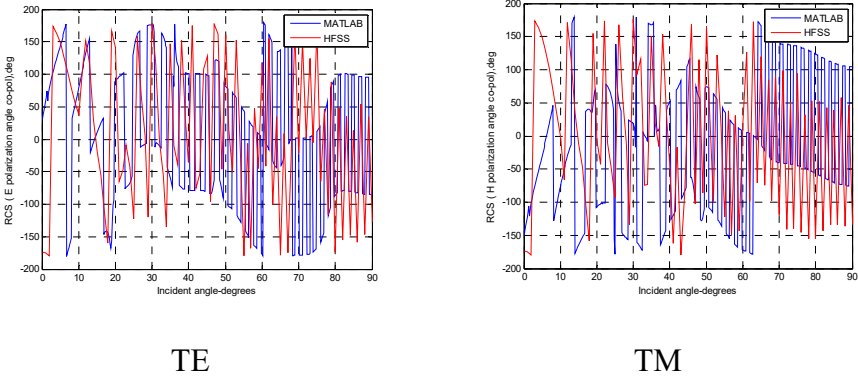


Figure 4.78: Phase comparison for TE and TM mode in MATLAB and HFSS (3.3 (~30 λ) meters in length by 0.165 (~1.5 λ) meters in radius at $\epsilon_r = 2.15$ for a dielectric cylinder without endcap). The phase shows mismatch for both TE and TM.

For the same size dielectric cylinder at $\epsilon_r = 2.15$ with endcap:

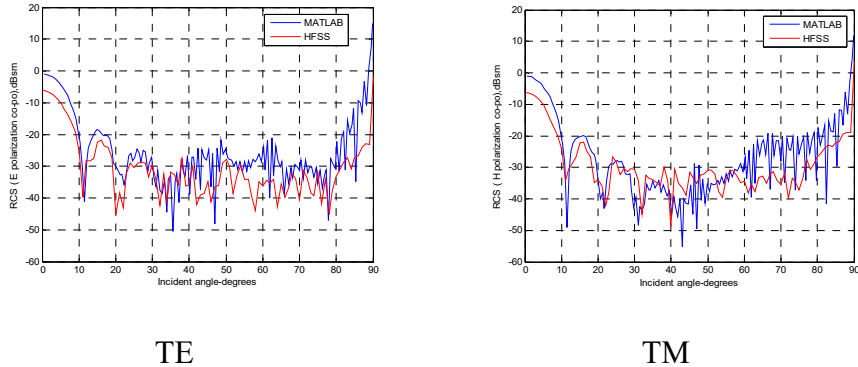


Figure 4.79: Amplitude comparison for TE and TM mode in MATLAB and HFSS (3.3 (~30 λ) meters in length by 0.165 (~1.5 λ) meters in radius at $\epsilon_r = 2.15$ for a dielectric cylinder with endcap). Amplitudes show differences of less than 10 dB at 0° for both TE and TM.

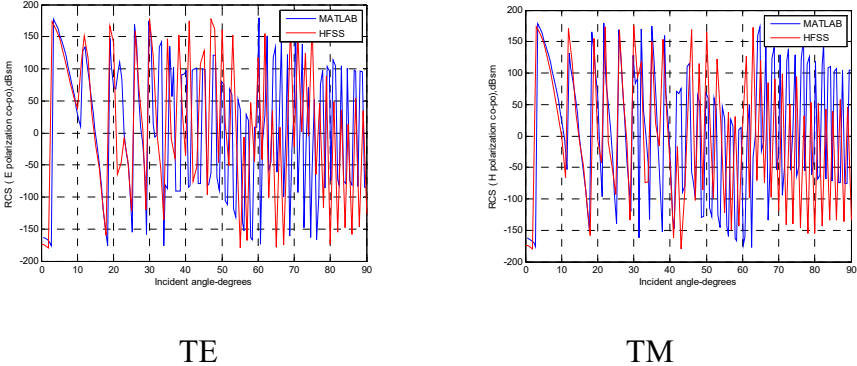


Figure 4.80: Phase comparison for TE and TM mode in MATLAB and HFSS (3.3 (~30 λ) meters in length by 0.165 (~1.5 λ) meters in radius at $\epsilon_r = 2.15$ for a dielectric cylinder with endcap). The phase is in good agreement with HFSS for both TE and TM.

For a dielectric cylinder at $\epsilon_r = 10-5j$ without endcap:

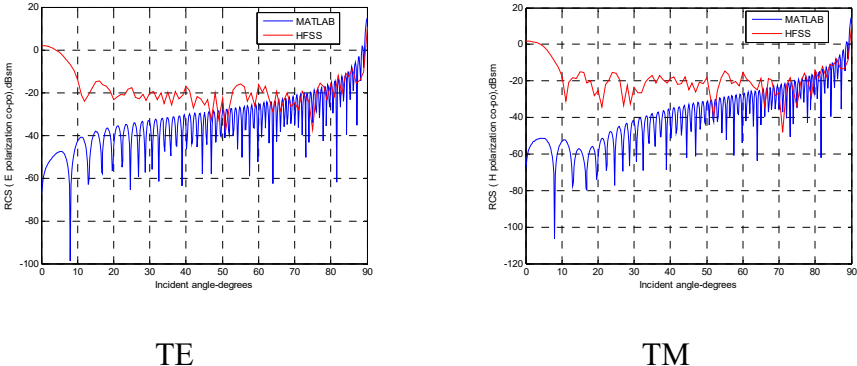


Figure 4.81: Amplitude comparison for TE and TM mode in MATLAB and HFSS (3.3 ($\sim 30 \lambda$) meters in length by 0.165 ($\sim 1.5 \lambda$) meters in radius at $\epsilon_r = 10-5j$ for a dielectric cylinder without endcap). Big gaps are observed at 0° for both TE and TM.

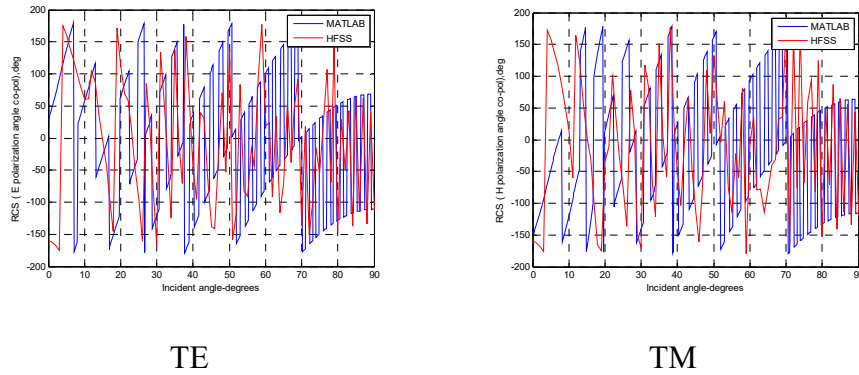


Figure 4.82: Phase comparison for TE and TM mode in MATLAB and HFSS (3.3 ($\sim 30 \lambda$) meters in length by 0.165 ($\sim 1.5 \lambda$) meters in radius at $\epsilon_r = 10-5j$ for a dielectric cylinder without endcap). The phase shows mismatch for both TE and TM.

For the same size dielectric cylinder at $\epsilon_r = 10-5j$ with endcap:

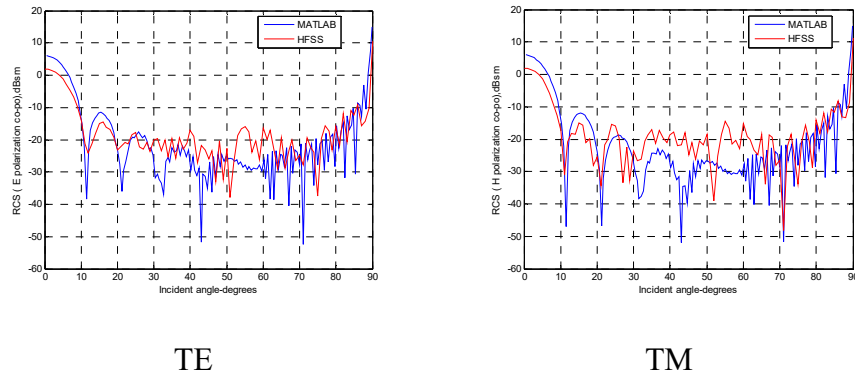


Figure 4.83: Amplitude comparison for TE and TM mode in MATLAB and HFSS (3.3 ($\sim 30 \lambda$) meters in length by 0.165 ($\sim 1.5 \lambda$) meters in radius at $\epsilon_r = 10-5j$ for a dielectric cylinder with endcap). Amplitudes have differences of less than 5 dB at 0° for both TE and TM.

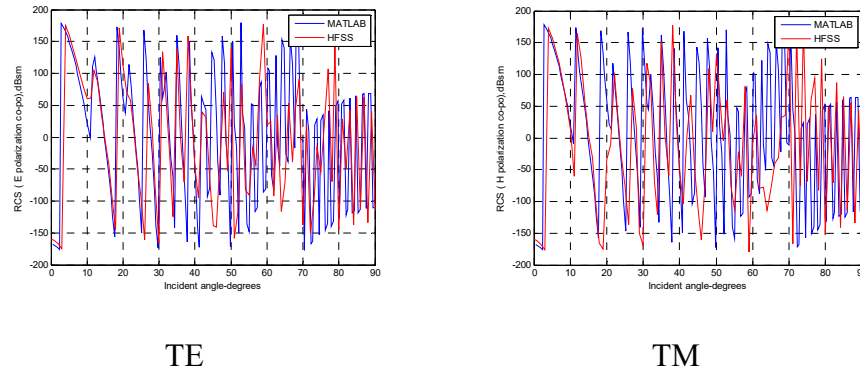


Figure 4.84: Phase comparison for TE and TM mode in MATLAB and HFSS (3.3 ($\sim 30 \lambda$) meters in length by 0.165 ($\sim 1.5 \lambda$) meters in radius at $\epsilon_r = 10-5j$ for a dielectric cylinder with endcap). The phase is in good agreement with HFSS for both TE and TM.

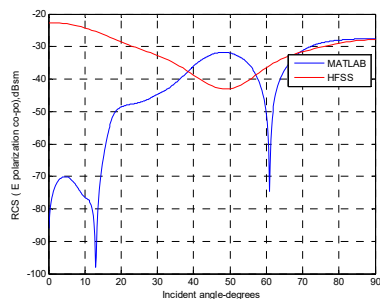
4.5 Short and fat dielectric cylinders

The relatively short and fat cylinders are 0.11 ($\sim 1 \lambda$) meters in length by 0.055 ($\sim 0.5 \lambda$) meters in radius; 0.1 ($\sim 1 \lambda$) meters in length by 0.11 ($\sim 1 \lambda$) meters in radius; 0.1 ($\sim 1 \lambda$) meters in length by 0.33 ($\sim 3 \lambda$) meters in radius. The discussion begins with small dimensions and moves to larger dimensions at different relative permittivity, as shown below.

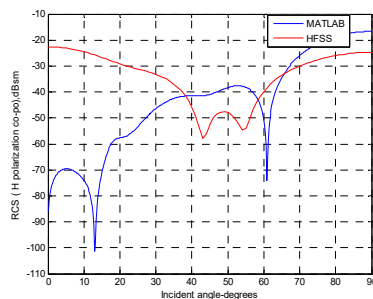
4.5.1 Analytical vs. simulated results with and without endcaps

Thickness is the same as diameter in a dielectric cylinder with radius = 0.5

λ at $\epsilon_r = 2.15$ without endcap:

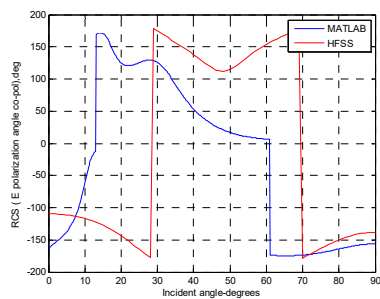


TE

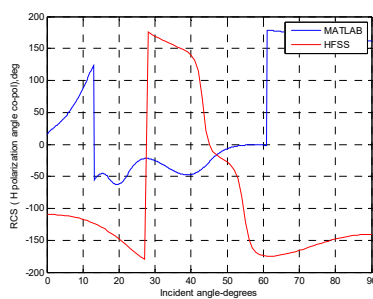


TM

Figure 4.85: Amplitude comparison for TE and TM mode in MATLAB and HFSS (0.11 (~1 λ) meters in length by 0.055 (~0.5 λ) meters in radius at $\epsilon_r = 2.15$ for a dielectric cylinder without endcap). Big gaps are observed at 0° for both TE and TM.



TE



TM

Figure 4.86: Phase comparison for TE and TM mode in MATLAB and HFSS (0.11 (~1 λ) meters in length by 0.055 (~0.5 λ) meters in radius at

$\epsilon_r = 2.15$ for a dielectric cylinder without endcap). The phase shows mismatch for both TE and TM.

For the same size dielectric cylinder with radius = 0.5λ at $\epsilon_r = 2.15$ with endcap:

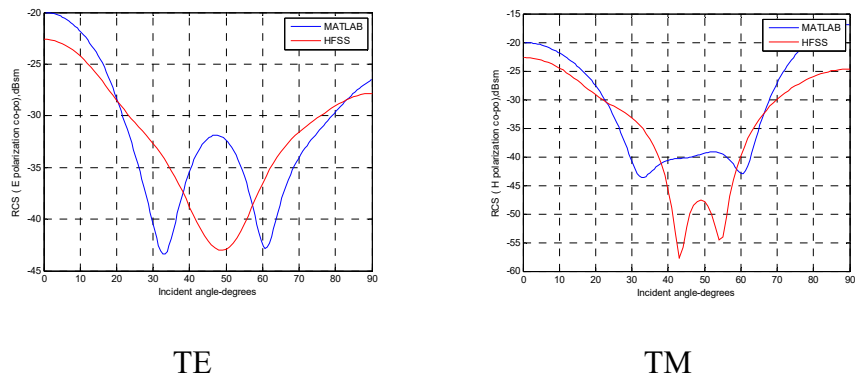


Figure 4.87: Amplitude comparison for TE and TM mode in MATLAB and HFSS (0.11 ($\sim 1 \lambda$) meters in length by 0.055 ($\sim 0.5 \lambda$) meters in radius at $\epsilon_r = 2.15$ for a dielectric cylinder with endcap). Amplitudes have a few dB differences for both TE and TM.

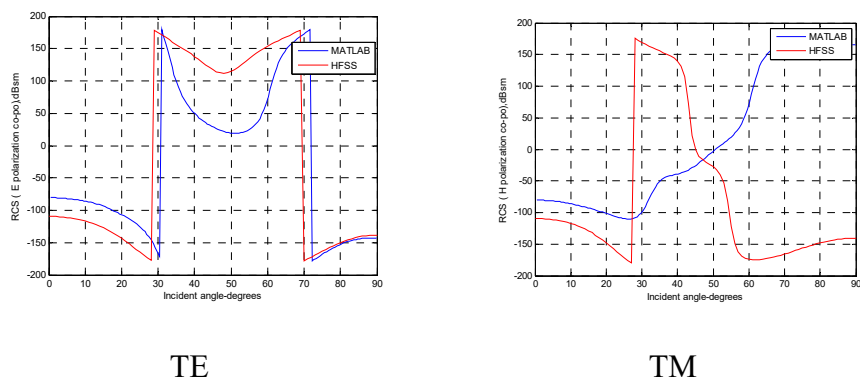
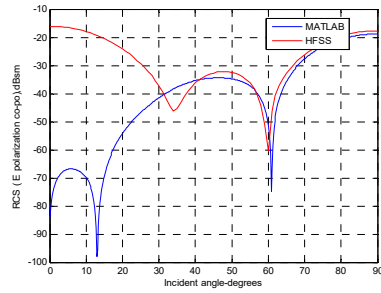


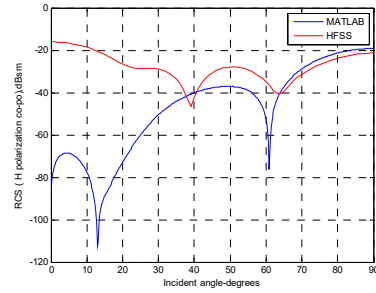
Figure 4.88: Phase comparison for TE and TM mode in MATLAB and HFSS (0.11 ($\sim 1\lambda$) meters in length by 0.055 ($\sim 0.5 \lambda$) meters in radius at ϵ_r ,

= 2.15 for a dielectric cylinder with endcap). The phase matches closely for both TE and TM.

For a dielectric cylinder with radius = 0.5λ at $\epsilon_r = 10-5j$ without endcap:

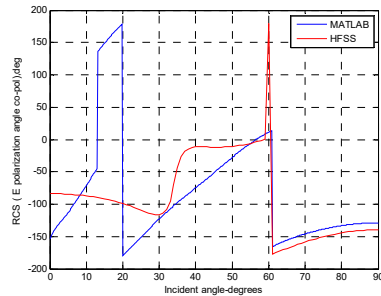


TE

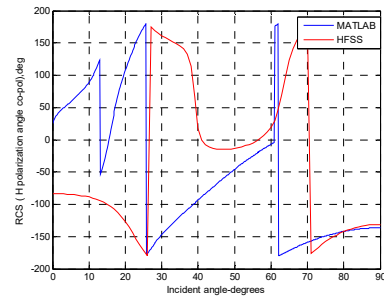


TM

Figure 4.89: Amplitude comparison for TE and TM mode in MATLAB and HFSS (0.11 ($\sim 1 \lambda$) meters in length by 0.055 ($\sim 0.5 \lambda$) meters in radius at $\epsilon_r = 10-5j$ for a dielectric cylinder without endcap). Amplitudes show big gaps at 0° for both TE and TM.



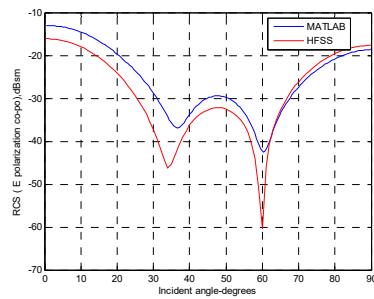
TE



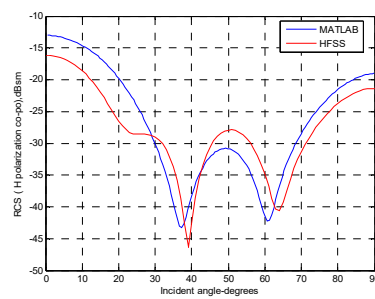
TM

Figure 4.90: Phase comparison for TE and TM mode in MATLAB and HFSS (0.11 (~1 λ) meters in length by 0.055 (~0.5 λ) meters in radius at $\epsilon_r = 10-5j$ for a dielectric cylinder without endcap). The phase shows mismatch for both TE and TM.

For the same size dielectric cylinder with radius = 0.5 λ at $\epsilon_r = 10-5j$ with endcap:

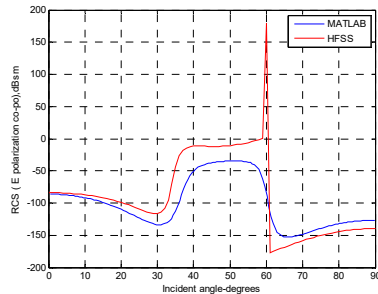


TE

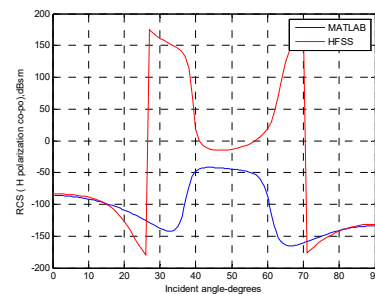


TM

Figure 4.91: Amplitude comparison for TE and TM mode in MATLAB and HFSS (0.11 (~1 λ) meters in length by 0.055 (~0.5 λ) meters in radius at $\epsilon_r = 10-5j$ for a dielectric cylinder with endcap). Amplitudes show a few dB differences for both TE and TM.



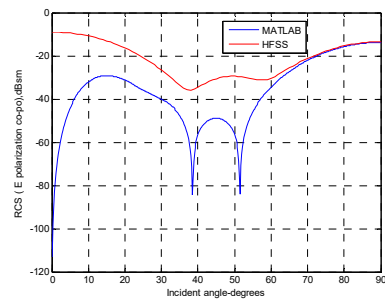
TE



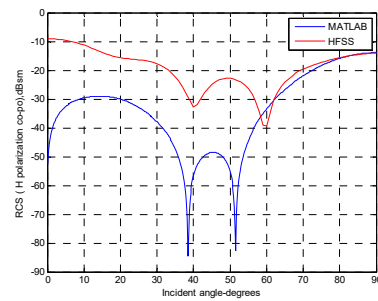
TM

Figure 4.92: Phase comparison for TE and TM mode in MATLAB and HFSS (0.11 (~1 λ) meters in length by 0.055 (~0.5 λ) meters in radius at $\epsilon_r = 10-5j$ for a dielectric cylinder with endcap). The phase matches closely for both TE and TM.

For the same size metal cylinder with radius = 0.5 λ at $\epsilon_r = 10^6$ without endcap:

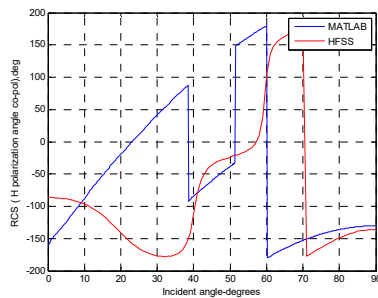
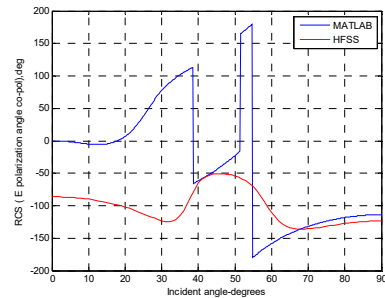


TE



TM

Figure 4.93: Amplitude comparison for TE and TM mode in MATLAB and HFSS (0.11 (~1 λ) meters in length by 0.055 (~0.5 λ) meters in radius at $\epsilon_r = 10^6$ for a metal cylinder without endcap). Big gaps are observed at 0° for both TE and TM.

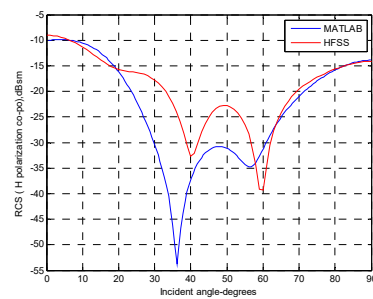
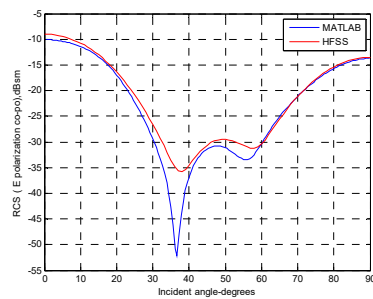


TE

TM

Figure 4.94: Phase comparison for TE and TM mode in MATLAB and HFSS (0.11 (~1 λ) meters in length by 0.055 (~0.5 λ) meters in radius at $\epsilon_r = 10^6$ for a metal cylinder without endcap). The phase shows mismatch for both TE and TM.

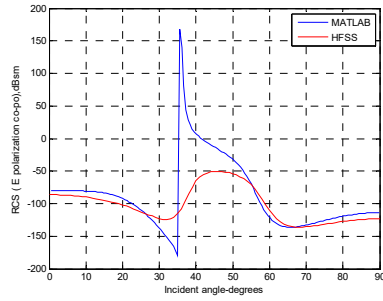
For the same size metal cylinder with radius = 0.5 λ at $\epsilon_r = 10^6$ with endcap:



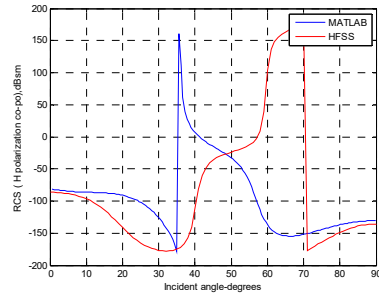
TE

TM

Figure 4.95: Amplitude comparison for TE and TM mode in MATLAB and HFSS (0.11 (~1 λ) meters in length by 0.055 (~0.5 λ) meters in radius at $\epsilon_r = 10^6$ for a metal cylinder with endcap). Amplitudes match well at 0° and 90°.



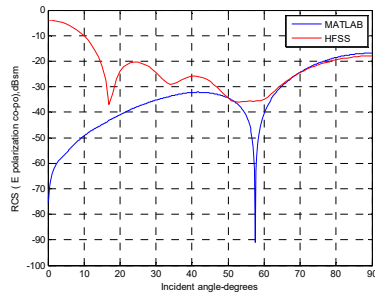
TE



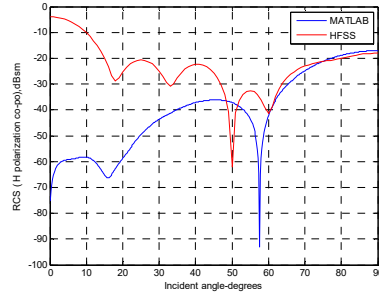
TM

Figure 4.96: Phase comparison for TE and TM mode in MATLAB and HFSS (0.11 ($\sim 1 \lambda$) meters in length by 0.055 ($\sim 0.5 \lambda$) meters in radius at $\epsilon_r = 10^6$ for a metal cylinder with endcap). The phase matches closely for both TE and TM.

For a dielectric cylinder with a diameter two times bigger than the thickness with radius = 0.11 ($\sim 1 \lambda$) meters at $\epsilon_r = 10-5j$ without endcap:



TE



TM

Figure 4.97: Amplitude comparison for TE and TM mode in MATLAB and HFSS (0.1 ($\sim 1 \lambda$) meters in length by 0.11 ($\sim 1 \lambda$) meters in radius at

$\epsilon_r = 10-5j$ for a dielectric cylinder without endcap). Big gaps are observed at 0° for both TE and TM.

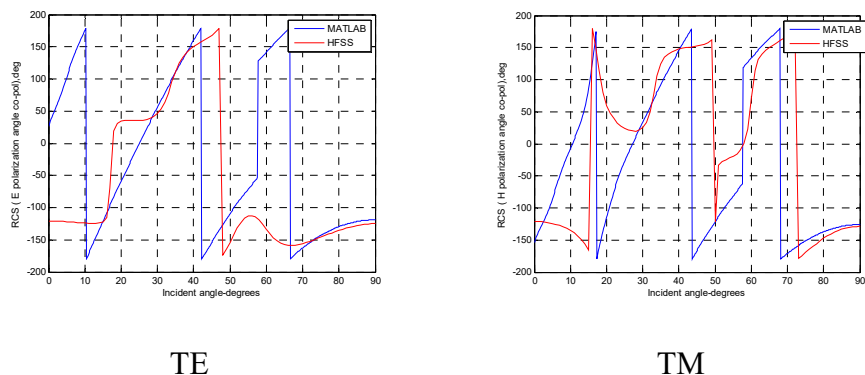


Figure 4.98: Phase comparison for TE and TM mode in MATLAB and HFSS (0.1 ($\sim 1 \lambda$) meters in length by 0.11 ($\sim 1 \lambda$) meters in radius at $\epsilon_r = 10-5j$ for a dielectric cylinder without endcap). The phase shows a gap at 0° for TE, and matches closely for TM.

For a dielectric cylinder with a diameter two times bigger than the thickness with radius = 0.11 ($\sim 1 \lambda$) meters at $\epsilon_r = 10-5j$ with endcap:

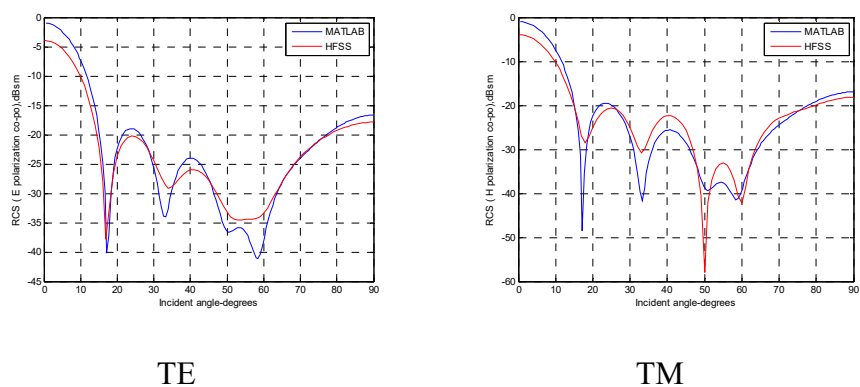
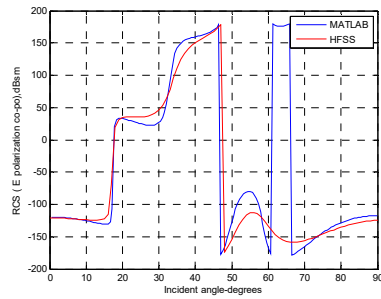
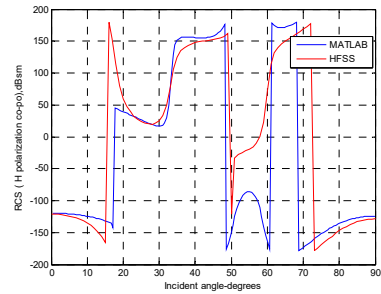


Figure 4.99: Amplitude comparison for TE and TM mode in MATLAB and HFSS (0.1 ($\sim 1 \lambda$) meters in length by 0.11 ($\sim 1 \lambda$) meters in radius at $\epsilon_r = 10-5j$ with endcap).

$\epsilon_r = 10-5j$ for a dielectric cylinder with endcap). Amplitudes match closely for both TE and TM.



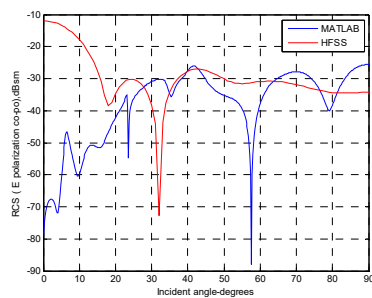
TE



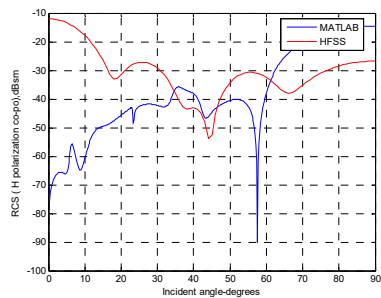
TM

Figure 4.100: Phase comparison for TE and TM mode in MATLAB and HFSS (0.1 ($\sim 1 \lambda$) meters in length by 0.11 ($\sim 1 \lambda$) meters in radius at $\epsilon_r = 10-5j$ for a dielectric cylinder with endcap). The phase matches closely for both TE and TM.

For a dielectric cylinder with a diameter two times bigger than the thickness with radius = 0.11 ($\sim 1 \lambda$) meters at $\epsilon_r = 2.15$ without endcap:



TE



TM

Figure 4.101: Amplitude comparison for TE and TM mode in MATLAB and HFSS (0.1 ($\sim 1 \lambda$) meters in length by 0.11 ($\sim 1 \lambda$) meters in radius at $\epsilon_r = 2.15$ for a dielectric cylinder without endcap). Big gaps are observed at 0° for both TE and TM.

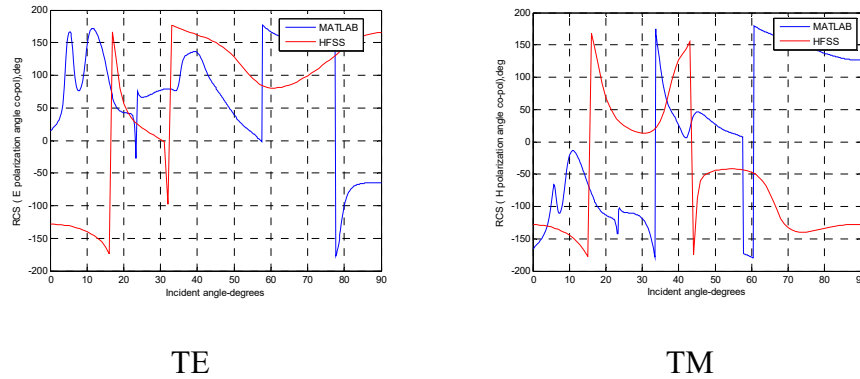


Figure 4.102: Phase comparison for TE and TM mode in MATLAB and HFSS (0.1 ($\sim 1 \lambda$) meters in length by 0.11 ($\sim 1 \lambda$) meters in radius at $\epsilon_r = 2.15$ for a dielectric cylinder without endcap). Big gaps are observed at 0° and 90° for both TE and TM.

For a dielectric cylinder with a diameter two times bigger than the thickness with radius = 0.11 ($\sim 1 \lambda$) meters at $\epsilon_r = 2.15$ with endcap:

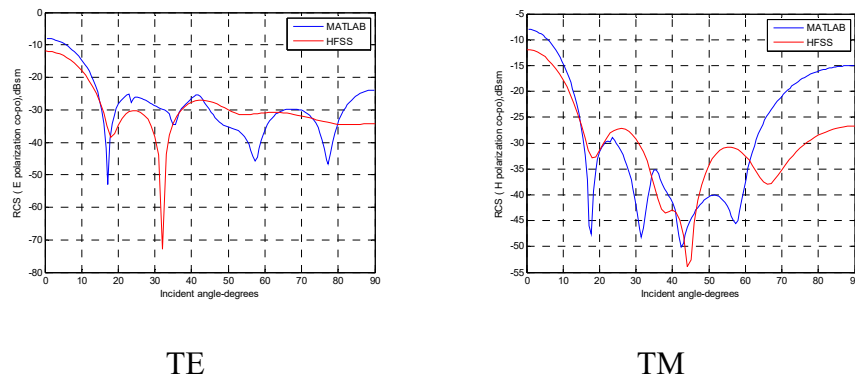


Figure 4.103: Amplitude comparison for TE and TM mode in MATLAB and HFSS (0.1 ($\sim 1 \lambda$) meters in length by 0.11 ($\sim 1 \lambda$) meters in radius at $\epsilon_r = 2.15$ for a dielectric cylinder with endcap). Gaps appear at 90° for both TE and TM.

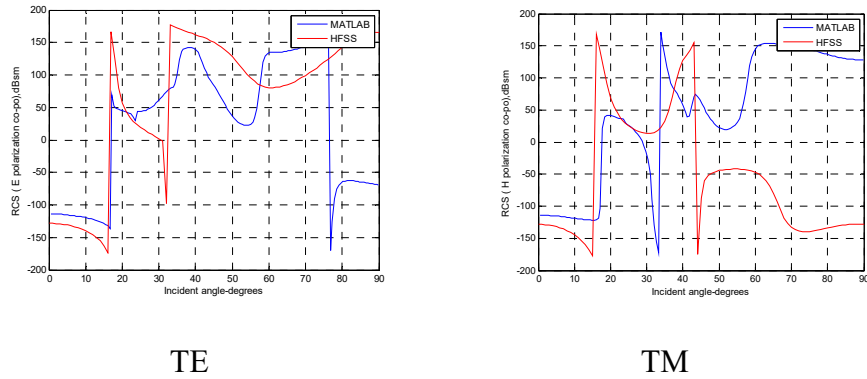


Figure 4.104: Phase comparison for TE and TM mode in MATLAB and HFSS (0.1 ($\sim 1 \lambda$) meters in length by 0.11 ($\sim 1 \lambda$) meters in radius at $\epsilon_r = 2.15$ for a dielectric cylinder with endcap). Gaps appear at 90° for both TE and TM.

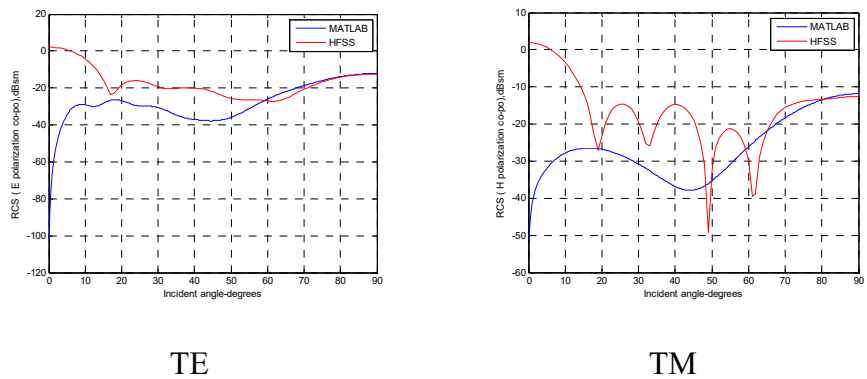


Figure 4.105: Amplitude comparison for TE and TM mode in MATLAB and HFSS (0.1 ($\sim 1 \lambda$) meters in length by 0.11 ($\sim 1 \lambda$) meters in radius at

$\epsilon_r = 10^6$ for a metal cylinder without endcap). Big gaps are observed at 0° for both TE and TM.

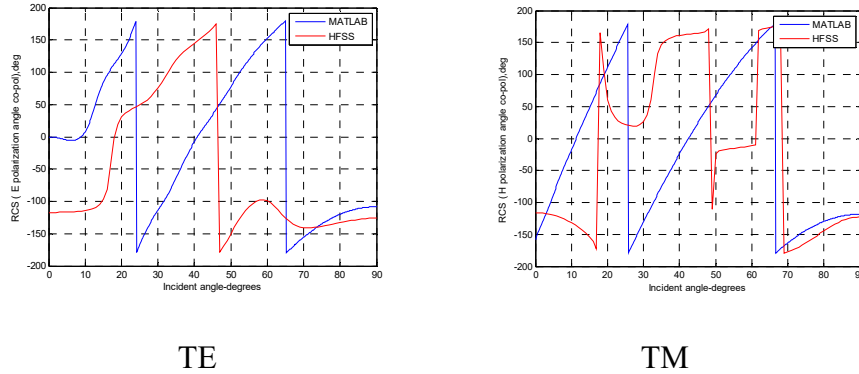


Figure 4.106: Phase comparison for TE and TM mode in MATLAB and HFSS (0.1 ($\sim 1 \lambda$) meters in length by 0.11 ($\sim 1 \lambda$) meters in radius at $\epsilon_r = 10^6$ for a metal cylinder without endcap). Big gaps are observed at 0° for both TE and TM.

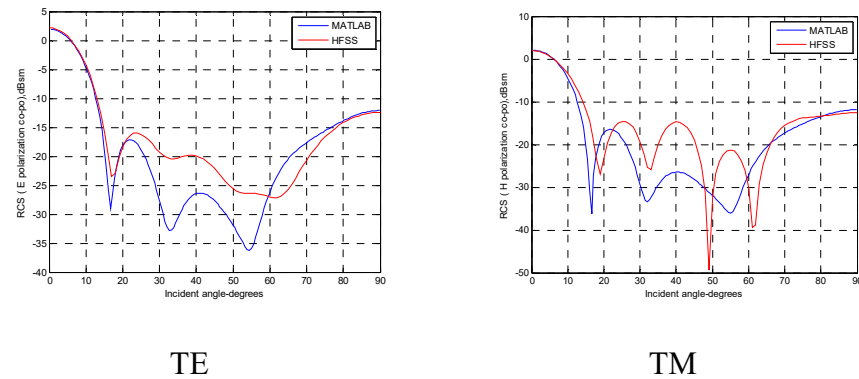
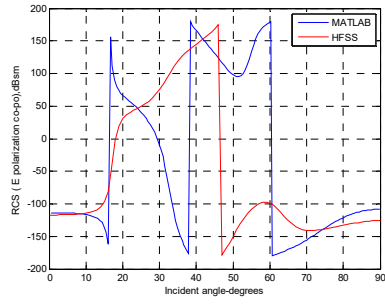
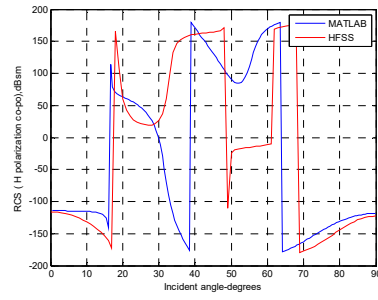


Figure 4.107: Amplitude comparison for TE and TM mode in MATLAB and HFSS (0.1 ($\sim 1 \lambda$) meters in length by 0.11 ($\sim 1 \lambda$) meters in radius at $\epsilon_r = 10^6$ for a metal cylinder with endcap). Big gaps are observed at 0° for both TE and TM.



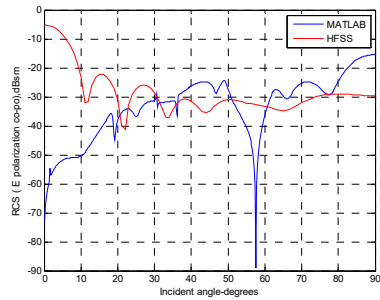
TE



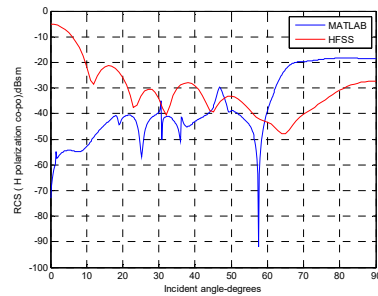
TM

Figure 4.108: Phase comparison for TE and TM mode in MATLAB and HFSS (0.1 ($\sim 1 \lambda$) meters in length by 0.11 ($\sim 1 \lambda$) meters in radius at $\epsilon_r = 10^6$ for a metal cylinder with endcap). Big gaps are observed at 0° for both TE and TM.

For a dielectric cylinder with radius = 1.5λ at $\epsilon_r = 2.15$ without endcap:

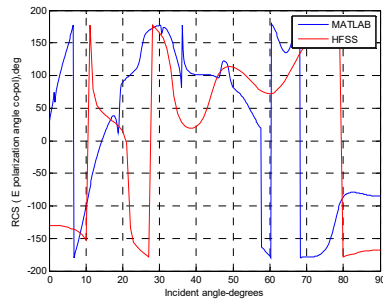


TE

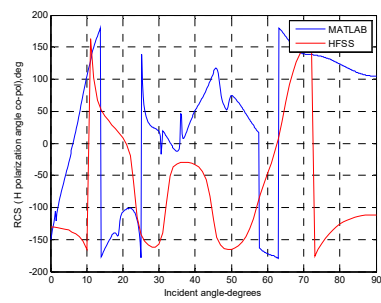


TM

Figure 4.109: Amplitude comparison for TE and TM mode in MATLAB and HFSS (0.1 ($\sim 1 \lambda$) meters in length by 0.165 ($\sim 1.5 \lambda$) meters in radius at $\epsilon_r = 2.15$ for a dielectric cylinder without endcap). Amplitudes show large gaps for both TE and TM.



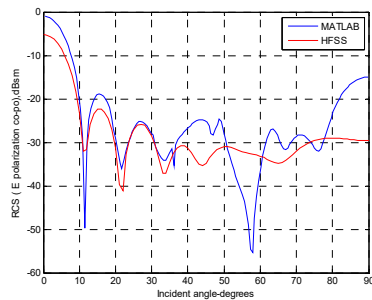
TE



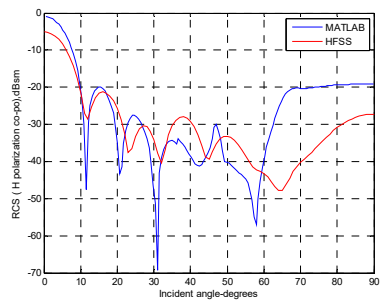
TM

Figure 4.110: Phase comparison for TE and TM mode in MATLAB and HFSS (0.1 ($\sim 1 \lambda$) meters in length by 0.165 ($\sim 1.5 \lambda$) meters in radius at $\epsilon_r = 2.15$ for a dielectric cylinder without endcap). The phase shows a big gap for both TE and TM.

For a dielectric cylinder with radius = 1.5λ at $\epsilon_r = 2.15$ with endcap:

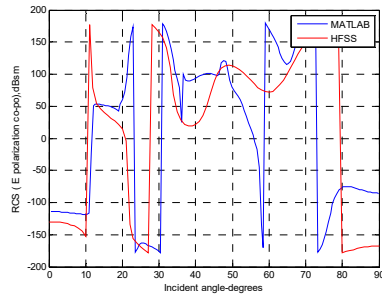


TE

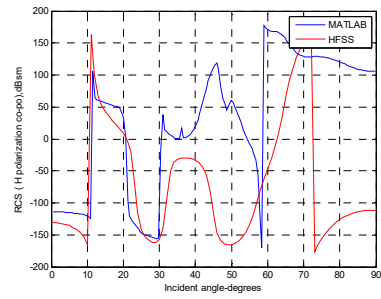


TM

Figure 4.111: Amplitude comparison for TE and TM mode in MATLAB and HFSS (0.1 ($\sim 1 \lambda$) meters in length by 0.165 ($\sim 1.5 \lambda$) meters in radius at $\epsilon_r = 2.15$ for a dielectric cylinder with endcap). Amplitudes have a few dB differences at 0° for both TE and TM.



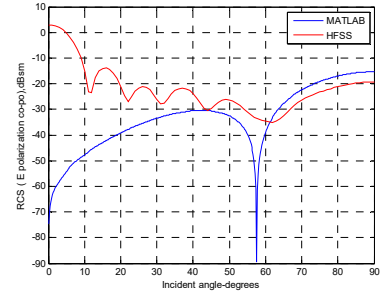
TE



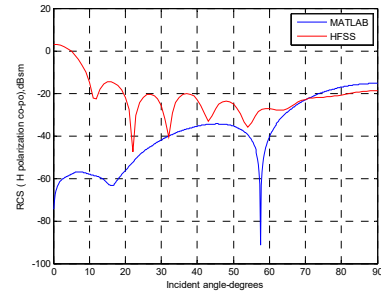
TM

Figure 4.112: Phase comparison for TE and TM mode in MATLAB and HFSS (0.1 (~1 λ) meters in length by 0.165 (~1.5 λ) meters in radius at $\epsilon_r = 2.15$ for a dielectric cylinder with endcap). The phase matches closely at 0° for both TE and TM.

For a dielectric cylinder with radius = 1.5 λ at $\epsilon_r = 10-5j$ without endcap:

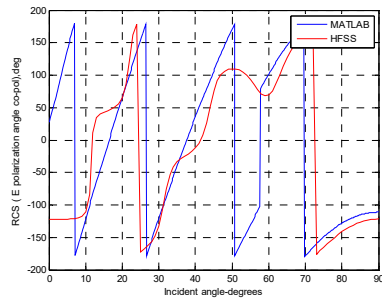


TE

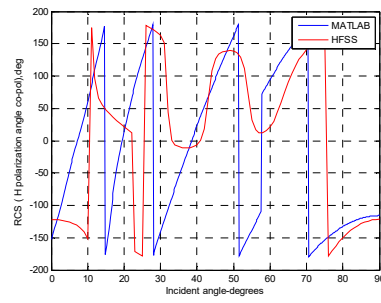


TM

Figure 4.113: Amplitude comparison for TE and TM mode in MATLAB and HFSS (0.1 (~1 λ) meters in length by 0.165 (~1.5 λ) meters in radius at $\epsilon_r = 10-5j$ for a dielectric cylinder without endcap). Amplitudes show big gaps at 0° for both TE and TM.



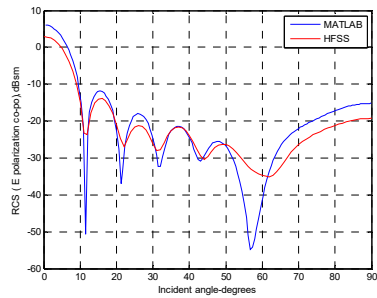
TE



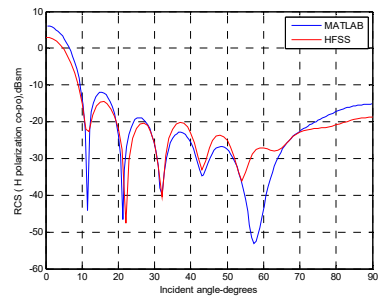
TM

Figure 4.114: Phase comparison for TE and TM mode in MATLAB and HFSS (0.1 ($\sim 1 \lambda$) meters in length by 0.165 ($\sim 1.5 \lambda$) meters in radius at $\epsilon_r = 10 - 5j$ for a dielectric cylinder without endcap). The phase shows a big gap at 0° for both TE and TM.

For a dielectric cylinder with radius = 1.5λ at $\epsilon_r = 10 - 5j$ with endcap:

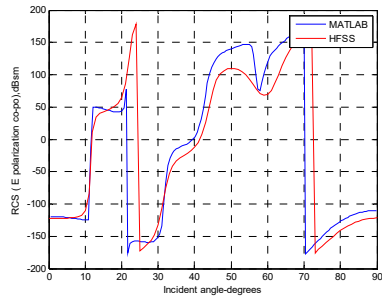


TE

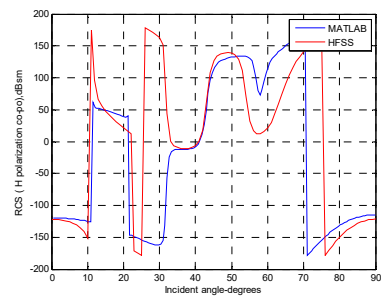


TM

Figure 4.115: Amplitude comparison for TE and TM mode in MATLAB and HFSS (0.1 ($\sim 1 \lambda$) meters in length by 0.165 ($\sim 1.5 \lambda$) meters in radius at $\epsilon_r = 10 - 5j$ for a dielectric cylinder with endcap). Amplitudes are in good agreement with HFSS for both TE and TM.



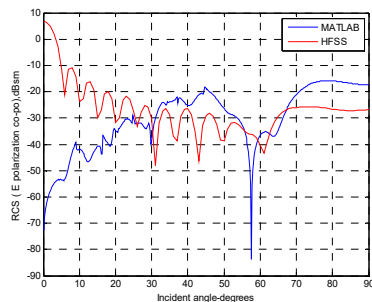
TE



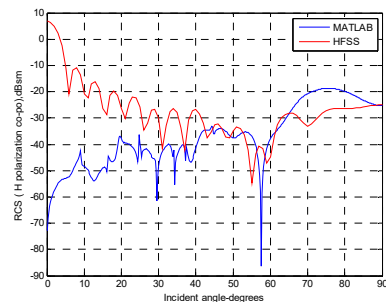
TM

Figure 4.116: Phase comparison for TE and TM mode in MATLAB and HFSS (0.1 ($\sim 1 \lambda$) meters in length by 0.165 ($\sim 1.5 \lambda$) meters in radius at $\epsilon_r = 10 - 5j$ for a dielectric cylinder with endcap). The phase is in good agreement with HFSS for both TE and TM.

For a dielectric cylinder with radius = 3λ at $\epsilon_r = 2.15$ without endcap:

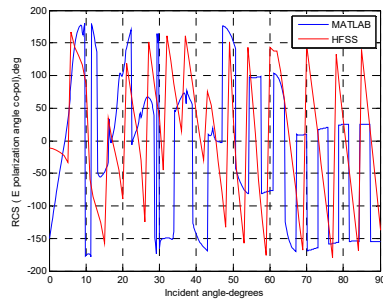


TE

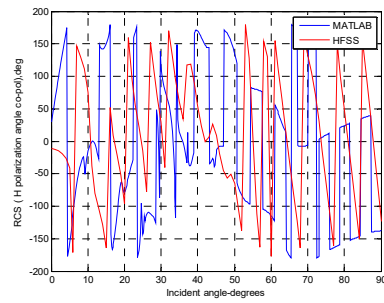


TM

Figure 4.117: Amplitude comparison for TE and TM mode in MATLAB and HFSS (0.1 ($\sim 1 \lambda$) meters in length by 0.33 ($\sim 3 \lambda$) meters in radius at $\epsilon_r = 2.15$ for a dielectric cylinder without endcap). Big gaps are observed at 0° for both TE and TM.



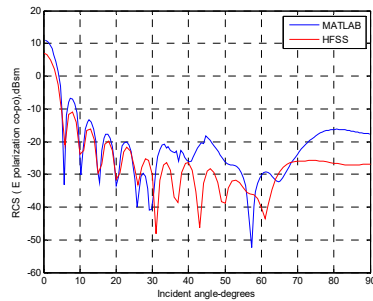
TE



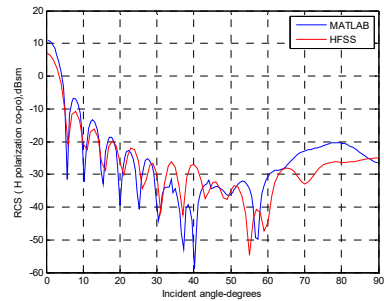
TM

Figure 4.118: Phase comparison for TE and TM mode in MATLAB and HFSS (0.1 ($\sim 1 \lambda$) meters in length by 0.33 ($\sim 3 \lambda$) meters in radius at $\epsilon_r = 2.15$ for a dielectric cylinder without endcap). The phase shows mismatch for both TE and TM.

For the same size dielectric cylinder with radius = 3λ at $\epsilon_r = 2.15$ with endcap:



TE



TM

Figure 4.119: Amplitude comparison for TE and TM mode in MATLAB and HFSS (0.1 ($\sim 1 \lambda$) meters in length by 0.33 ($\sim 3 \lambda$) meters in radius at

$\epsilon_r = 2.15$ for a dielectric cylinder with endcap). Amplitudes have a few dB differences at 0° for both TE and TM.

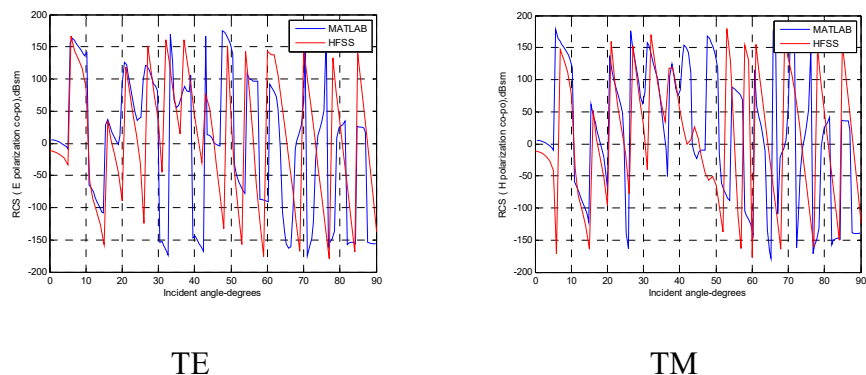


Figure 4.120: Phase comparison for TE and TM mode in MATLAB and HFSS (0.1 ($\sim 1 \lambda$) meters in length by 0.33 ($\sim 3 \lambda$) meters in radius at $\epsilon_r = 2.15$ for a dielectric cylinder with endcap). The phase is in good agreement with HFSS for both TE and TM.

4.5.2 Comparing short cylinders to thin sheet results

Thin sheets measuring 0.00011 ($\sim 0.001 \lambda$) meters in depth by 0.055 ($\sim 0.5 \lambda$) meters in radius have a thickness that is 1000 times smaller than the thickness of a short dielectric cylinder measuring 0.11 meters by 0.055 meters. The length of the same dielectric cylinder is also 2 times bigger than the radius at $\epsilon_r = 10 - 5j$. when comparing the two, amplitude of a thin sheet (Figure 3.41) is lower than a short dielectric cylinder by about 25 dB for both TE and TM, as shown in Figure 4.121; and amplitude for a thin sheet (Figure 3.39) is lower than a short dielectric cylinder by about 40 dB

at $\epsilon_r = 2.15$ for both TE and TM, as shown in Figure 4.122. Amplitude for a metal thin sheet (Figure 3.9) overlaps at 0° with a metal cylinder, but has a gap with a metal cylinder at 90° , as shown in Figure 4.123.

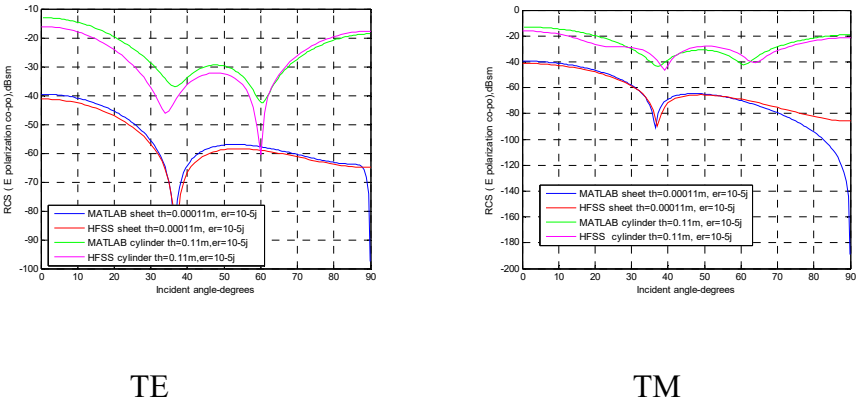


Figure 4.121: Amplitude comparison for TE and TM mode in MATLAB and HFSS (0.11 (~1 λ) meters in length by 0.055 (~0.5 λ) meters in radius at $\epsilon_r = 10-5j$ for a dielectric cylinder with endcap in comparison to a sheet 0.00011 (~0.001 λ) meters in thickness by 0.055 (~0.5 λ) meters in radius). Amplitude shows 25 dB differences for both TE and TM.

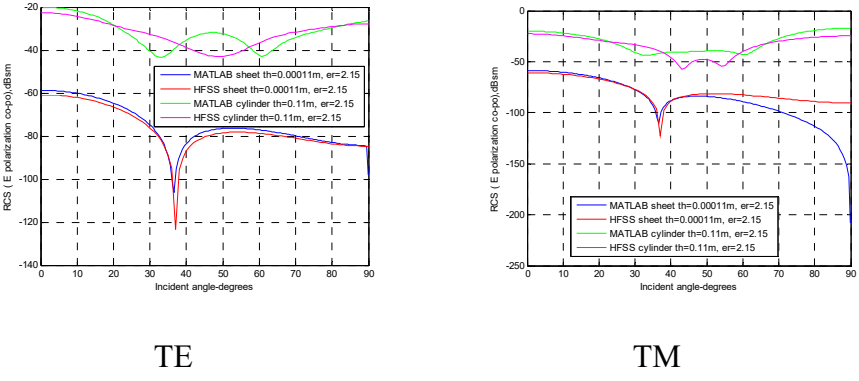


Figure 4.122: Amplitude comparison for TE and TM mode in MATLAB and HFSS (0.11 ($\sim 1 \lambda$) meters in length by 0.055 ($\sim 0.5 \lambda$) meters in radius at $\epsilon_r = 2.15$ for a dielectric cylinder with endcap in comparison to a sheet 0.00011 ($\sim 0.001 \lambda$) meters in thickness by 0.055 ($\sim 0.5 \lambda$) meters in radius). Amplitudes show 40 dB differences for both TE and TM.

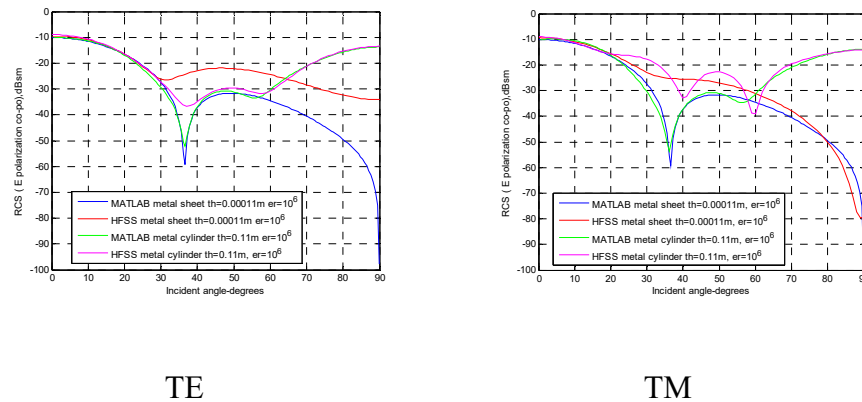


Figure 4.123: Amplitude comparison for TE and TM mode in MATLAB and HFSS (0.11 ($\sim 1 \lambda$) meters in length by 0.055 ($\sim 0.5 \lambda$) meters in radius at $\epsilon_r = 10^6$ for a metal cylinder with endcap in comparison to a sheet 0.00011 ($\sim 0.001 \lambda$) meters in thickness by 0.055 ($\sim 0.5 \lambda$) meters in radius). Amplitudes for a metal thin sheet overlap with a metal cylinder at 0° , but have a gap with a metal cylinder at 90° for both TE and TM.

A thin sheet that measures 0.0001 ($\sim 0.001 \lambda$) meters in depth by 0.11 ($\sim 1 \lambda$) meters in radius is 1000 times smaller in thickness when compared to a short dielectric cylinder that measures 0.1 ($\sim 1 \lambda$) meters in thickness by 0.11 ($\sim 1 \lambda$) meters in radius with a length that is the same as radius at

$\epsilon_r = 10^{-5}j$. When comparing the two, the amplitude of a thin sheet (Figure 3.43) is lower by about 30 dB for TE and TM when compared to a short cylinder, as shown in Figure 4.124; and amplitude for a thin sheet (Figure 3.80) is lower by about 40 dB at $\epsilon_r = 2.15$ for TE and TM when compared to a short cylinder, as shown in Figure 4.125. Amplitudes for a metal thin sheet (Figure 3.11) overlap at 0° with a metal cylinder, but show a gap with a metal cylinder at 90° , as shown in Figure 4.126.

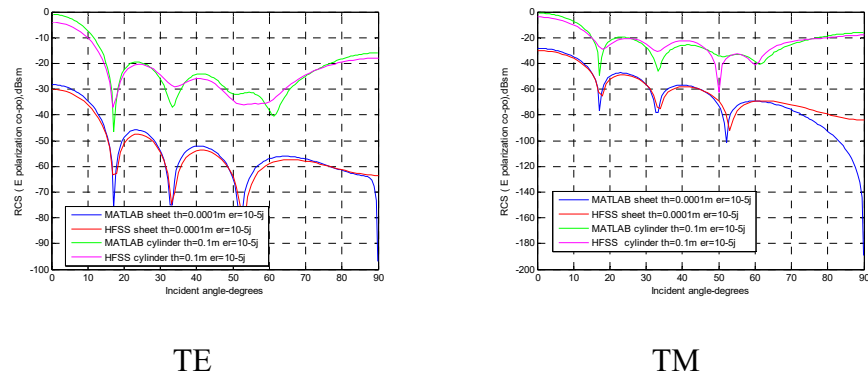
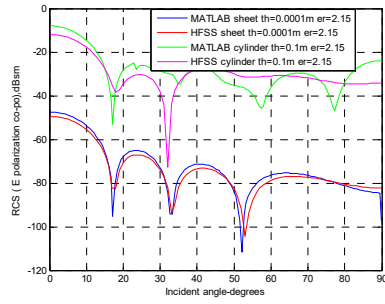
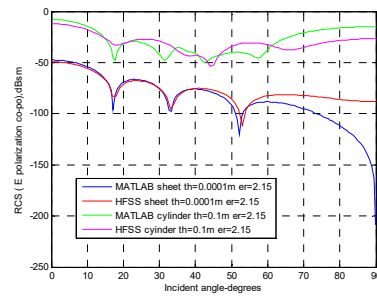


Figure 4.124: Amplitude comparison for TE and TM mode in MATLAB and HFSS (0.1 ($\sim 1 \lambda$) meters in length by 0.11 ($\sim 1 \lambda$) meters in radius at $\epsilon_r = 10^{-5}j$ for a dielectric cylinder with endcap in comparison to a sheet 0.0001 ($\sim 0.001 \lambda$) meters in thickness by 0.11 ($\sim 1 \lambda$) meters in radius). Amplitudes differ by about 30 dB for both TE and TM.

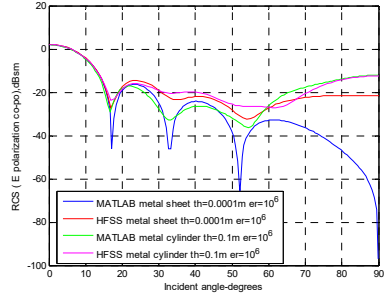


TE

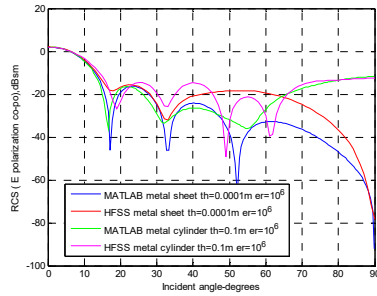


TM

Figure 4.125: Amplitude comparison for TE and TM mode in MATLAB and HFSS (0.1 (~1 λ) meters in length by 0.11 (~1 λ) meters in radius at $\epsilon_r = 2.15$ for a dielectric cylinder with endcap in comparison to a sheet 0.0001 (~0.001 λ) meters in thickness by 0.11 (~1 λ) meters in radius). Amplitudes differ by about 40 dB for both TE and TM.



TE



TM

Figure 4.126: Amplitude comparison for TE and TM mode in MATLAB and HFSS (0.1 (~1 λ) meters in length by 0.11 (~1 λ) meters in radius at $\epsilon_r = 10^6$ for a metal cylinder with endcap in comparison to a sheet 0.0001 (~0.001 λ) meters in thickness by 0.11 (~1 λ) meters in radius).

Amplitudes for a metal thin sheet overlap with a metal cylinder at 0° , but show a gap with a metal cylinder at 90° for both TE and TM.

When comparing a thin sheet 0.0001 ($\sim 0.001 \lambda$) meters in depth by 0.165 ($\sim 1.5 \lambda$) meters in radius whose thickness is 1000 times smaller than the thickness of a short dielectric cylinder that measures 0.1 ($\sim 1 \lambda$) meters in thickness by 0.165 ($\sim 1.5 \lambda$) meters in radius which its length is 0.6 times smaller than radius at $\epsilon_r = 10 - 5j$, amplitude of a thin sheet (Figure 3.108) is lower by about 25-30 dB for both TE and TM when compared to a short cylinder, as shown in Figure 4.127; and amplitude for a thin sheet (Figure 3.102) is lower by about 40 dB at $\epsilon_r = 2.15$ for both TE and TM when compared to a short cylinder, as shown in Figure 4.128. Amplitudes for a metal thin sheet (Figure 3.17) overlap at 0° with a metal cylinder, but a gap is apparent with a metal cylinder at 90° , as shown in Figure 4.129.

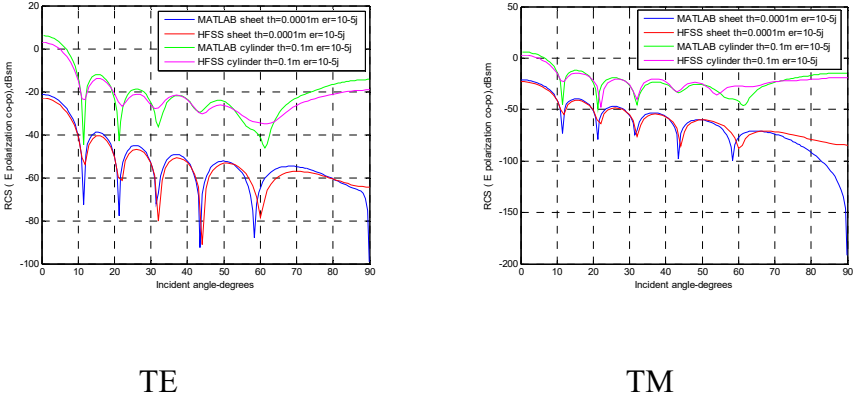
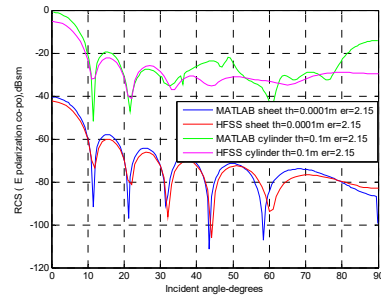


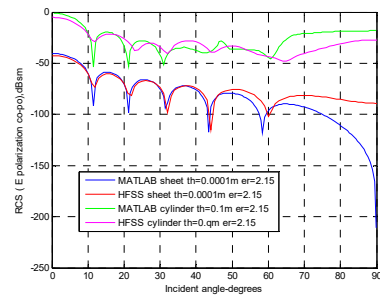
Figure 4.127: Amplitude comparison for TE and TM mode in MATLAB and HFSS (0.1 ($\sim 1 \lambda$) meters in length by 0.165 ($\sim 1.5 \lambda$) meters in radius

at $\epsilon_r = 10 - 5j$ for a dielectric cylinder with endcap in comparison to a sheet 0.0001 ($\sim 0.001 \lambda$) meters in thickness by 0.165 ($\sim 1.5 \lambda$) meters in radius).

Amplitudes differ by about 25-30 dB for both TE and TM.



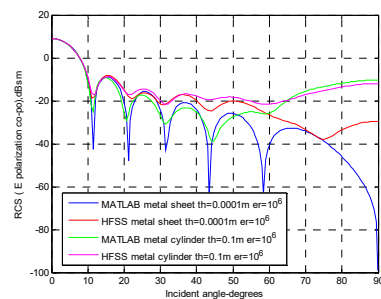
TE



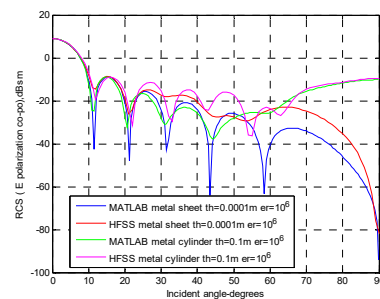
TM

Figure 4.128: Amplitude comparison for TE and TM mode in MATLAB and HFSS (0.1 ($\sim 1 \lambda$) meters in length by 0.165 ($\sim 1.5 \lambda$) meters in radius at $\epsilon_r = 2.15$ for a dielectric cylinder with endcap in comparison to a sheet 0.0001 ($\sim 0.001 \lambda$) meters in thickness by 0.165 ($\sim 1.5 \lambda$) meters in radius).

Amplitudes differ by about 40 dB for both TE and TM.



TE



TM

Figure 4.129: Amplitude comparison for TE and TM mode in MATLAB and HFSS (0.1 (~1 λ) meters in length by 0.165 (~1.5 λ) meters in radius at $\epsilon_r = 10^6$ for a metal cylinder with endcap in comparison to a metal sheet 0.0001 (~0.001 λ) meters in thickness by 0.165 (~1.5 λ) meters in radius). Amplitudes for a metal thin sheet overlap with a metal cylinder at 0°, but have gap with a metal cylinder at 90° for both TE and TM.

For a thin sheet (Figure 3.45) that measures 0.0002 (~0.002 λ) meters in depth by 0.33 (~3 λ) meters in radius, its thickness is 500 times smaller than the thickness of a short dielectric cylinder, which measures 0.1 (~1 λ) meters in thickness by 0.33 (~3 λ) meters in radius with a length 0.3 times smaller than radius at $\epsilon_r = 2.15$. When comparing the two, amplitude for a thin sheet is lower than a short dielectric cylinder by about 30 dB at $\epsilon_r = 2.15$ for both TE and TM.

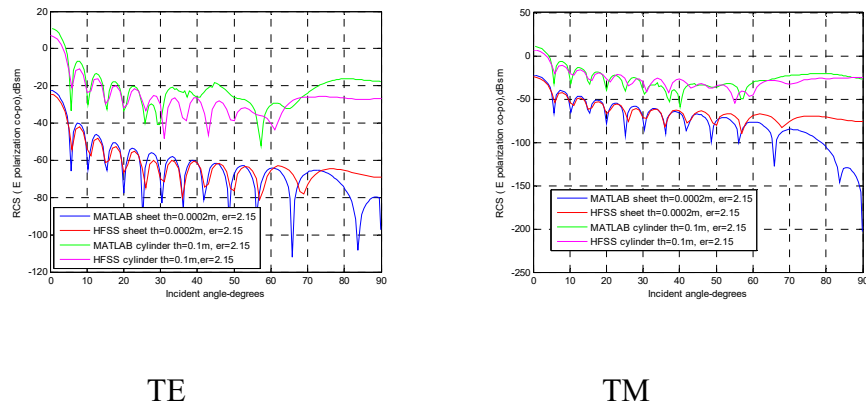


Figure 4.130: Amplitude comparison for TE and TM mode in MATLAB and HFSS (0.1 (~1 λ) meters in length by 0.33 (~3 λ) meters in radius at

$\epsilon_r = 2.15$ for a dielectric cylinder with endcap in comparison to a sheet 0.0002 ($\sim 0.002 \lambda$) meters in thickness by 0.33 ($\sim 3 \lambda$) meters in radius). Amplitudes differ by 30 dB for both TE and TM.

4.5.3 Summary

For a limiting case, as the skin depth $t \rightarrow 0$, surface resistivity $R_s \rightarrow \infty$, the reflection coefficient would be zero. Resistive thin sheets have a penetrable surface; here thickness = 0.001λ or $0.002 \lambda \ll \lambda$ resulting in more transmission going through the material and less reflection.

A short cylinder for $\epsilon_r = 10 - 5j$ shows better results than $\epsilon_r = 2.15$ in terms of overlapping for all sizes tested. This is because cylindrical material property on broadside mainly contributes to the RCS of the whole body with specular scattering domination and depolarization characteristics. However, a thin sheet still has a gap at 90 degrees due to edge effect not being taken into account by PO.

The amplitude of a dielectric thin sheet is lower by 20-40 dB when compared to a short cylinder at different relative permittivity. This is because sheets are more penetrable than cylinders.

The results also show that metal thin sheet analytical results match HFSS well at 0° , and the same fact seems to apply to the metal cylinders. This is because of the incident wave reflecting from a conducting body with a reflection coefficient near 1. A metal thin sheet behaves the same as

a metal plate (Jenn 2005) since there is no possible transmission through the material. However, as the incident angle approaches to 90 degrees, a gap appears for a metal sheet because the edge effect is ignored by PO. In this scenario, a metal cylinder is a better choice when compared to a metal thin sheet for modeling circular shaped RCS.

It is better to analyze the dimension of an object between 0.01λ and 50λ comparable to the wavelength by full wave simulation such as HFSS. All comparison to MATLAB in this dissertation shows that HFSS gives more accurate results. Both HFSS and analytical methods are more suitable at this dimension range. For radius $> 1 \lambda$, all plots for MATLAB simulation take a few minutes, while HFSS takes at least 30 minutes for short cylinders ($0.1 (\sim 1 \lambda)$ meters in length), and may take several days for longer cylinders ($3.3 (\sim 30 \lambda)$ meters in length by $0.165 (\sim 1.5 \lambda)$ meters in radius). MATLAB takes less time than HFSS, but HFSS presents more precise results.

Chapter 5

Example applications

5.1 Leaf library generation examples

5.1.1 Describe and discuss the coordinate transformations to generate a library

The purpose of the coordinate transformation system is to set up a laboratory reference frame from which the orientation of the object can be illustrated. The direction of polarization \mathbf{E} and \mathbf{H} fields and wave vector \mathbf{k} can also be specified with it.

The radar is located at the origin of the spherical polar (R, θ, ϕ) coordinate system, where R is the distance between the source and observer. Figure 1 (Jenn 2005) specifies the electromagnetic wave in the spherical coordinate system, and Figure 2 (Mishchenko 2000) illustrates the transformation of the laboratory reference system xyz into the radar reference coordinate system $x' y' z'$. If \mathbf{p} represents a vector in the “radar” system and \mathbf{P} represents a vector in the “local” system, the transformation relationship between the two vectors using \mathbf{T} matrix are $\mathbf{P}=\mathbf{T}\mathbf{p}$. We specify radar H-pol pointing in the X-direction denoted as \hat{x} , and V-pol pointing in the Y-direction denoted as \hat{y} . Based on the transformation relationship, the local polarizations can be transformed to the radar scattering polarizations.

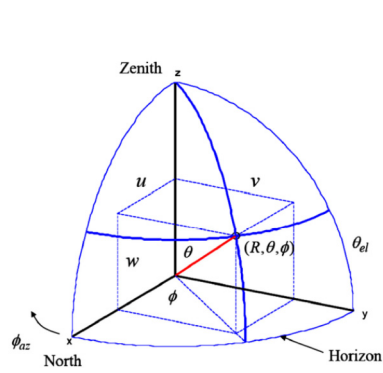


Figure 5.1

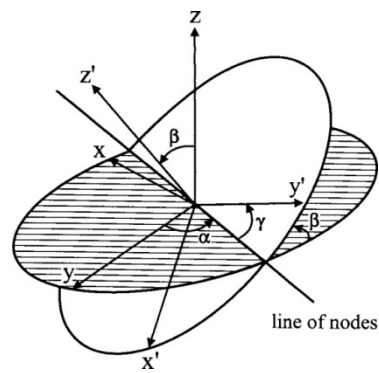


Figure 5.2

Figure 5.1: Spherical coordinate system used to specify the direction and the polarization state of a transverse electromagnetic wave. (Mishchenko 2000)

Figure 5.2: Transformation of the laboratory reference system xyz into the particle reference frame $x' y' z'$. (Mishchenko 2000)

Figure 5.2 can also be illustrated in detail with three axis (xyz) rotation as a whole transformation of the coordinate system.

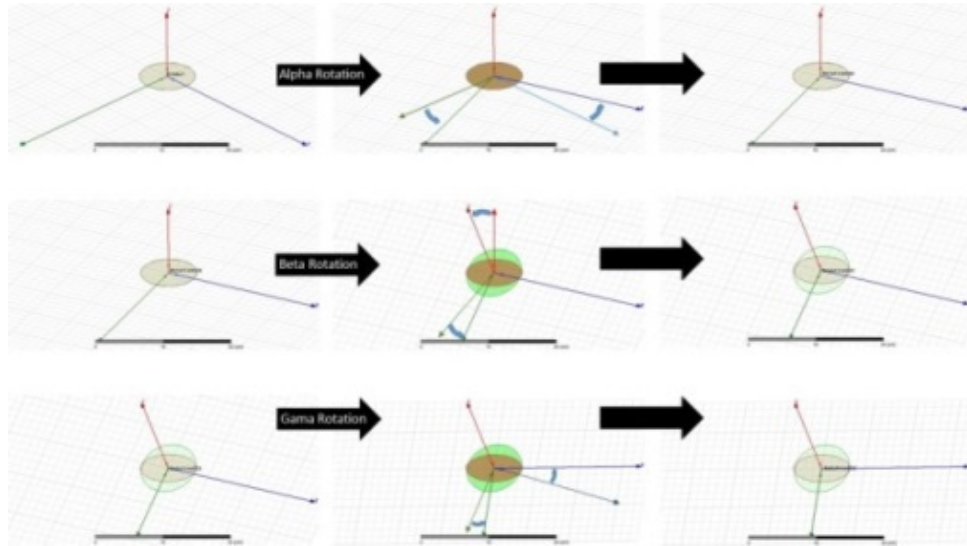


Figure 5.3: Rotation of three axes for radar-laboratory transformation system.

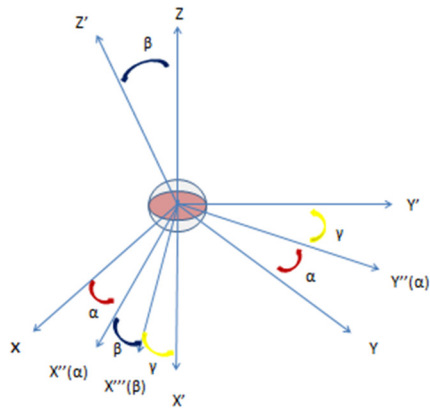


Figure 5.4: Rotation of three axes for radar-laboratory transformation system.

There are three steps to show how the transformations system works.

Rotating three Euler angles of rotation α , β and γ for each time, the

laboratory reference system xyz can be translated into the radar system $x' y' z'$.

First, by rotating the z axis, which is accomplished by moving the x and y axis through the angle α counter-clockwise in the $x y$ plane, the x and y axis become a new $x'' (\alpha)$ axis and a new $y'' (\alpha)$ axis.

Second, by rotating the new $y'' (\alpha)$ axis, which is accomplished by moving the z axis and the new $x'' (\alpha)$ axis through the angle β counter-clockwise in the $z x'' (\alpha)$ plane, the z axis and the $x'' (\alpha)$ axis become the new $z' (\beta)$ and the new $x''' (\beta)$. The $z' (\beta)$ is therefore simplified to z' axis.

Third, by rotating the new $z' (\beta)$ axis, which is accomplished by moving the new $x''' (\beta)$ and the new $y'' (\alpha)$ axis through angle γ counter-clockwise in the $x''' (\beta) y'' (\alpha)$ plane, the new $x''' (\beta)$ and the new $y'' (\alpha)$ axis become $x' (\gamma)$ and $y' (\gamma)$, simplified to x' axis and y' axis.

Here, $x'' (\alpha)$, $y'' (\alpha)$, $x''' (\beta)$ are used as transaction states for each step of the movement of each axis.

5.1.2 Analytical simulation for a single leaf

The complex RCS of scattering matrix S with four complex elements is denoted to specify the amplitude of co-pol and cross-pol for TE (horizontal) and TM (vertical) scattering polarization return signal, as shown below (Kahny 1988):

$$S = \begin{bmatrix} S_{hh} & S_{hv} \\ S_{vh} & S_{vv} \end{bmatrix}$$

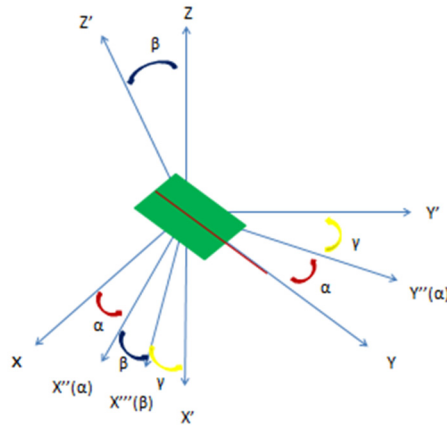


Figure 5.5: Leaf rotations under the coordinate transformation system.

The analytical simulation for the different sizes of a single leaf (from big to small), with all polarizations under the radar transformation systems at 2.8 GHz and 10 GHz, are shown below. The “real” leaf combines two individual objects: a dielectric thin sheet to simulate a leaf body and a long thin cylinder to simulate a stem. FEKO simulations are followed by each analytical simulation for the purpose of comparison. The results show that they are very similar for the same size.

Co-pol and Cross-pol polarization of a leaf at 2.8 GHz

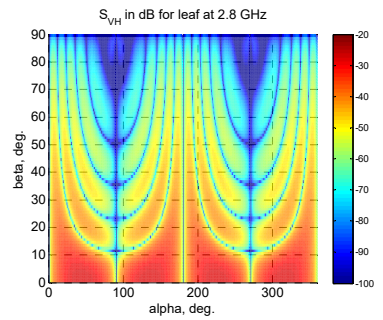
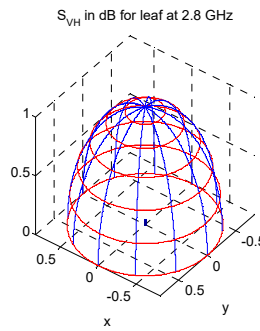
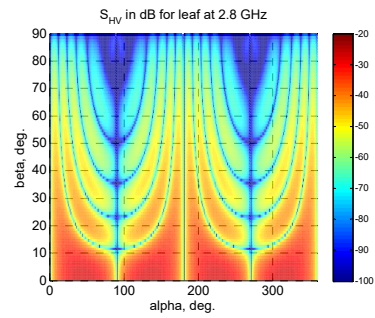
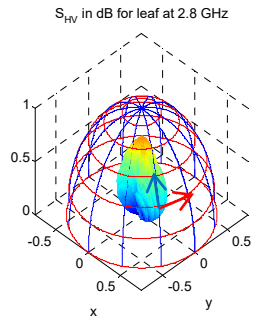
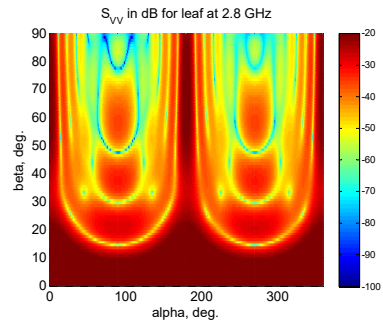
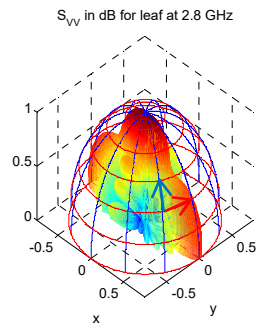
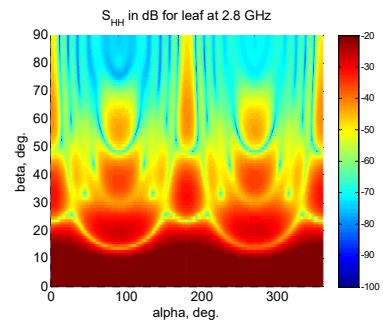
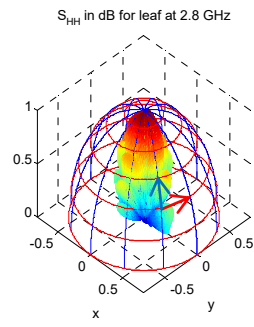
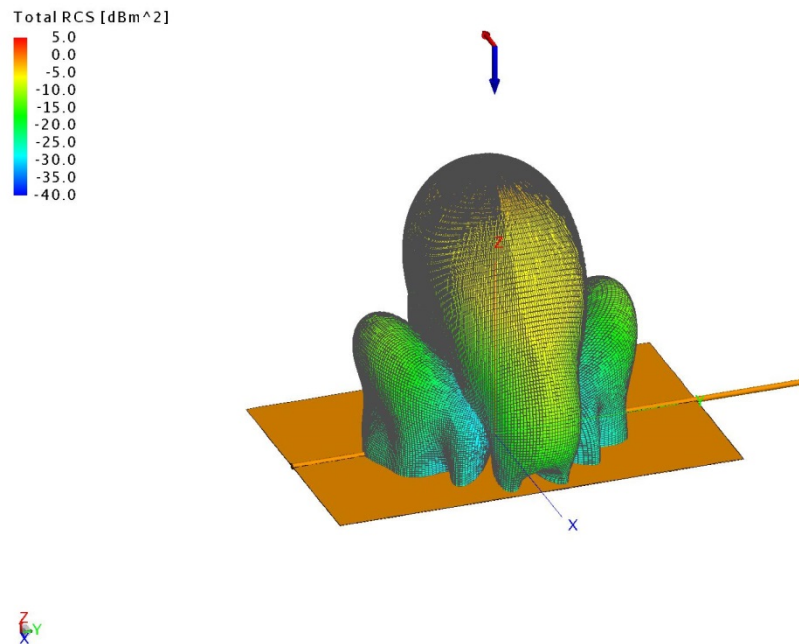


Figure 5.6: An example of the RCS database for a maple leaf, which is comprised of the co-pol amplitude of E polarization S_{HH} (top), co-pol amplitude of H polarization S_{VV} (middle), and cross-pol amplitude of E polarization S_{HV} (bottom) of far-field RCS for a resistive sheet with stem (cylinder) (width = 14 cm, height = 22 cm, thickness = 0.2 mm, stem length = 280 mm, stem diameter = 3.0 mm, moisture content: 80%) at 2.8 GHz. The red and blue arrows represent the horizontal and vertical polarizations, respectively.

FEKO simulation:



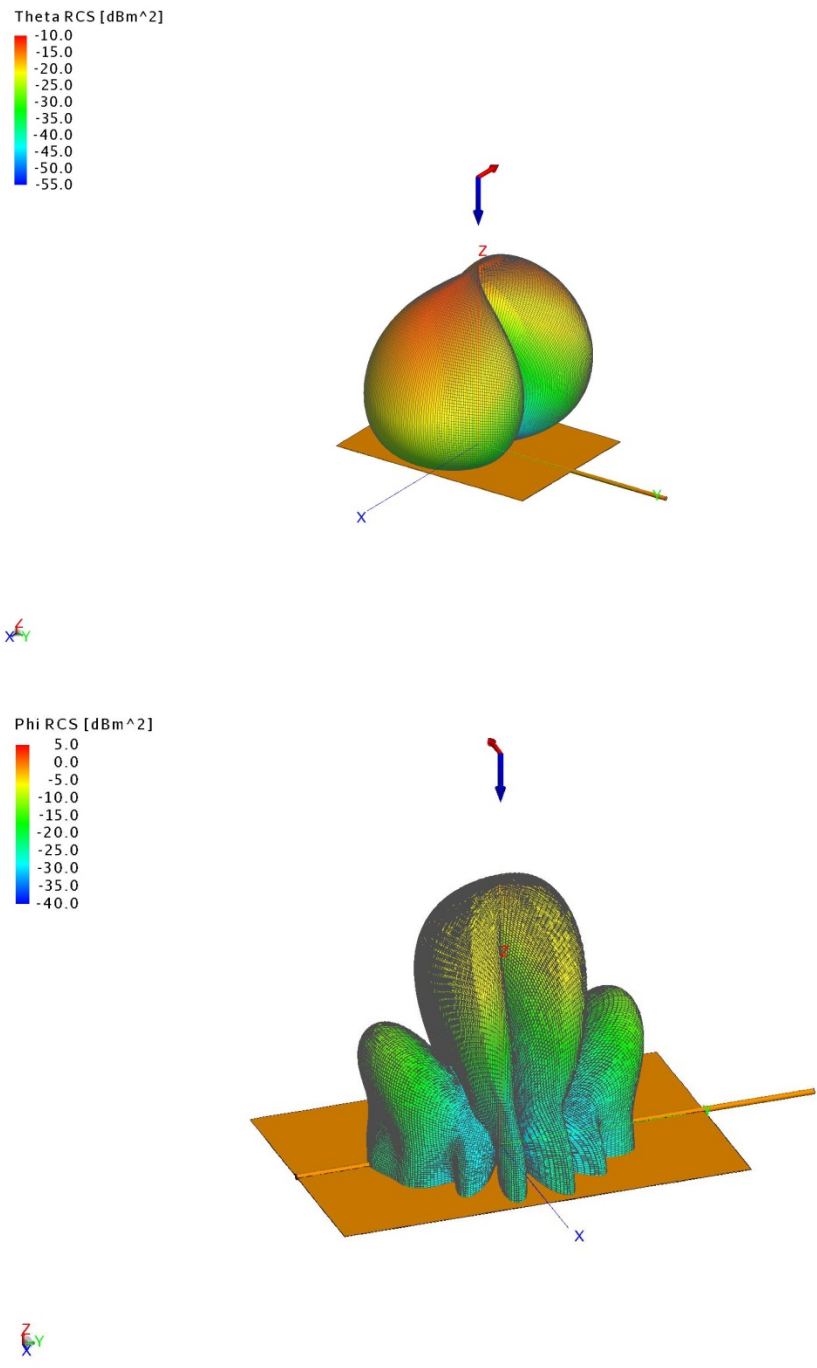


Figure 5.7: FEKO simulation for RCS of the same size leaf at a different polarization angle (total, theta, phi) at 2.8 GHz.

Co-pol and Cross-pol polarization of a leaf at 10 GHz

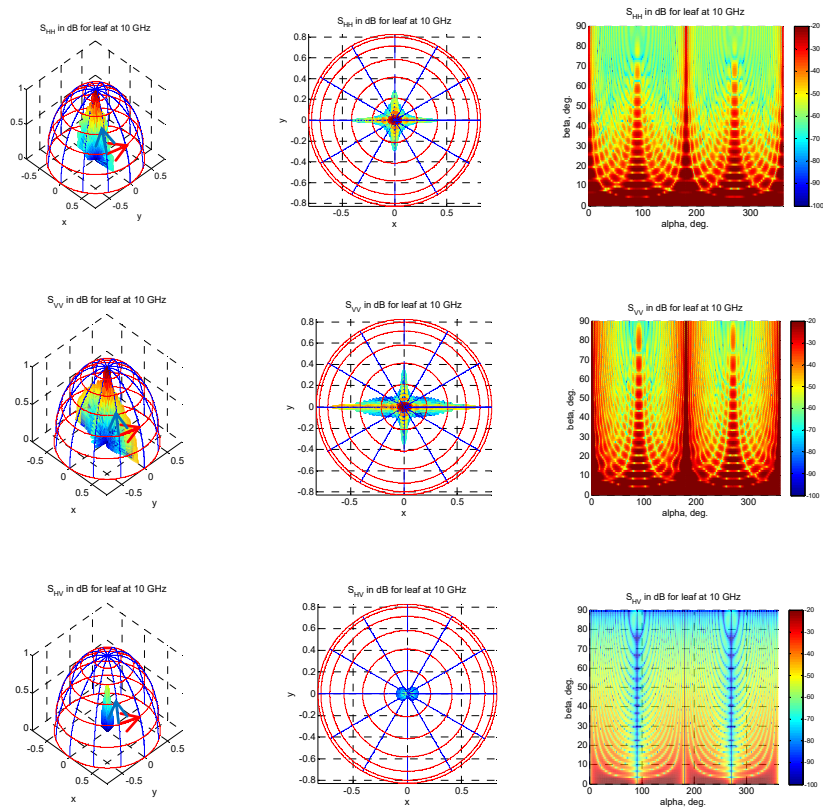
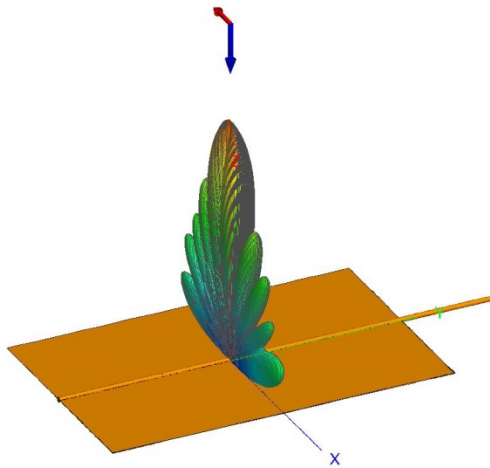
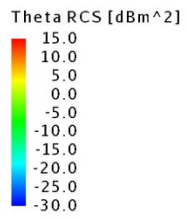
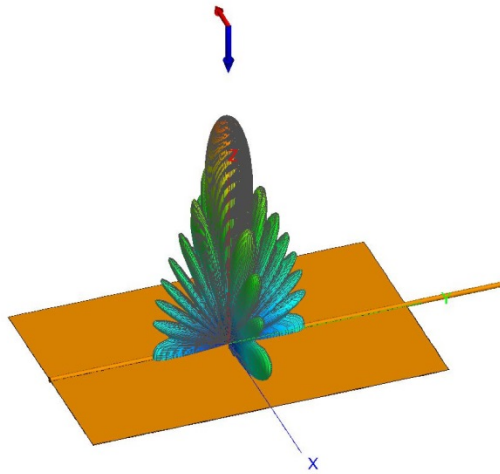
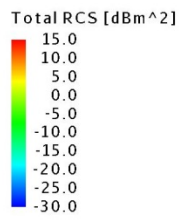


Figure 5.8: An example of the RCS database for a maple leaf, which is comprised of the co-pol amplitude of E polarization S_{HH} (top), co-pol amplitude of H polarization S_{VV} (middle), and cross-pol amplitude of E polarization S_{HV} (middle) and H polarization S_{VH} (bottom) of far-field RCS for a resistive sheet with a stem (cylinder) (width = 14 cm, height = 22 cm, thickness = 0.2 mm, stem length = 280 mm, stem diameter = 3.0 mm, moisture content: 80%) at 10 GHz. The red and blue arrows represent the horizontal and vertical polarizations, respectively.

FEKO simulation:



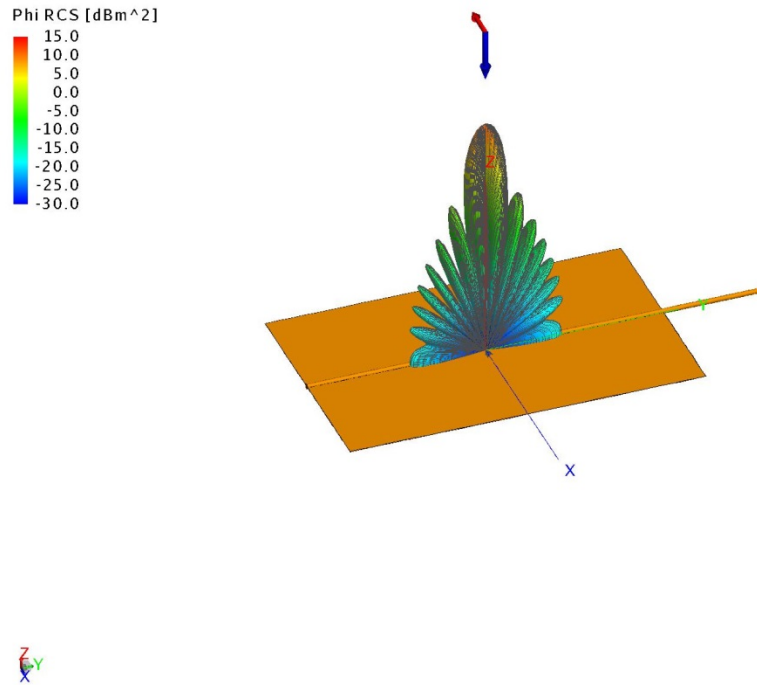
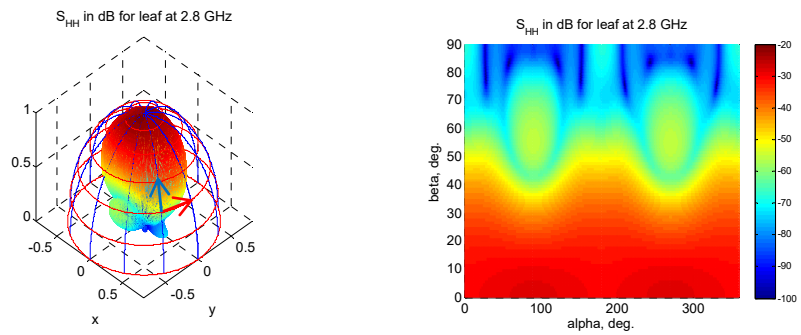


Figure 5.9: FEKO simulation for the RCS of the same size leaf at a different polarization angle (total, theta, phi) at 10 GHz.

Co-pol and Cross-pol polarization of a leaf at 2.8 GHz



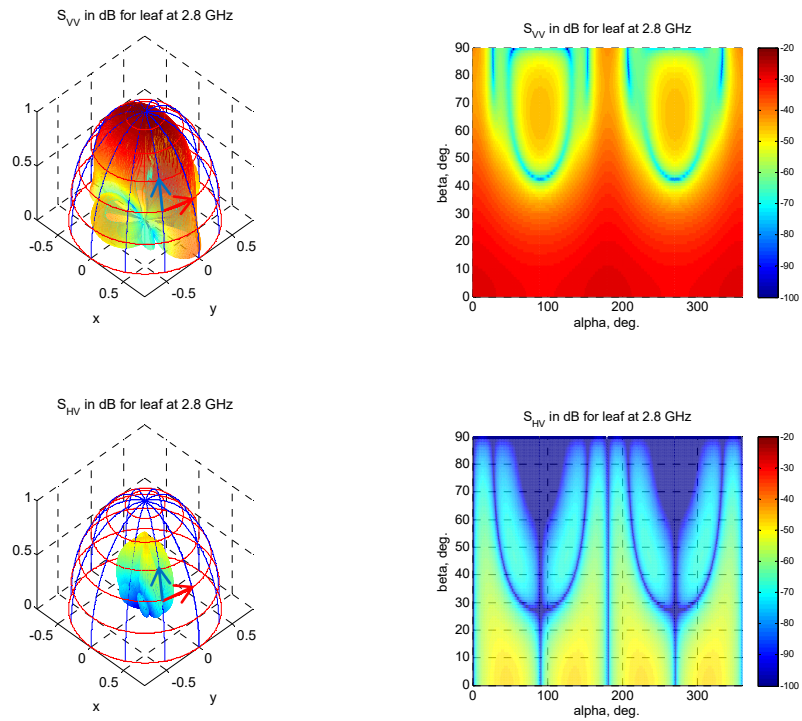
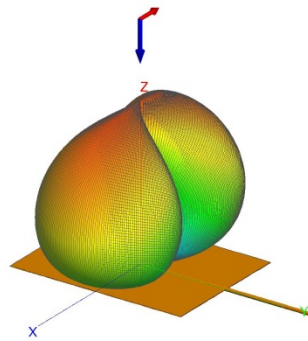
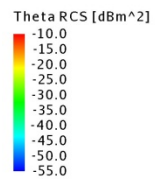
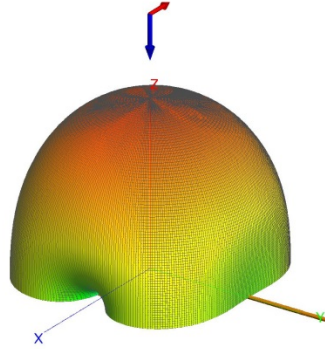
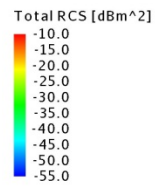


Figure 5.10: An example of the RCS database for a leaf, which is comprised of the co-pol amplitude of E polarization S_{HH} (top), co-pol amplitude of H polarization S_{VV} (middle), and cross-pol amplitude of E polarization S_{HV} (bottom) of far-field RCS for a resistive sheet with stem (cylinder) (width = 6 cm, height = 8 cm, thickness = 0.2 mm, stem length = 120 mm, stem diameter = 1.5 mm, moisture content: 80%) at 2.8 GHz. The red and blue arrows represent the horizontal and vertical polarizations, respectively. (Cheong, Bodine, Zhu et al. 2015)

FEKO simulation:



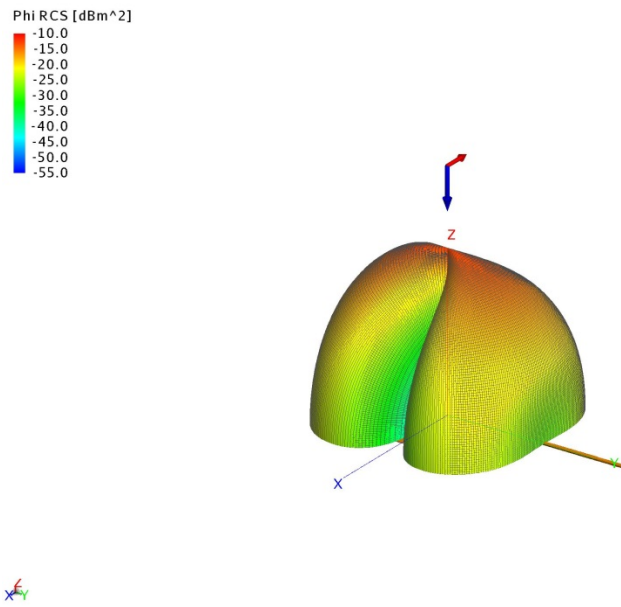
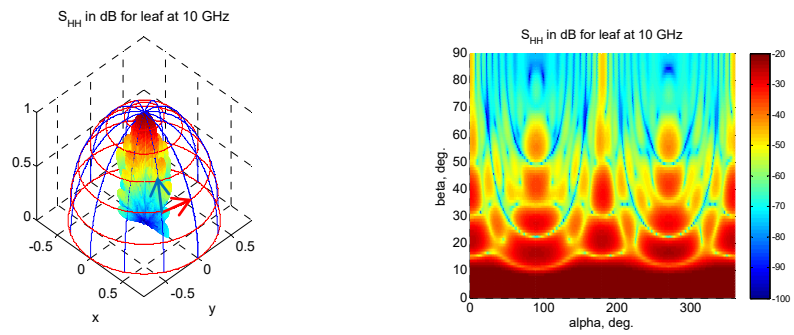


Figure 5.11: FEKO simulation for the RCS of the same size leaf at a different polarization angle (total, theta, phi) at 2.8 GHz.

Co-pol and Cross-pol polarization of a leaf at 10 GHz



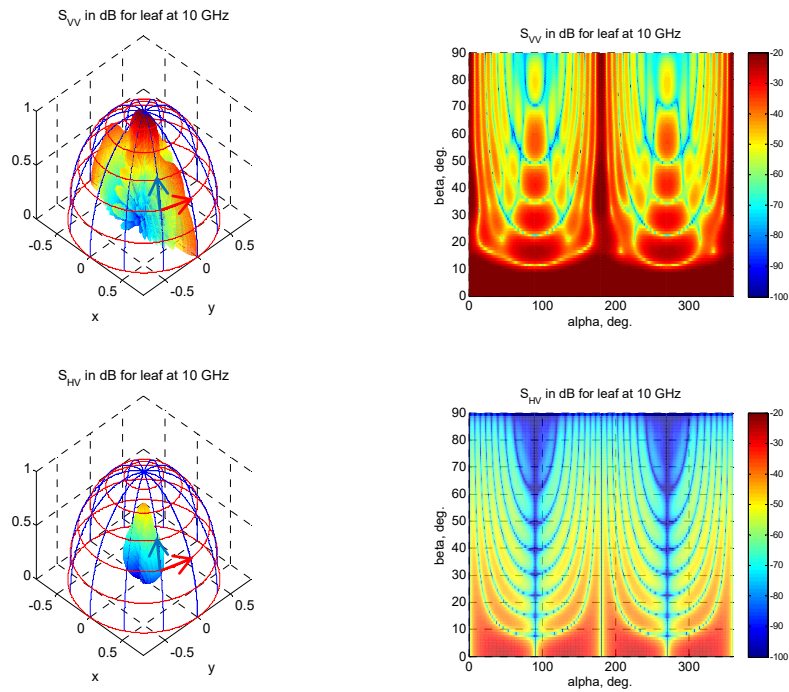
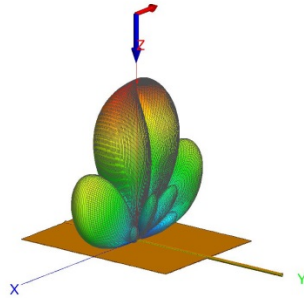
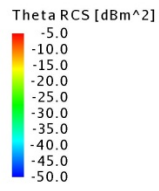
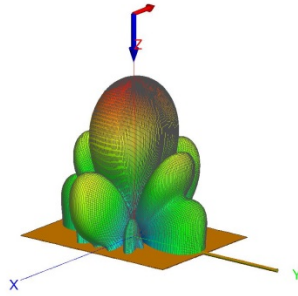
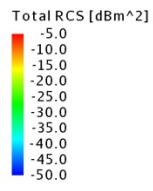


Figure 5.12: An example of the RCS database for a leaf, which is comprised of the co-pol amplitude of E polarization S_{HH} (top), co-pol amplitude of H polarization S_{VV} (middle), and cross-pol amplitude of E polarization S_{HV} (bottom) of far-field RCS for a resistive sheet with a stem (cylinder) (width = 6 cm, height = 8 cm, thickness = 0.2 mm, stem length = 120 mm, stem diameter = 1.5 mm, moisture content: 80%) at 10 GHz. The red and blue arrows represent the horizontal and vertical polarizations, respectively.

FEKO simulation:



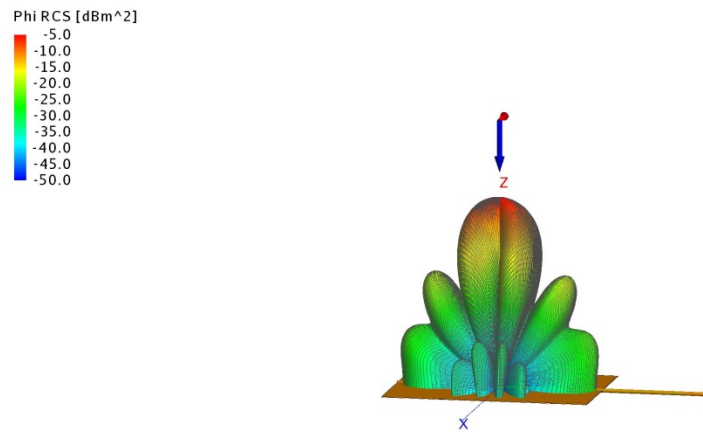
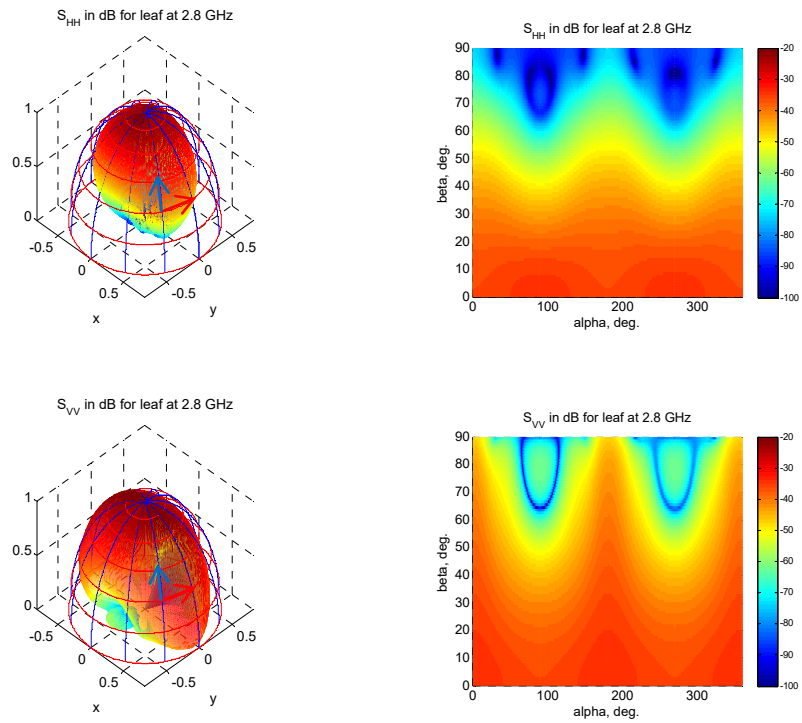


Figure 5.13: FEKO simulation for the RCS of the same size leaf at a different polarization angle (total, theta, phi) at 10 GHz.

Co-pol and Cross-pol polarization of a leaf at 2.8 GHz



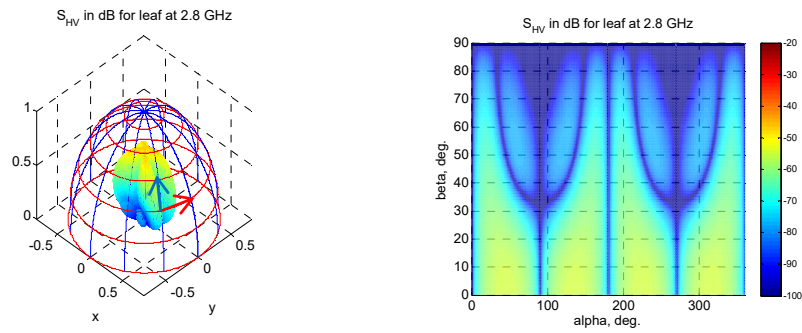
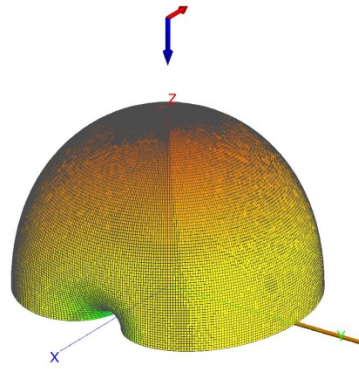
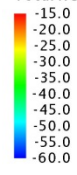


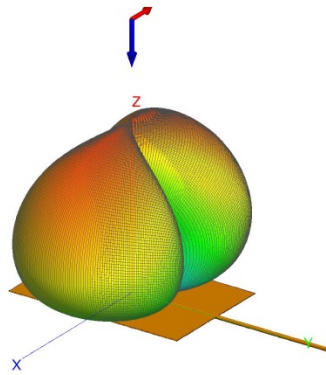
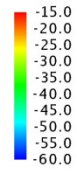
Figure 5.14: An example of the RCS database for a leaf, which is comprised of the co-pol amplitude of E polarization S_{HH} (top), co-pol amplitude of H polarization S_{VV} (middle), and cross-pol amplitude of E polarization S_{HV} (bottom) of far-field RCS for a resistive sheet with a stem (cylinder) (width = 4 cm, height = 6 cm, thickness = 0.2 mm, stem length = 100 mm, stem diameter = 1.2 mm, moisture content: 80%) at 2.8 GHz. The red and blue arrows represent the horizontal and vertical polarizations, respectively.

FEKO simulation:

Total RCS [dBm²]



Theta RCS [dBm²]



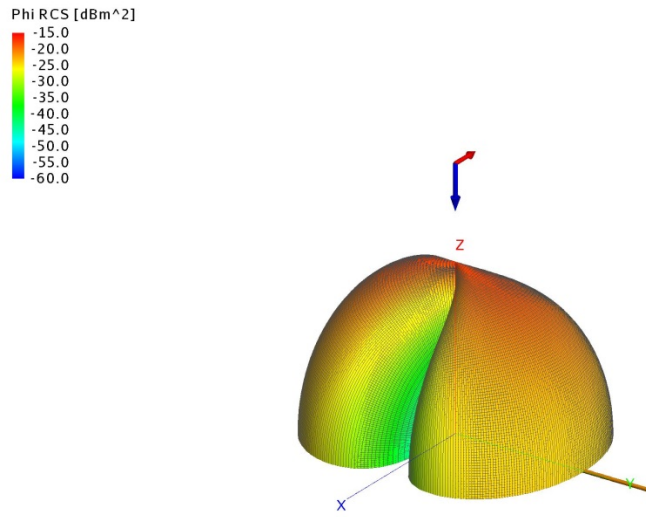
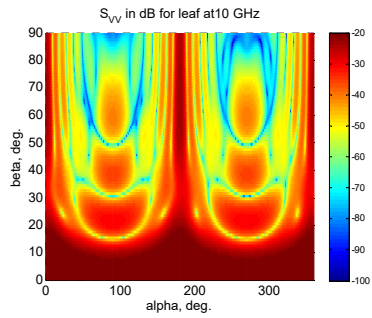
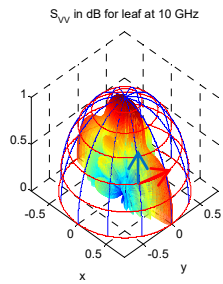
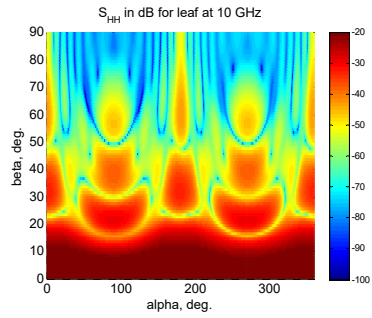
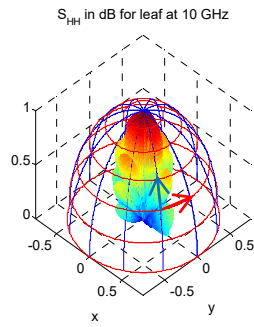


Figure 5.15: FEKO simulation for the RCS of the same size leaf at a different polarization angle (total, theta, phi) at 2.8 GHz.

Co-pol and Cross-pol polarization of a leaf at 10 GHz



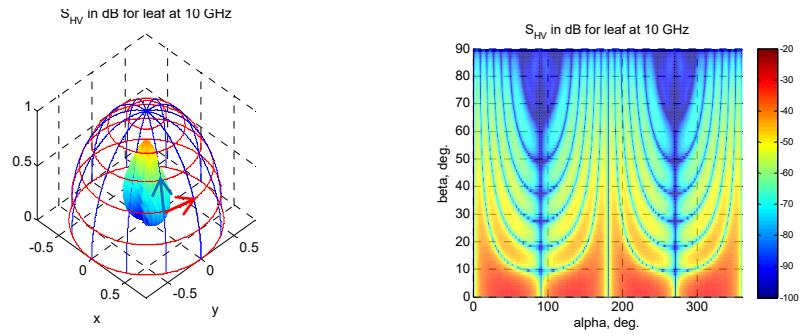
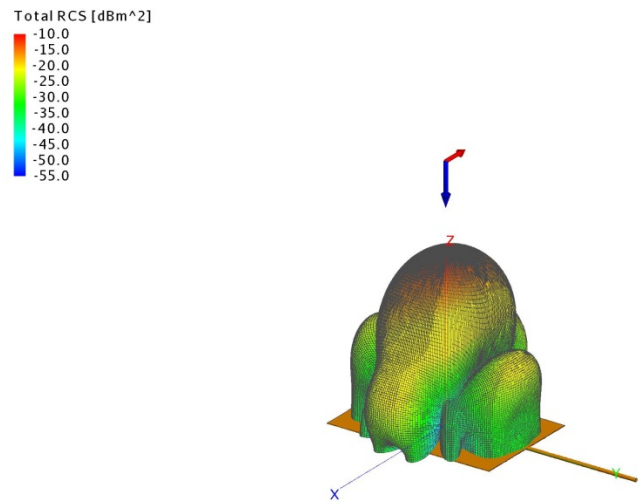
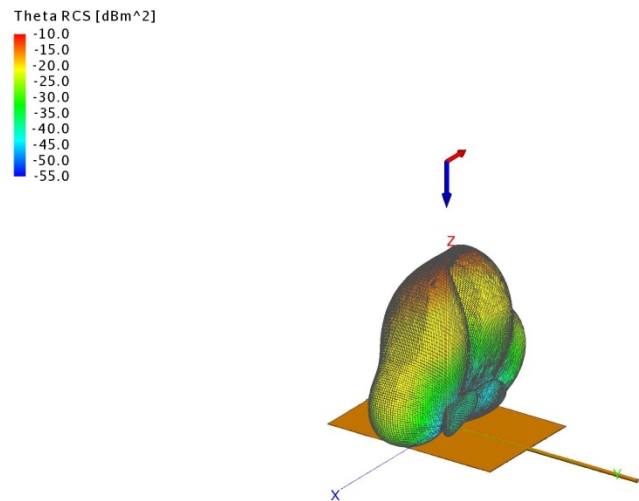


Figure 5.16: An example of the RCS database for a leaf, which is comprised of the co-pol amplitude of E polarization S_{HH} (top), co-pol amplitude of H polarization S_{VV} (middle), and cross-pol amplitude of E polarization S_{HV} (bottom) of far-field RCS for a resistive sheet with a stem (cylinder) (width = 4 cm, height = 6 cm, thickness = 0.2 mm, stem length = 100 mm, stem diameter = 1.2 mm, moisture content: 80%) at 10 GHz. The red and blue arrows represent the horizontal and vertical polarizations, respectively.

FEKO simulation:



x y z



x y z

Figure 5.17: FEKO simulation for the RCS of the same size leaf at a different polarization angle (total, theta, phi) at 10 GHz.

Co-pol and Cross-pol polarization of a leaf at 2.8 GHz

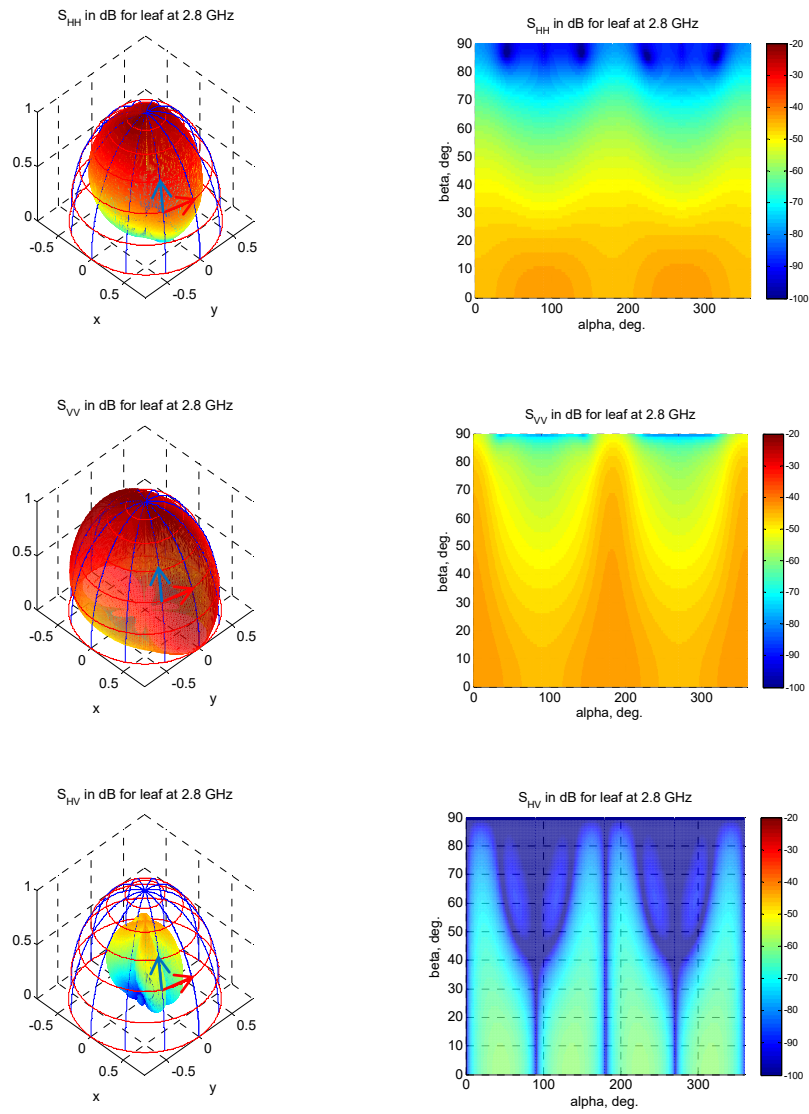
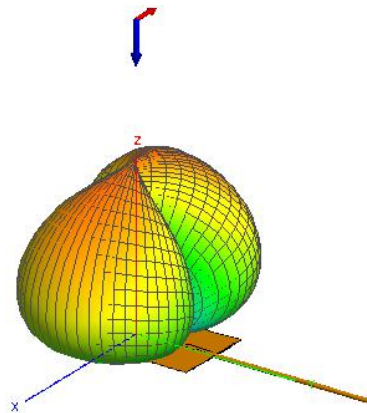
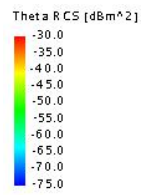
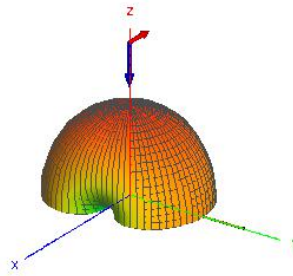
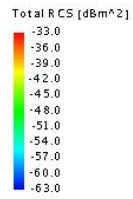


Figure 5.18: An example of the RCS database for a leaf, which is comprised of the co-pol amplitude of E polarization S_{HH} (top), co-pol amplitude of H polarization S_{VV} (middle), and cross-pol amplitude of E polarization S_{HV} (bottom) of far-field RCS for a resistive sheet with a stem (cylinder) (width = 2 cm, height = 4 cm, thickness = 0.2 mm, stem length = 80 mm, stem diameter = 1.0 mm, moisture content: 80%) at 2.8 GHz.

The red and blue arrows represent the horizontal and vertical polarizations, respectively.

FEKO simulation:



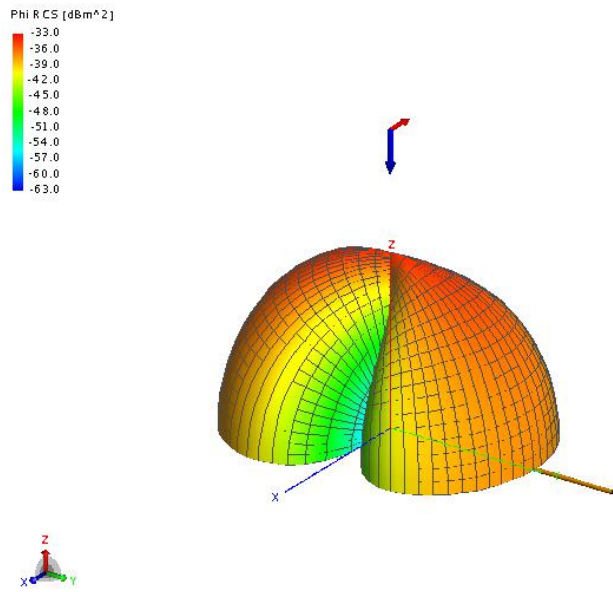
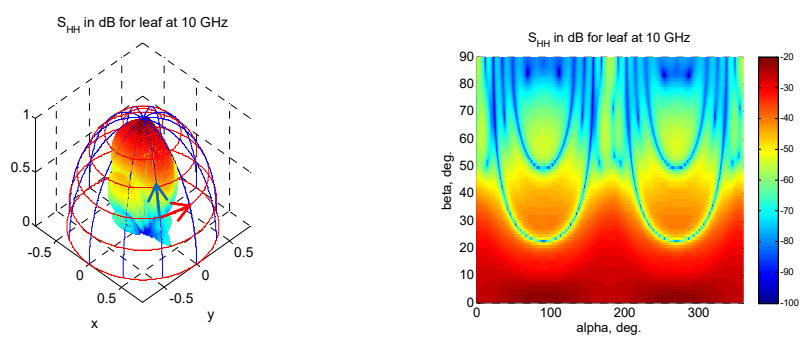


Figure 5.19: FEKO simulation for the RCS of the same size leaf at a different polarization angle (total, theta, phi) at 2.8 GHz.

Co-pol and Cross-pol polarization of a leaf at 10 GHz



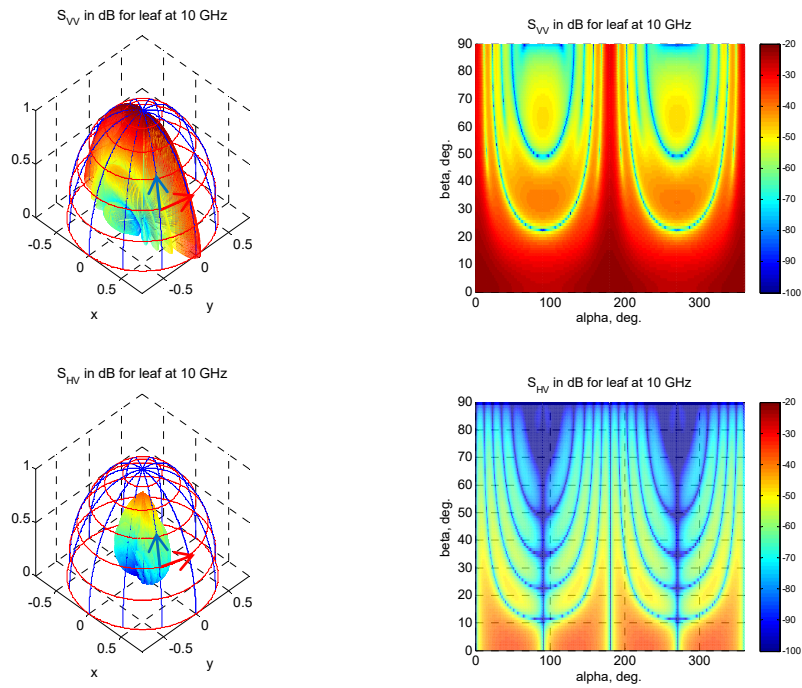
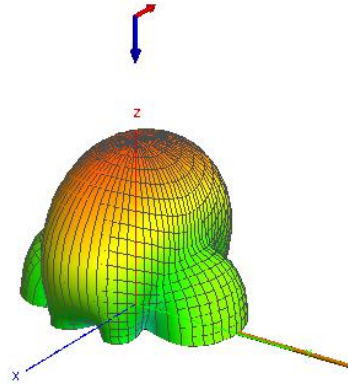
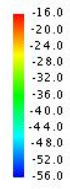


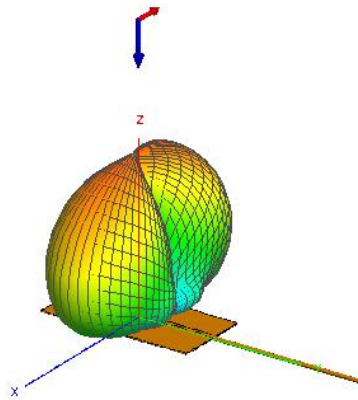
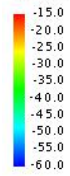
Figure 5.20: An example of the RCS database for a leaf, which is comprised of the co-pol amplitude of E polarization S_{HH} (top), co-pol amplitude of H polarization S_{VV} (middle), and cross-pol amplitude of E polarization S_{HV} (bottom) of far-field RCS for a resistive sheet with a stem (cylinder) (width = 2 cm, height = 4 cm, thickness = 0.2 mm, stem length = 80 mm, stem diameter = 1.0 mm, moisture content: 80%) at 10 GHz. The red and blue arrows represent the horizontal and vertical polarizations, respectively.

FEKO simulation:

Total RCS [dBm²]



Theta RCS [dBm²]



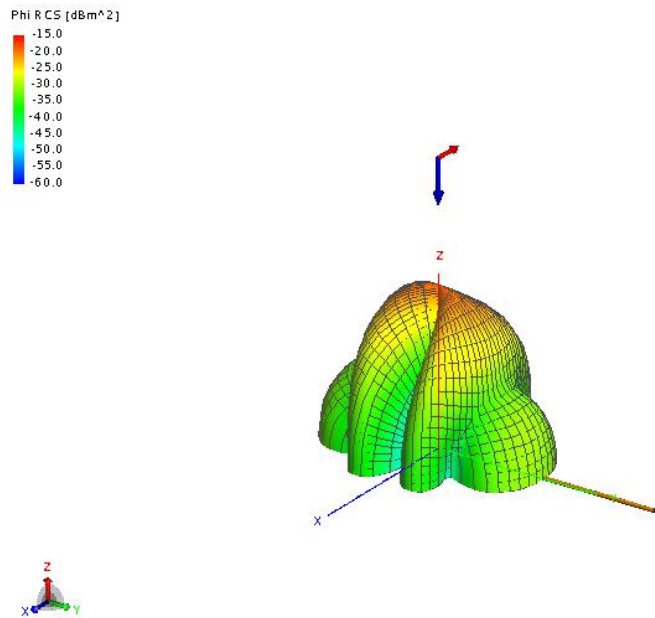
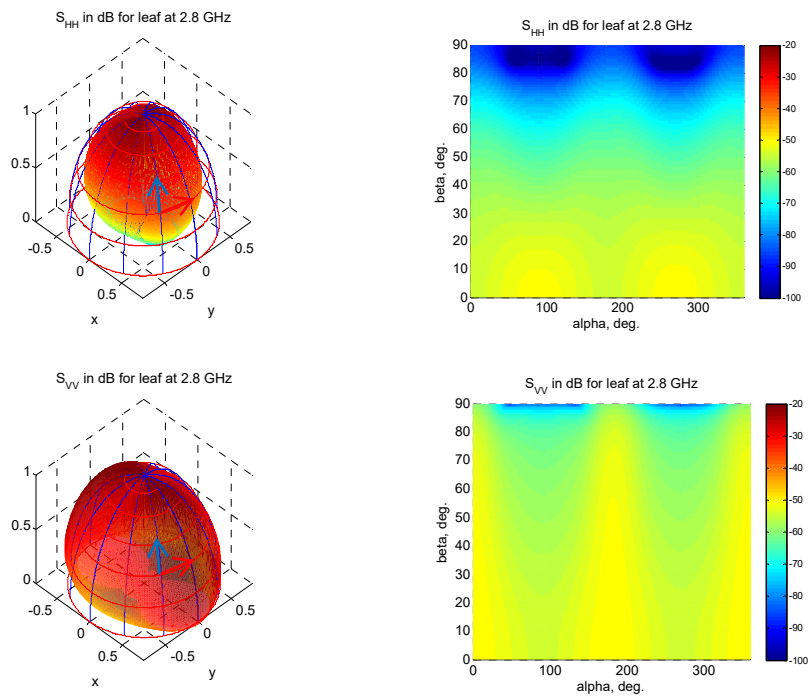


Figure 5.21: FEKO simulation for the RCS of the same size leaf at a different polarization angle (total, theta, phi) at 10 GHz.

Co-pol and Cross-pol polarization of a leaf at 2.8 GHz



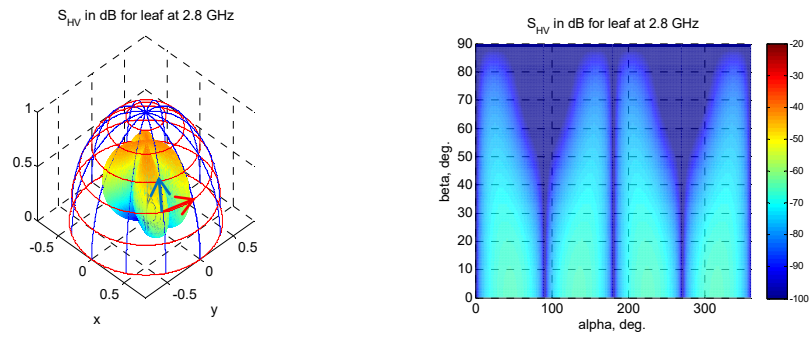
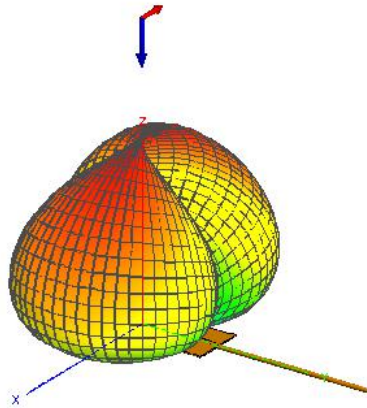
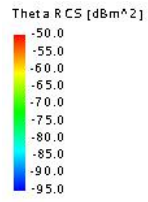
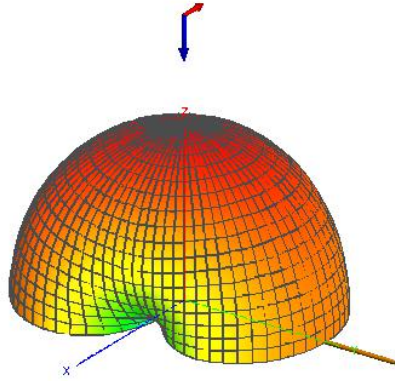
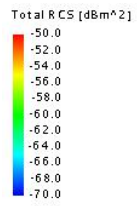


Figure 5.22: An example of the RCS database for a leaf, which is comprised of the co-pol amplitude of E polarization S_{HH} (top), co-pol amplitude of H polarization S_{VV} (middle), and cross-pol amplitude of E polarization S_{HV} (bottom) of far-field RCS for a resistive sheet with stem (cylinder) (width = 1 cm, height = 3 cm, thickness = 0.2 mm, stem length = 60 mm, stem diameter = 0.8 mm, moisture content: 80%) at 2.8 GHz. The red and blue arrows represent the horizontal and vertical polarizations, respectively.

FEKO simulation:



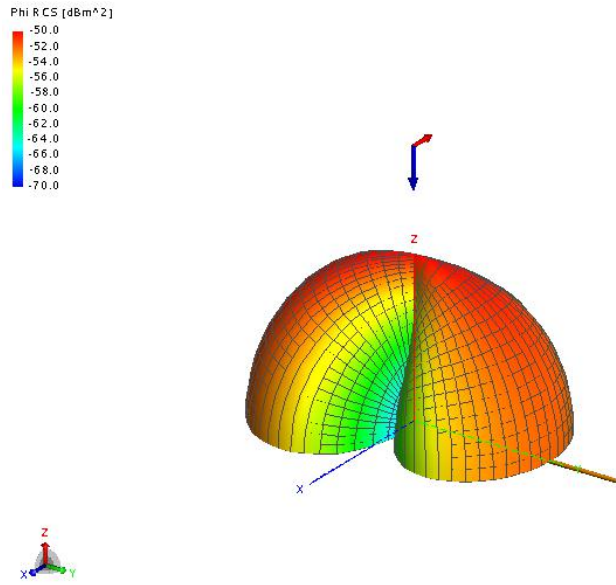
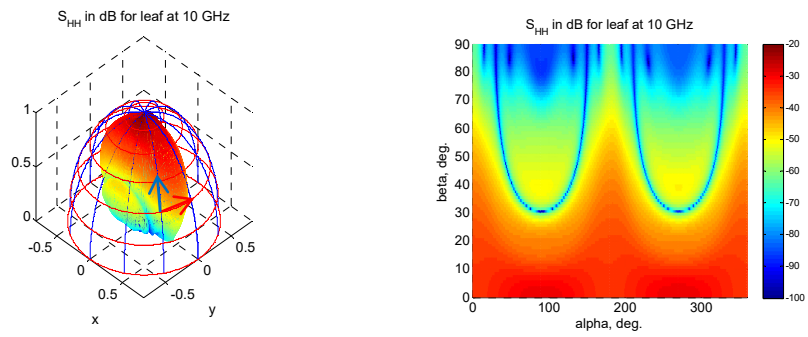


Figure 5.23: FEKO simulation for the RCS of the same size leaf at a different polarization angle (total, theta, phi) at 2.8 GHz.

Co-pol and Cross-pol polarization of a leaf at 10 GHz



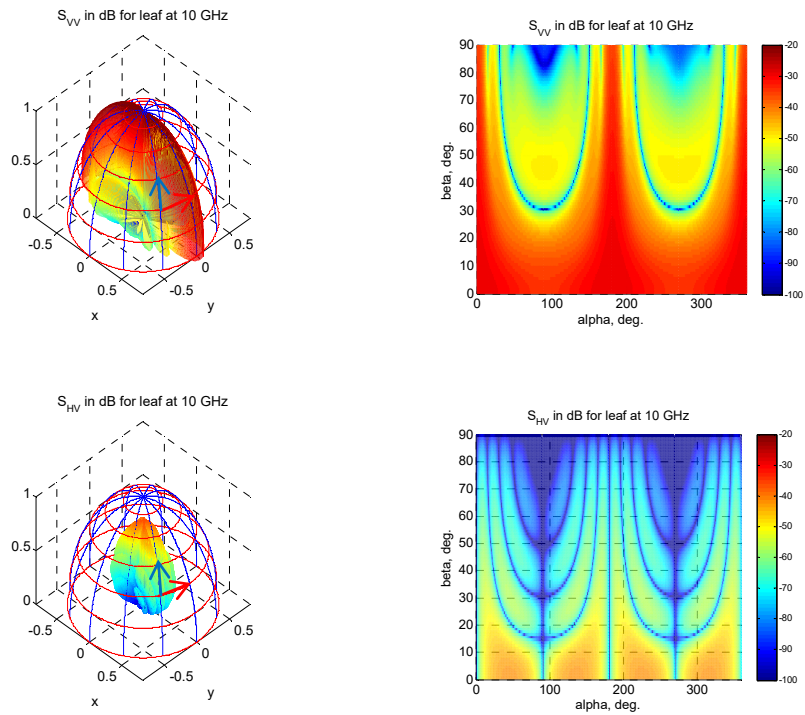
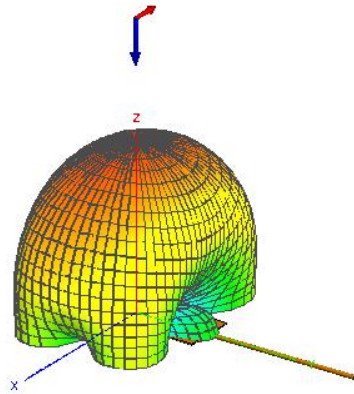
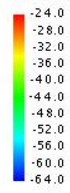


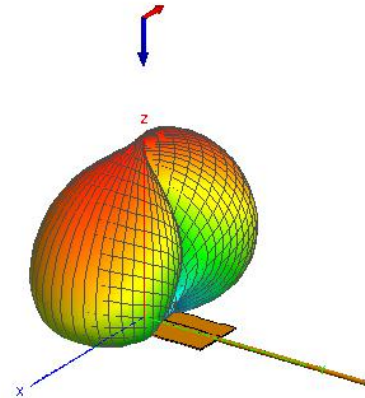
Figure 5.24: An example of the RCS database for a leaf, which is comprised of the co-pol amplitude of E polarization S_{HH} (top), co-pol amplitude of H polarization S_{VV} (middle), and cross-pol amplitude of E polarization S_{HV} (bottom) of far-field RCS for a resistive sheet with a stem (cylinder) (width = 1 cm, height = 3 cm, thickness = 0.2 mm, stem length = 60 mm, stem diameter = 0.8 mm, moisture content: 80%) at 10 GHz. The red and blue arrows represent the horizontal and vertical polarizations, respectively.

FEKO simulation:

Total RCS [dBm²]



Theta RCS [dBm²]



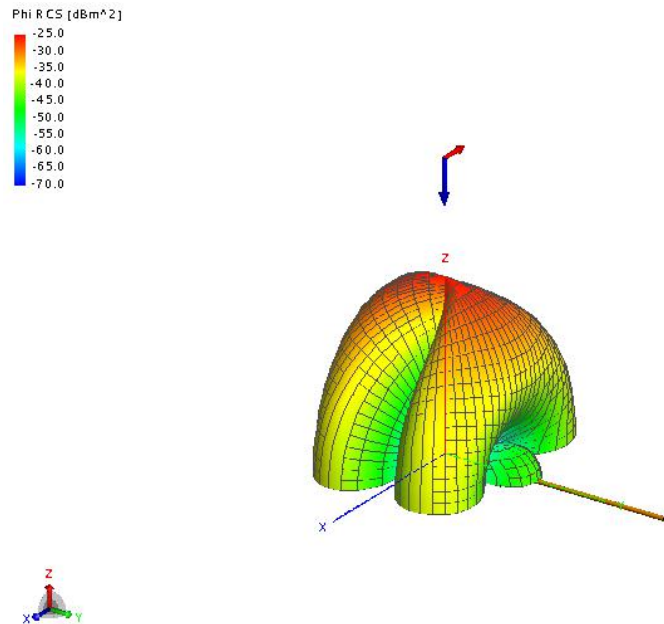


Figure 5.25: FEKO simulation for the RCS of the same size leaf at a different polarization angle (total, theta, phi) at 10 GHz.

5.2 Mean RCS of wood board study

5.2.1 Motivation

RCS calculations are required for the comparison of transmission matrix calculations (Waterman 1969, 1971) and electromagnetic scattering calculations using PO “Simulated frequency dependence of radar observations of tornadoes” (Bodine et al. 2015). This is one of the RCS applications towards tornadic debris scatterers. My contribution in a

previously published work as a co-author is to calculate the mean RCS value of wood board.

The purpose of the comparison is to examine some problems with the T-matrix calculations. One problem is that the T-matrix is not able to converge on very large sized particles, or particles with large eccentricities and high refractive indices. The T-matrix also cannot compute irregular size objects with sharp edges. The T-matrix is successful in obtaining accurate results for spheroids, but this is an idealized debris type. In the T-matrix calculation, an equivalent reflectivity factor Z_e is calculated from rain concentrations at different radar frequencies with the equation,

$$Z_e = \frac{\lambda^4}{\pi^5 |K_w|^2} \int_0^\infty \sigma_b(D) N(D) dD, \quad \text{where } \lambda \text{ is the radar wavelength, } K_w \text{ is a}$$

function of the refractive index of water (Doviak and Zrnic' 1993), $\sigma_b(D)$ is the mean value of backscattering RCS, D is the particle diameter, and $N(D)$ is the particle size distribution.

A wood board has the same volume of a sphere with a radius varying linearly from 9.5-95 mm for 10 sizes ($r = 9.5, 19, 28.5, \dots, 95$ mm) at five different higher frequencies: $f = 2.8$ GHz, 5.5 GHz, 9.7 GHz, 37.5 GHz, and 100 GHz. The thickness of thin wood board ranges from less than a few 10^{th} of a wavelength to 10 times that of a wavelength with $\lambda = 0.11$ meters. In terms of specific measurements, the lengths of the square wood

board used are 41.57 mm, 83.14 mm, and so on up to 415.7 mm; and the thickness is relative to length, measuring 1/20 of the board length (2.08 mm, 4.16 mm, and so on up to 20.79 mm). A complex relative permittivity ϵ_r is defined as $2 - 0.2j$, which is broadly consistent with values measured by Daian (2006) and Nawfal (2011). Based on the request of reviewers, the wet wood board ϵ_r is calculated by $4.65-1.46j$ with 20% moisture content.

5.2.2 Calculation of the mean value of RCS for wood board

First, how does one determine the reflection and transmission of the electromagnetic field when electromagnetic wave scattering in the lossless or lossy and infinitely long media (two-dimensional geometry) by a planar boundary for one single layer? Several things need to be considered:

1. How the direction of a traveling wave refers to the angle of incidence (normal or oblique incidence), the rough or planar interface between two media, whether these media are lossless or lossy, and wave polarization. These are the main factors required to determine the reflection and transmission coefficient. In general, the reflection and transmission coefficients are complex. Oblique incidence wave and lossy media will cause even more complexity for the calculation.
2. For convenience, if separating electrical field traveling to the boundary into two polarizations can be accomplished, perpendicular and parallel

individually, then the total transmitted and reflected field will be the sum of the two polarizations.

3. Reflection and transmission coefficients are derived by applying boundary conditions, in which the tangential components of electric and magnetic fields are continuous at the boundary. In other words, the total of the incident and the reflected tangential components of electrical and magnetic fields are equal to the transmitted tangential components of the field.
4. The transmitted angle in lossy media is complex, but for a good conductor, $\cos \theta_t$ is 1(real) not complex for lossy media, as indicated by an example 5-8 in Chapter 5 in Banalis's research (2012).
5. Snell's law and Fresnel's law can be applied in any media (lossless or lossy), and from this the reflection coefficient and transmission coefficient can be calculated.
6. Critical angle can be neglected because the source wave is a radar beam. If the source beam incident is in the high-density medium layer between the air, then this angle will allow the total internal reflection of energy. In other words, the incident wave will not come out and travel inside the medium as a waveguide.
7. The Brewster angle matters because it will allow total transmission in the layer. The Brewster angle is important in the RCS measurement in

the anechoic chamber because it significantly reduces reflection. Theoretically, the incident Brewster angle exists only if the polarization of the wave is parallel (vertical); no real incidence angle will reduce the reflection coefficient for perpendicular polarization to zero.

8. A wood board is considered to be lossy media due to the dielectric property, which results in dielectric loss in the media.

Next, there were two ways to calculate the RCS for wood board: approximation and non-approximation. Approximate reflection coefficient formulation (Senior et al. 1987) for resistive thin sheets is the starting point for determining the approximate amplitude of RCS wood board.

The non-approximated calculation formulation was drawn from Balanis's book (2012), Chapter 5 (a typo-corrected version of 5.5.2.D) and 11 (Section 11.3.2). This recursive process for multi-layer structures can be applied to the wood board to determine the reflection and transmission coefficients with oblique incidence wave. The recursive process for multi-layer structures is based on the calculations of the reflection coefficient using PO in the front of interface of an infinite half-plane, on which the uniform plane wave at an oblique incident angle is polarized. The recursive technique is employed as a common method to formulate a process, in which the impedance calculation in the media is embedded in the reflection coefficient calculation for each boundary. This leads to the

overall reflection coefficient calculations in front of the first boundary. The recursive formulation makes the calculation process much easier, especially given the several considerations detailed above.

Next, each RCS value calculated by the method above is entered in the coordinate transformation radar system. Radar direction with 651 points uniformly distributed over a far-field sphere pointing to each wood board with a set of discrete, sufficient oblique incident angles, which verify the overall convergence after averaging the RCS value of each object.

Table 5.1 and Table 5.2, which illustrate both approximation and non-approximation calculations, are presented for comparison. The wood boards are dry wood with $\epsilon_r = 2-0.2j$. The values for both calculations are small, but later calculations seem more reasonable for targets 40 feet away from the radar, based on two-way plane wave with a round trip phase. The new RCS values for wet wood board with $\epsilon_r = 4.65-1.46j$ are calculated by 20% moisture content, and are presented in Table 5.3.

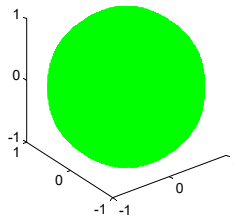
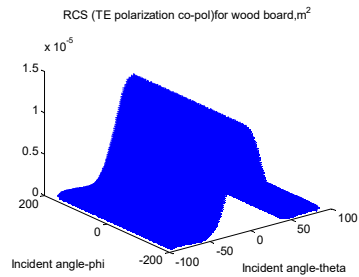
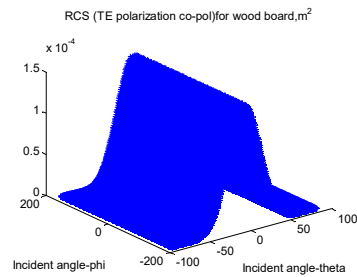


Figure 5.26: Sphere for radar direction pointing to the wood slab with 651 points.

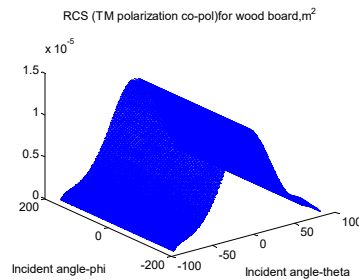


Dry wood board

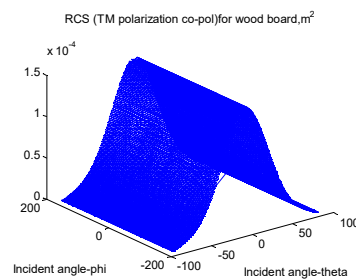


Wet wood board

Figure 5.27: RCS TE polarization on dry wood board (0.04157x 0.04157 meters) (left) and RCS TE polarization on wet wood board (0.04157x 0.04157 meters) (right) with two incident angles theta and phi scattered.



Dry wood board



Wet wood board

Figure 5.28: RCS TM polarization on dry wood board (0.04157x 0.04157 meters) (left) and RCS TM polarization on wet wood board (0.04157x 0.04157 meters) (right) with two incident angles theta and phi scattered.

The five figures illustrate the radar polarization and RCS values for one dry or wet wood board at 0.04157 by 0.04157 meters at 2.8 GHz. The following 9 sizes can also be generated accordingly. (Table 5.1, Table 5.2 and Table 5.3)

5.2.3 The list of wood to a typical house and establishing an RCS library

A board foot is a standard measure for wood lumber. For example, a piece of lumber one-inch thick (depth), one foot wide, and one foot long can be written as 1" x 12" x 12' as a board foot.

For example, an average 2,000 square foot home requires 13,000 board feet of lumber. This number is calculated by considering lumber of different sizes, as follows:

2x6 lumber 13,000 feet long = $1625 \times 8'$ 2x6 = $6500 \times 2'$ 2x6;

2x4 lumber 19,500 feet long = $2437.5 \times 8'$ 2x4 = $9750 \times 2'$ 2x4;

1x12 lumber 13,000 feet long = $1625 \times 8'$ 1x12 = $6500 \times 2'$ 1x12;

3x4 lumber 13,000 feet long = $1625 \times 8'$ 3x4 = $6500 \times 2'$ 3x4;

3x6 lumber 8,666.67 feet long = $1083.3 \times 8'$ 3x6 = $4333.33 \times 2'$ 3x6 etc.

A study from Dr. Paul Emrath for the National Association of Home Builders reports the average size house built in 2011 was 2,480 square feet, while the median size house built in 2011 was 2,233 square feet. The typical 2,400 square foot, single-family home requires about 16,000 board feet of framing lumber, and over 14,000 square feet of other wood products, including plywood, oriented strand board, glulam beams, wood I-joists, laminated veneer lumber, hardboard, particleboard and medium-density fiberboard (MDF).

In order to establish the RCS library, the wood board should be divided by wood type and size. For example, how many tree species for different lengths of 2x4 wood lumbers are required to compile a representative sample? To establish an RCS library for framing lumber, three things require specification and verification from the following picture. First, there are two grades to classify moisture content: S-dry and S-Grn (for green). S-dry means the board has water weight less than 19%. S-Grn means the board has water weight over 19%.

Second, species is a category that requires consideration for the RCS. This study addresses four species: Southern Pine, Spruce-Pine-Fir, Douglas Fir, and Hem-Fir. Each has a different dielectric property and structural strength.

Finally, there are four lumber grades that are used in most homes: SEL STR, No.1, No.2 and No.3. SEL STR (select structural) is nearly knot-free lumber. The remaining three lumber grades are designed by how many defects or knots the boards have, as this affects the lumber's strength and properties.

Penn State Pointers ▶ Selecting the Proper Wood

Homeowners need to be sure to select the right materials for their remodeling and do-it-yourself projects.

Look for the grade stamp on each board or piece of lumber.
Stamps allow consumers to purchase the proper lumber for the proper application.

Certification and Mill I.D. ...
Varies by geographic region.

LUMBER GRADE...
Most homeowners will use:

- **SEL STR** - Select Structural (nearly knot-free)
- **NO. 1**
- **NO. 2**
- **NO. 3**

 Graded by how many defects or knots appear in the board and how that affects the lumber's strength.

SPECIES...
The more popular (in the northeastern U.S.) are:

- **SOUTHERN PINE**
- **SPRUCE - PINE - FIR**
- **DOUGLAS FIR**
- **HEM-FIR**

MOISTURE CONTENT...

- **S-GRN** (over 19% water weight) can shrink or warp if used undried.
- **S-DRY** (under 19% water weight) can be used immediately.

Visit us at
["http://aginfo.psu.edu/psp/index.html"](http://aginfo.psu.edu/psp/index.html)

Graphics / illustration: Tom Lunt, College of Agricultural Sciences, Copyright Penn State.

Figure 5.29 Four lumber grades of lumber that homeowners need to see.

(<http://www.oldhouseweb.com/how-to-advice/buying-guides/what-to-look-for-when-buying-framing-lumber.shtml>)

Table 5.1: Approximation of RCS values for dry wood board for 10 square sizes at 5 different frequencies (2.8, 5.5, 9.7, 37.5, and 100 GHz).

Frequencies /mean RCS Dimensions (meters)	$\lambda=107$ mm f=2.8 Ghz		$\lambda=55$ mm f=5.5 Ghz		$\lambda=31$ mm f=9.7 Ghz		$\lambda=8$ mm f=37.5 Ghz		$\lambda=3$ mm f=100 Ghz	
	TE	TM	TE	TM	TE	TM	TE	TM	TE	TM
0.04157x 0.04157	3.36 e-06	1.48 e-06	1.17 e-05	8.59 e-06	3.46 e-05	2.95 e-05	2.91 e-04	2.85 e-04	6.2 e-04	6.18 e-04
0.08314x 0.08314	4.87 e-05	3.58 e-05	1.72 e-04	1.52 e-04	4.61 e-04	4.34 e-04	0.0021	0.0021	0.0030	0.0030
0.12471x 0.12471	2.33 e-04	1.97 e-04	7.94 e-04	7.37 e-04	0.0019	0.0018	0.0058	0.0058	0.0074	0.0074
0.16628x 0.16628	7.13 e-04	6.3 e-04	0.0022	0.0021	0.0048	0.0047	0.0113	0.0113	0.0141	0.0141
0.20785x 0.20785	0.0017	0.0015	0.0049	0.0047	0.0095	0.0094	0.0185	0.0185	0.0232	0.0232
0.24942x 0.24942	0.0033	0.003	0.0090	0.0087	0.0161	0.0160	0.0276	0.0276	0.0336	0.0336
0.29099x 0.29099	0.0057	0.0054	0.0147	0.0144	0.0246	0.0244	0.0388	0.0388	0.0439	0.0439
0.33256x 0.33256	0.0092	0.0088	0.0222	0.0218	0.0349	0.0347	0.0523	0.0523	0.0699	0.0699
0.37413x 0.37413	0.0140	0.0134	0.0315	0.0311	0.0471	0.0469	0.0683	0.0683	0.1171	0.1171
0.4157x 0.4157	0.0200	0.0193	0.0427	0.0423	0.0612	0.0610	0.0867	0.0867	0.1773	0.1773

Table 5.2: Non-approximation of RCS values for dry wood board for 10 square sizes at 5 different frequencies (2.8, 5.5, 9.7, 37.5, and 100 GHz).

Frequencies /mean RCS Dimensions (meters)	$\lambda=107$ mm f=2.8 Ghz		$\lambda=55$ mm f=5.5 Ghz		$\lambda=31$ mm f=9.7 Ghz		$\lambda=8$ mm f=37.5 Ghz		$\lambda=3$ mm f=100 Ghz	
	TM	TE	TM	TE	TM	TE	TM	TE	TM	TE
0.04157x 0.04157	1.1653 e-06	3.3361 e-06	7.6325 e-06	1.1333 e-05	2.5193 e-05	3.1131 e-05	4.4810 e-05	4.7935 e-05	6.4121 e-06	6.9383 e-06
0.08314x 0.08314	3.1854 e-05	4.7135 e-05	1.2587 e-04	1.5091 e-04	2.7773 e-04	3.0533 e-04	2.5639 e-04	2.6183 e-04	5.5906 e-05	5.7025 e-05
0.12471x 0.12471	1.7033 e-04	2.1527 e-04	5.2645 e-04	5.8924 e-04	6.8277 e-04	7.3144 e-04	2.2187 e-04	2.2519 e-04	1.4710 e-04	1.4882 e-04
0.16628x 0.16628	5.1943 e-04	6.1936 e-04	0.0012	0.0013	6.1761 e-04	6.6218 e-04	1.6886 e-04	1.7504 e-04	2.7508 e-04	2.7765 e-04
0.20785x 0.20785	0.0012	0.0013	0.0020	0.0021	9.3155 e-05	1.1170 e-04	8.3099 e-04	8.4033 e-04	7.6276 e-04	7.6550 e-04
0.24942x 0.24942	0.0022	0.0024	0.0023	0.0025	5.5712 e-04	5.7095 e-04	0.0013	0.0013	0.0015	0.0015
0.29099x 0.29099	0.0034	0.0038	0.0020	0.0021	0.0025	0.0025	9.1410 e-04	9.2371 e-04	0.0025	0.0025
0.33256x 0.33256	0.0049	0.0053	9.9573 e-04	0.0011	0.0041	0.0042	0.0010	0.0011	0.0041	0.0042
0.37413x 0.37413	0.0064	0.0070	2.1121 e-04	2.6239 e-04	0.0033	0.0034	0.0017	0.0017	0.0068	0.0068
0.4157x 0.4157	0.0078	0.0083	6.5480 e-04	6.8752 e-04	0.0011	0.0011	0.0017	0.0017	0.0101	0.0101

Table 5.3: Non-approximation of RCS values for wet wood board for 10 square sizes at 5 different frequencies (2.8, 5.5, 9.7, 37.5, and 100 GHz). (Moisture content 20%, $\epsilon_r = 4.6500 - 1.4600i$)

Frequencies /mean RCS Dimen- sions (meters)	$\lambda=107$ mm f=2.8 Ghz		$\lambda=55$ mm f=5.5 Ghz		$\lambda=31$ mm f=9.7 Ghz		$\lambda=8$ mm f=37.5 Ghz		$\lambda=3$ mm f=100 Ghz	
	TM	TE	TM	TE	TM	TE	TM	TE	TM	TE
0.04157x 0.04157	1.6198 e-05	3.6280 e-05	7.9515 e-05	1.0242 e-04	1.8251 e-04	2.0562 e-04	8.3258 e-05	8.6074 e-05	1.1101 e-04	1.1252 e-04
0.08314x 0.08314	3.2846 e-04	3.3300 e-04	8.2706 e-04	9.1555 e-04	9.6061 e-04	0.0010	5.0180 e-04	5.0994 e-04	4.6650 e-04	4.6968 e-04
0.12471x 0.12471	0.0014	0.0016	0.0023	0.0024	6.8124 e-04	7.2152 e-04	0.0012	0.0012	8.9782 e-04	9.0264 e-04
0.16628x 0.16628	0.0034	0.0037	0.0033	0.0035	0.0016	0.0016	0.0020	0.0020	0.0015	0.0015
0.20785x 0.20785	0.0061	0.0066	0.0025	0.0027	0.0044	0.0045	0.0030	0.0030	0.0038	0.0038
0.24942x 0.24942	0.0091	0.0097	0.0018	0.0019	0.0046	0.0047	0.0042	0.0042	0.0072	0.0072
0.29099x 0.29099	0.0117	0.0123	0.0046	0.0048	0.0047	0.0048	0.0054	0.0055	0.0119	0.0119
0.33256x 0.33256	0.0128	0.0135	0.0099	0.0101	0.0086	0.0088	0.0064	0.0064	0.0200	0.0201
0.37413x 0.37413	0.0118	0.0124	0.0142	0.0145	0.0109	0.0110	0.0068	0.0068	0.0323	0.0323
0.4157x 0.4157	0.0092	0.0098	0.0151	0.0155	0.0111	0.0113	0.0074	0.0074	0.0484	0.0484

Chapter 6

Conclusions

The final decision for choosing a PO technique is based on the geometry of the debris types, as well as the complexity, limitation, and accuracy of the analytical method. Even though PO is not as accurate as other approaches like MoM, GTD, etc., these methods require an excessive computation in terms of time and math complexity; the benefits of using PO outweigh these shortcomings. Moreover, edge diffraction is not taken into account for PO. PO is sufficiently able to analyze plate-like objects.

Calculating and simulating the polarimetric RCS of simple objects, such as plate-like (including sheets) and cylindrical objects with endcaps, works reasonably. Plots further confirmed theoretical limitations and approximations.

For non-penetrable plate-like objects, amplitudes for sheets are the same as plates, as formulation indicated. HFSS is not in good agreement with analytical results, as the incident angle approaches to 90 degrees due to the edge effect not being taken into account for PO.

For penetrable plate-like structures, all rectangular and circular plots match well as the incident angle is less than 40 degrees. This observation confirms the theoretical limitation and approximation that more accurate

results appear as the incident angle becomes closer to normal due to the restriction of surface impedance principle.

Two-layer plate structures are calculated towards multilayer approaches. FEKO is utilized to construct two layers with different media since HFSS has no such function. The plots generated from FEKO are in good agreement with analytical results.

RCS amplitudes for thin and thicker plates are compared and distinguishable. The difference is as large as about 20 dB at $\epsilon_r = 2.15$, or 10 dB at $\epsilon_r = 10-5j$ between each thickness (0.001λ , 0.01λ , and 0.1λ) on selected plate sizes.

Unlike the sphere, whose symmetry allows an exact RCS solution for the wave equation, a finite cylinder has no such solution. The solution for the broadside of the finite conducting cylinder formulated in Balanis's research (2012) is not as accurate when compared to the infinite long cylinder. The plots show gaps at 0° (more than 20 dB) between MATLAB and HFSS for the most selected sizes of cylinders.

This study took advantage of theoretical accuracy for a circular plate by adding the endcap, which compensated the deficiency of the cylinder's amplitude since the incident wave approaches normal at the endcap surface. The results become more accurate when the radius is larger than 0.3λ and the length is larger than 6λ . This is indicated from the RCS

modeling developed. Some selected cylinders almost perfectly overlap at the range of 0-90 degrees in terms of scattering angle. Although there are still gaps between 40-50 degrees for incident angle on the selected sizes of cylinders, this is most likely because the edge between endcap and cylinder broadside is ignored by PO approximation, and because the amplitude increases significantly between the ranges of 0 to 60 degrees of the incident angle. This study also found that amplitudes of cross-pols of TE and TM for a dielectric cylinder are imperceptibly low, falling within a range of -200 to -400 dB. The analytical plots for cross-pols are not shown in the dissertation.

The benefit discovered through the use of endcaps marks a pivotal moment in this study, and exemplifies the spirit and passion that foregrounds this dissertation. The process of finding methods that yield more accurate results for RCS modeling helps us better understand the limitations for the PO technique.

In terms of computational time, cylindrical objects ($\lambda = 0.11$ meters, for example) with radii at 0.1λ , 0.2λ , 0.3λ , 0.36λ , 0.5λ , 0.55λ , 1λ , 1.5λ and lengths of 3.64λ , 5.5λ , 7.27λ , 10λ , 30λ are examples of thin, long cylinders (several λ 's in length). The MATLAB calculations for RCS modeling on the selected sizes require less time than HFSS simulations. Plate-like objects also require less time in MATLAB calculations when compared to HFSS, especially for a short, fat cylinders with up to 3λ in

radius and 1λ in length. HFSS simulation takes over 30 minutes, whereas MATLAB only takes a few minutes.

A further motivation for completing this study is to validate modeling with measurements. Past studies indicated that a short cylinder has a higher monostatic RCS than a long cylinder of the same maximum dimensions, which defines a bounding box as a limiting factor in far-field measurements since it must fit within the measurement facility's quiet zone.

For complex shapes, examples of Japanese roof tiles are given:

Length 0.375 meters, Thickness 0.0219 meters; $L/T = 19$

Length 0.175 meters, Thickness 0.0109 meters

Length 0.075 meters, Thickness 0.0055 meters

(75 mm-375 mm lengths, 5.5 mm-21.9 mm thickness)

These objects increase math complexity because the surface is not flat and has holes. If these variations make the object too computationally intensive, then measurement is a good choice.

Toward the end of this dissertation, examples of applications of "real" debris scatterer using radar coordinate transformations systems for a single leaf and wood board study are presented. The "real" leaf modeling combines a thin flat sheet (to represent the leaf body) (Senior 1987) and a long thin finite cylinder (to represent the stem), thereby developing a new approach for making more complex objects for modeling purposes. The

leaf sizes are designed to represent a range of leaves from small to large in order to establish a “real” leaf RCS library. FEKO simulation is used to compare with analytical results, since this software makes it easy to combine two objects as a whole. The RCS values for all polarizations in the dry wood board study are calculated starting from 651 points uniformly distributed over a far-field sphere. The radar will point to each wood board with a set of discrete, sufficient angles to ensure the convergence of overall RCS mean values for each object. The study requires a set of high frequencies at 2.8, 5.5, 9.7, 37.5, 100 GHz, and so on. The reflection coefficient for each RCS value is calculated from a recursive process formulation in Balanis’s research (2012). The thickness of the wood boards (square plates) are 1/20 of their length, which range approximately from a few 10th’s of a wavelength ($\lambda = 0.11$ meters at 2.8 GHz, for example) to 10 times a wavelength for 10 values at each frequency. Wood boards (0.01 meters ($\sim 0.1 \lambda$) in thickness) with a uniformly coated water layer on the top make the amplitude of RCS go up by about 10 dB or 5 dB, except when the thickness of water is less than 0.0003 meters. Uniformly wet wood boards in 10 different thicknesses with 20% moisture content make the amplitude of RCS increase by about 6 dB when compared to dry wood boards.

Answering the poorly understood research questions that this dissertation poses makes an invaluable contribution to the field of tornadic debris study, and helps us clarify some fundamental concepts.

In terms of answering fundamental questions in this dissertation:

- a. What debris types and characteristics lead to observed polarimetric scattering signatures?

Based on tornado debris storm observations, tornadic debris features polarimetric characteristics. These may vary in the size, geometry and concentration on debris types. In most cases, lofted sand and dust particles and wood debris comprise the visible debris around the tornado. Currently, T-matrix calculations are performed for dust, sand particles, and spheroid wood debris, all which lead to observed polarimetric scattering signatures (Bodine 2014). As described, dust in the range 10 to 10^4 μm , sand diameter $D > 0.1$ mm, and prolate or oblate spheroids in a range of 0-160 mm with axis ratios of 3 and 1/3 wood spheroids have been evaluated for Z_{HH} and correlation coefficient. Both were performed in the Rayleigh and Mie regions. These debris types lead to observed polarimetric scattering signatures since their sizes are dominant factors that affect polarimetric variables. However, T-matrix calculations have limitations or errors for objects associated with dimensions and shapes.

Compared to these scatterers, RCS modeling on similar sizes of plate-like and small cylindrical objects, which T-Matrix cannot do, will be significant in the study of electromagnetic scattering characteristics. Therefore, RCS modeling is best represented by radar signature in terms of size-based theoretical analysis. For example, leaves (4 cm x 6 cm, 0.0001 meters in thickness), metal circular plates ($> 0.3 \lambda$ in radius), non-metal circular plates ($> 1 \lambda$ in radius), conducting cylinders ($> 0.3 \lambda$ in radius, $> 6 \lambda$ in length) and dielectric larger cylinders ($> 0.5 \lambda$ in radius, $> 1 \lambda$ in length) are in good agreement for both E and H polarizations with HFSS ($\lambda = 0.11$ meters at 2.8 GHz). By further validating with measurements, conclusions will be drawn based on selected-sizes of objects leading to a polarimetric scattering signature.

- b. What types of debris can be reasonably approximated in a computationally-efficient way for the purposes of this research?
 - i. RCS modeling of plate-like objects, as question (a) indicated.
 - ii. RCS modeling of perfect conducting cylinders with endcaps, $> 0.3 \lambda$ in radius with the same length 7.3λ (0.8 meters) can be reasonably approximated. (For example, 0.04 ($\sim 0.3 \lambda$) meters in radius by 0.8 ($\sim 7.3 \lambda$) meters in length, and 0.06 ($\sim 0.55 \lambda$) meters in radius by 0.8 ($\sim 7.3 \lambda$) meters in length).
 - iii. RCS modeling of metal cylinders with endcaps 0.5λ (0.055 meters) in radius with 10λ (1.1 meters) in length; 1λ (0.11

meters) in radius with 10λ (1.1 meters) in length; 0.3λ (0.033 meters) in radius with 30λ (3.3 meters) in length; and 1.5λ (0.165 meters) in radius with 30λ (3.3 meters) in length all performed well.

- iv. RCS modeling of dielectric cylinders at relative permittivity $\epsilon_r = 10 - 5j$, dielectric cylinders $> 0.5 \lambda$ (0.055 meters) in radius with 10λ (1.1 meters) in length; $> 1 \lambda$ (0.11 meters) in radius with 10λ (1.1 meters) in length; and $> 1.5 \lambda$ (0.165 meters) in radius with 30λ (3.3 meters) in length all performed well.

These selected sizes of plate-like and cylindrical objects require less time in MATLAB when compared to full-wave simulation HFSS, and are in good agreement with HFSS. Therefore, they are better options for a computationally-efficient way to obtain results for the purposes of this research.

- c. How should one determine which approach to use when adding the RCS database to a simulator?

When modeling the polarimetric RCS of simple objects (such as plate-like, cylindrical objects) based on the theories and research published, the goal is to emulate the radar return signal with thousands of different debris scatterers. In general, computer modeling is able to provide a variety of plots from 2D to 3D, which are also visualized. The analytical data

obtained from programming may easily be processed by the central computer facility (GPU) available at the University of Oklahoma.

RCS modeling can be used in the event that the measurement of an antenna is not feasible. Certain situations that cause any instability in the surrounding environment, such as being in moving vehicle, may cause inaccurate experiment data. In other words, if there is instability, the data analysis cannot be done in real time, and requires the data to be treated for statistical analysis later. It is very dangerous physically, for example, to capture the real data from the radar vehicle when it is moving closer to a tornado. Measurement accuracy is strongly dependent on the accuracy of the chosen instrumentation and method. Therefore, modeling based on theory and simulation has an advantage of obtaining more accurate data over the measurement.

On the other hand, when adding RCS data into a larger data processing network, computational efficiency is one of the most important factors to consider. When computational efficiency from modeling larger objects derived from theory and simulation is not high enough, measurement becomes necessary. Moreover, if RCS modeling differences between theoretical analysis and full-wave simulation HFSS are not trivial, measurement becomes a crucial component for obtaining accurate data.

Ultimately, any decision regarding obtaining accurate results must consider how well theory, simulation and measurement agree with one

another. By controlling and measuring the RCS of a single scatterer, the ultimate goal is to incorporate common objects with unique characteristics through the RCS database into the radar simulator.

d. In terms of accuracy, is the approach of simulating individual scatterers more suitable for answering the fundamental research questions posed in this dissertation?

A good advantage for simulating individual scatterers is that the detailed distinguishable analytical scattering characteristic becomes relatively easy if multiple scattering involves thousands to millions of angle combinations when the cross-polarized return signal is involved. Thus, the RCS database can be built with a unique characteristic for each object. In addition, as illustrated by the “real” leaf in Chapter 5, a single object can be combined to model more complex objects.

In addition, the complex received radar signals in the radar system are the sum of the signals of the individual debris object. The approach of modeling RCS of individual scatterers is more efficient to estimate the errors for the signals of the individual object. Therefore, RCS prediction is more accurate when considering polarimetric variable measurements by evaluating these errors.

Simulating individual scatterers is more suitable in terms of accuracy when compared to measurement; this is because RCS measurement does

not require high accuracy due to many errors and approximations from measurement instrumentation and method.

The basic nature of RCS modeling on discrete objects without multiple reflections is the science of fundamental electromagnetic scattering. Simulating the individual scatterer requires a strong knowledge of fundamental theory to serve as a starting point for solving more challenging, complex problems.

Analytical simulation and HFSS simulation are two major tools used in this doctoral study. Future work includes anechoic chamber measurements are the next exciting steps towards determining how well theory calculation for individual scatterer compares to radar returns.

References

- Abramowitz, M. I., A. Stegun, 1972: Handbook of mathematical functions. Dover Publications, New York.
- Aguilar, A. G., P. H. Pathak, M. Sierra-Perez, Oct. 2013: A canonical UTD solution for electromagnetic scattering by an electrically large impedance circular cylinder illuminated by an obliquely incident plane wave. *IEEE Transactions on Antennas and Propagation*, **61(10)**, 5144-5154.
- Balanis, C.A., 2005: Antenna Theory: Analysis and Design. 3rd edition, Copyright, John Wiley & Sons, Inc.
- Balanis, C., 2012: Advanced Engineering Electromagnetics. 2nd edition, Wiley.
- Blacksmith, P. Jr., R. E. Hiatt, R. B. Mack, Aug.1965: Introduction to radar cross-section measurements. *Proc. IEEE*, vol. **53**, 901-920.
- Bluestein, H. B., M. M. French, R. L. Tanamachi, S. Frasier, K. Hardwick, F. Junyent, and A. Pazmany, 2007: Close-range observations of tornadoes in supercells made with a dual-polarization, X-band, mobile Doppler radar. *Mon. Wea. Rev.*, **135**, 1522–1543.
- Bodine, D. J., M. R. Kumjian, R. D. Palmer, P. L. Heinselman, and A. V. Ryzhkov, 2013: Tornado damage estimation using polarimetric radar. *Wea. Forecasting*, **28**, 139–158.
- Bodine, D. J., R. D. Palmer, T. Maruyama, C. Fulton, Y. Zhu and B. L. Cheong, 2015: Simulated Frequency Dependence of Radar Observations of Tornadoes, *37th Conference on Radar Meteorology*, Norman, Oklahoma, September 14-18.
- Bodine, D. J., R. D. Palmer, T. Maruyama, C. Fulton, Y. Zhu, and B. L. Cheong, 2015: Simulated Frequency Dependence of Radar Observations of Tornadoes, *JTech.*, 2016 accepted.
- Bodine, D.J., 2014: Polarimetric radar observations and numerical simulations of tornadic debris. Dissertation.
- Brill, D. G., C. Gaunard, 1990: High frequency monostatic echoes from finite-length cylinders. Tome 51, France.

Capsoni, C., and M. D'Amico, 1998: A Physically Based Radar Simulator. *J. Atmos. Oceanic Technol.*, **15**, 593–598.

Cheong, B. L., D. Bodine, Y. Zhu, C. Fulton, S. Torres, T. Maruyama, R. Palmer, 2015: Emulating Polarimetric Radar Signals from Tornadic Debris Using a Radar-Cross-Section Library, *12th European Radar Conference*, Paris, France, September 6-11.

Cheong, B. L., D. Bodine, Y. Zhu, C. Fulton, S. Torres, T. Maruyama and R. Palmer, 2015: Emulating Polarimetric Radar Signals from Tornadic Debris Using a Radar-Cross-Section Library, *4th International Symposium on Earth-science Challenges*, Norman, Oklahoma, September 20-23.

Cheong, B. L., D. Bodine, Y. Zhu, C. Fulton, S. Torres, T. Maruyama, R. Palmer, Understanding Tornadic Debris Echoes Using a Radar Time-Series Emulator, 2015: *IEEE International Radar Conference*, Arlington, Virginia, May 11-15.

Cheong, B. L., R. D. Palmer, and M. Xue, 2008: A Time Series Weather Radar Simulator Based on High-Resolution Atmospheric Models. *J. Atmos. Oceanic Technol.*, **25**, 230–243.

Chiu, T., K. Sarabandi, May 1999: Electromagnetic scattering interaction between a dielectric cylinder and a slightly rough surface. *IEEE Transactions On antennas And Propagation*, Vol. **47**, No. 5, 902-913.

Cottard, G., Y. Arien, 2006: Anechoic chamber measurement improvement. *Microwave journal*.

Crowe, C., C. Schultz, M. Kumjian, L. Carey, and W. Petersen, 2012: Use of dual-polarization signatures in diagnosing tornadic potential. *Electronic J. Operational Meteor.*, Vol. **13**, 57–78.

Daian, G., A. Taube, A. Birnboim, M. Daian, Y. Shramkov, 2006: Modeling the dielectric properties of wood. *Wood Sci Tech.*, **40**, 237-246.

Doviak, R. J., D. S. Zrnic, 1993: Doppler Radar and Weather Observations. Dover Publications. Inc., 2nd edition. Mineola, New York.

Doviak, R. J., V. Bringi, A. Ryzhkov, A. Zahrai, and D. Zrni'c, 2000: Considerations for polarimetric upgrades to operational WSR-88D radars. *J. Atmos. Oceanic Technol.*, **17**, 257 – 278.

Dowell, D. C., C. R. Alexander, J. M. Wurman, and L. J. Wicker, 2005: Centrifuging of Hydrometeors and Debris in Tornadoes: Radar-Reflectivity Patterns and Wind- Measurement Errors. *Mon. Wea. Rev.*, **133**, 1501–1524.

Dybdal, R. B., Apr. 1987: Radar cross section measurements. *Proceedings of the IEEE*, Vol. **75**, No.4, 498-516.

Elsherbeni, A.Z., and A. Kishk, Jan. 1992: Modeling of cylindrical objects by circular cylinder. *IEEE Trans. Antennas. Propagat.*, Vol. **40**, No. 1, 96-99.

Fung, A., F. Ulaby, 1978: A scatter model for leafy vegetation. *IEEE Trans. Geosci. Electron.*, Vol **16**, No.4, 281-286.

Harrington, R. F., J. R. Mautz, 1975: An impedance sheet approximation for thin dielectric shells. *IEEE Trans. Antennas Propag.*, Ap-25, 531-534.

Harrington, R.F., 1961: Field Computation by Moment Methods. Macmillan, New York.

Henin, B. H., A. Z. Elsherbeni, M. Al Sharkawy, 2007: Oblique incidence plane wave scattering from an array of circular dielectric cylinders” *Progress In Electromagnetics Research*, PIER **68**, 261-279.

Herman, M.I., and J. L. Volakis, 1987: High-frequency scattering by a resistive strip and extensions to conductive and impedance strips. *Radio Sci.*, **22**,335-349.

IEEE Standard Test Procedures for Antennas, IEEE Std.149-1979.New York, NY: Wiley-Interscience.

Jebbor, N., S. Bri, A. Nakheli, L. Bejjit, M. Hdddad, A. Mamouni, Dec. 2011: Complex Permittivity Determination with the Transmission / Reflection Method. *Int. J. Emerg. Sci.*, **1(4)**, 682-695.

Jenn, D. C., 2005: Radar and laser cross section engineering. *AIAA*, 2nd edition.

Kahny, D., S. Riegger, G. Schone, W. Wiesbeck, Jan. 1988: Coherent polarimetric signatures of coniferous trees- A survey. *Proceedings of the 4th International Colloquium on Spectral Signatures of Objects in Remote Sensing*, France, 18-22.

Karam, M. A., A. K. Fung, 1988: Electromagnetic scattering from a layer of finite length, randomly oriented, dielectric, circular cylinders over a rough interface with application to vegetation. *Int. J. Remote Sensing*. Vol. **9**, No.6, 1109-1134.

Knott, E. F., 2006: Radar cross section measurements. *SciTech Publishing*.

Kouyoumjian, R. G., and P. H. Pathak, 1974: A uniform geometrical theory of diffraction for an edge in a perfectly conducting surface. *Proc. IEEE*, **62(11)**, 1448-1461.

Kumjian, M. R., and A. V. Ryzhkov, 2008: Polarimetric signatures in supercell thunderstorms. *J. Appl. Meteor. Climatol.*, **48**, 1940–1961.

Kummer, W.H., and E. S. Gillespie, Apr.1978: Antenna measurements. *Proc. IEEE*, Vol.**66**, 483-507.

Lambour, R., N. Rajan, T. Morgan, I. Kupiec, E. Stansbery, 2004: Assessment of orbital debris size estimation from radar cross-section measurements. *Advances in Space Research*, **34**, 1013-1020.

Lang, R. H., J. S. Sidhu, 1983: Electromagnetic backscattering from a layer of vegetation: A discrete approach. *IEEE Transactions on Geoscience and Remote Sensing*. Vol. **GE-21**, No.1, 62-71.

Liou, Kuo-nan., 1972: Electromagnetic scattering by arbitrarily oriented ice cylinders. *Appl Opt.*, **11(3)**, 667-74.

Mack, C. L., JR. and B. Reiffen, 1964: RF characteristics of thin dipoles. *Proceeding of the IEEE*. Vol. **52**, 533-542.

Maliuzhinets, G.D., 1958: Excitation, reflection and emission of surface waves from a wedge with given wave impedances. *Soviet Physics: Doklady*, Vol. **3**, 752–754.

McDonald, K.T., Oct. 2011: Scattering of a plane electromagnetic wave by a small conducting cylinder. Princeton University.

Mishchenko, M.I., 2000: Calculation of the amplitude matrix for a nonspherical particle in a fixed orientation. *Appl. Opt.*, **39(6)**, 1026-31.

Mishchenko, M.I., L.D. Travis, and D.W. Mackowski, 1996: T-matrix computations of light scattering by nonspherical particles: A review. *J. Quant. Spectrosc. Radiat. Transfer.*, **55**, 535-575.

Palmer, R. D., D. Bodine, M. Kumjian, B. Cheong, G. Zhang, Q. Cao, H. B. Bluestein, A. Ryzhkov, T.-Y. Yu, and Y. Wang, 2011: The 10 May 2010 tornado outbreak in central Oklahoma: Potential for new science with high-resolution polarimetric radar. *Bull. Amer. Meteor. Soc.*, **92**, 871–891.

Park, H.S., A. V. Ryzhkov, D. S. Zrnić, and Kyung-Eak Kim, 2009: The Hydrometeor Classification Algorithm for the Polarimetric WSR-88D: Description and Application to an MCS. *Wea. Forecasting*, **24**, 730–748.

Penny, C.W., R.J. Luebbers, J.W. Schuster, 1996: Scattering from coated targets using a frequency-dependent, surface impedance boundary condition in FDTD. *IEEE Transactions on Antennas Propagation*, Vol. **44**, No. 4, 434-443.

Riegger, S., 1987: Measurement and calculation of the complex scattering matrix for a dielectric cylinder. *Proceedings of the 17th EMC*, Rome, 800-805.

Ruck, G. T., D. E. Barrick, W. D. Stuart, and C. K. Krichbaum, 1970: Radar Cross Section Handbook. New York.

Ryzhkov, A., D. Burgess, D. Zrnić, T. Smith, and S. Giangrande, 2002: Polarimetric analysis of a 3 May 1999 tornado. *Preprints, 21th Conf. on Severe Local Storms*, Amer. Meteor. Soc., Ed., San Antonio, TX.

Ryzhkov, A.V., T. J. Schuur, D.W. Burgess, and D. S. Zrnić, 2005: Polarimetric tornado detection. *J. Appl. Meteor.*, **44**, 557–570.

Sarabandi, K., P. F. Polatin, Apr.1994: Electromagnetic scattering from two adjacent objects. *IEEE Transactions on Antennas and Propagation*, Vol. **42**, No. 4, 510-516.

Sarabandi, K., P. F. Polatin, F. T. Ulaby, 1993: Monte Carlo simulation of scattering from a layer of vertical cylinders. *IEEE Transactions on Antennas and Propagation*. Vol. **41**, No. 4, 465-475.

Sarabandi, K., T.B.A. Senior, 1990: Low frequency scattering from cylindrical structure at oblique incidence. *IEEE Trans. Geosci. Remote Sensing*. Vol. **28**, 879-885.

Schultz, C. J., L. D. Carey, E. V. Schultz, B. C. Carcione, C. B. Darden, C. C. Crowe, P. N. Gatlin, D. J. Nadler, W. A. Petersen, and K. R. Knupp, 2012a: Dual-polarization tornadic debris signatures Part I: Examples and utility in an operational setting. *Electronic J. Operational Meteor.*, **13**, 120 – 137.

Schultz, C. J., S. E. Nelson, L. D. Carey, L. Belanger, B. C. Carcione, C. B. Darden, T. Johnstone, A. L. Molthan, G. J. Jedlovec, E. V. Schultz, C. C. Crowe, and K. R. Knupp, 2012b: Dual-polarization tornadic debris signatures Part II: Comparisons and caveats. *Electronic J. Operational Meteor.*, **13**, 138–158.

Seker, S., 1986: Microwave backscattering from a layer of randomly oriented discs with application to scattering from vegetation. *IEEE Proc. Microwave. Antennas and Propagation. H.*, 497-502.

Seker, S., A. Schneider, 1985: Electromagnetic scattering from finite-length dielectric cylinders. *Digest of International Geoscience and Remote Sensing Symposium*. Vol. **1**, 523-526.

Senior, T. B. A., 1952: Diffraction by a semi-infinite metallic sheet. *Proc. R. Soc. London, Set. A*, **213(1115)**, 436-458.

Senior, T. B. A., 1985: Scattering by resistive strips and plates. Rep. 388919-1-F, *Univ. of Mich. Radiat. Lab.*, Ann Arbor, Mich.

Senior, T. B. A., K. Sarabandi, and F. T. Ulaby, 1987: Measuring and modeling the backscattering cross section of a leaf. *Radio Sci.*, **22**, 1109 – 1116.

Simmons, K. M., D. Sutter, 2005: WSR-88D radar tornado warnings and tornado casualties. *Wea. Forecasting*, vol. **20**, 301–310.

Snyder, J. C., and Bluestein, H. B. 2014: Some considerations for the use of high-resolution mobile radar data in tornado intensity determination. *Wea. Forecasting*, **29**, 799 – 827.

Straka, J. M., D. S. Zrnica, A.V. Ryzhkov, 2000: Bulk Hydrometeor Classification and Quantification Using Polarimetric Radar Data: Synthesis of Relations. *J. Appl. Meteor.*, **39**, 1341–1372.

Stratton, J. A., 1941: Electromagnetic theory. McGraw-Hill Book Company, Inc., New York.

Sutrakar, V. K., P. Vasistha, and K.N. Shamanna, 2012: RCS measurement in anechoic chamber and its validation by comparison with simulation data. *ATMS*.

Tiberio, R., G. Pelosi, and G. Manara, 1985b: A uniform GTD formulation for the diffraction by a wedge with impedance faces. *IEEE Trans. Antennas Propag.*, AP-33, 867- 873.

Tice, T. E., Feb. 1990: An overview of radar cross section measurement techniques. *IEEE Transactions on Instrumentation and Measurement*. Vol. **39**, No.1, 205-207.

Tricomi, F.G., F. Oberhettinger, W. Magnus, A. Erdelyi, 1953: Higher transcendental functions. *McGraw Book Company Inc.*, New York, Vol. **2**, 102.

Ulaby, F. T., C. Elachi, Eds., 1990: Scattering models for distributed target. *Radar Polarimetry for Geoscience Applications*. Norwood, MA, Artech House. 111-190.

Ulaby, F.T., T.E. Van Deventer, J.R. East, T.F. Haddock, May 1988: Millimeter-wave bistatic scattering from ground and vegetation targets. *IEEE Transactions on Geoscience and Remote Sensing*, Vol. **26**, No. 3, 229-243.

Wait, J. R., 1955: Scattering of a plane wave from a circular dielectric cylinder at oblique incidence. *Canadian J. Phys.*, **33**, 189 – 195.

Waterman, P. C., 1969: New Formulation of Acoustic Scattering, *J. Acoust. Soc. Am.*, **45**, 1417 - 1429.

Waterman, P.C., 1971: Symmetry, unitarity, and geometry in electromagnetic scattering. *Phys Rev D*. **3**, 825-39.

Wolf, M. E., 1965: Principles of Optics. Pergamon, New York, 378.

Workshop on Polarimetric Radar, *US Army Missile Command*. GIGIAC, ITT Res. Inst., Chicago, IL.

Zhang, Linxi, K. Ding, Nanjing Li, J. Ren, 2010: High-resolution RCS measurement inside an anechoic chamber. *International forum on information technology and applications*. 252-255.

Zrnic, D.S., and Ryzhkov, A.V., 1999: Polarimetry for Weather Surveillance Radars. *Bull. Amer. Meteor. Soc.*, **80**, 389–406.

<http://dspace.mit.edu/bitstream/handle/1721.1/61254/701906470.pdf>

<http://faculty.nps.edu/jenn/EC4630/TheoremsandConceptsV2.pdf>

<http://www.eecs.umich.edu/RADLAB/html/techreports/RL681.pdf>

http://www.nahb.org/fileUpload_details.aspx?contentID=85253

www.cst.com CST MWS workshop series 2011

www.microwavevision.com

www.orbitfr.com/usa/content/locate-sales-representative

Appendix A

List of Acronyms

ARPS	Advanced Regional Prediction
DDA	Discrete Dipole Approximation
FDTD	Finite-difference time-domain
PEC	Perfect electrical conducting
FEKO	FEldberechnung für Körper mit beliebiger Oberfläche
FEM	Finite element method
FDTD	Finite Difference Time Domain method
PTD	Physical theory of diffraction
GO	Geometrical optics
GPU	Graphics processing unit
GTD	Geometrical Theory of Diffraction
HFSS	High Frequency Structural Simulator
IE	Integral equations
LES	Large Eddy Simulation
MoM	Method of moments
PO	Physical optics
RCS	Radar Cross Section
TDS	Tornadic debris signature
UTD	Uniform Theory of Diffraction

Appendix B

List of Symbols

D	Diameter of target (m)
E_s	Scattering electric field ($V\ m^{-1}$)
E_i	Incident electric field ($V\ m^{-1}$)
H_i	Incident magnetic field ($V\ m^{-1}$)
H_s	Scattered magnetic field ($V\ m^{-1}$)
J_s	Surface current
k	Propagation constant (m^{-1})
K_w	Function of the refractive index of water
L_{DR}	Linear depolarization ratio (dB)
$N(D)$	Particle size distribution
R	Resistivity (ohm)
r	Radius (m)
S	Scattering matrix
S_{hh}	Amplitude of horizontal co-polarization (dBsm)
S_{hv}	Amplitude of horizontal cross-polarization (dBsm)
S_{vv}	Amplitude of vertical co-polarization (dBsm)
S_{vh}	Amplitude of vertical cross-polarization (dBsm)
T	T matrix
T_E	E polarization of transmission coefficient

T_H	H polarization of transmission coefficient
Z_e	Equivalent radar reflectivity factor (dBZ)
Z_{DR}	Differential reflectivity threshold (dB)
Z_{HH}	Horizontal radar reflectivity factor (dBZ)
Z_{VV}	Vertical radar reflectivity factor (dBZ)
$Z (1/Y)$	Intrinsic impedance
Z_s	Normalized surface impedance (ohm)
ρ_{HV}	Co-polar cross-correlation coefficient
δ_{dp}	Backscatter differential phase ($^\circ$)
$\alpha (\varphi)$	Orientation angle in xy polarization plane ($^\circ$)
$\beta (\theta)$	Orientation angle in zx polarization plane ($^\circ$)
γ	Orientation angle in yx polarization plane ($^\circ$)
σ	Radar cross-sections (m^2)
λ	Wavelength (m)
\hat{n}	Unit vector normal to the surface
Γ_E	E polarization of reflection coefficient
Γ_H	H polarization of reflection coefficient
ϵ_r	Complex relative permittivity
η_s	Surface impedance (ohm)
a_n^s	TM polarization coefficient
b_n^s	TM polarization coefficient

σ_b	Backscatter cross-section (m ²)
μ	Relative permeability
ρ	Cylindrical radius (m)
J_n	Bessel function of first kind
$H_n^{(2)}$	Hankel function of second kind